UNDERSTANDING THE SYMBIOSIS IN ANAEROBIC OXIDATION OF METHANE THROUGH METABOLIC, BIOSYNTHETIC AND TRANSCRIPTOMIC ACTIVITIES

Thesis by

Hang Yu (Hank)

In Partial Fulfillment of the Requirements for

the degree of

Doctor of Philosophy

CALIFORNIA INSTITUTE OF TECHNOLOGY

Pasadena, California

2017

(Defended on April 26, 2017)

ORCID: 0000-0002-7600-1582

ACKNOWLEDGEMENTS

My accomplishments today would not have been possible without the contributions and guidance from the following individuals:

I would like to thank my thesis advisor Professor Victoria Orphan. She has opened up a world of possibilities for me since joining her lab. I am very grateful to have the rare opportunity and freedom to learn the best techniques and explore my own ideas in science in the past six years, while knowing that she will always be there to support and guide regardless of the situation. She has helped to build a solid foundation for me to pursue whichever career path I decide on next.

I would also like to thank Professor Jared Leadbetter. He is my thesis advisory committee chair and a living encyclopedia of microbiology. I have been fortunate to interact and learn from him since my first day at Caltech. Not only have I been fortunate to perform research in his laboratory, but I have also learned a lot by being a teaching assistant in his class for three consecutive years and chatting with him about microbial physiology and microbiology in general.

Professors Dianne Newman and Woodward Fischer have also provided excellent guidance as members in my thesis advisory committee. Their extremely approachable personalities combined with their immense knowledge in fields of microbial metabolism, microbial interactions, and geobiology helped to improve this thesis from the small details to the big picture.

The faculty members in the Department of Environmental Sciences and Engineering and the Division of Geological and Planetary Sciences have together made Caltech education truly exceptional. Professor Joe Kirschvink is one of the kindest people I know; it has been difficult to not learn when given the opportunities to go to amazing places like Baja California and Antarctica. Professors Alex Sessions, Jason Saleeby, John Eiler and Michael Lamb all have dedicated their time outside of their work to teach students and lead division

trips to New Zealand and Hawaii. Other faculties such as Professors Paul Wennberg, Jess Adkins, Andy Thompson, Tapio Schneider, and Mike Hoffmann are all top scientists in their research area, and yet still try their very best to teach and help students in every way they could. Together, these classroom and field experiences greatly expanded my horizons in the past six years.

A very special gratitude goes out to the students and staff in the department and the division. I would like to thank the students in ESE 166 Microbial Physiology and GE 246 Molecular Geobiology Seminar for giving me the opportunity to practice teaching and also learn from them. I would like to thank Clement Cid and Xing Xie for their help in different projects. I would like to thank Drs. Fenfang Wu, Yunbin Guan and Nathan Delleska for running excellent analytical facilities, teaching me about their ways around the instruments, and saving me from a lot of potential frustrations. I would also like to thank the excellent administrative staff, especially Elizabeth Boyd, Julie Lee, Nora Oshima, and Jan Haskell, for being incredibly considerate and made my time in Caltech significantly more pleasant and enjoyable.

I would like to thank my fellow labmates for the discussions, collaborations and all the fun we have had together. Connor Skennerton, Grayson Chadwick, Patricia Tavormina, Roland Hatzenpichler, Shawn McGlynn and Silvan Scheller have directly assisted me in this thesis and wonderful to work with. Stephanie Connon did her very best to fulfill the needs of every project in the lab, and managed to not have a single fire incident during my time here with such a big chaotic group. I am also very thankful for the chances to interact with very talented individuals past and present in the lab, including Abigail Green-Saxena, Alexis Pasulka, Alice Michel, Anne Dekas, Ariel O'Neill, Daan Speth, David Case, Derek Smith, Elizabeth Trembath-Reichert, Fabai Wu, Greg Wanger, Haley Sapers, Hiro Imachi, Jeffrey Marlow, Jennifer Glass, Joshua Steele, Kat Dawson, Kyle Metcalfe, Lizzy Wilbanks, Masataka Aoki, Michelle Fry, Min Sub Sim, Paul Magyar, Ranjani Murali, Sean Mullin,

Shana Goffredi, Sujung Lim, Tetsuya Yamada, and Usha Lingappa. Together, you have created such a pleasant and supportive atmosphere that fostered this work.

Caltech is also special because of its small size. I would like to thank all the friends I have made across all disciplines on campus. This includes the people I spent time together on division field trips, in various on-campus and off-campus events, and those I met in the Caltech Chinese Association. I will not list everyone here, but I hope you know who you are if you ever read this. I have learned a tremendous amount from you, and I hope our friendships continue in the years to come.

I would also like to thank my mentors in the past, including Drs. Bill Mohn, Martin Hartmann, Hao Xiao, Sebastian Sudek and Alex Worden. I would not be doing this work if it were not for your generosity and passion that inspired me to study microbiology.

I would like to thank Yuling Zhang for encouraging and cheering me on during the ups and downs in my studies. Thank you for always being there and your understanding, especially when the experiments run late or when I need to work evenings, weekends and holidays. Your confidence in me and your smile has made a positive impact on this work.

Finally, to my parents, Lin Yu and Xiaobing Li. Thank you for providing me the best in everything to reach for the stars and chase my dreams. I rarely tell you how grateful I am to be your son, but I truly am. To my dad, thank you for showing me the way to be a better scientist, and to my mom, thank you for showing me the way to be a better person. This thesis is only possible with your unconditional support and love.

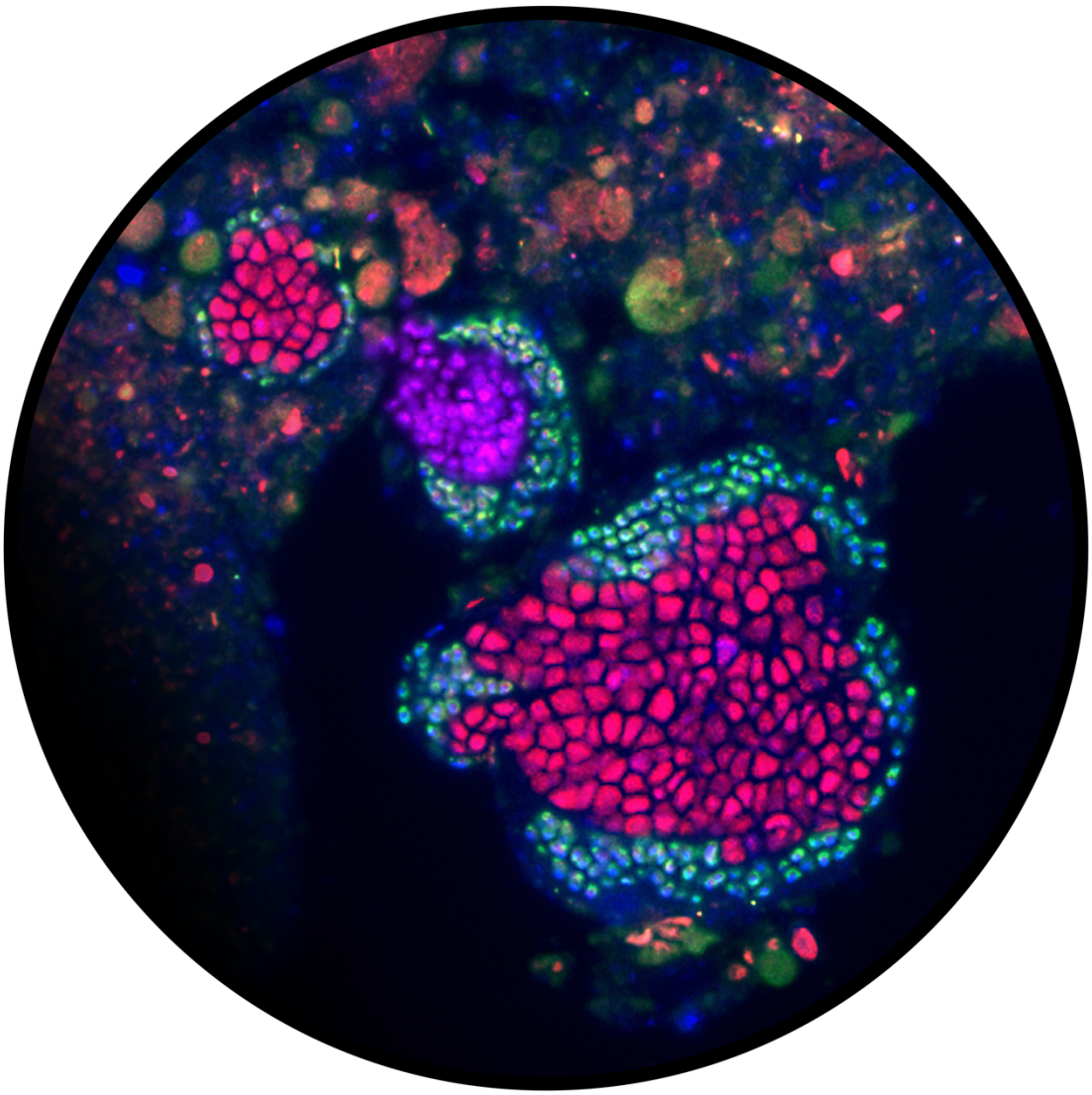

ABSTRACT

Microorganisms provide essential ecological services to our planet. Their combined activities control and shape our environment as we know today. In the deep sea, a microbial mediated process known as anaerobic oxidation of methane (AOM) consumes large amounts of methane, a potent greenhouse gas and a valuable energy resource. How this symbiosis works is poorly understood.

In this thesis, I tested current hypotheses on the symbiotic mechanisms in AOM microbial consortia, consisting of a partnership between anaerobic methanotrophic archaea (ANME) and sulfate-reducing bacteria (SRB). Sediments collected from methane seeps offshore Oregon and California and dominated by AOM consortia were used in these investigations. A range of compounds were amended to sediment microcosms, and their effects on the metabolic activities of ANME or SRB were monitored by tracking the rates of methane oxidation or sulfate reduction on timescales varying from hours to months. A lack of stimulation or inhibition on the AOM consortia, combined with long-term community profiles, suggest that diffusible compounds are unlikely to be involved in the symbiosis in AOM. I further examine ANME genomes, focusing the role of sulfur in methane seep ecosystems. Phylogenetic analyses revealed multiple poorly characterized genes in the sulfur pathway, and comparisons with methanogenic archaea related to ANME provided a better understanding of their roles in the cell. Transcriptional responses combined with protein modeling were used to predict the potential substrate of a sulfite reductase related enzyme. These predictions were validated using genetics, and together point to an assimilatory rather than dissimilatory sulfur pathway in methane-utilizing archaea in general. Then, the AOM symbiosis was decoupled for the first time using soluble electron acceptors. ANME remained metabolically and biosynthetically active without their SRB partner, suggesting that the electrons are transferred directly in this partnership. This observation was investigated to a greater depth with transcriptomics. Membrane proteins and multiheme cytochromes critical in extracellular electron transfer in ANME and SRB were expressed. These results together illuminate the path electrons may take to exit or enter the AOM consortia. Overall, multiple activity analyses used here piece together a clearer view on how the symbiosis in AOM works, with potential applications in future energy generation from methane.

PUBLISHED CONTENT AND CONTRIBUTIONS

Scheller, S., Yu, H., Chadwick, G.L., McGlynn, S.E., and Orphan, V.J. (2016). "Artificial Electron Acceptors Decouple Archaeal Methane Oxidation from Sulfate Reduction". In: *Science*, 351.627, pp. 703–7. doi: 10.1126/science.aad7154.

H.Y. participated in conception of project, designed study, prepared data and analysis, and participated in writing of the manuscript.

TABLE OF CONTENTS

Acknowledgements iii
Abstract vii
Published Content and Contributions viii
Table of Contents ix

Introduction 1
References 5

Chapter 1: Comparative genomics and functional characterization of assimilatory sulfate reduction in methanogenic and methanotrophic archaea 8
1.1 Abstract 9
1.2 Introduction 10
1.3 Materials and Methods 13
1.4 Results 25
1.5 Discussions 34
1.6 Tables and Figures 38
1.7 Supplementary Information 58
1.8 Acknowledgements 58
1.9 Author Contributions 59
1.10 References 60

Chapter 2: Artificial Electron Acceptors Decouple Archaeal Methane Oxidation from Sulfate Reduction 68
2.1 Abstract 69
2.2 Report 70
2.3 Tables and Figures 77
2.4 References in the Report 97
2.5 Materials and Methods 101
2.6 References in the Materials and Methods 112
2.7 Acknowledgements 116
2.8 Author Contributions 116

Chapter 3: Transcriptional Responses of Deep-sea Archaea Decoupled from Their Syntrophic Sulfate-Reducing Bacteria Partner 117
3.1 Abstract 118
3.2 Introduction 119
3.3 Materials and Methods 121
3.4 Results and Discussions 127

3.5 Tables and Figures....133
3.6 Author Contributions....150
3.7 References....151

Appendix A: Investigating the Effects of Diffusible Metabolites on Anaerobic Methane Oxidizing Consortia....154
Explanation for Appendix....155
Abstract....157
Introduction....158
Materials and Methods....159
Results and Discussions....161
Tables and Figures....168
References....179

Conclusions and Future Directions....182

Introduction

Methane (CH_4) is an important chemical in the global carbon cycle. It is the simplest hydrocarbon and the primary component of natural gas, and thus represents a valuable energy resource. 34% of electricity generation in the U.S. is from natural gas in 2016 (United States Energy Information Administration 2017). On the other hand, methane is a potent greenhouse gas with global warming potential 86 times that of carbon dioxide (CO_2) (IPCC 2014). Given its wide usage and significant impact on climate, discovering a more efficient way to utilize methane and improving our understanding of its biogeochemical cycle is a necessary area of research in environmental sciences.

Microorganisms control the cycling of methane by catalyzing 85% of its production and 60% of its consumption on our planet (Knittel and Boetius 2009). Oceanic sediments are a particularly large reservoir and source of methane, with 3,000,000 teragram (Tg) stored as methane hydrates and 85 Tg produced annually (Reeburgh 2007). Geochemical measurements of methane in marine sediments since the 1970s have repeatedly identified a concave-up shaped profile showing a depletion of methane under anoxic conditions with sulfate depletion, and subsequent studies of its oxidation rates and natural isotopes confirmed that this process is biologically mediated, and later termed it the anaerobic oxidation of methane (AOM) (Reeburgh 2007 and references therein). Sulfate is the main electron acceptor coupled to methane oxidation given its high concentration in seawater, but it was not until the turn of the century that a series of three studies pinned down the biological identities that controls AOM with sulfate (Hinrichs et al. 1999; Boetius et al. 2000; Orphan et al. 2001). This process involves a syntrophic consortium of anaerobic methanotrophic archaea (ANME) and partner sulfate-reducing bacteria (SRB) that pass an, as yet unidentified, metabolic intermediate between ANME and SRB to couple their metabolisms. The main goal of my thesis is to experimentally examine the various hypotheses regarding the mechanism of this symbiosis and the identity of the intermediate passed between ANME and SRB.

There are multiple groups of ANME and SRB, and they may use different symbiotic mechanisms. Although AOM is the unifying metabolism that gave the name ANME to these microorganisms, they are phylogenetically distinct, belonging to different orders in the class Methanomicrobia under phylum Euryarchaeaota and domain Archaea (Knittel and Boetius 2009). There are also multiple groups of SRB in the class Deltaproteobacteria under phylum Proteobacteria and domain Bacteria (Knittel et al. 2003; Schreiber et al. 2010). In order to distinguish these different uncultured groups of ANME and SRB, I will use their specific group names wherever possible in this thesis (eg. ANME-2a and Seep-SRB1).

A range of possible metabolic intermediates have been proposed for AOM symbiosis and can be grouped into three categories:

The first category includes substrates that can be used by methanogenic archaea. These relatives of ANME can grow with hydrogen, formate, acetate or methylated compounds to generate methane (Thauer et al. 2008), and it was also shown using metagenomics that ANME operate the methanogenesis pathway in reverse to oxidize methane (Hallam et al. 2004). Together, these compounds could be produced by ANME as a result of AOM, and then passed to and consumed by their SRB partner (Hoehler et al. 1994; Valentine and Reeburgh 2000; Moran et al. 2008; Alperin and Hoehler 2009). These potential intermediates have been tested by adding them to incubations with ANME-2a/2c and Seep-SRB1 collected from Hydrate Ridge (Nauhaus et al. 2002; Nauhaus et al. 2005), ANME-1 and Seep-SRB2 collected from Black Sea (Nauhaus et al. 2005), ANME-2a and various Deltaproteobacteria or Bacteroidetes enriched from Eckernförde Bay (Meulepas et al. 2010), ANME-1 and HotSeep-1 enriched from Guaymas Basin (Wegener et al. 2015), ANME-2a/2b/2c and Seep-SRB2 enriched from Mediterranean island Elba (Wegener et al. 2016), and ANME-1 and Seep-SRB2 enriched from Guaymas Basin (Wegener et al. 2016). These feeding experiments have shown no stimulation in terms of metabolic rate as measured by either rates of AOM or sulfide production or growth of SRB in the AOM

consortia, suggesting that these methanogenic substrates are unlikely the metabolic intermediate used in AOM symbiosis.

The second scenario involves a sulfur based metabolic intermediate. It might be possible that ANME carry out both methane oxidation and sulfate reduction. This could explain the microscopy observations of ANME only aggregates without SRB partner in environmental samples (Orphan et al. 2002; Treude et al. 2007). By investigating enrichments from Mediterranean Isis Mud Volcano containing ANME-2a/2c and Seep-SRB1, Milucka and colleagues observed higher zero-valent sulfur content in ANME and a unique 7:1 sulfide:sulfate production stoichiometry indicative of disulfide disproportionation, suggesting that zero-valent sulfur is the metabolic intermediate produced from partial sulfate reduction by ANME (Milucka et al. 2012).

The last scenario hypothesizes that electrons are transferred directly from ANME to SRB. This was first proposed with identification of secreted multiheme c-type cytochromes in ANME-1 metagenome and metatranscriptome (Meyerdierks et al. 2010). Subsequently, two studies on ANME-1 and ANME-2b/2c both suggest that AOM consortia transfer electrons directly without a diffusible intermediate based on cellular activity patterns, physiological studies and genomic findings of potential proteins used in direct interspecies electron transfer. The thermophilic partner of ANME-1, namely HotSeep-1 or Candidatus Desulfofervidus auxilii, grew independently with hydrogen (Krukenberg et al. 2016), but the rate of hydrogen production in thermophilic AOM cultures when sulfate reduction was inhibited were much lower than the level needed to support partner HotSeep-1 (Wegener et al. 2015). However, ANME still could not be decoupled to grow independently from their SRB partner and the symbiotic mechanism in AOM remains enigmatic.

In this thesis, I use various experimental and bioinformatics approaches to test all three of these scenarios.

- Appendix A investigates both the first and second scenarios using sediment containing a mixture of ANME-1/2a/2b/2c and Seep-SRB1 collected from Hydrate Ridge and Santa Monica Basin.

- Chapter 1 investigates the second scenario using a combination of bioinformatics analyses and genetic characterizations to elucidate sulfur pathways in ANME-1/2a/2b and Candidatus Methanoperedens.

- Chapter 2 investigates the third scenario by amending different soluble electron acceptors to sulfate-free incubations.

- Chapter 3 further explores the symbiotic mechanism in AOM by studying single-cell anabolic activity and changes in RNA expression of these consortia containing ANME-2a/2c.

Together, the work presented here help us to better understand the physiology and inner workings of the enigmatic AOM consortia. The discoveries on how microbes work together and mediate methane consumption is important in characterizing one of the largest sinks for methane on Earth, and may lead to potential applications in future energy generation from methane.

REFERENCES

Alperin, Marc J, and Tori M Hoehler. 2009. "Anaerobic Methane Oxidation by Archaea/Sulfate-Reducing Bacteria Aggregates: 1. Thermodynamic and Physical Constraints." *American Journal of Science* 309 (10): 869–957. doi:10.2475/10.2009.01.

Boetius, Antje, Katrin Ravenschlag, Carsten J Schubert, Dirk Rickert, Friedrich Widdel, Armin Gieseke, Rudolf Amann, Bo Barker Jørgensen, Ursula Witte, and Olaf Pfannkuche. 2000. "A Marine Microbial Consortium Apparently Mediating Anaerobic Oxidation of Methane." *Nature* 407 (6804): 623–26. doi:10.1038/35036572.

Hallam, Steven J, Nik Putnam, Christina M Preston, John C Detter, Daniel Rokhsar, Paul M Richardson, and Edward F DeLong. 2004. "Reverse Methanogenesis: Testing the Hypothesis with Environmental Genomics.." *Science* 305 (5689). American Association for the Advancement of Science: 1457–62. doi:10.1126/science.1100025.

Hinrichs, Kai U, John M Hayes, Sean P Sylva, Peter G Brewer, and Edward F DeLong. 1999. "Methane-Consuming Archaebacteria in Marine Sediments.." *Nature* 398 (6730): 802–5. doi:10.1038/19751.

Hoehler, Tori M, Marc J Alperin, Daniel B Albert, and Christopher S Martens. 1994. "Field and Laboratory Studies of Methane Oxidation in an Anoxic Marine Sediment: Evidence for a Methanogen-Sulfate Reducer Consortium." *Global Biogeochemical Cycles* 8 (4): 451–63. doi:10.1029/94GB01800.

IPCC. 2014. "Climate Change 2014: Synthesis Report. Contribution of Working Groups I, II and III to the Fifth Assessment Report of the Intergovernmental Panel on Climate Change." Edited by Core Writing Team, R K Pachauri, and L A Meyer. Geneva, Switzerland.

Knittel, Katrin, and Antje Boetius. 2009. "Anaerobic Oxidation of Methane: Progress with an Unknown Process.." *Annual Review of Microbiology* 63: 311–34. doi:10.1146/annurev.micro.61.080706.093130.

Knittel, Katrin, Antje Boetius, Andreas Lemke, Heike Eilers, Karin Lochte, Olaf Pfannkuche, Peter Linke, and Rudolf Amann. 2003. "Activity, Distribution, and Diversity of Sulfate Reducers and Other Bacteria in Sediments Above Gas Hydrate (Cascadia Margin, Oregon)." *Geomicrobiology Journal* 20 (4): 269–94. doi:10.1080/01490450303896.

Krukenberg, Viola, Katie Harding, Michael Richter, Frank Oliver Glöckner, Harald R Gruber Vodicka, Birgit Adam, Jasmine S Berg, et al. 2016. "Candidatus Desulfofervidus Auxilii, a Hydrogenotrophic Sulfate-Reducing Bacterium Involved in the Thermophilic Anaerobic Oxidation of Methane.." *Environmental Microbiology* 18 (9): 3073–91. doi:10.1111/1462-2920.13283.

Meulepas, Roel J W, Christian G Jagersma, Ahmad F Khadem, Alfons J M Stams, and Piet N L Lens. 2010. "Effect of Methanogenic Substrates on Anaerobic Oxidation of Methane and Sulfate Reduction by an Anaerobic Methanotrophic Enrichment.." *Applied Microbiology and Biotechnology* 87 (4): 1499–1506. doi:10.1007/s00253-010-2597-0.

Meyerdierks, Anke, Michael Kube, Ivaylo Kostadinov, Hanno Teeling, Frank Oliver

Glöckner, Richard Reinhardt, and Rudolf Amann. 2010. "Metagenome and mRNA Expression Analyses of Anaerobic Methanotrophic Archaea of the ANME-1 Group.." *Environmental Microbiology* 12 (2). Blackwell Publishing Ltd: 422–39. doi:10.1111/j.1462-2920.2009.02083.x.

Milucka, Jana, Timothy G Ferdelman, Lubos Polerecky, Daniela Franzke, Gunter Wegener, Markus Schmid, Ingo Lieberwirth, Michael Wagner, Friedrich Widdel, and Marcel M M Kuypers. 2012. "Zero-Valent Sulphur Is a Key Intermediate in Marine Methane Oxidation.." *Nature* 491 (7425): 541–46. doi:10.1038/nature11656.

Moran, James J, Christopher H House, Jennifer M Vrentas, and Katherine H Freeman. 2008. "Methyl Sulfide Production by a Novel Carbon Monoxide Metabolism in Methanosarcina Acetivorans.." *Applied and Environmental Microbiology* 74 (2): 540–42. doi:10.1128/AEM.01750-07.

Nauhaus, Katja, Antje Boetius, Martin Krüger, and Friedrich Widdel. 2002. "In Vitro Demonstration of Anaerobic Oxidation of Methane Coupled to Sulphate Reduction in Sediment From a Marine Gas Hydrate Area.." *Environmental Microbiology* 4 (5): 296–305.

Nauhaus, Katja, Tina Treude, Antje Boetius, and Martin Krüger. 2005. "Environmental Regulation of the Anaerobic Oxidation of Methane: a Comparison of ANME-I and ANME-II Communities.." *Environmental Microbiology* 7 (1): 98–106. doi:10.1111/j.1462-2920.2004.00669.x.

Orphan, Victoria J, Christopher H House, Kai U Hinrichs, Kevin D McKeegan, and Edward F DeLong. 2001. "Methane-Consuming Archaea Revealed by Directly Coupled Isotopic and Phylogenetic Analysis.." *Science* 293 (5529). American Association for the Advancement of Science: 484–87. doi:10.1126/science.1061338.

Orphan, Victoria J, Christopher H House, Kai-Uwe Hinrichs, Kevin D McKeegan, and Edward F DeLong. 2002. "Multiple Archaeal Groups Mediate Methane Oxidation in Anoxic Cold Seep Sediments.." *Proceedings of the National Academy of Sciences of the United States of America* 99 (11). National Acad Sciences: 7663–68. doi:10.1073/pnas.072210299.

Reeburgh, William S. 2007. "Oceanic Methane Biogeochemistry.." *Chemical Reviews* 107 (2): 486–513. doi:10.1021/cr050362v.

Schreiber, Lars, Thomas Holler, Katrin Knittel, Anke Meyerdierks, and Rudolf Amann. 2010. "Identification of the Dominant Sulfate-Reducing Bacterial Partner of Anaerobic Methanotrophs of the ANME-2 Clade.." *Environmental Microbiology* 12 (8): 2327–40. doi:10.1111/j.1462-2920.2010.02275.x.

Thauer, Rudolf K, Anne-Kristin Kaster, Henning Seedorf, Wolfgang Buckel, and Reiner Hedderich. 2008. "Methanogenic Archaea: Ecologically Relevant Differences in Energy Conservation.." *Nature Reviews Microbiology* 6 (8): 579–91. doi:10.1038/nrmicro1931.

Treude, Tina, Victoria Orphan, Katrin Knittel, Armin Gieseke, Christopher H House, and Antje Boetius. 2007. "Consumption of Methane and CO2 by Methanotrophic Microbial Mats From Gas Seeps of the Anoxic Black Sea.." *Applied and Environmental Microbiology* 73 (7): 2271–83. doi:10.1128/AEM.02685-06.

United States Energy Information Administration. 2017. "Annual Energy Outlook 2017,

with Projections to 2050." Accessed April 10. www.eia.gov/aeo.

Valentine, D L, and W S Reeburgh. 2000. "New Perspectives on Anaerobic Methane Oxidation.." *Environmental Microbiology* 2 (5). Blackwell Science Ltd: 477–84. doi:10.1046/j.1462-2920.2000.00135.x.

Wegener, Gunter, Viola Krukenberg, Dietmar Riedel, Halina E Tegetmeyer, and Antje Boetius. 2015. "Intercellular Wiring Enables Electron Transfer Between Methanotrophic Archaea and Bacteria." *Nature* 526 (7574). Nature Publishing Group: 587–90. doi:10.1038/nature15733.

Wegener, Gunter, Viola Krukenberg, S Emil Ruff, Matthias Y Kellermann, and Katrin Knittel. 2016. "Metabolic Capabilities of Microorganisms Involved in and Associated with the Anaerobic Oxidation of Methane." *Frontiers in Microbiology* 7 (17). Frontiers: 869. doi:10.3389/fmicb.2016.00046.

Chapter 1

COMPARATIVE GENOMICS AND FUNCTIONAL CHARACTERIZATION OF ASSIMILATORY SULFATE REDUCTION IN METHANOGENIC AND METHANOTROPHIC ARCHAEA

Hang Yu[1,2], Dwi Susanti[3], Shawn McGlynn[1,7], Connor Skennerton[1], Karuna Chourey[4], Ramsunder Iyer[4], Silvan Scheller[1,8], Patricia Tavormina[1], Robert L. Hettich[4], Biswarup Mukhopadhyay[3,5,6], Victoria Orphan[1]

[1]Division of Geological and Planetary Sciences, California Institute of Technology, Pasadena, California, 91125, USA

[2]Ronald and Maxine Linde Center for Global Environmental Science, California Institute of Technology, Pasadena, CA 91125, USA

[3]Department of Biochemistry, Virginia Tech, Blacksburg, VA 24061, USA

[4]Oak Ridge National Laboratory, Oak Ridge, USA

[5]Biocomplexity Institute, Virginia Tech, Blacksburg, VA 24061, USA

[6]Virginia Tech Carilion School of Medicine, Virginia Tech, Blacksburg, VA 24061, USA

[7]Present Affiliation: Earth-Life Science Institute, Tokyo Institute of Technology, Ookayama, Meguro-ku, Tokyo, Japan

[8]Present Affiliation: Department of Biotechnology and Chemical Technology, Aalto University, Kemistintie 1, 02150 Espoo, Finland

This chapter is in preparation for publication.

1.1 ABSTRACT

ANME and its related methanogenic archaea can all use sulfide as a source of sulfur for biosynthetic processes. Alternative sulfur sources such as sulfate, sulfite, thiosulfate, and elemental sulfur can be present in their environments. However, the capability and genetic mechanism of assimilation or even dissimilation of these more oxidized sulfur sources is not well understood. Here, the genomes of methanogenic and methanotrophic archaea were analyzed, and a previously overlooked pathway for assimilatory but not dissimilatory sulfate reduction is presented. Phylogenetic analyses suggest that while use of sulfur species of intermediate oxidation states may be widespread, the ability to activate sulfate is restricted. Multiple homologs of sulfite reductases were found in methanotrophic archaeal genomes, and their transcriptional responses to different sulfur species were consistent between ANME and a cultured relative *Methanococcoides burtonii*. In particular, Group II Fsr, a sulfite reductase homolog found in all methane seep environments surveyed, was only upregulated in the presence of thiosulfate. Analysis of inferred protein structures identified active site residue variations consistent with the hypothesis that this enzyme may serve a different function than sulfite reduction, in particular that it may accommodate a larger substrate molecule than sulfite. Heterologous expression studies showed that this enzyme is functional as a thiosulfate reductase, and ANME containing microcosms were insensitive to thiosulfate, but were sensitive to sulfite. Together these findings reveal a new function for a sulfite reductase homolog and also identify a hitherto unknown pathway of sulfur assimilation in these methane metabolizing archaea.

1.2 INTRODUCTION

The anaerobic oxidation of methane (AOM) is an important biogeochemical process in the global carbon cycle, and is the primary sink for methane in anoxic ocean sediments (Reeburgh 2007). The diffusion of seawater sulfate into sediments serves as the major electron acceptor for this process, fueling a syntrophic association between as yet uncultured anaerobic methanotrophic archaea (ANME) and sulfate-reducing bacteria (SRB) in regions where methane seepage is occuring. The underlying mechanism supporting this globally important process has not been definitively determined, but there have been a number of hypotheses proposed since the initial description of the AOM process by geochemists (Reeburgh 2007) and discovery of AOM syntrophs (Hinrichs et al. 1999; Boetius et al. 2000; Orphan et al. 2001). It has been proposed that methane oxidation might be coupled to sulfate reduction to zero-valent sulfur for catabolism (Milucka et al. 2012). This could resolve the long-standing question of how methane oxidation is metabolically coupled to sulfate reduction, but a genetic and biochemical basis for this hypothesis is lacking. Additionally, ANME and related methanogenic archaea often live in sulfidic environments, and all cultured methanogens have accordingly been shown to derive anabolic sulfur from sulfide (Y. Liu, Beer, and Whitman 2012). However, the phylogenetic and physiological diversity of these organisms is considerable (Y. Liu and Whitman 2008; Knittel and Boetius 2009; Borrel et al. 2014), and since some methane-metabolizing archaea live in environments low in sulfide, alternative sources and assimilatory mechanisms for sulfur may exist.

Sulfate can be reduced via assimilatory or dissimilatory sulfate reduction pathways to sulfide for anabolism or catabolism. A variety of sulfur species of intermediate oxidation states (+4 to 0) such as sulfite, thiosulfate and zero-valent sulfur can form from biotic and abiotic reactions. The first step in sulfate reduction is the activation of sulfate (oxidation state +6) using ATP that is catalyzed by two non-homologous ATP sulfurylase enzymes. The heterodimeric ATP sulfurylase can be found in some archaea and bacteria for sulfate

assimilation, and is composed of a regulatory GTPase subunit CysN (sulfate adenylyltransferase large subunit or subunit 1) and a catalytic subunit CysD (sulfate adenylyltransferase small subunit or subunit 2), together forming an enzyme composed of four heterodimers (Mougous et al. 2006). This process has a high energetic cost, consuming one GTP and one ATP per sulfate activated (C. Liu, Martin, and Leyh 1994). The more wide-spread ATP sulfurylase Sat, present across all three domains of life, exists as homo-oligomers and is used for both assimilatory and dissimilatory sulfate reduction, costing one ATP per reaction (Parey et al. 2013; Herrmann et al. 2014; Sperling et al. 2001; Ullrich, Blaesse, and Huber 2001).

Once sulfate is activated to adenosine-5'-phosphosulfate (APS, oxidation state +6), it can be reduced directly to sulfite (oxidation state +4) using APS reductase or via a further phosphatation step via 3'-phosphoadenosine-5'-phosphosulfate (PAPS, oxidation state +6) using APS kinase and PAPS reductase (Verschueren and Wilkinson 2005) . APS and PAPS differ by only one phosphate-group and their respective reductase enzymes are homologous proteins that use the same catalytic mechanism (Carroll et al. 2005). APS reductase can be distinguished from PAPS reductase by the presence of conserved cysteines that bind an iron-sulfur cluster as its cofactor (Chartron et al. 2006). However, distantly related APS reductase and PAPS reductase found in archaea that lack iron-sulfur clusters were described in *Methanocaldococcus jannaschii* (Lee et al. 2011; Cho 2013). Given the similarity between these newly characterized APS and PAPS reductases in archaea, it is unclear whether they could be easily distinguished bioinformatically based on their protein sequences.

After reduction, sulfite can be further reduced to sulfide (oxidation state -2) using sulfite reductase. Several homologs of this enzyme exist that may have iron-sulfur cluster or FAD binding domains in addition to the central siroheme binding domain, and best studied members are in the assimilatory sulfite reductase (aSir) and dissimilatory sulfite reductase (Dsr) groups. Related to these proteins are a number of not well understood homologs. These include the low-molecular weight sulfite reductase (alSir) that was purified from *Desulfovibrio vulgaris*, *Desulforomonas acetoxidans*, and *Methanosarcina barkeri* to carry out sulfite to sulfide conversion (Moura et al. 1986). alSir, also refered to as Group III Dsr-

like protein (Group III Dsr-LP) (Susanti and Mukhopadhyay 2012), can be distinguished by its low-spin state siroheme, but its physiological function remains unknown (Moura and Lino 1994). Other sulfite reductase homologs include the assimilatory anaerobic sulfite reductase (asrC) and Group I Dsr-like proteins (Group I Dsr-LP) (Dhillon et al. 2005; Loy, Duller, and Wagner 2008; Susanti and Mukhopadhyay 2012). An additional sulfite reductase, coenzyme F_{420}-dependent sulfite reductase (Fsr), has been described recently from *M. jannaschii*. This novel protein is a fusion of the beta subunit of the $F_{420}H_2$ dehydrogenase (FrhB) at the N-terminal and dissimilatory-type siroheme sulfite reductase at the C-terminal, together coupling the $F_{420}H_2$ oxidation to sulfite reduction (Johnson and Mukhopadhyay 2005). Expression of this protein into sulfite-sensitive *Methanococcus maripaludis* enables sulfite tolerance and also the use of sulfite as the sole sulfur source, which indicates that Fsr can detoxify or assimilate sulfite from the environment (Johnson and Mukhopadhyay 2008). This enzyme is found in a number of methanogens including *Methanosarcinales*, *Methanococcales*, *Methanobacteriales* and *Methanopyrales* as well as ANME (Susanti and Mukhopadhyay 2012).

In this study, comparative genomics, transcriptomics, and preliminary biochemical experiments were conducted to understand the sulfur pathways in methane-metabolizing archaea in general. Given the hypothesis of a novel sulfate reduction pathway as proposed by Milucka and colleagues (2012), new genome bins from methane seep sediment ANME groups were studied in comparison to published genomes. Although the physiological characteristic of anaerobic oxidation of methane (AOM) is the unifying metabolism that gave the name ANME to these organisms, they are phylogenetically distinct: ANME-1 is distantly related to *Methanosarcinales* and *Methanomicrobiales*, whereas ANME-2 and ANME-3 belong to *Methanosarcinales* (Knittel and Boetius 2009). In addition to this phylogenetic diversity, they also exhibit physiological diversity. While *Candidatus* Methanoperedens (ANME-2d) has been shown to couple AOM to nitrate reduction (Haroon et al. 2013; Arshad et al. 2015), other ANME groups (ANME-1a/1b/2a/2b/3) are believed to couple AOM to sulfate reduction with syntrophic bacterial partners (Knittel and Boetius 2009).

Genome analysis identified an apparently complete assimilatory sulfate reduction pathway in ANME-1 and ANME-2, despite the fact that they live in sulfidic environments symbiotically with sulfate-reducing deltaproteobacteria partners. The identified sulfite reductases are notably different from conventional assimilatory or dissimilatory pathways, and therefore were further investigated by studying *Methanococcoides burtonii*, a cultured methylotrophic methanogenic archaeaon (Franzmann et al. 1992; Allen et al. 2009) which harbors a close relative of the apparent sulfite reductase found in ANME. Gene expression, protein structure, and enzymatic activity studies revealed the activity and physiological consequences of this protein, and together, these analyses points to a broader sulfur-assimilating potential in ANME and methane-metabolizing archaea.

1.3 MATERIALS AND METHODS

1.3.1 Sample collection, DNA extraction, sequencing, and assembly

The recovery of a near complete genome (95.73% complete, 0.06% contamination) from the ANME-2b group was obtained from a bulk metagenome from a methane seep from Hydrate Ridge on the Cascadia Margin offshore of Oregon USA (sample ID 5133; 44◦40.02N; 125◦6.00W; water depth of 597 m; below a white microbial mat). Previous studies of the microbial community within this sample suggested the potential for multiple sulfur cycling processes directly and indirectly associated with AOM (Trembath-Reichert, Case, and Orphan 2016). In addition to the published ANME-1b genome bin (Meyerdierks et al. 2010), we also used an ANME-1b genome bin obtained from a single aggregate sorted from sample ID 7142 (methane seep in Santa Monica Basin; 35 37.3431N, 118 40.0997W; water depth of 860.5 m; below a white microbial mat) using an activity-based flow cytometry method to verify our findings (Hatzenpichler *et al.* 2016, Skennerton *et al.* In preparation).

In addition, DNA extracts from 4 methane seep sediments were used to survey the ANME gene distribution in different environment with the following sample IDs: 3730, 5059, 5207, 5547. These were collected from Hydrate Ridge (offshore Oregon, USA) on

two separate sampling cruises: sample ID 3730 (location 44˚ 43.09N; 125˚ 9.14W; water depth 776 m; below a *Calyptogena* clam bed) was collected on cruise AT 15-38 in August 2010; the others including sample IDs 5059 (location 44˚ 40.19N; 125˚ 5.88W; water depth of 595 m; below a clam field), 5207 (location 44◦40.02N 125◦6.00W; water depth of 601 m; below a white microbial mat), and 5547 (location 44◦34.19N 125◦8.86W; water depth of 775 m; below a white microbial mat) were collected on cruise AT 18-10 in September 2011, using the HOV Alvin (2010) or ROV JASON II (2011) on board of the R/V Atlantis. Anoxic 0.22 μm filtered bottom seawater collected on cruise AT 18-10 was mixed in 2:1 ratio with sediment and maintained under 2 bar of methane prior to subsampling for DNA analysis. DNA was extracted using PowerSoil DNA extraction kit following manufacturer's instructions (Mo Bio Laboratories Inc., Carlsbad, CA, USA).

1.3.2 Comparative genomic of sulfur pathways in ANME groups

Protein sequences for ANME groups were retrieved from IMG Submission ID 36455 for ANME-2a (Wang et al. 2014), NCBI GenBank ID AY714844 for ANME-2c (Hallam et al. 2004), NCBI BioProject PRJNA224116 and PRJNA296416 for *Ca.* Methanoperedens nitroreducens and *Ca.* Methanoperedens sp. BLZ1 (Haroon et al. 2013; Arshad et al. 2015), and ANME-1b and ANME-2b metagenome bins generated in this study. Other reference sequences were retrieved from databases NCBI Refseq and Integrated Microbial Genomes with Microbiome Samples (IMG/MER) (Pruitt et al. 2012; Markowitz et al. 2012). For phylogenetic analysis, alignments were done using Clustal Omega (Sievers et al. 2011). The results were imported into the ARB package (Ludwig et al. 2004) and manually checked. After excluding columns with mostly gaps, 418 and 276 aligned amino acids were used for phylogenetic analysis for *cysD* and *cysN*/EF-1A/EF-Tu, respectively. For APS/PAPS reductases, since some homologs have acquired extra N- or C-terminus domains (Supplementary Figure S2), only 168 aligned amino acids from the central shared region excluding columns with mostly gaps were used for phylogenetic analysis. For sulfite reductases, since different groups have acquired extra domains for flavin or iron-sulfur cluster

binding, or $F_{420}H_2$ oxidation, only the shared catalytic and siroheme binding region with 224 amino acid residues was used for phylogenetics (Supplementary Figure S5). The trees were built using a mixed amino acid model with burn-in set to 25% and stop value set to 0.01 in MrBayes v.3.2.1 (Ronquist et al. 2012) and edited using iTOL (Letunic and Bork 2016).

1.3.3 Protein homology modeling of Group II Fsr

Protein structural prediction was done using I-TASSER and the best matching template was dissmilatory sulfite reductase alpha subunit from *Archaeoglobus fulgidus* (PDB 3mm5 Chain A) (Yang et al. 2015). ANME Fsr sequence was trimmed to contain only the c-terminal sulfite reductase half of the protein as done previously (Johnson and Mukhopadhyay 2005). The structural alignment results were imported and viewed in PyMOL Molecular Graphics System (Delano 2002).

1.3.4 Targeted analysis: Primer design and amplification of Group II Fsr from marine methane seep sediment samples

We designed both degenerate and non-degenerate primer sets to study alSir and Group II Fsr in environmental samples (Supplementary Table S3a). For degenerate primers, PCR was done using the TaKaRa Ex Taq® DNA Polymerase kit (Takara Bio USA) with the following conditions: 1.0 µl of 10× buffer, 0.2 µl of dNTP, 0.2 µl of Taq polymerase, 0.2 µl of each forward and reverse primer, 7.2 µl of PCR water, and 1 µl of DNA sample. The cycling conditions were as follows: 95˚C for 40 s, 94˚C for 20 s, annealing at 59˚C for 30 s, extension at 72˚C for 1:40 min, for 40 cycles, and a final extension step at 72˚C for 4 min, cooled down to 4˚C and then immediately proceeded to cloning. The non-degenerate primer set was designed based on the Fsr found in ANME-2c (Hallam et al. 2004), only modified to add a restriction digest site and four leading bases for better annealing (Supplementary Table S3a). PCR was done using the NEB Q5 HotStart High Fidelity kit with the following conditions: 25 µl of Q5 master mix, 1.25 µl each of forward and reverse primers from 10

mM stock solutions, 5ul of DNA extracts at 10 ng/μl, and 17.5 μl of PCR water. The cycling conditions were as follows: 98˚C for 40 s, 98˚C for 10 s, annealing at 65˚C for 20 s, extension at 72˚C for 1 min, for 30 cycles, and a final extension step at 72˚C for 2 min, and stored at 4˚C.

For cloning, the amplified products were first purified with QIAquick PCR Purification kit (Qiagen, Valencia, CA, USA). Vector pMev2.1.1 was isolated using QIAprep Spin Miniprep kit (Qiagen, Valencia, CA, USA) from *Escherichia coli* transformants containing these plasmids as previously (Johnson and Mukhopadhyay 2008). Both the purified PCR products and pMev2.1.1 plasmids were double digested with NsiI and BamHI (NEB, Ipswich, MA, USA) at 37˚C for 5 hr, and inactivated at 65˚C for 20 min. Digested products were purified with the QIAquick PCR Purification kit (Qiagen), and ligated into pMev plasmid using the NxGen T4 DNA Ligase (Lucigen, WI, USA) with 5 μl of 10x buffer, 1 μl of T4 ligase, 8 μl of vector, and 36 μl of PCR insert with the vector and insert amounts at 1:3 ratio. The ligation reaction was performed at 4˚C for 48 hr before inactivation at 70˚C for 10 min. The products were purified using Multiscreen HTS plates (Millipore, Billerica, MA, USA), and checked for concentration and successful insertion using PCR with same primers and conditions as described earlier. Transformation was done using Top10 Escherichia coli competent cells and kit as instructed (Invitrogen, Carlsbad, CA, USA). Over 100 transformants were observed on plate with 20ul of initial cells. Clones were grown overnight, confirmed for correct insertion with PCR and restriction digest with SphI and HaeIII (NEB). Sequencing was done at Laragen Sequencing (Culver City, CA, USA) by mixing 9 μl of PCR products from transformed cells and 1 μl of either forward or reverse primers to confirm that no mutation has occurred in the process.

1.3.5 Metatranscriptome analysis of ANME Fsr/alSir expression

We performed microcosm experiments using sediment sample 5207 by amending different sulfur species of intermediate oxidation states. First, sediment sample 5207 was

mixed with 0.22 μm filtered natural bottom seawater collected on cruise AT 18-10 in 1:2 ratio. Then, 10 ml of mixed sediment seawater slurry was aliquoted into 30 ml bottles and capped with a black rubber stopper in the N_2:H_2 (95:5) anaerobic chamber. The incubations were then flushed with N_2 for 10 minutes. Thiosulfate and sulfite were added to a final concentration of 10 mM from anaerobic stock solutions, or as powder in the case for sulfur to a final amount of 50 mg in duplicates. The microcosms were incubated in the dark at 4°C. The overlaying seawater above the sediments was taken out approximately each month (Supplementary Figure S8), and sulfide concentration was monitored using the methylene-blue assay (Cline 1969). Subsequently, 20 ml of filtered anaerobic natural seawater and amendments was added to the same final concentration as before. At the end of the experiment (Supplementary Figure S8), 0.5 ml of settled sediment was sampled and flash frozen in liquid nitrogen for RNA analysis and extracted as previously described (Dekas et al. 2016).

RNA integrity was assessed using RNA 6000 Pico Kit for Bioanalyzer (Agilent Technologies, Santa Clara, CA, USA). RNA-seq libraries were constructed using NEBNext Ultra RNA Library Prep Kit for Illumina (NEB) following manufacturer's instructions. Briefly, 1-4 ng of total RNA was fragmented to the average size of 200 nt by incubating at 94°C for 15 min in first strand buffer, cDNA was synthesized using random primers and ProtoScript II Reverse Transcriptase followed by second strand synthesis using NEB Second Strand Synthesis Enzyme Mix. Resulting DNA fragments were end-repaired, dA tailed, and ligated to NEBNext hairpin adaptors (NEB). After ligation, adaptors were converted to the 'Y' shape by treating with USER enzyme and DNA fragments were size selected using Agencourt AMPure XP beads (Beckman Coulter, Brea, CA, USA) to generate fragment sizes between 250 and 350 bp. Adaptor-ligated DNA was PCR amplified followed by AMPure XP bead clean up. Libraries were quantified with a Qubit dsDNA HS Kit (Invitrogen) and the size distribution was confirmed with a High Sensitivity DNA Kit for Bioanalyzer (Agilent Technologies). Libraries were sequenced on Illumina HiSeq2500 in single read mode with the read length of 50 nt following manufacturer's instructions. Base

calls were performed with RTA 1.13.48.0 followed by conversion to FASTQ with bcl2fastq 1.8.4. Approximately 20 million sequences were obtained for each sample. rRNA sequences were removed by using BLAST against the RDP 16s database. The remaining mRNA sequences were processed using Tophat 2 with --no-novel-juncs option and Cuffdiff (Trapnell et al. 2012), using a methane seep metagenome database with the addition of full-lgenth Group II Fsr sequences generated in this study (Marlow, Skennerton, Li, Chourey, Hettich, Pan, and Orphan 2016a).

1.3.6 Quantitative PCR analysis of *M. burtonii* Fsr/alSir expression

Methanococcoides burtonii was obtained from DSMZ culture collection (DSMZ6242). Cultures were initiated in the DSM280 media, and then transferred to a minimal media without sulfate containing the following ingredients (per 1L media): 0.34 g of KCl, 8.2 g of $MgCl_2 \cdot 6H_2O$, 0.25 g of NH_4Cl, .014 g of $CaCl_2 \cdot 2H_2O$, 0.14 g of K_2HPO_4, 18 g of NaCl, 5 g of $NaHCO_3$, 0.5 g of $Na_2S \cdot 9H_2O$ and trace elements and DSM141 vitamin. Growth was monitored using photospectrometer based on absorbance at wavelength 600 nm.

DNA was extracted from *M.burtonii* cultures using Qiagen kit, and full length Fsr was amplified using primer sets designed based on its genome (Supplementary Table S3a) (Allen et al. 2009). To study the response of *M.burtonii* to different sulfur amendments, 60 ml of exponentially growing cells were diluted into 90 ml of the minimal media without sulfide, and then 5 ml of the mixture was distributed into Balch tubes in an anaerobic chamber. Additional sulfide was added to a final concentration of 1 mM to keep the cultures in reducing condition. The cultures were then flushed and pressurized with N_2:CO_2 (80:20) to 0.5 bar first, then pressurized to 0.7 bar with argon gas. When the cultures reached mid-exponential growth phase, different sulfur amendments from anaerobic stock solutions were spiked into the cultures in replicates of 4 to the following final concentrations: 0.5mM of sulfite, 1.0 mM of polythionate, 1.0mM of polysulfide, 10 mM of thiosulfate, and 5 mM of

NaHS. Polythionate solutions were prepared following a previously described protocol (Steudel, Göbel, and Holdt 1989), and polysulfide solutions were prepared by autoclaving sulfide solutions in an excess of elemental sulfur powder. After 1 hr of amendments, 5 ml of RNAlater solution was added. Then cultures were mixed and centrifuged at 5000 x g for 10 minutes. The pellet was flash frozen in liquid nitrogen and stored at -80˚C until further processing.

RNA extraction was carried out using a Qiagen RNeasy Plus Mini Kit and purified using a Qiagen RNeasy Mini purification kit following the kit's instructions. The extracts were then reverse transcribed using the AB High Capacity cDNA RT kit with 5 µl of RNA extract added to the recommended reaction mixture and incubated at 25˚C for 10 min, 37˚C for 120 min, and 85˚C for 5 min before cooling down to 4˚C. DNA was removed from the extract using Mobio Dnase kit following manufacturer's instructions. Quantitative PCR was done using iTaq Universal SYBR Green reagent in Biorad CFX96 Touch Real Time PCR Detection System (Biorad, Hercules, CA, USA). The following qPCR reaction mixture was used for Fsr: 5 µl of iTaq supermix, 0.5 µl of each forward and reverse primers (Supplementary Table S3b), 1 µl of cDNA, 0.4 µl of 25mM $MgCl_2$, and 2.6 µl of PCR water; and for alSir: 5 µl of iTaq supermix, 0.4 µl of each forward and reverse primers (Supplementary Table S3b), 1 µl of cDNA, 0.4 µl of 25mM $MgCl_2$, and 2.8 µl of PCR water. The amplification products of qPCR primers were checked by sequencing to confirm the correct products. Controls with no reverse transcriptase added in the cDNA generation step showed no signal, indicating no DNA contamination. Given the changes in expression of 16s rRNA or "housekeeping" genes based on our previous study, the copies of the gene targets obtained via qPCR were instead normalized to the amount (µg) of RNA extracted (Tavormina et al. 2017).

1.3.7 Metaproteome analysis of sulfur pathways in methane seeps

Metaproteomes were generated from methane seep samples from three geographical locations: Hydrate Ridge (AD4635), Santa Monica (T796 0-12 cm at 4 cm depth intervals), and Eel River (T863 0-20 cm at 10 cm intervals). Details of these sites information have been published (Marlow, Skennerton, Li, Chourey, Hettich, Pan, and Orphan 2016a). All chemicals used for sample preparation and mass spectrometry analysis were obtained from Sigma Chemical Co. (St Louis, MO, USA), unless mentioned otherwise. High performance liquid chromatograpy (HPLC) grade water and other solvents were obtained from Burdick & Jackson (Muskegon, MI).

For protein extraction, 5 grams of thawed seep sediments was suspended in 10 ml of detergent lysis buffer and then subjected to cellular lysis as described previously (Chourey et al. 2010). The suspension was subsequently cooled down at room temperature and centrifuged for 5 min at 8000 g to allow the sediment to settle. An aliquot containing the clear supernatant was treated with 100% trichloroacetic acid (TCA) precipitation and kept at -20°C overnight. The supernatant was then centrifuged at 21,000 x g for 20 mins to obtain a protein pellet. This pellet was washed thrice with chilled acetone, air dried, and subsequently solubilized in a buffer containing 6 M guanidine (6 M guanidine in 10 mM dithiothreitol [DTT] in Tris-$CaCl_2$ buffer (50 mM Tris; 10 mM $CaCl_2$, pH 7.8) and incubated for three hours at 60°C. 25 µl of this aliquot was then used for protein estimation, which was carried out using RC/DC protein estimation kit (Bio-Rad Laboratories, Hercules, CA, USA). The remaining protein sample was diluted six-fold using Tris-$CaCl_2$ buffer and subjected to proteolytic digestion using sequencing-grade trypsin (Promega, Madison, WI, USA) based on the protein estimation results (40 µg/ 1-3 mg of total protein). This digestion was carried out overnight at 37°C with minor mixing and the resulting peptides were reduced by adding DTT (10 mM). These peptides were then desalted using a Seppak column and subjected to solvent exchange (Thompson et al. 2007).

Proteolytic peptide samples were analyzed via an online nano 2D LC–MS/MS system interfaced with LTQ-Velos Pro MS (ThermoFisher Scientific, San Jose, CA, USA).

A 100 μg aliquot of peptide mixture was pressure loaded onto a biphasic silica back-column which was packed with SCX (Luna, Phenomenex, Torrance, CA, USA) and C18 (Aqua, Phenomenex, Torrance, CA, USA), as described previously (Thompson et al. 2007; Brown et al. 2006). The back column was then washed offline with solvent A (95% HPLC grade water, 5% acetonitrile, 0.1% formic acid [FA] (EM Science, Darmstadt, Germany)) for 20 min, followed by a 25 min gradient to solvent B (70% acetonitrile, 30% HPLC grade water, 0.1% FA). This sample column was then connected to the C18 packed nanospray tip (New objective, Woburn, MA, USA) mounted on a nanospray source (Odense, Denmark) and analyzed by twelve step MudPIT (Multidimentional protein identification technology) over a course of 24 h, as described previously (Thompson et al. 2007; Brown et al. 2006; Sharma et al. 2012). For LTQ-Velos Pro measurements, each full scan (1 microscan) was followed by collision activated dissociation (CID) based fragmentation using 35% normalized collision energy of the 10 most abundant parent ions (2 micrscans) having a mass exclusion width of 0.2 m/z and a dynamic exclusion duration of 60 s.

MS/MS spectra were analyzed using the following software protocol: a decoy database of reversed protein sequences and common contaminants from keratin and trypsin was appended to the target database containing sulfur pathway genes from ANME genome bins (Figure 1). The fragmentation spectra was searched with Myrimatch v2.1 algorithm (Tabb, Fernando, and Chambers 2007) with the following configuration parameters: fully tryptic peptides with any number of miscleavages, an average precursor mass tolerance of 1.5 m/z, and a fragment mass tolerance of 0.5 m/z. Static cysteine and dynamic oxidation modifications were not included in the search parameters. Peptide identifications were filtered with IDPicker v3.1 6 to achieve peptide-level FDR of < 1%. At the protein level, a minimum of 1 total peptide and 1 unique peptide were required per protein call as described previously (Marlow, Skennerton, Li, Chourey, Hettich, Pan, and Orphan 2016b). Protein abundances for a subset of proteins were estimated using normalization of spectral counts, as described previously (Paoletti et al. 2006; Neilson et al. 2013). Briefly, to account for the fact that larger proteins tend to contribute more peptide/spectra, spectral counts were divided by

protein length to obtain a spectral abundance factor (SAF). These SAF values were then normalized against the sum of all SAF values in the run, allowing the comparison of protein levels across individual replicates. These values were then balanced and converted to normalized spectral counts (nSpC).

1.3.8 Stable isotope probing of thiosulfate as AOM intermediate

Microcosms were setup using methane-seep sediment sample 7142 and artificial seawater containing 20 mM $^{34}SO_4^{2-}$ as the sole S-source. The recipe for artificial seawater used and microcosm setup were the same as our previous experiment (Scheller et al. 2016), and $^{34}SO_4^{2-}$ was synthesized in-house from $^{34}S^0$ (99.8% ^{34}S, Trace Sciences International Inc., Wilmington, DE, USA) using the previously described protocol (Dawson et al. 2016). One incubation was amended with 10 mM thiosulfate of natural isotopic abundance. Sulfur samples were taken after 25 days of incubation using the bromobimane preservation method and measured via LC-MS for quantification and isotopic values (Smith et al. 2017).

1.3.9 Heterologous expression of Group II Fsr from ANME and *M.burtonii* in *M.maripaludis*

Two full-length clones of ANME Fsr (ANME Fsr-5207-6D and ANME Fsr-5059-7A) and one *M.burtonii* Fsr were picked for heterologous expression in the host *Methanococcus maripaludis* (Supplementary Figure S6). We designed internal primers and validated that no insertions or deletions were in the products (Supplementary Table S3a). Three E. coli transformants were grown up overnight in 100ml of LB media with 6 μg/ml of ampicilin at 37˚C with shaking at 200 rpm. Plasmids were isolated using Qiagen Plasmid Maxi kit (cat 12162) as kit protocol, and were then transformed into *M. maripaludis* by the use of PEG mediated DNA uptake method (Tumbula, Makula, and Whitman 1994). The transformants were plated on McCas solid media containing neomycin.

M. maripaludis strain S2 was grown in the McN minimum medium or McCas medium (McN with casamino acid, 0.2% w/v) with H_2 and CO_2 as methanogenic substrates as described previously (Whitman et al. 1987). Briefly, for McN medium, a solution with the following composition was made anaerobic by three cycles of alternate vacuum and pressure of a mixture of H_2 and CO_2 (80:20 vol/vol, 3 bar) (ingredient, final concentration): K_2HPO_4, 0.72 mM; KCl, 4.02 mM; $NaHCO_3$, 53.33 mM; NaCl, 336.87 mM; $MgCl_2 \cdot 6H_2O$, 49.19 mM; NH_4Cl, 18.7 mM; $CaCl_2 \cdot 2H_2O$, 4 mM; resazurin, 0.0001%, and 10 ml of a 100-fold-concentrated mineral solution per ml (Johnson and Mukhopadhyay 2008). The anaerobic medium was sterilized and then a sulfur source, $Na_2S \cdot 9H_2O$ or Na_2SO_3 or $Na_2S_2O_3$, was added to a final concentration of 2 mM. When Na_2SO_3 or $Na_2S_2O_3$ was the sulfur source, titanium citrate at a final concentration of 137.5 μM was used as the reductant for the media (A. Neumann, Wohlfarth, and Diekert 1996). For growth in liquid culture, 25 mL of McN or McCas in a 150 mL serum bottle sealed with a butyl rubber stopper of 20 mm diameter and an aluminum crimp was used. Inoculated cultures were incubated at 37°C with shaking at 200 rpm in a C24 Incubator Shaker (New Brunswick Scientific, Edison, NJ, USA). For growth on solid media, agar (1.5% w/v) was added as a solidifying agent to the medium and the plates were incubated inside an anaerobic jar filled with a mixture of H_2 and CO_2 (80:20 vol/vol) containing 7.5 ppm of H_2S at a pressure of 0.2 MPa; the jar was placed inside an anaerobic chamber maintained at 37°C. To select *M. maripaludis* strains harboring pMev 2.1.1, a *M. maripaludis-Escherichia coli* shuttle vector (Lin and Whitman 2004), or its derivatives, neomycine was added to the medium at a final concentration of 1 mg/mL.

To determine whether the expression of a Group II Fsr homolog enabled the growth of *M. maripaludis* in McN media with Na_2SO_3 or $Na_2S_2O_3$ as a sulfur source, 100 μl of inoculum from a culture grown with sulfide was transferred into McN media containing these compounds at a final concentration of 2 mM. When the growth observed, two additional sequential transfers to McN media containing the same sulfur source were

performed to confirm the phenotype. *M. maripaludis* strain S2 harboring pMev2.1.1 was used as a control.

To further confirm the findings from the growth studies, *M. maripaludis* cell lysates were assayed for their sulfite reductase or thiosulfate reductase activities. For this purpose, cell extracts from *M. maripaludis* cells expressing Group II Fsr homologs were obtained by osmotic lysis and an aliquot of the resulting cell extracts (30 μg protein) was added to the following mixture (total volume of 100 μL): potassium phosphate buffer, Na_2SO_3 or $Na_2S_2O_3$, and methyl viologen at final concentrations of 100, 1, and 0.1 mM. The reaction mixtures were incubated at room temperature for 1 hr under H_2 at a pressure of 1.35 bar. Methyl viologen was used as a redox mediator between Fsr and the H_2/H_2-ase electron donor system of the cell lysate. The amount of sulfide generated in the reactions was measured by employing methylene blue procedure as described previously (Johnson and Mukhopadhyay 2005; Trüper and Schlegel 1964).

1.4 RESULTS

1.4.1 Assimilatory and dissimilatory sulfate reduction pathways in ANME inferred from methane seep metagenomes

Analysis of ANME genomes revealed multiple candidate genes, which are associated with sulfate assimilation pathway (Figure 1). Potential sulfate transporters were identified, but given the substrate promiscuity of these transporter systems for different oxyanions (Aguilar-Barajas et al. 2011), the specificity and enzyme activity for sulfate is uncertain. The heterodimeric sulfate adenylyltransferase, encoded by the *cysDN* genes, was previously reported in ANME-1b (Meyerdierks et al. 2010). Due to the sequence and structural similarity between cysN and elongation factor 1-alpha (EF1a), *cysN* may be misannotated as EF1a (Mougous et al. 2006). There are two homologs of *cysN* in all of the ANME genomes, with the exception of ANME-2a, one of which is closely related phylogenetically to other archaeal EF1a, and thus likely an elongation factor for translation (Supplementary Figure S1a). The second homolog shows an early divergence in the split between EF1a and *cysN*, but they are all positioned in an operon with *cysD* suggesting that they are bona fide ATP sulfurylase (Supplementary Figure S1B). The homo-oligomeric ATP sulfurylase, encoded by *sat*, was only identified in *Ca.* Methanoperedens.

Activated sulfate in the form of APS can be reduced directly using either assimilatory or dissimilatory APS reductase, or indirectly via PAPS using APS kinase then PAPS reductase. Dissimilatory APS reductase (*aprAB*) was not identified in any ANME genome bins, while APS kinase was only found in ANME-1b and *Ca.* Methanoperedens (Figure 1 and Supplementary Table S2). Assimilatory APS reductase and PAPS reductase are homologous and therefore are often misannotated. Phylogenetic analysis of potential assimilatory APS or PAPS reductase genes from ANME genome bins showed a divergent group of APS or PAPS reductases that were exclusively associated with archaea and distinct from those in bacteria or eukaryotes (Supplementary Figure S2). While *Ca.*

Methanoperedens contained an APS reductase similar to those commonly found in bacteria, it also had the putative APS/PAPS reductase that were also found in ANME-2a and ANME-2b genome bins. These proteins vary in length from 239 to 896 amino acids with additional proteins domains (Supplementary Figure S2). Previous studies characterized the putative APS reductase and PAPS reductase, which are 411 and 480 amino acids long respectively, with an iron-sulfur cluster binding domain in *M. jannaschii*, and confirmed their biochemical functions (Lee et al. 2011; Cho 2013). In each ANME genome bin, two homologs were found, with extra iron-sulfur cluster binding domains (conserved $CX_2CX_2CX_3C$ motif) at N- or C-terminus of the proteins in addition to the central iron-sulfur cluster binding domain (total lengths from 456 to 637 amino acids) compared to previously characterized ones in *M. jannaschii* (Supplementary Figure S2).

The final step in sulfate reduction is to convert sulfite to sulfide. There are at least seven groups of sulfite reductases for assimilatory or dissimilatory purposes (Dhillon et al. 2005; Loy, Duller, and Wagner 2008; Susanti and Mukhopadhyay 2012). All but two of these groups were identified in ANME genomes (Figure 1); the only two groups not identified in any ANME were the canonical dissimilatory sulfite reductase (*dsrAB*) and *asrC* (Figure 2). While Group I Dsr-LP and/or aSir were found only in the *Ca.* Methanoperedens genomes, alSir was found in all ANME (Supplementary Figure S4). The ANME genome bins also contained the F_{420}-dependent sulfite reductase (Fsr) (Johnson and Mukhopadhyay 2005). In addition, Fsr and alSir were found on a fosmid of ANME-2c (Hallam et al. 2004) indicating that ANME have potentially two mechanisms for sulfite reduction, possibly by coupling oxidation of $F_{420}H_2$ generated in the course of methane reduction to the formation of sulfide.

Phylogenetic analysis of the functional units of different sulfite reductases showed that Fsr from *M. janaschii* cluster with other Fsr found in non-cytochrome containing methanogens, which we call Group I Fsr (Figure 2). Several species in *Methanosarcinales* including ANME-1b, ANME-2a, ANME-2b and ANME-2c contained Fsr, and these

genes form a well-supported sub-clade, which we call Group II Fsr (Figure 2). This may indicate a diversification of Fsr and possibly a different physiological function.

There were also other proteins that could be involved in sulfur assimilation. Rhodanese-like proteins (or thiosulfate sulfurtransferase, *tst*) are found in ANME-1b and *Ca.* Methanoperedens genome bins. Based on the presence of rhodanese or other protein domains, they could be classified as single-domain (Ga0123266_104918, KCZ72772.1, KPQ43738.1), tandem-domain (CBH36927.1, CBH36931.1, CBH36927.1, CBH37402.1, KCZ72976.1), or multi-domain proteins (Ga0123266_10257, Ga0123266_11066, KCZ71040.1, KPQ45278.1) (Cipollone, Ascenzi, and Visca 2007). This protein superfamily transfers a thiol group from thiosulfate or possibly polysulfide with potential physiological roles ranging from cyanide detoxification, sulfur transport, cysteine and iron-sulfur protein cofactors synthesis, as well as sulfur energy metabolism (Westley 1973; Cipollone, Ascenzi, and Visca 2007; Aussignargues et al. 2012). Thiosulfate may serve as electron acceptor for some groups of ANME-1 (Jagersma et al. 2012), but the exact role of *tst* in ANME remains to be elucidated given that more recent study of another thermophilic ANME-1 enrichment culture could not grow on thiosulfate (Wegener et al. 2016).

Taken together, ANME groups appear to have different pathways to assimilate sulfate or potentially sulfur species of intermediate oxidation states such as thiosulfate. ANME-2b and *Ca.* Methanoperedens have heterodimeric ATP sulfurylases (*cysDN*), putative APS reductase, and a sulfite reductase alSir to completely reduce sulfate to sulfide. In addition, they possess a putative PAPS reductase, but its function is unknown given that APS kinase is not found in the genome bins. Additionally, Group II Fsr was found in all ANME except *Ca.* Methanoperedens, but this group had additional genes for sulfur metabolism. *Ca.* M. nitroreducens has an additional assimilatory sulfate reduction pathway including the homo-oligomeric ATP sulfurylase (*sat*), bacterial APS reductases, and aSir. This second pathway is not identified in *Ca.* Methanoperedens sp. BLZ1, which has Group

I Dsr-LP instead. This indicates that there may be some species-level differences in *Ca.* Methanoperedens or other ANME groups and more genomic information is needed to confirm these findings. ANME-1b, which is distantly related to ANME-2a/2b/2c and *Ca.* Methanoperedens, may also have a different assimilatory sulfate reduction pathway that includes *cysDN*, APS kinase, APS/PAPS reductasae and alSir. However, the APS/PAPS reductase in ANME-1b is too distantly related to those in other archaea or bacteria to be assigned a putative function (Supplementary Figure S2). ANME-1b also has Group II Fsr or Tst and may assimilate sulfur species such as thiosulfate. These observed differences in sulfur pathways of different ANME groups may be explained by their phylogenetic and ecological differences.

1.4.2 Genes involved in sulfur assimilation in methanogenic archaea

Of 88 methanogens, only three had *cysDN*, and the closely related genes phylogenetically were found in bacteria, suggesting a possible horizontal gene transfer (Supplementary Figure S1 and Supplementary Table S2). Two methanogens, namely *Methanothermococcus thermolithotrophicus* and *Methanobrevibacter ruminantium*, was reported to use sulfate as the sole sulfur source (Rajagopal and Daniels 1986; Daniels, Belay, and Rajagopal 1986), and neither contained *cysDN* in their genomes. Only *sat*, similar to that in *Ca.* Methanoperedens, was found in *M. thermolithotrophicus* but not *M. ruminantium*. However, it is unclear what the sulfur source is for *M. ruminantium*, given that its growth is dependent on coenzyme M and yeast extract was present in its medium (Taylor et al. 1974; Rajagopal and Daniels 1986).

7 out of 88 representative methanogen genomes contained an assimilatory APS reductase similar to that found in bacteria (Supplementary Figure S2), but not all had ATP sulfurylase to activate sulfate (Supplementary Table S2). In addition, putative APS/PAPS reductases were prevalent in many methanogens (Supplementary Table S2). The previously characterized APS reductase from *M. jannschii* represented the simplest version without any

additional functional domains, while the PAPS reductase from *M. jannaschii* had an extra iron-sulfur binding domain at the N-terminus (Supplementary Figure S2). Homologs of these in other methanogens also occurred with two iron-sulfur binding domains at the C-terminus that may be involved in electron transferring processes. Additionally, a few were found to have a cysteine desulfurylase domain at the C-terminus (Supplementary Figure S2). Most genomes also contained two copies of the putative APS/PAPS reductases, suggesting that these genes could be specialized for either APS or PAPS reduction. Furthermore, *Methanothermococcus thermolithotrophicus* that was reported to reduce sulfate also contain homologs of dissimilatory APS reductase alpha and beta subunits (*aprAB*). Despite the prevalence of APS/PAPS reductases in methanogenic and methanotrophic archaeal genomes, the origin of APS or PAPS is unclear, given that many of the genomes do not have homologs to ATP sulfurylase or APS kinase (Supplementary Table S2).

None of the methanogen genomes contained dissimilatory sulfite reductase (*dsrAB*) homologs, including *Methanothermococcus thermolithotrophicus* that has holomogs of *sat* and *aprAB* (Supplementary Table S2). It is likely then that *Methanothermococcus thermolithotrophicus* cannot perform dissimilatory sulfate reduction. aSir that was found in *Ca.* M. nitroreducens, was only found in two other methanogens, while Dsr-like proteins (alSir/Group I Dsr-LP and Group III Dsr-LP) were found in a number of methanogens. The physiological functions of these Dsr-like proteins are unknown and requires further study to see if they interact with ATP sulfurylase and putative APS/PAPS reductases. Overall, the comparative genomic study of methanogenic and methanotrophic archaea show a limited ability to reduce sulfate directly, but they may be able to assimilate sulfur species of intermediate oxidation states using poorly characterized APS/PAPS reductase and sulfite reductases that need to be further studied.

1.4.3 Metaproteome expression of ANME sulfur pathways, and predicted structure and diversity of the Group II coenzyme F_{420}-dependent sulfite reductase (Group II Fsr) in the methane-seep sediments

Metaproteomes of methane-seep sediments showed expression of sulfur pathways encoded in the ANME genome bins (Supplementary Table 4). For both ANME-1b and *Ca.* Methanoperedens, the results indicate that these two clades assimilate sulfate in the environment: ANME-1b expressed CysN subunit of the heterodimeric ATP sulfurylase, APS kinase and APS/PAPS reductase like protein, while *Ca.* Methanoperedens expressed CysN, different APS/PAPS reductases and two different sulfite reductases including aSir and Group I Dsr-LP. For ANME-2a/2b/2c, only two sulfite reductases, namely alSir and Group II Fsr, were expressed in addition to a potential sulfate transporter. These results show a more restricted sulfur utilization in these later ANME groups, but the relatively high expression alSir and Fsr in comparison to other sulfur genes by multiple ANME groups highlights the importance of these sulfite reductases in AOM.

Sulfite reductases, despite their different physiological roles, have conserved amino acid residues to bind siroheme and sulfite (Dhillon et al. 2005; Schiffer et al. 2008; Susanti and Mukhopadhyay 2012). We then focused our study on Fsr for its potential interaction with $F_{420}H_2$, a key cofactor produced by methane-metabolizing archaea. By aligning ANME Fsr sequences to Fsr in methanogens and other sulfite reductases, conservation of siroheme-[FeS] binding cysteines known from Dsr sequences was found (Supplementary Figure S5). However, the key residues that bind sulfite, conserved amongst Group I Fsr and Dsr, are not conserved in Group II Fsr (Supplementary Figure S5). In the sulfite reducing enzymes Arg98, Arg170, Lys211, Lys213 in *Archaeoglobus fulgidus* DsrA are catalytically important in positioning sulfite at the axial position of the siroheme cofactor (Schiffer et al. 2008). In Group II Fsr, Arg98 and Arg170 in DsrA were replaced with Lys and Gly, respectively, perhaps indicating a potential alteration in substrate binding (Supplementary Figure S5). This was also evident in protein homology modeling that shows conservation in overall structure and 3D positioning of siroheme-[FeS] binding cysteines (Supplementary Figure S3a), but a presumably larger active site pocket due to the replacement of Arg with Lys or Gly (Supplementary Figure S3b). These results suggest that the ANME Fsr has conserved cofactors but may use a substrate other than sulfite.

To judge the distribution of Group II Fsr in environmental samples, the presence of Group II Fsr was investigated in samples collected from four different methane seeps. Both specific and degenerate primers designed based on ANME *fsr* amplified this gene from four methane seep sediment samples surveyed. The amplicons cluster with known *fsr* from ANME2a/b/c (Supplementary Figure S6). ANME-2a had two copies of Group II Fsr in its genome, but the primer designed with specificity for one of the variants (ANME2a_03223) failed to amplify in our samples. Together, these results show that ANME *fsr* can be found in diverse methane seep ecosystems.

1.4.4 Functional characterization of Group II Fsr by heterologous expression in *M. maripalutis*

Previous studies of Group I Fsr suggested that it is used to detoxify sulfite and enable methanogens to use sulfite as its sole sulfur source (Johnson and Mukhopadhyay 2005; Johnson and Mukhopadhyay 2008). We attempted to characterize Group II Fsr of ANME recovered from methane seep sediment, as well as the closest Fsr-containing relative of ANME, *M. burtonii*, using heterologous expression to better understand the function of Group II Fsr. Addition of a sulfite concentration (1.0 mM) is inhibitory to the cells, as evident in the reduced methane oxidation rate for ANME or growth cessation for *M. burtonii* (Supplementary Figure S9). This result is in contrast with previous Group I Fsr studies in which *M. jannaschii* displayed growth in >2 mM of sulfite without any effect on growth rate. Growth inhibition is also in contrast to experiments where *M. jannaschii* Fsr was heterologously expressed in a sulfite-sensitive non-Fsr containing methanogen, *Methanococcus maripaludis*, enabling cultures to tolerate and grow in similar concentrations of sulfite. This suggests that Group II Fsr is not used for detoxification and/or assimilation of sulfite.

Subsequently, we amended various sulfur compounds of intermediate oxidation states such as sulfite, sulfur, thiosulfate, polysulfide and polythionate to incubations and studied the

RNA response of ANME and *M. burtonii*. Metatranscriptomic results showed changes in the expression of Group II Fsr and alSir when sulfite, thiosulfate, or sulfur powder was added to methane seep microcosms (Supplementary Figure S7a). Increased expression of alSir was observed in the presence of sulfite and thiosulfate, compared with control microcosms growing only with methane and sulfate without amendments. The expression of ANME Fsr was upregulated only when in the presence of thiosulfate, but not sulfite. A similar response was also observed in exponentially growing *M. burtonii* cultures upon the addition of various sulfur compounds. By measuring the Group II Fsr and alSir expression with qPCR, we observed a similar response to amendments in *M. burtonii* cultures as ANME microcosms (Supplementary Figure S7b).

Given the RNA expression response of Group II Fsr and its altered enzyme active site, we hypothesized that this enzyme might use thiosulfate as its substrate instead of sulfite. In the case of ANME, $F_{420}H_2$ regenerated from methane oxidation could be coupled to thiosulfate reduction using Group II Fsr. The energy yield for AOM with thiosulfate ($\Delta G^{0'}$=-38.4 kJ/mol CH_4) is more favorable than AOM with sulfate ($\Delta G^{0'}$=-16.5 kJ/mol CH_4). To check the possibility of ANME using thiosulfate as electron acceptor, we incubated ANME-containing sediment samples in the presence of ^{34}S labelled sulfate with or without thiosulfate. If ANME could respire thiosulfate, then sulfate reduction might stop when a more favorable electron acceptor was added. In the sediment incubation with 10 mM of thiosulfate with natural isotope abundance (95.0% ^{32}S) added, a small amount of ^{32}S-sulfide is produced, indicating that some thiosulfate was consumed and reduced to sulfide (Supplementary Table S1). However, the majority of sulfide is still ^{34}S-labelled, indicating that sulfate reduction continued even in the presence of high amounts of thiosulfate (Supplementary Table S1). This result suggests that thiosulfate cannot be used as an alternative electron acceptor for methane oxidation, and thus the function of Group II Fsr in ANME is likely not used for dissimilatory thiosulfate reduction.

To investigate if Group II Fsr could use thiosulfate as substrate, we heterologously expressed Group II Fsr from ANME and *M. burtonii* in *M. maripaludis* similar to the previous study (Johnson and Mukhopadhyay 2008). Based on the known diversity of Group II Fsr, primers are designed to amplify two different full-length ANME-Fsr and the full-length Fsr from *M. burtonii* (Supplementary Figure S6). All three Group II Fsr from either ANME or *M. burtonii* were successfully amplified, cloned, and expressed in *M. maripaludis*, as confirmed by re-sequencing and SDS-PAGE protein profiles of the *M. maripaludis* cell extracts. A protein band of a molecular mass (~70 kDa) characteristic of Fsr, as described previously, could be seen from extracts of *M. maripaludis* harbouring pMev plasmids with Mbur- and ANME-Fsr. The control cell extract from *M. maripaludis* harboring only the plasmid did not contain this band. To probe thiosulfate reductase activity by Group II Fsr, *in-vitro* thiosulfate reductase assays were performed with the *M. maripaludis* cell extracts expressing the Fsr homologs. Only the Mbur-Fsr containing *M. maripaludis* cell extract reduced thiosulfate (Figure 3). Negligible reduction of sulfite was observed in all cell extracts. Furthermore, Mbur-Fsr containing *M. maripaludis* grew with thiosulfate but not sulfite as its sole sulfur source for growth. This *M. maripaludis* strain, however, exhibited a long lag phase and reached stationary phase at a much lower cell density when grown on thiosulfate compared to when sulfide was supplied as sulfur source, and a similar observation is found in *M. burtonii* cultures (data not shown). Expression of two ANME-Fsr homologs did not allow *M. maripaludis* to use either thiosulfate or sulfite as its sole sulfur source. Taken together, these results show that Mbur-Fsr enables reduction and assimilation of thiosulfate but not sulfite.

1.5 DISCUSSIONS

All known life has an obligate requirement for sulfur. In methane-metabolizing archaea, sulfur occurs in the cell in different oxidation states including +4 in coenzyme M and -2 that is found in most organosulfur molecules. These anaerobes in general use sulfide as their sulfur source (Y. Liu, Beer, and Whitman 2012). Our comparative genomic analysis reveals an assimilatory sulfate reduction pathway in ANME and a few methanogens that could have been overlooked due to misannotation in the genomes and limited biochemical data (Figure 1). Heterodimeric sulfate-activating *cysDN* is presently restricted within the Archaea to ANME, Bathyarchaeota genome bins, and three methanogens (Supplementary Table S2). *cysN* and *cysD* phylogenetic trees have similar species topologies, suggesting that the two subunits co-evolved and are both required for their functions (Supplementary Figure S1). Given that *cysN* and elongation factor 1 alpha are homologous, annotation for "sulfate adenylyltransferase subunit 1" or similar that denotes *cysN* needs to be taken with caution, unless *cysD* could also be identified in the same operon. On the other hand, *Ca.* Methanoperedens has homo-oligomeric ATP sulfurylase (*sat*) in its genome. This represents a different way to activate sulfate and was found in nine other methanogens (Supplementary Table S2).

Some methanogens have been reported to grow with sulfur compounds of intermediate oxidation states such as elemental sulfur, thiosulfate, and sulfite as their sole sulfur sources (Daniels, Belay, and Rajagopal 1986; Rajagopal and Daniels 1986). A range of methanogens have also been found to perform high rates of sulfur reduction (Stetter and Gaag 1983), but the genetic mechanism remains elusive and this was also found to lead to diminished growth in some cases. Two homologs of APS/PAPS reductases are found in each ANME genome bin, and they cluster into two well-supported phylogenetic groups (Supplementary Figure S2). Given that one is more similar to APS reductase of *M. janaschii* while the other is more similar to PAPS reductase of *M. janaschii*, we hypothesize that ANME groups process both APS and PAPS reductases in their genome, and the extra iron-

sulfur cluster at N- or C-terminus of the proteins could be used to transfer electrons that reduce APS and PAPS to sulfite. These APS and PAPS reductases, as well as different sulfite reductases, have wide distributions in methanogenic archaea and may be used in sulfur assimilation (Supplementary Table S2). Moreover, rhodanese-like proteins are found in ANME-1b and *Ca.* Methanoperedens. Little is known about the physiological roles of this protein superfamily, but they may be important during growth on different sulfur compounds (Ramirez et al. 2002; Cipollone, Ascenzi, and Visca 2007).

By comparing draft genomes of four ANME groups ANME-1/2a/2b and *Ca.* Methanoperedens, we identify significant differences in their sulfur pathways. These differences underscore the phylogenetic as well as physiological differences between different ANME groups. Two potential pathways of sulfur assimilation from sulfate are found in *Ca.* M. nitroreducens: a complete assimilatory sulfate reduction pathway, which includes *sat*, assimilatory APS reductase, and aSir, and another pathway involving *cysDN*, putative assimilatory APS reductase and alSir (Figure 1). This set of sulfur genes may help *Ca.* Methanoperedens thrive as freshwater nitrate reducers, and they could be enriched with sulfate as the sole sulfur source (Haroon et al. 2013; Arshad et al. 2015). Previous transcriptome result from *Ca.* M. nitroreducens shows expression of both pathways, with the *sat*-assimilatory APS reductase-aSir pathway having higher expression levels compared to the cysDN-putative APS reductase-alSir pathway (Haroon et al. 2013). Our metaproteome result shows partial expression of both pathways, which may due to under-sampling of complex environmental samples.

Perhaps more puzzling is the finding of an apparently complete sulfate reduction pathway (*cysDN*-putative APS reductase-alSir) in ANME1b and ANME-2b similar to *Ca.* Methanoperedens. Additional experiments are needed to show that these genes can function together to reduce sulfate to sulfide. Based on previous studies of *cysDN* and homologs of putative assimilatory APS reductase, these genes in ANME are likely used for assimilatory function. Dissimilatory functions, including sulfate reduction to zero-valent sulfur (Milucka

et al. 2012), is unlikely based on our genomic characterization and also their metaproteome expression. Moreover, this is supported by recent experimental studies of ANME-1b and ANME-2a/2b/2c enrichments (Wegener et al. 2015; Wegener et al. 2016).

Group II Fsr is identified in different marine methane seeps, in particular in the genome of ANME1b, ANME-2a and ANME-2b, and is expressed in the metaproteome. We identify a similar RNA expression pattern and enzyme active site in ANME and *M. burtonii*, and show thiosulfate reductase activity with *M. burtonii* Fsr. Our results suggest that thiosulfate maybe the substrate for Group II Fsr as opposed to sulfite for previously studied Group I Fsr from *M. jannaschii* (Johnson and Mukhopadhyay 2005; Johnson and Mukhopadhyay 2008), given that: 1) elevated expressions of ANME and *M. burtonii* Fsr were only observed with thiosulfate but not sulfite or other sulfur sources tested, 2) cultures of *M. burtonii* and *M. burtonii* Fsr-containing *M. maripaludis* only grew with thiosulfate but not sulfite as the sole sulfur source, and 3) the cell lysate of *M. burtonii* Fsr-containing *M. maripaludis* reduced thiosulfate but showed negligible reduction of sulfite. The thiosulfate reductase activity of Group II Fsr likely serves an assimilatory instead of dissimilatory role. It remains possible that Group II Fsr reacts with other sulfur molecules such as trithionate, which have been shown to react with purified Dsr proteins (Parey et al. 2010). Our attempts to express ANME Fsr in *M. maripaludis* did not allow transformed cells grow with thiosulfate or sulfite as the sole sulfur source, and we did not find thiosulfate reductase activity of ANME-Fsr containing *M. maripaludis* cell lysate. Even though the proteins were expressed, it is difficult to know whether they have the correct folding and cofactor compliments without detailed biochemical analysis. In addition, ANME-2 are psychrophiles with a lower optimal growth temperature range (4-15°C) compared to *M. burtonii* (23-24°C) and *M. maripaludis* (38°C) (Nauhaus et al. 2005; Franzmann et al. 1992; Jones, Paynter, and Gupta 1983). This could lead to misfolding of ANME proteins at higher temperatures due to their lower thermal stabilities (D'Amico et al. 2002). Given that ANME Fsr is most closely related to *M. burtonii* Fsr, it is possible that ANME Fsr serves the same assimilatory thiosulfate reductase function.

This study explores potential genes used by methane-metabolizing archaea to expand their sulfur substrate range beyond sulfide, potentially assimilating sulfate, thiosulfate, or other sulfur species of intermediate oxidation states. In anoxic sulfidic environments, such as the shallow marine sediments where ANME and methanogens thrive, there could be perturbation of the sediments causing mixing with the overlying waters that might lead to periodic oxygenation, abiotic sulfide oxidation, or influx of more oxidized sulfur species from the sediment surface, providing an addition source of sulfur. There are also anoxic environments in which methanogenic or methanotrophic archaea exist that are low in sulfide such as freshwater sediments, rumen, coal beds, and terrestrial environments (Y. Liu and Whitman 2008; Knittel and Boetius 2009; Strapoc et al. 2011). Under these conditions, the ability to scavenge additional sulfur species for anabolism could be beneficial. In the case of AOM with sulfate, finding that ANME-1b, ANME-2a, and ANME-2b can potentially use sulfate or thiosulfate is particularly intriguing given that their syntrophic lifestyle with sulfate-reducing bacterial partners. However, sulfate is not necessarily the only electron acceptor for ANME-1b and ANME-2a/2b/2c communities. ANME could be found together with organisms other than deltaproteobacterial sulfate reducers (Hatzenpichler et al. 2016). Also, ANME-2a and ANME-2c remained active under laboratory conditions without sulfate using electron acceptors including AQDS, humic acids and $Fe^{(III)}$ (Scheller et al. 2016). In these cases, an expanded sulfur utilizing ability may help ANME, or methane-metabolizing archaea in general, to broaden their environmental niche and thrive in environments regardless of the oxidation state of sulfur.

1.6 TABLES AND FIGURES

Figure 1. Sulfur assimilatory and dissimilatory pathways in ANMEs. Squares are color-filled based on the presence of particular gene in the corresponding ANME (meta)genome: ANME-1b (Meyerdierks et al. 2010) and this study, ANME-2a (Wang et al. 2014), ANME-2b (this study), and *Ca.* Methanoperedens nitroreducens (Haroon et al. 2013). Solid lines indicate the presence of a pathway in ANME-2 performing AOM with sulfate.

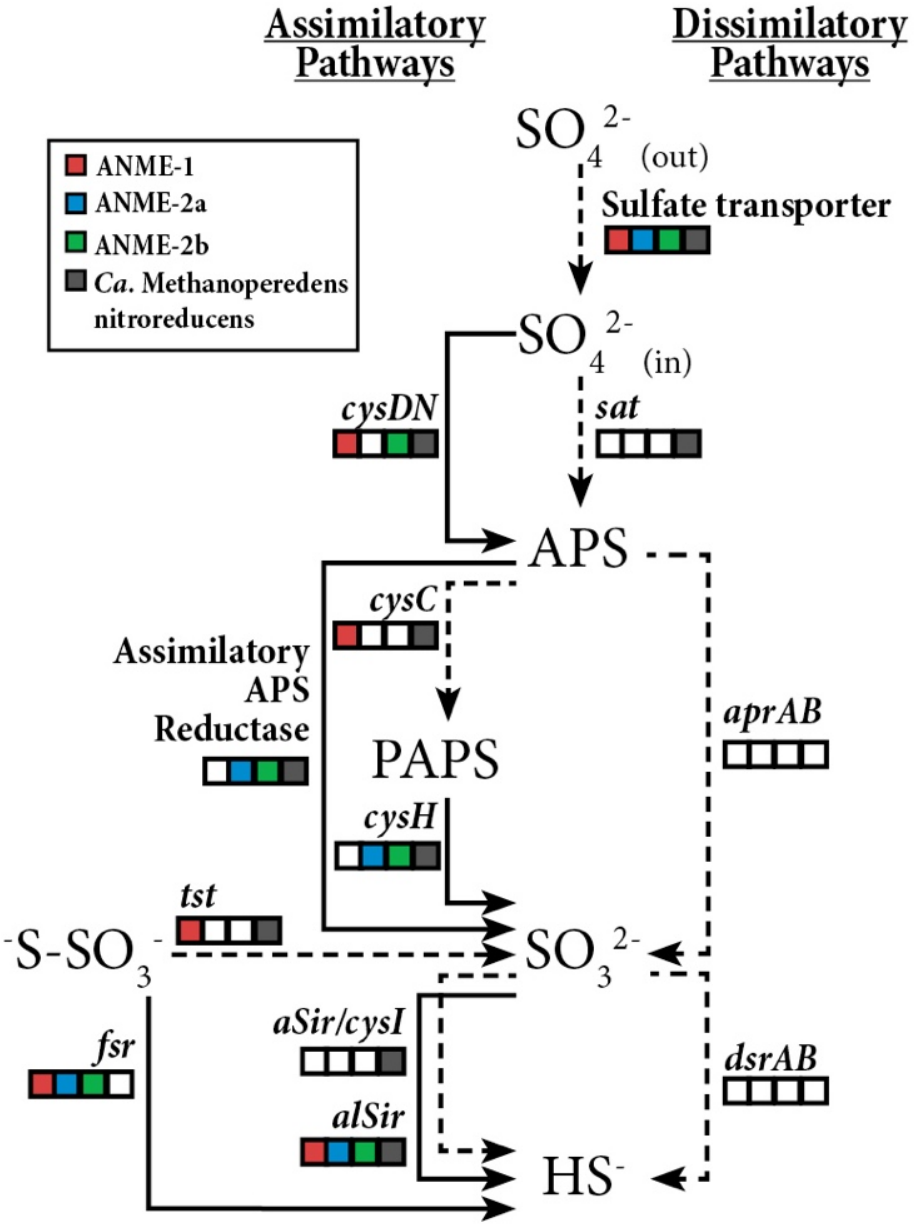

Figure 2. Bayesian phylogeny of 224 amino acid residues of sulfite reductases showing Fsr and alSir. Black dots on the branches represent Bayesian posterior probability values greater than 90%. Scale bar indicates the number of amino acid substitutions per site.

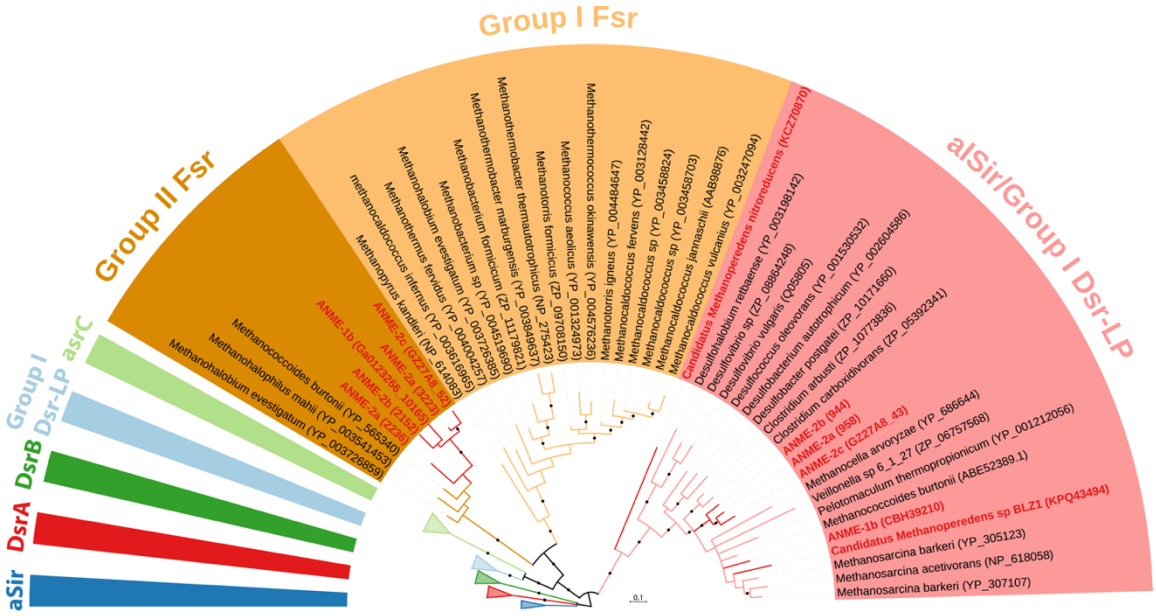

Figure 3. *In-vitro* thiosulfate reductase assay using cell extracts of the indicated M. maripaludis strains expressing Group II Fsr homologs from M. burtonii (Mm S2 pMeV-Mbur-Fsr) and ANME.

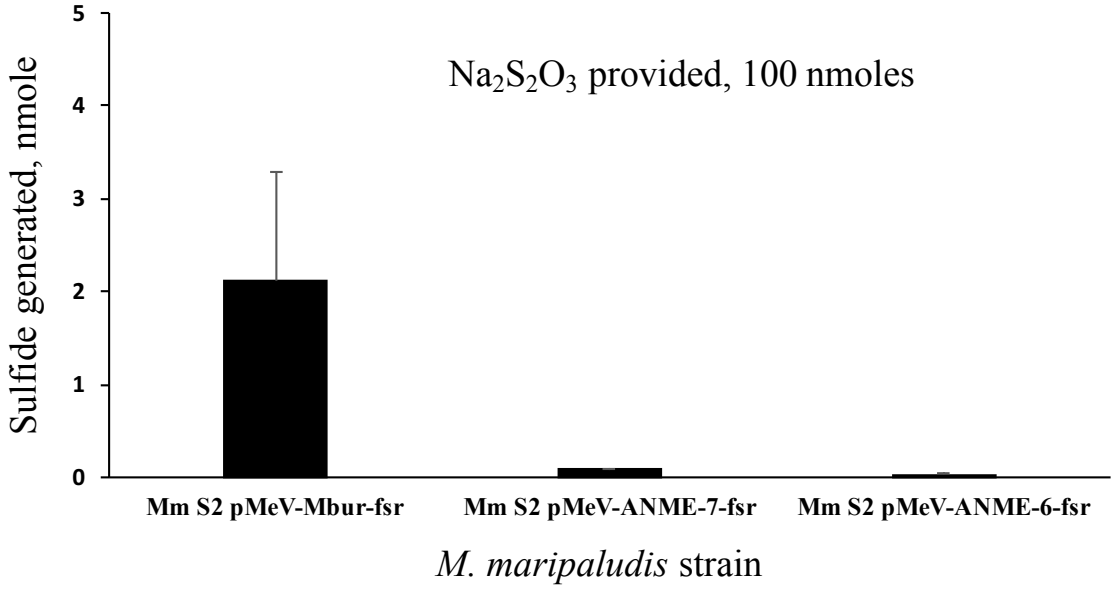

Supplementary Figure S1. Phylogeny of heterodimeric ATP sulfurylase (CysDN) subunits. (**a**) Bayesian phylogeny of 418 amino acid residues of assimilatory sulfate adenylyltransferase large subunit (CysN) and elongation factor 1 alpha (EF-1A) or elongation factor thermo unstable (EF-Tu) proteins. EF-1A and EF-Tu are in blue, CysN is in green, and proteins from ANME metagenomes are bolded and in red. (**b**) Bayesian phylogeny of 276 amino acid resudes of assimilatory sulfate adenylyltransferase small subunit (CysD) in green. Proteins from ANME metagenomes are bolded and in red Asterisks (*) indicate proteins that have been studied biochemically or structurally (Andersen et al. 2000; Vitagliano et al. 2001; Schmeing et al. 2009; Kobayashi et al. 2010; Thirup et al. 2015; Liu, Martin, and Leyh 1994; Mougous et al. 2006). Black dots on the branches represent Bayesian posterior probability values greater than 90%. Scale bar indicates the number of amino acid substitutions per site.

a

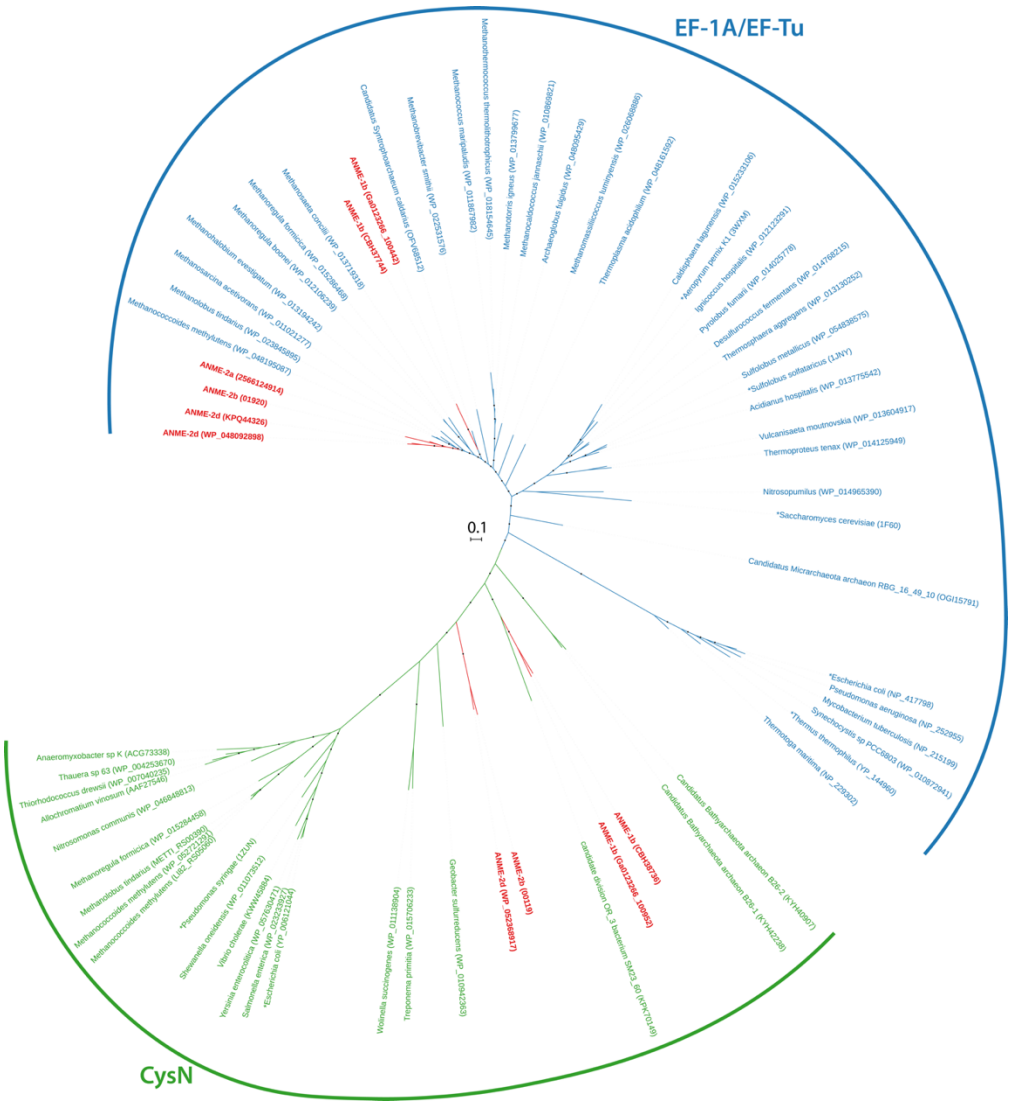

b

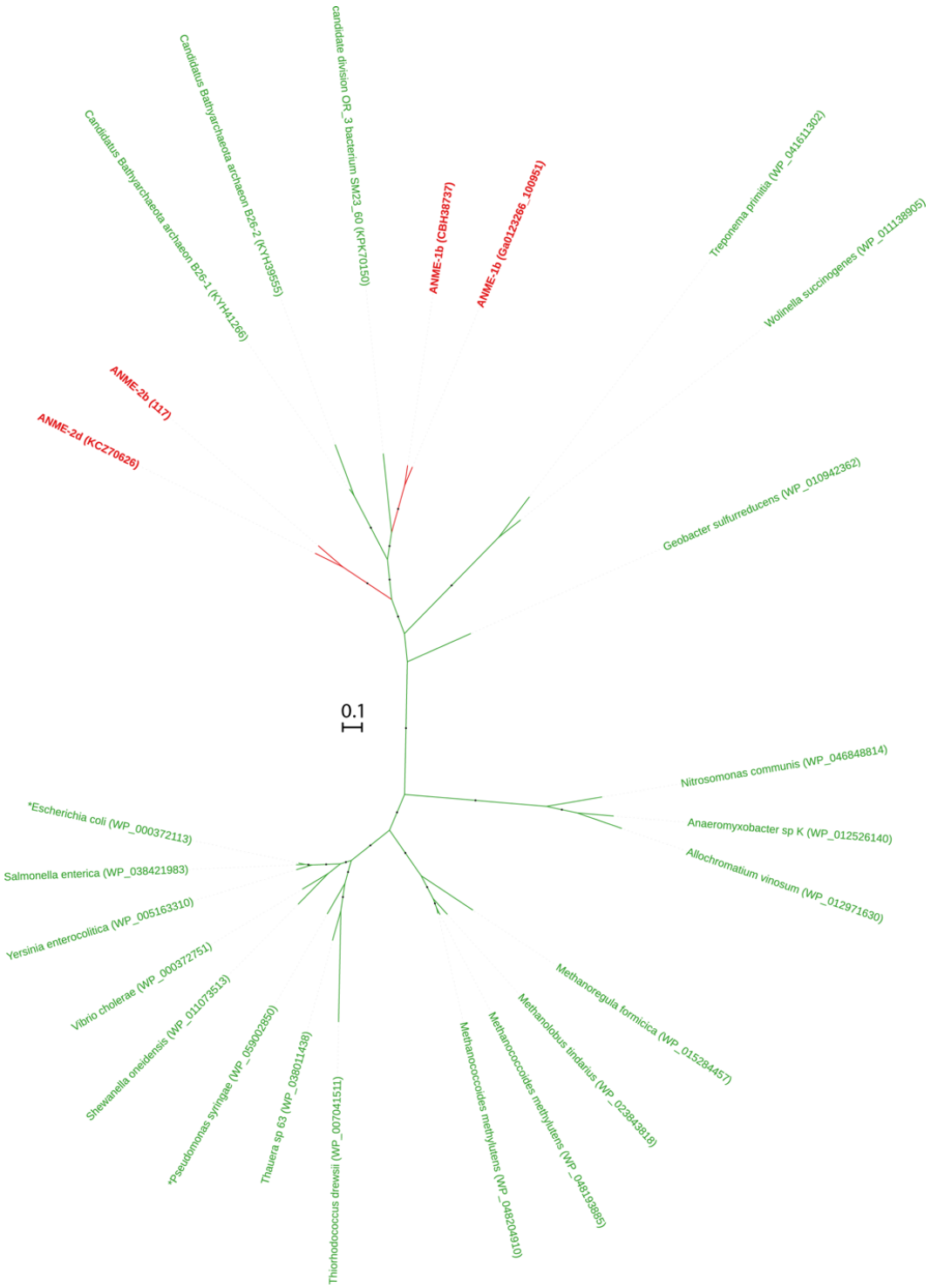
candidate division OR_3 bacterium SM23_60 (KPK70150)
Candidatus Bathyarchaeota archaeon B26-2 (KYH39555)
Candidatus Bathyarchaeota archaeon B26-1 (KYH41266)
ANME-1b (CBH38737)
ANME-1b (Ga0123266_100951)
Treponema primitia (WP_041611302)
Wolinella succinogenes (WP_011138905)
ANME-2b (117)
ANME-2d (KCZ70626)
Geobacter sulfurreducens (WP_010942362)
0.1
Nitrosomonas communis (WP_046848814)
Anaeromyxobacter sp K (WP_012526140)
Allochromatium vinosum (WP_012971630)
*Escherichia coli (WP_000372113)
Salmonella enterica (WP_038421983)
Yersinia enterocolitica (WP_005163310)
Vibrio cholerae (WP_000372751)
Shewanella oneidensis (WP_011073513)
*Pseudomonas syringae (WP_059002850)
Thauera sp 63 (WP_038011438)
Thiorhodococcus drewsii (WP_007041511)
Methanococcoides methylutens (WP_048204910)
Methanococcoides methylutens (WP_048193885)
Methanolobus tindarius (WP_023843818)
Methanoregula formicica (WP_015284457)

Supplementary Figure S2. Bayesian phylogeny of 168 amino acid residues of assimilatory adenyl-sulfate (APS) reductases and phosphoadenylyl-sulfate (PAPS) reductases. Nodes and branches of APS or PAPS reductases are in green or blue respectively, and proteins from ANME metagenomes are bolded and in red. Asterisks (*) indicate proteins that has been studied biochemically or structurally (Savage et al. 1997; Yu et al. 2008; Berndt et al. 2004; Kim et al. 2004; Gutierrez-Marcos et al. 1996; Suter et al. 2000; Lee et al. 2011; Cho 2013). Protein lengths range from 239 to 896 amino acids with the addition of protein domains, which are shown with filled symbols. Numbers on the branches represent Bayesian posterior probability values greater than 50%. Scale bar indicates the number of amino acid substitutions per site.

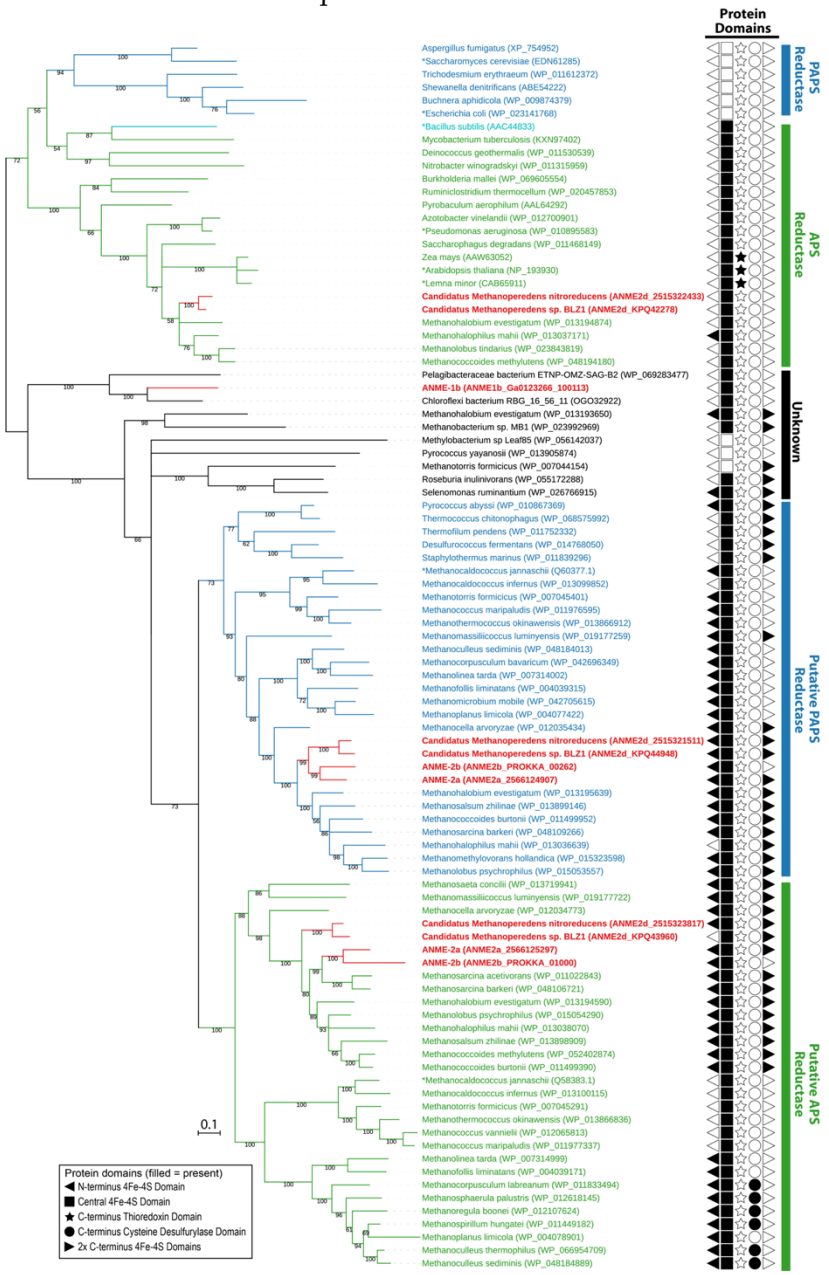

Supplementary Figure S3. Protein homology modeling of the c-terminus domain of Group II Fsr. (**a**) The overall 3D structural similarity between c-terminus of Group II Fsr found in ANME-2a (ANME2a_02262 in orange) and dissmilatory sulfite reductase (3mm5A in gray) found in *Archaeoglobus fulgidus* (RMSD=0.93). (**b**) Close-up active site showing differences in active site residues between DsrA and ANME-2a Group II Fsr. The four key residues for positioning of sulfite are shown by stick representations, and the dashed yellow lines and numbers indicate their distances to sulfite in Angstrom (shown in yellow). Other co-factors siroheme (white/red/blue) and iron sulfur clusters (yellow/orange) involved in the catalysis are also shown.

a

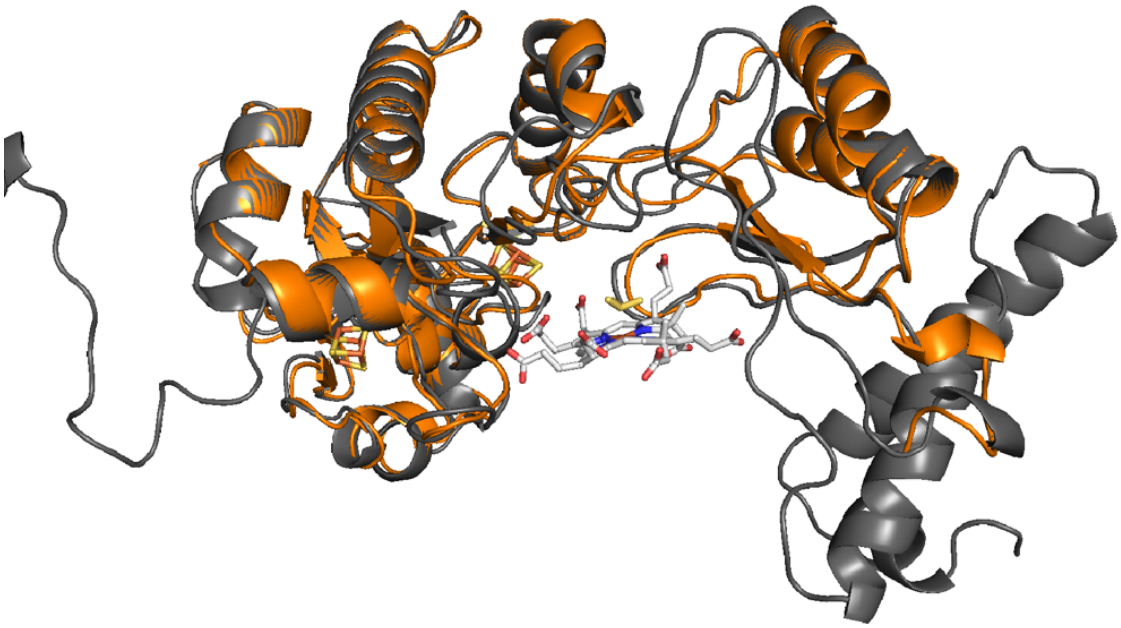

b

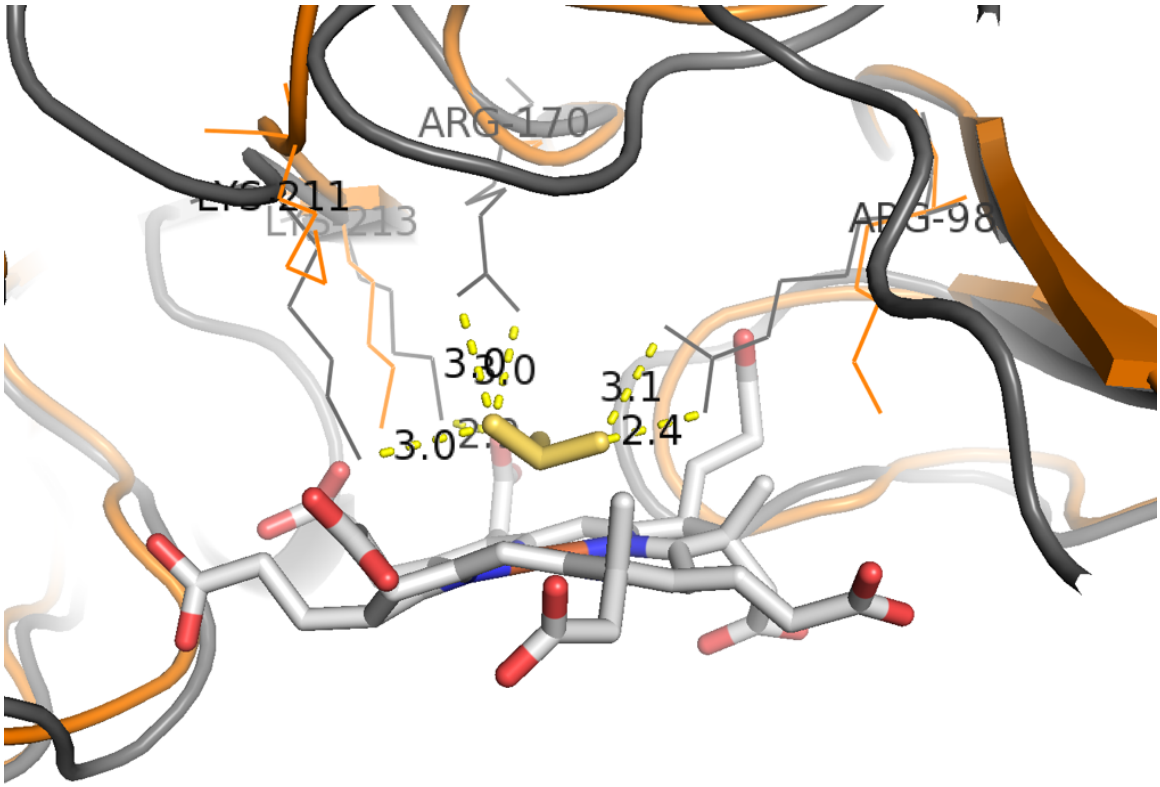

Supplementary Figure S4. Bayesian phylogeny of 224 amino acid residues of sulfite reductases. Nodes and branches to sulfite reductases found in ANME genome bins are highlighted in red. Black dots on the branches represent Bayesian posterior probability values greater than 90%. Scale bar indicates the number of amino acid substitutions per site.

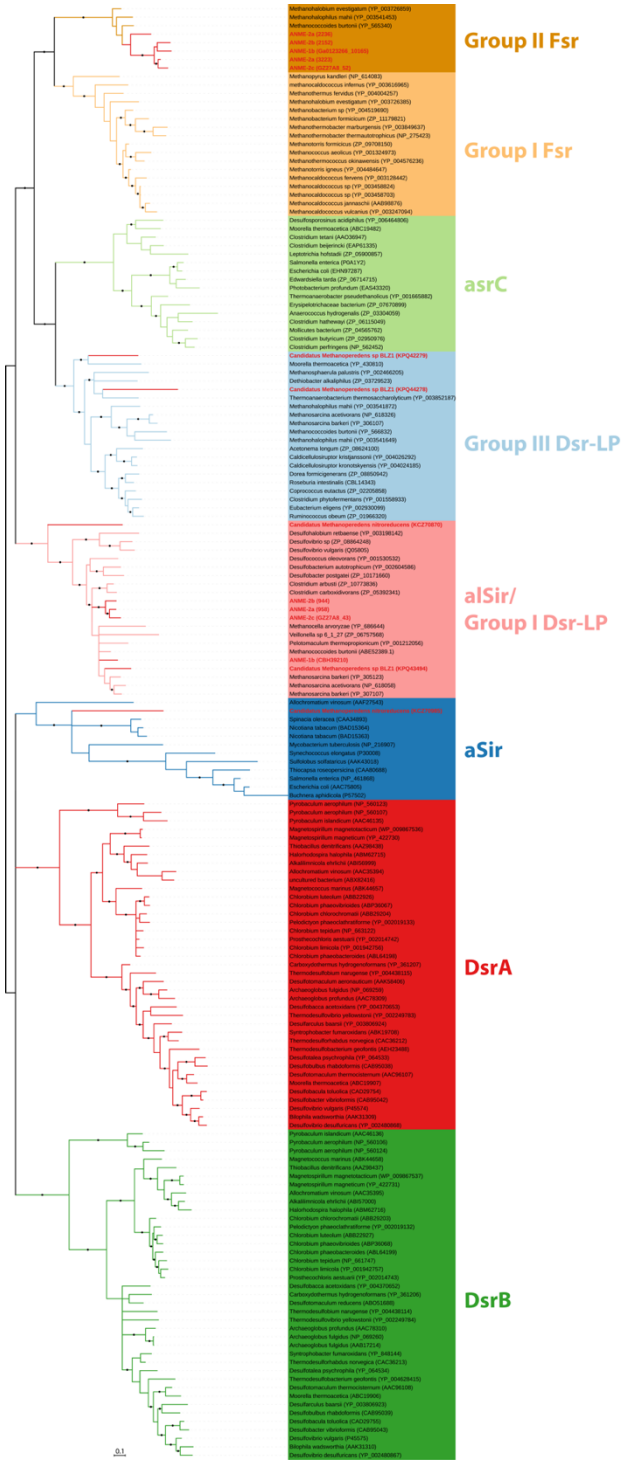

Supplementary Figure S5. Alignment of Group I and II Fsr to DsrAB. Four key residues that DsrA use for the positioning of sulfite are highlighted with red boxes and a red dot above. The residues in siroheme-binding motif ($CX_5CX_nCX_3C$) and one of the iron sulfur motifs ($CX_2CX_2CX_3C$) in DsrAB are highlighted with orange and black dots, respectively. Other highly conserved residues between Fsr and DsrAB are highlighted in blue boxes. Arrows indicate the sulfite- and siroheme-binding region used for phylogenetic analysis. Only a portion of the full alignment is shown here.

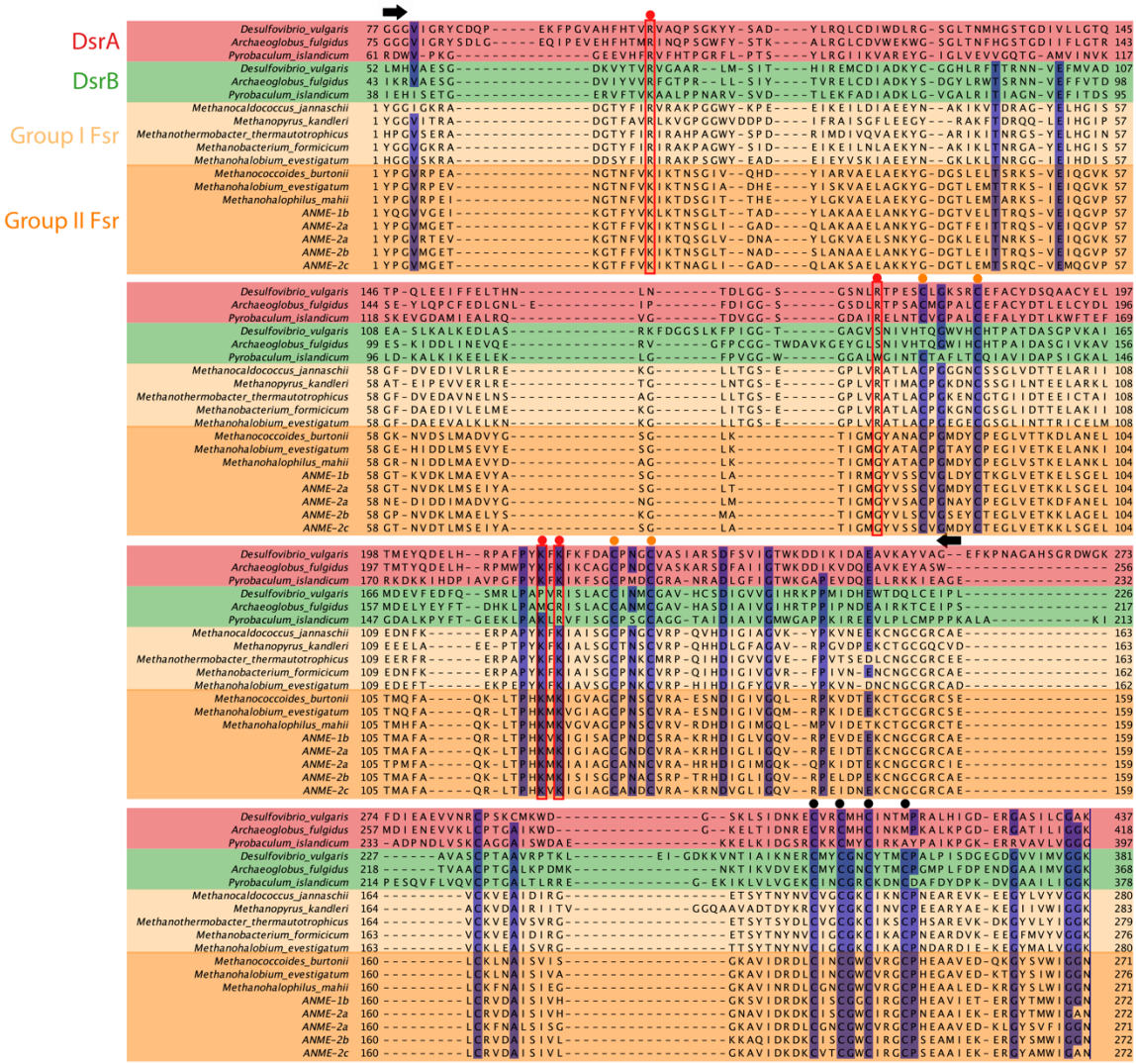

Supplementary Figure S6. Bayesian phylogeny of 615 amino acid residues of Fsr with environmental clones inserted. Three sets of primers (*=Fsr_GZ_Full_F+Fsr_GZ_full_R, **=Fsr_ANME_259F11 & Fsr_1923R2, ***=Fsr_ANME_265F13 & Fsr_1923R3) were used to amplify Group II Fsr from 4 methane seep samples 3730, 5207, 5059 and 5547 as indicated in the clone names. Black dots on the branches represent Bayesian posterior probability values greater than 90%. Scale bar indicates the number of amino acid substitutions per site. Three underlined Group II Fsr from ANME and *M. burtonii* were heterologously expressed in *Methanococcus maripaludis* for functional characterization.

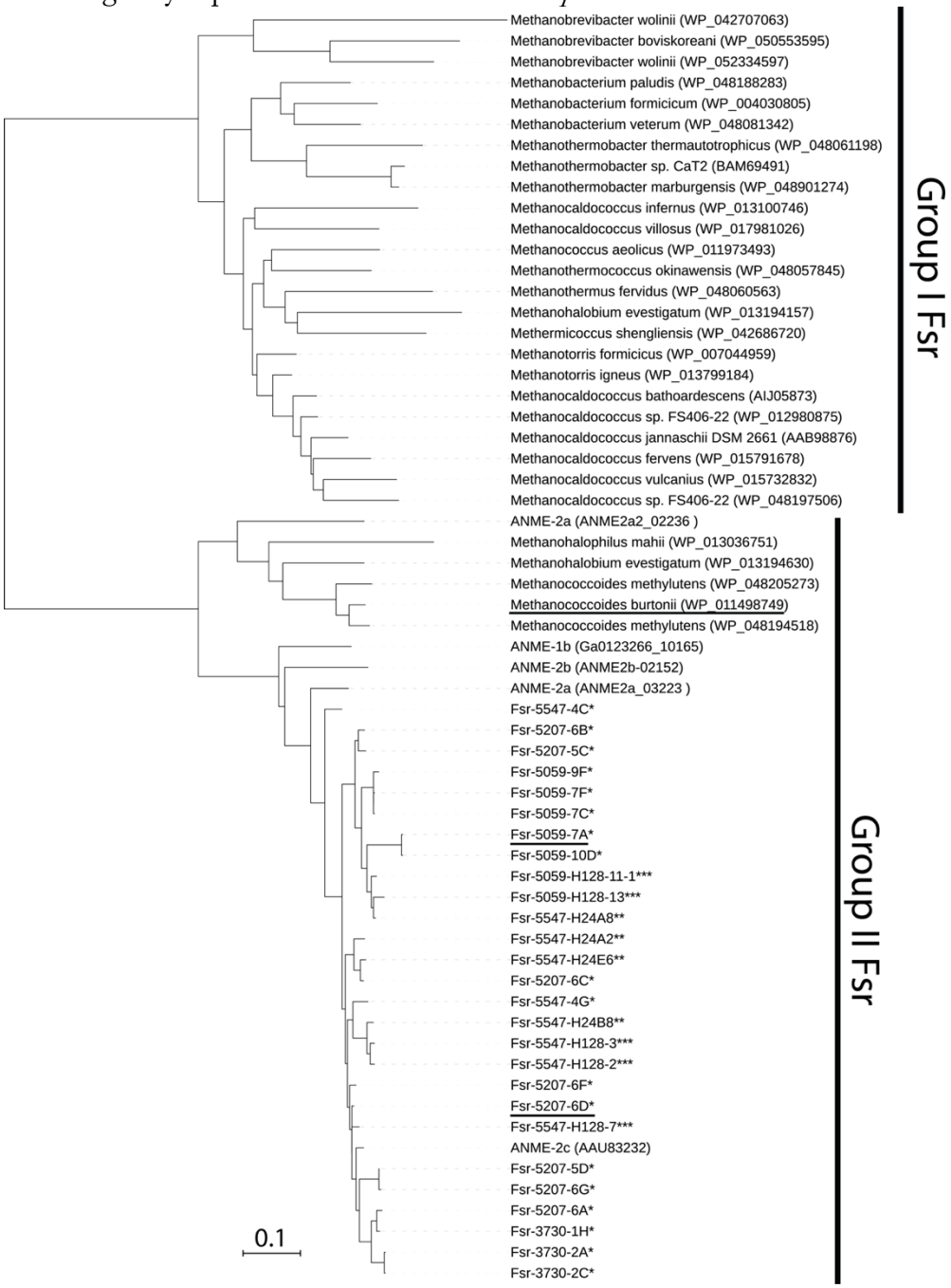

Supplementary Figure S7. RNA response of Group II Fsr and alSir in (**a**) ANME and (**b**) *M. burtonii* to various sulfur amendments. The expression data has been normalized to either the control CH_4+SO_4^{2-} condition with FPKM (Fragments Per Kilobase of transcript per Million mapped reads) values of 242 and 16 for Group II Fsr and alSir, respectively in panel **a**, or to the no addition control condition with $1.35x10^4$ and $1.57x10^3$ copies per µg RNA for Group II Fsr and alSir respectively in panel **b**. Error bars represent standard error for triplicate cultures.

a

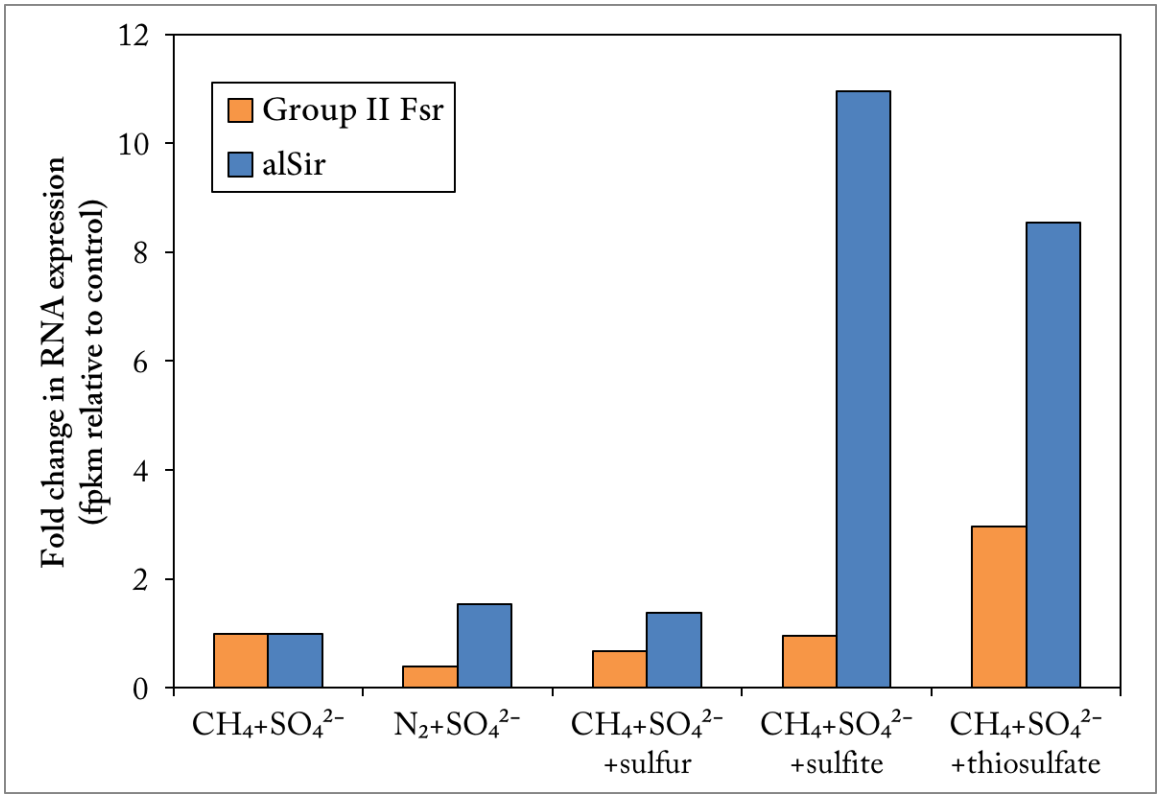

b

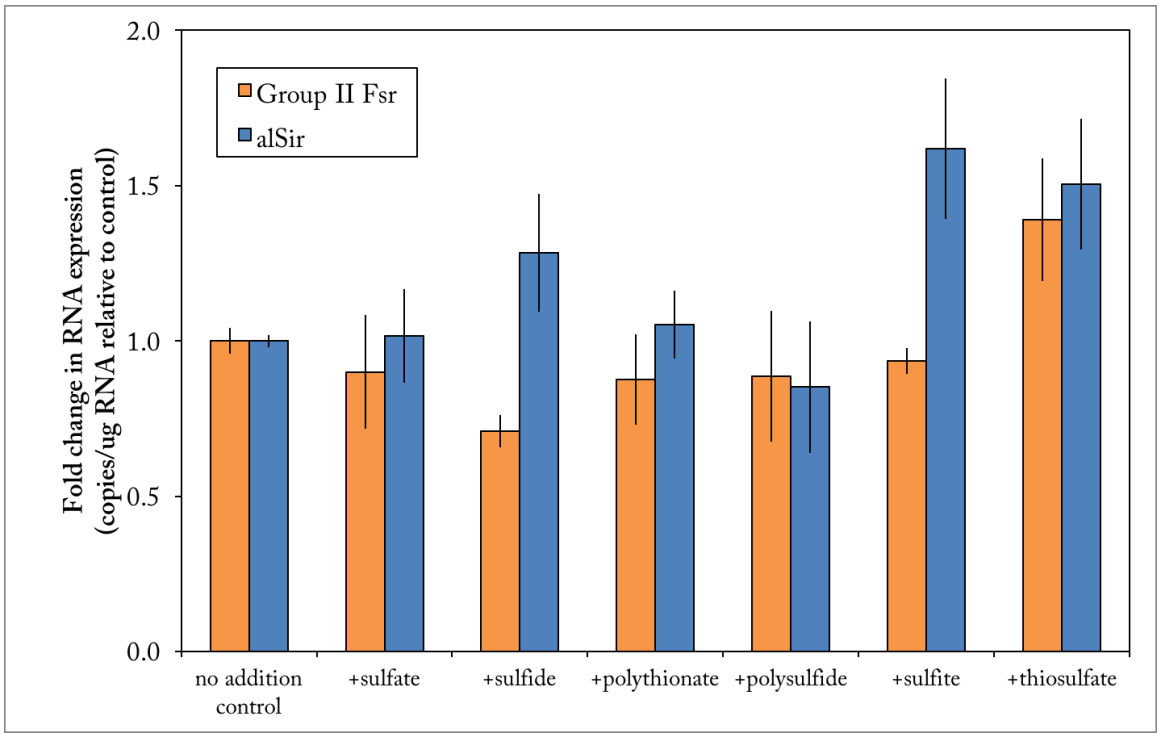
2.0
1.5
1.0
0.5
0.0
Fold change in RNA expression (copies/ug RNA relative to control)
Group II Fsr
alSir
no addition control
+sulfate
+sulfide
+polythionate
+polysulfide
+sulfite
+thiosulfate

Supplementary Figure S8. Sulfide production from methane seep microcosms amended with various sulfur compounds. Arrows indicate times when seawater was replaced and new seawater with amendments were added. At the end of the experiment (day 91), samples were taken for RNA analysis.

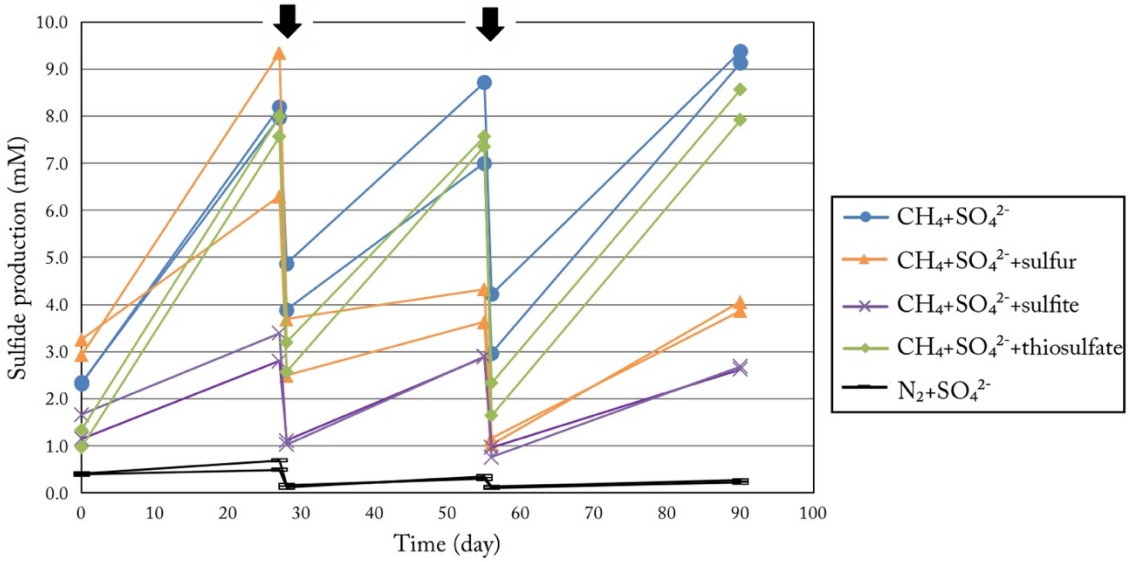

Supplementary Figure S9. Responses of (**a**) ANME and (**b**) *M. burtonii* to addition of various sulfur compounds. Arrows indicate time of amendments.

a

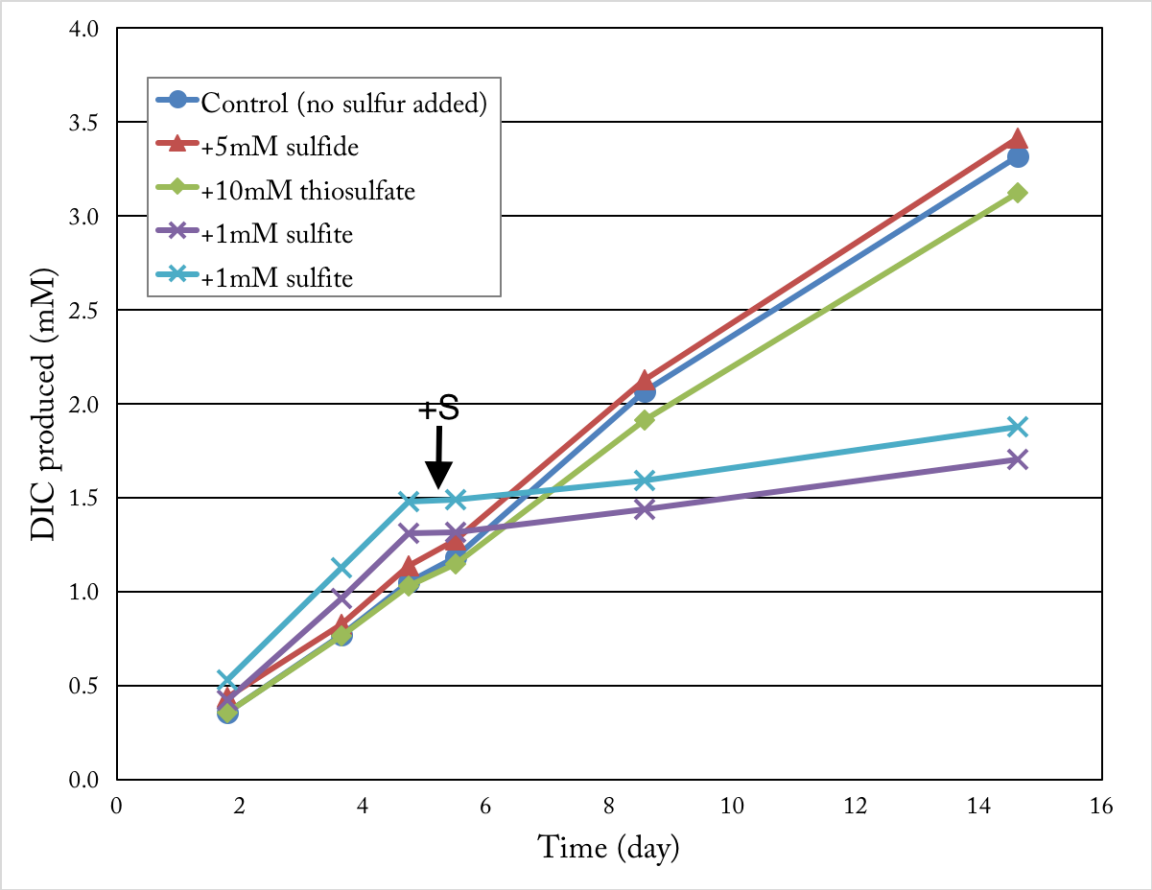

b

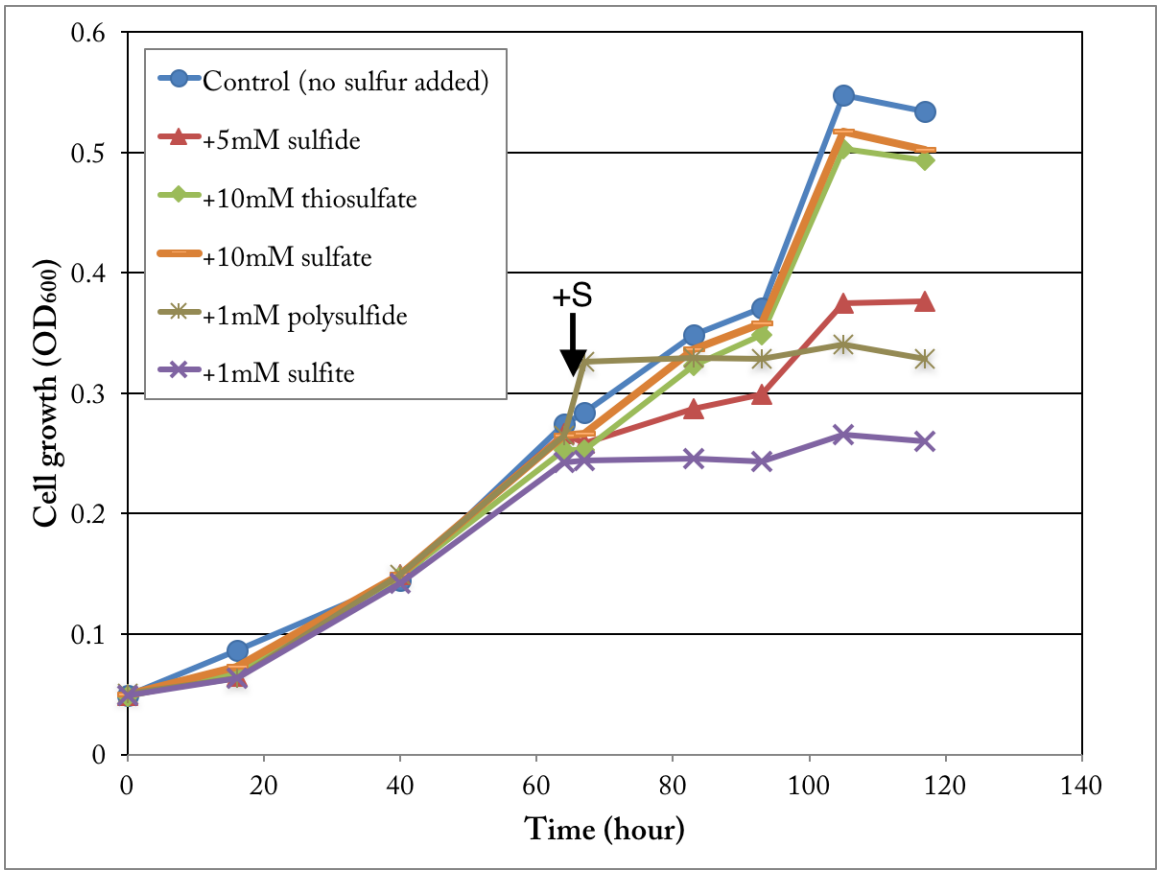
Control (no sulfur added)
+5mM sulfide
+10mM thiosulfate
+10mM sulfate
+1mM polysulfide
+1mM sulfite
+S
Cell growth (OD600)
Time (hour)
0
0.1
0.2
0.3
0.4
0.5
0.6
0
20
40
60
80
100
120
140

Supplementary Table S1. Bromobimane preservation and LC-MS measurement of ^{32}S- and ^{34}S-sulfide production (mM) from methane seep microcosms containing 20 mM labelled (99.8% ^{34}S) sulfate after 25-day incubation with or with unlabeled (95% ^{32}S) thiosulfate addition.

	^{32}S-Sulfide	**^{34}S-Sulfide**	**Sulfide total**
CH_4+^{34}S-Sulfate	0	5.9	5.9
CH_4+^{34}S-Sulfate +^{32}S-Thiosulfate	0.7	3.3	4

Supplementary Table S2. Sulfur pathways in representative genomes of methanogenic or methanotrophic archaea.
(Attached separately in Excel file)

Supplemetnary Table S4. Expression of ANME sulfur pathways in methane seep metaproteomes.
(Attached separately in Excel file)

Supplementary Table S3. Primer sequences used in either (**a**) PCR, or (**b**) qPCR experiments to study Group II Fsr in ANME and *M. burtonii*.

a

Primer name	Primer sequence	Note
Fsr_ANME_259F11	TGTACMYTCTGCGGCGC	Degenerate primer
Fsr_ANME_265F13	YTMTGCGGYGCATGTGC	Degenerate primer
Fsr_1923R2	CKGAYRCACCATCCACA	Degenerate primer
Fsr_1923R3	CTGATRCACCAKCCACA	Degenerate primer
Fsr_GZ_full_F	GCGCATGCATATGGCAAACGAAGAATATAAATGG	Contains NsiI digest site ATGCAT
Fsr_GZ_full_R	TAATGGATCCTCACACCTGATCCAGAACCTCT	Contains the reverse complement of BamHI digest site GGATCC
Fsr_Mbur_full_F	GCGC ATGCAT ATGTCAGAAGAATATAAATG	
Fsr_Mbur_full_R	GACA GGATCC TTATTCTTTCAGAACTTCAC	
Fsr-136R-ANME	CCGTTTCTCGGACACTCTTC	Internal primer
Fsr-136R-4C	CCGTTTCTCGGACACTCCTC	Internal primer
Fsr-136R-MBUR	CCATTCCTGTAGCATTCTTC	Internal primer
Fsr-1609F-ANME	TCAATCGTTCTTGGAAAGGC	Internal primer
Fsr-1609F-MBUR	TCTGTGATCTCAGGAAAAGC	Internal primer

b

Primer name	Primer sequence
Fsr1519F-bur	CACAAAATGAAGATCGGTGT
Fsr1590R-bur	ATACCAATGTCATTACTCTC
alsir427F-bur	AAGTTCAAGATCGGTGTTTC
alsir489R-bur	ACATCTTTTATGGCATTCTC

1.7 SUPPLEMENTARY INFORMATION

1.7.1 Assimilatory sulfate reduction pathway in different organisms

In bacteria such as *Escherichia coli* and *Salmonella typhimurium*, the assimilatory sulfate reduction pathway proceeds through heterodimeric ATP sulfurylase (*cysDN*), APS kinase (cysC), PAPS reductase (cysH) and assimilatory sulfite reductase (alSir or cysI) (Verschueren and Wilkinson 2005). In anoxygenic phototrophic bacteria, a dedicated sulfate assimilatory pathway exist and skips PAPS as the intermediate, using *cysDN* or *sat*, APS reductase and aSir (S. Neumann et al. 2000; Frigaard and Dahl 2008). In yeast, the assimilatory pathway is similar to that in *E. coli*, except *cysDN* has been swapped with the homo-oligomeric ATP sulfurylase *sat* (Ullrich, Blaesse, and Huber 2001; Thomas and Surdin-Kerjan 1997). In plants, the assimilatory sulfate reduction pathway is similar to that in anoxygenic phototrophic bacteria skipping PAPS and involves sat, APS reductase and aSir (also called ferredoxin-dependent sulfite reductase), although PAPS molecules are still produced from APS using APS kinase for sulfation reactions (Leustek et al. 2000).

1.8 ACKNOWLEDGEMENTS

We would like to thank the Environmental Analysis Center at Caltech and its director Nathan Delaskas for the help and support analyzing samples using ion chromatography and liquid chromatography coupled mass spectroscopy. We would like to thank the Millard and Muriel Jacobs Genetics and Genomics Laboratory at Caltech for performing RNA sequencing. We would like to thank Katherine Dawson and Derek Smith for their help with measuring and analyzing the intermediate sulfur species using the bromobimane method. Also, we would like to thank Katherine Dawson and Grayson Chadwick for their comments on the manuscript.

1.9 AUTHOR CONTRIBUTIONS

HY, RLH, BM, VJO devised the study. HY, DS, SM, CS, KC, RI, SS, PT conducted the experiments and analyses. HY and VJO wrote the manuscript with contributions from all authors, including data analysis, figure generation, and the final manuscript.

1.9 REFERENCES

Aguilar-Barajas, Esther, Cesar Diaz-Perez, Martha I Ramirez-Diaz, Hector Riveros-Rosas, and Carlos Cervantes. 2011. "Bacterial Transport of Sulfate, Molybdate, and Related Oxyanions." *Biometals* 24 (4). Springer Netherlands: 687–707. doi:10.1007/s10534-011-9421-x.

Allen, Michelle A, Federico M Lauro, Timothy J Williams, Dominic Burg, Khawar S Siddiqui, Davide De Francisci, Kevin W Y Chong, et al. 2009. "The Genome Sequence of the Psychrophilic Archaeon, Methanococcoides Burtonii: the Role of Genome Evolution in Cold Adaptation.." *Isme Journal* 3 (9): 1012–35. doi:10.1038/ismej.2009.45.

Arshad, Arslan, Daan R Speth, Rob M de Graaf, Huub J M Op den Camp, Mike S M Jetten, and Cornelia U Welte. 2015. "A Metagenomics-Based Metabolic Model of Nitrate-Dependent Anaerobic Oxidation of Methane by Methanoperedens-Like Archaea.." *Frontiers in Microbiology* 6 (273). Frontiers: 1423. doi:10.3389/fmicb.2015.01423.

Aussignargues, Clément C, Marie-Cécile MC Giuliani, Pascale P Infossi, Elisabeth E Lojou, Marianne M Guiral, Marie-Thérèse MT Giudici-Orticoni, and Marianne M Ilbert. 2012. "Rhodanese Functions as Sulfur Supplier for Key Enzymes in Sulfur Energy Metabolism.." *The Journal of Biological Chemistry* 287 (24): 19936–48. doi:10.1074/jbc.M111.324863.

Boetius, Antje, Katrin Ravenschlag, Carsten J Schubert, Dirk Rickert, Friedrich Widdel, Armin Gieseke, Rudolf Amann, Bo Barker Jørgensen, Ursula Witte, and Olaf Pfannkuche. 2000. "A Marine Microbial Consortium Apparently Mediating Anaerobic Oxidation of Methane." *Nature* 407 (6804): 623–26. doi:10.1038/35036572.

Borrel, Guillaume, Nicolas Parisot, Hugh M B Harris, Eric Peyretaillade, Nadia Gaci, William Tottey, Olivier Bardot, et al. 2014. "Comparative Genomics Highlights the Unique Biology of Methanomassiliicoccales, a Thermoplasmatales-Related Seventh Order of Methanogenic Archaea That Encodes Pyrrolysine.." *Bmc Genomics* 15 (1). BioMed Central: 679. doi:10.1186/1471-2164-15-679.

Brown, Steven D, Melissa R Thompson, Nathan C Verberkmoes, Karuna Chourey, Manesh Shah, Jizhong Zhou, Robert L Hettich, and Dorothea K Thompson. 2006. "Molecular Dynamics of the Shewanella Oneidensis Response to Chromate Stress.." *Molecular & Cellular Proteomics : MCP* 5 (6). American Society for Biochemistry and Molecular Biology: 1054–71. doi:10.1074/mcp.M500394-MCP200.

Carroll, Kate S, Hong Gao, Huiyi Chen, C David Stout, Julie A Leary, and Carolyn R Bertozzi. 2005. "A Conserved Mechanism for Sulfonucleotide Reduction.." *PLoS Biology* 3 (8): e250. doi:10.1371/journal.pbio.0030250.

Chartron, Justin, Kate S Carroll, Carrie Shiau, Hong Gao, Julie A Leary, Carolyn R Bertozzi, and C David Stout. 2006. "Substrate Recognition, Protein Dynamics, and Iron-Sulfur Cluster in Pseudomonas Aeruginosa Adenosine 5'-Phosphosulfate Reductase.." *Journal of Molecular Biology* 364 (2): 152–69. doi:10.1016/j.jmb.2006.08.080.

Cho, Myung Kook. 2013. "Discovery of Novel 3'-Phosphoadenosine-5'-Phosphosulfate (PAPS) Reductase From Methanarcheon Methanocaldococcus Jannaschii.." Edited by

Sung-Kun Kim. Waco, Texas.

Chourey, Karuna, Janet Jansson, Nathan VerBerkmoes, Manesh Shah, Krystle L Chavarria, Lauren M Tom, Eoin L Brodie, and Robert L Hettich. 2010. "Direct Cellular Lysis/Protein Extraction Protocol for Soil Metaproteomics.." *Journal of Proteome Research* 9 (12): 6615–22. doi:10.1021/pr100787q.

Cipollone, Rita R, Paolo P Ascenzi, and Paolo P Visca. 2007. "Common Themes and Variations in the Rhodanese Superfamily.." *Iubmb Life* 59 (2): 51–59. doi:10.1080/15216540701206859.

Cline, Joel D. 1969. "Spectrophotometric Determination of Hydrogen Sulfide in Natural Waters." *Limnology and Oceanography* 14: 454–58.

D'Amico, Salvino, Paule Claverie, Tony Collins, Daphné Georlette, Emmanuelle Gratia, Anne Hoyoux, Marie-Alice Meuwis, Georges Feller, and Charles Gerday. 2002. "Molecular Basis of Cold Adaptation." *Philosophical Transactions of the Royal Society of London. Series B, Biological Sciences* 357 (1423). The Royal Society: 917–25. doi:10.1098/rstb.2002.1105.

Daniels, Lacy, Negash Belay, and B S Rajagopal. 1986. "Assimilatory Reduction of Sulfate and Sulfite by Methanogenic Bacteria.." *Applied and Environmental Microbiology* 51 (4): 703–9.

Dawson, Katherine S, Silvan Scheller, Jesse G Dillon, and Victoria J Orphan. 2016. "Stable Isotope Phenotyping via Cluster Analysis of NanoSIMS Data as a Method for Characterizing Distinct Microbial Ecophysiologies and Sulfur-Cycling in the Environment.." *Frontiers in Microbiology* 7 (243). Frontiers: 774. doi:10.3389/fmicb.2016.00774.

Dekas, Anne E, Stephanie A Connon, Grayson L Chadwick, Elizabeth Trembath-Reichert, and Victoria J Orphan. 2016. "Activity and Interactions of Methane Seep Microorganisms Assessed by Parallel Transcription and FISH-NanoSIMS Analyses.." *The ISME Journal* 10 (3): 678–92. doi:10.1038/ismej.2015.145.

Delano, Warren L. 2002. *The PyMOL Molecular Graphics System*. Delano Scientific. doi:10.1234/12345678.

Dhillon, Ashita, Sulip Goswami, Monica Riley, Andreas Teske, and Mitchell Sogin. 2005. "Domain Evolution and Functional Diversification of Sulfite Reductases.." *Astrobiology* 5 (1): 18–29. doi:10.1089/ast.2005.5.18.

Franzmann, P D, N Springer, W Ludwig, E C Demacario, and M Rohde. 1992. "A Methanogenic Archaeon From Ace Lake, Antarctica - Methanococcoides-Burtonii Sp-Nov." *Systematic and Applied Microbiology* 15 (4): 573–81. doi:10.1016/S0723-2020(11)80117-7.

Frigaard, Niels-Ulrik, and Christiane Dahl. 2008. "Sulfur Metabolism in Phototrophic Sulfur Bacteria." In, 54:103–200. Advances in Microbial Physiology. Elsevier. doi:10.1016/S0065-2911(08)00002-7.

Hallam, Steven J, Nik Putnam, Christina M Preston, John C Detter, Daniel Rokhsar, Paul M Richardson, and Edward F DeLong. 2004. "Reverse Methanogenesis: Testing the Hypothesis with Environmental Genomics.." *Science* 305 (5689). American Association for the Advancement of Science: 1457–62. doi:10.1126/science.1100025.

Haroon, Mohamed F, Shihu Hu, Ying Shi, Michael Imelfort, Jurg Keller, Philip Hugenholtz, Zhiguo Yuan, and Gene W Tyson. 2013. "Anaerobic Oxidation of Methane Coupled to Nitrate Reduction in a Novel Archaeal Lineage.." *Nature* 500 (7464): 567–70. doi:10.1038/nature12375.

Hatzenpichler, Roland, Stephanie A Connon, Danielle Goudeau, Rex R Malmstrom, Tanja Woyke, and Victoria J Orphan. 2016. "Visualizing in Situ Translational Activity for Identifying and Sorting Slow-Growing Archaeal–Bacterial Consortia." *Proceedings of the National Academy of Sciences of the United States of America*, June. National Acad Sciences, 201603757. doi:10.1073/pnas.1603757113.

Herrmann, Jonathan, Geoffrey E Ravilious, Samuel E McKinney, Corey S Westfall, Soon Goo Lee, Patrycja Baraniecka, Marco Giovannetti, Stanislav Kopriva, Hari B Krishnan, and Joseph M Jez. 2014. "Structure and Mechanism of Soybean ATP Sulfurylase and the Committed Step in Plant Sulfur Assimilation.." *The Journal of Biological Chemistry* 289 (15). American Society for Biochemistry and Molecular Biology: 10919–29. doi:10.1074/jbc.M113.540401.

Hinrichs, Kai U, John M Hayes, Sean P Sylva, Peter G Brewer, and Edward F DeLong. 1999. "Methane-Consuming Archaebacteria in Marine Sediments.." *Nature* 398 (6730): 802–5. doi:10.1038/19751.

Jagersma, Christian G, Roel J W Meulepas, Peer H A Timmers, Agata Szperl, Piet N L Lens, and Alfons J M Stams. 2012. "Enrichment of ANME-1 From Eckernförde Bay Sediment on Thiosulfate, Methane and Short-Chain Fatty Acids." *Journal of Biotechnology* 157 (4): 482–89. doi:10.1016/j.jbiotec.2011.10.012.

Johnson, Eric F, and Biswarup Mukhopadhyay. 2005. "A New Type of Sulfite Reductase, a Novel Coenzyme F420-Dependent Enzyme, From the Methanarchaeon Methanocaldococcus Jannaschii.." *The Journal of Biological Chemistry* 280 (46): 38776–86. doi:10.1074/jbc.M503492200.

Johnson, Eric F, and Biswarup Mukhopadhyay. 2008. "Coenzyme F420-Dependent Sulfite Reductase-Enabled Sulfite Detoxification and Use of Sulfite as a Sole Sulfur Source by Methanococcus Maripaludis.." *Applied and Environmental Microbiology* 74 (11): 3591–95. doi:10.1128/AEM.00098-08.

Jones, W Jack, M J B Paynter, and R Gupta. 1983. "Characterization of Methanococcus Maripaludis Sp. Nov., a New Methanogen Isolated From Salt Marsh Sediment." *Archives of Microbiology* 135 (2). Springer-Verlag: 91–97. doi:10.1007/BF00408015.

Knittel, Katrin, and Antje Boetius. 2009. "Anaerobic Oxidation of Methane: Progress with an Unknown Process.." *Annual Review of Microbiology* 63: 311–34. doi:10.1146/annurev.micro.61.080706.093130.

Lee, Jong-Sun, Ethan White, Sang Gon Kim, Sara Rae Schlesinger, Sang Yeol Lee, and Sung-Kun Kim. 2011. "Discovery of a Novel Adenosine 5′-Phosphosulfate (APS) Reductase From the Methanarcheon Methanocaldococcus Jannaschii." *Process Biochemistry* 46 (1): 154–61. doi:10.1016/j.procbio.2010.08.004.

Letunic, Ivica, and Peer Bork. 2016. "Interactive Tree of Life (iTOL) V3: an Online Tool for the Display and Annotation of Phylogenetic and Other Trees.." *Nucleic Acids Research*, April. Oxford University Press, gkw290. doi:10.1093/nar/gkw290.

Leustek, Thomas, Melinda N Martin, Julie Ann Bick, and John P Davies. 2000. "Pathways and Regulation of Sulfur Metabolism Revealed Through Molecular and Genetic Studies." *Annual Review of Plant Physiology and Plant Molecular Biology* 51 (1): 141–65. doi:10.1146/annurev.arplant.51.1.141.

Lin, Winston, and William B Whitman. 2004. "The Importance of porE and porF in the Anabolic Pyruvate Oxidoreductase of Methanococcus Maripaludis.." *Archives of Microbiology* 181 (1): 68–73. doi:10.1007/s00203-003-0629-1.

Liu, Changxian, Eugene Martin, and Thomas S Leyh. 1994. "GTPase Activation of ATP Sulfurylase: the Mechanism." *Biochemistry* 33 (8): 2042–47. doi:10.1021/bi00174a009.

Liu, Yuchen, and William B Whitman. 2008. "Metabolic, Phylogenetic, and Ecological Diversity of the Methanogenic Archaea.." *Annals of the New York Academy of Sciences* 1125 (1). Blackwell Publishing Inc: 171–89. doi:10.1196/annals.1419.019.

Liu, Yuchen, Laura L Beer, and William B Whitman. 2012. "Methanogens: a Window Into Ancient Sulfur Metabolism.." *Trends in Microbiology* 20 (5): 251–58. doi:10.1016/j.tim.2012.02.002.

Loy, Alexander, Stephan Duller, and Michael Wagner. 2008. "Evolution and Ecology of Microbes Dissimilating Sulfur Compounds: Insights From Siroheme Sulfite Reductases." In *Microbial Sulfur Metabolism*, 46–59. Berlin, Heidelberg: Springer Berlin Heidelberg. doi:10.1007/978-3-540-72682-1_5.

Ludwig, Wolfgang, Oliver Strunk, Ralf Westram, Lothar Richter, Harald Meier, Yadhukumar, Arno Buchner, et al. 2004. "ARB: a Software Environment for Sequence Data.." *Nucleic Acids Research* 32 (4): 1363–71. doi:10.1093/nar/gkh293.

Markowitz, Victor M, I-Min A Chen, Krishna Palaniappan, Ken Chu, Ernest Szeto, Yuri Grechkin, Anna Ratner, et al. 2012. "IMG: the Integrated Microbial Genomes Database and Comparative Analysis System." *Nucleic Acids Research* 40 (D1): D115–22. doi:10.1093/nar/gkr1044.

Marlow, Jeffrey J, Connor T Skennerton, Zhou Li, Karuna Chourey, Robert L Hettich, Chongle Pan, and Victoria J Orphan. 2016a. "Proteomic Stable Isotope Probing Reveals Biosynthesis Dynamics of Slow Growing Methane Based Microbial Communities.." *Frontiers in Microbiology* 7 (386). Frontiers: 563. doi:10.3389/fmicb.2016.00563.

Marlow, Jeffrey, Connor Tobias Skennerton, Zhou Li, Karuna Chourey, Robert Hettich, Chongle Pan, and Victoria Orphan. 2016b. "Proteomic Stable Isotope Probing Reveals Biosynthesis Dynamics of Slow Growing Methane Based Microbial Communities." *Frontiers in Microbiology* 7 (386). Frontiers: 563. doi:10.3389/fmicb.2016.00563.

Meyerdierks, Anke, Michael Kube, Ivaylo Kostadinov, Hanno Teeling, Frank Oliver Glöckner, Richard Reinhardt, and Rudolf Amann. 2010. "Metagenome and mRNA Expression Analyses of Anaerobic Methanotrophic Archaea of the ANME-1 Group.." *Environmental Microbiology* 12 (2). Blackwell Publishing Ltd: 422–39. doi:10.1111/j.1462-2920.2009.02083.x.

Milucka, Jana, Timothy G Ferdelman, Lubos Polerecky, Daniela Franzke, Gunter Wegener, Markus Schmid, Ingo Lieberwirth, Michael Wagner, Friedrich Widdel, and Marcel M M Kuypers. 2012. "Zero-Valent Sulphur Is a Key Intermediate in Marine Methane Oxidation.." *Nature* 491 (7425): 541–46. doi:10.1038/nature11656.

Mougous, Joseph D, Dong H Lee, Sarah C Hubbard, Michael W Schelle, David J Vocadlo, James M Berger, and Carolyn R Bertozzi. 2006. "Molecular Basis for G Protein Control of the Prokaryotic ATP Sulfurylase.." *Molecular Cell* 21 (1): 109–22. doi:10.1016/j.molcel.2005.10.034.

Moura, I, A R Lino, J J Moura, A V Xavier, G Fauque, H D Peck, and J LeGall. 1986. "Low-Spin Sulfite Reductases: a New Homologous Group of Non-Heme Iron-Siroheme Proteins in Anaerobic Bacteria.." *Biochemical and Biophysical Research Communications* 141 (3): 1032–41.

Moura, I, and A R Lino. 1994. "Low-Spin Sulfite Reductases." *Methods in Enzymology: Methods in Methane Metabolism, Pt A* 243: 296–303.

Nauhaus, Katja, Tina Treude, Antje Boetius, and Martin Krüger. 2005. "Environmental Regulation of the Anaerobic Oxidation of Methane: a Comparison of ANME-I and ANME-II Communities.." *Environmental Microbiology* 7 (1): 98–106. doi:10.1111/j.1462-2920.2004.00669.x.

Neilson, Karlie A, Tim Keighley, Dana Pascovici, Brett Cooke, and Paul A Haynes. 2013. "Label-Free Quantitative Shotgun Proteomics Using Normalized Spectral Abundance Factors.." *Methods in Molecular Biology (Clifton, N.J.)* 1002 (Chapter 17). Totowa, NJ: Humana Press: 205–22. doi:10.1007/978-1-62703-360-2_17.

Neumann, A, G Wohlfarth, and G Diekert. 1996. "Purification and Characterization of Tetrachloroethene Reductive Dehalogenase From Dehalospirillum Multivorans." *The Journal of Biological Chemistry* 271 (28): 16515–19.

Neumann, S, A Wynen, Hans G Trüper, and Christiane Dahl. 2000. "Characterization of the Cys Gene Locus From Allochromatium Vinosum Indicates an Unusual Sulfate Assimilation Pathway.." *Molecular Biology Reports* 27 (1): 27–33.

Orphan, Victoria J, Christopher H House, Kai U Hinrichs, Kevin D McKeegan, and Edward F DeLong. 2001. "Methane-Consuming Archaea Revealed by Directly Coupled Isotopic and Phylogenetic Analysis.." *Science* 293 (5529). American Association for the Advancement of Science: 484–87. doi:10.1126/science.1061338.

Paoletti, Andrew C, Tari J Parmely, Chieri Tomomori-Sato, Shigeo Sato, Dongxiao Zhu, Ronald C Conaway, Joan Weliky Conaway, Laurence Florens, and Michael P Washburn. 2006. "Quantitative Proteomic Analysis of Distinct Mammalian Mediator Complexes Using Normalized Spectral Abundance Factors.." *Proceedings of the National Academy of Sciences of the United States of America* 103 (50). National Acad Sciences: 18928–33. doi:10.1073/pnas.0606379103.

Parey, Kristian K, Eberhard E Warkentin, Peter M H PM Kroneck, and Ulrich U Ermler. 2010. "Reaction Cycle of the Dissimilatory Sulfite Reductase From Archaeoglobus Fulgidus.." *Audio, Transactions of the IRE Professional Group on* 49 (41): 8912–21. doi:10.1021/bi100781f.

Parey, Kristian, Ulrike Demmer, Eberhard Warkentin, Astrid Wynen, Ulrich Ermler, and Christiane Dahl. 2013. "Structural, Biochemical and Genetic Characterization of Dissimilatory ATP Sulfurylase From Allochromatium Vinosum.." Edited by Inês A Cardoso Pereira. *PloS One* 8 (9). Public Library of Science: e74707. doi:10.1371/journal.pone.0074707.

Pruitt, Kim D, Tatiana Tatusova, Garth R Brown, and Donna R Maglott. 2012. "NCBI Reference Sequences (RefSeq): Current Status, New Features and Genome Annotation Policy.." *Nucleic Acids Research* 40 (Database issue): D130–35. doi:10.1093/nar/gkr1079.

Rajagopal, Basavapatna S, and Lacy Daniels. 1986. "Investigation of Mercaptans, Organic Sulfides, and Inorganic Sulfur-Compounds as Sulfur Sources for the Growth of Methanogenic Bacteria." *Current Microbiology* 14 (3): 137–44.

Ramirez, Pablo, Hector Toledo, Nicolas Guiliani, and Carlos A Jerez. 2002. "An Exported Rhodanese-Like Protein Is Induced During Growth of Acidithiobacillus Ferrooxidans in Metal Sulfides and Different Sulfur Compounds." *Applied and Environmental Microbiology* 68 (4). American Society for Microbiology: 1837–45. doi:10.1128/AEM.68.4.1837-1845.2002.

Reeburgh, William S. 2007. "Oceanic Methane Biogeochemistry.." *Chemical Reviews* 107 (2): 486–513. doi:10.1021/cr050362v.

Ronquist, Fredrik, Maxim Teslenko, Paul van der Mark, Daniel L Ayres, Aaron Darling, Sebastian Höhna, Bret Larget, Liang Liu, Marc A Suchard, and John P Huelsenbeck. 2012. "MrBayes 3.2: Efficient Bayesian Phylogenetic Inference and Model Choice Across a Large Model Space.." *Systematic Biology* 61 (3): 539–42. doi:10.1093/sysbio/sys029.

Scheller, Silvan, Hang Yu, Grayson L Chadwick, Shawn E McGlynn, and Victoria J Orphan. 2016. "Artificial Electron Acceptors Decouple Archaeal Methane Oxidation From Sulfate Reduction.." *Science* 351 (6274): 703–7. doi:10.1126/science.aad7154.

Schiffer, Alexander, Kristian Parey, Eberhard Warkentin, Kay Diederichs, Harald Huber, Karl O Stetter, Peter M H Kroneck, and Ulrich Ermler. 2008. "Structure of the Dissimilatory Sulfite Reductase From the Hyperthermophilic Archaeon Archaeoglobus Fulgidus.." *Journal of Molecular Biology* 379 (5): 1063–74. doi:10.1016/j.jmb.2008.04.027.

Sharma, Ritin, Brian D Dill, Karuna Chourey, Manesh Shah, Nathan C Verberkmoes, and Robert L Hettich. 2012. "Coupling a Detergent Lysis/Cleanup Methodology with Intact Protein Fractionation for Enhanced Proteome Characterization.." *Journal of Proteome Research* 11 (12). American Chemical Society: 6008–18. doi:10.1021/pr300709k.

Sievers, Fabian, Andreas Wilm, David Dineen, Toby J Gibson, Kevin Karplus, Weizhong Li, Rodrigo Lopez, et al. 2011. "Fast, Scalable Generation of High-Quality Protein Multiple Sequence Alignments Using Clustal Omega." *Molecular Systems Biology* 7 (October): –. doi:10.1038/msb.2011.75.

Smith, Derek A, Alex L Sessions, Katherine S Dawson, Nathan Dalleska, and Victoria J Orphan. 2017. "Rapid Quantification and Isotopic Analysis of Dissolved Sulfur Species.." *Rapid Communications in Mass Spectrometry : RCM*, March. doi:10.1002/rcm.7846.

Sperling, Detlef, Ulrike Kappler, Hans G Trüper, and Christiane Dahl. 2001. "Dissimilatory ATP Sulfurylase From Archaeoglobus Fulgidus." *Methods in Enzymology: Methods in Methane Metabolism, Pt A* 331: 419–27.

Stetter, Karl O, and Günther Gaag. 1983. "Reduction of Molecular Sulphur by Methanogenic Bacteria" 305 (5932). Nature Publishing Group: 309–11. doi:10.1038/305309a0.

Steudel, Ralf, Thomas Göbel, and Gabriele Holdt. 1989. "The Molecular Nature of the Hydrophilic Sulfur Prepared From Aqueous Sulfide and Sulfite (Selmi Sulfur Sol)." *Zeitschrift Für Naturforschung. B, a Journal of Chemical Sciences* 44 (5). Verlag der

Zeitschrift für Naturforschung: 526–30.

Strapoc, Dariusz, Maria Mastalerz, Katherine Dawson, Jennifer Macalady, Amy V Callaghan, Boris Wawrik, Courtney Turich, and Matthew Ashby. 2011. "Biogeochemistry of Microbial Coal-Bed Methane." *Annual Review of Earth and Planetary Sciences, Vol 39* 39 (1): 617–56. doi:10.1146/annurev-earth-040610-133343.

Susanti, Dwi, and Biswarup Mukhopadhyay. 2012. "An Intertwined Evolutionary History of Methanogenic Archaea and Sulfate Reduction" 7 (9). Public Library of Science: e45313. doi:10.1371/journal.pone.0045313.

Tabb, David L, Christopher G Fernando, and Matthew C Chambers. 2007. "MyriMatch: Highly Accurate Tandem Mass Spectral Peptide Identification by Multivariate Hypergeometric Analysis.." *Journal of Proteome Research* 6 (2): 654–61. doi:10.1021/pr0604054.

Tavormina, Patricia L, Matthias Y Kellermann, Chakkiath Paul Antony, Elitza I Tocheva, Nathan F Dalleska, Ashley J Jensen, David L Valentine, et al. 2017. "Starvation and Recovery in the Deep-Sea Methanotroph Methyloprofundus Sedimenti.." *Molecular Microbiology* 103 (2): 242–52. doi:10.1111/mmi.13553.

Taylor, C D, B C McBride, R S Wolfe, and M P Bryant. 1974. "Coenzyme-M, Essential for Growth of a Rumen Strain of Methanobacterium-Ruminantium." *Journal of Bacteriology* 120 (2). American Society for Microbiology (ASM): 974–75.

Thomas, Dominique, and Yolande Surdin-Kerjan. 1997. "Metabolism of Sulfur Amino Acids in Saccharomyces Cerevisiae.." *Microbiology and Molecular Biology Reviews : MMBR* 61 (4). American Society for Microbiology: 503–32.

Thompson, Melissa R, Nathan C Verberkmoes, Karuna Chourey, Manesh Shah, Dorothea K Thompson, and Robert L Hettich. 2007. "Dosage-Dependent Proteome Response of Shewanella Oneidensis MR-1 to Acute Chromate Challenge.." *Journal of Proteome Research* 6 (5): 1745–57. doi:10.1021/pr060502x.

Trapnell, Cole, Adam Roberts, Loyal Goff, Geo Pertea, Daehwan Kim, David R Kelley, Harold Pimentel, Steven L Salzberg, John L Rinn, and Lior Pachter. 2012. "Differential Gene and Transcript Expression Analysis of RNA-Seq Experiments with TopHat and Cufflinks.." *Nature Protocols* 7 (3): 562–78. doi:10.1038/nprot.2012.016.

Trembath-Reichert, Elizabeth, David H Case, and Victoria J Orphan. 2016. "Characterization of Microbial Associations with Methanotrophic Archaea and Sulfate-Reducing Bacteria Through Statistical Comparison of Nested Magneto-FISH Enrichments.." *PeerJ* 4. PeerJ Inc.: e1913. doi:10.7717/peerj.1913.

Trüper, Hans G, and H G Schlegel. 1964. "Sulphur Metabolism in Thiorhodaceae I. Quantitative Measurements on Growing Cells ofChromatium Okenii." *Antonie Van Leeuwenhoek* 30 (1): 225–38. doi:10.1007/BF02046728.

Tumbula, Debra L, Ronald A Makula, and William B Whitman. 1994. "Transformation of Methanococcus Maripaludis and Identification of a PstI-Like Restriction System." *FEMS Microbiology Letters* 121 (3). The Oxford University Press: 309–14. doi:10.1111/j.1574-6968.1994.tb07118.x.

Ullrich, T C, M Blaesse, and R Huber. 2001. "Crystal Structure of ATP Sulfurylase From Saccharomyces Cerevisiae, a Key Enzyme in Sulfate Activation.." *The EMBO Journal* 20

(3). EMBO Press: 316–29. doi:10.1093/emboj/20.3.316.

Verschueren, Koen HG, and Anthony J Wilkinson. 2005. *Sulfide: Biosynthesis From Sulfate*. Chichester, UK: John Wiley & Sons, Ltd. doi:10.1038/npg.els.0001405.

Wang, Feng-Ping, Yu Zhang, Ying Chen, Ying He, Ji Qi, Kai-Uwe Hinrichs, Xin-Xu Zhang, Xiang Xiao, and Nico Boon. 2014. "Methanotrophic Archaea Possessing Diverging Methane-Oxidizing and Electron-Transporting Pathways.." *Isme Journal* 8 (5): 1069–78. doi:10.1038/ismej.2013.212.

Wegener, Gunter, Viola Krukenberg, Dietmar Riedel, Halina E Tegetmeyer, and Antje Boetius. 2015. "Intercellular Wiring Enables Electron Transfer Between Methanotrophic Archaea and Bacteria." *Nature* 526 (7574). Nature Publishing Group: 587–90. doi:10.1038/nature15733.

Wegener, Gunter, Viola Krukenberg, S Emil Ruff, Matthias Y Kellermann, and Katrin Knittel. 2016. "Metabolic Capabilities of Microorganisms Involved in and Associated with the Anaerobic Oxidation of Methane." *Frontiers in Microbiology* 7 (17). Frontiers: 869. doi:10.3389/fmicb.2016.00046.

Westley, John. 1973. "Rhodanese." In *Advances in Enzymology and Related Areas of Molecular Biology*, edited by Alton Meister, 39:327–68. Hoboken, NJ, USA: John Wiley & Sons, Inc. doi:10.1002/9780470122846.ch5.

Whitman, William B, SeeHyang Sohn, SeungUk Kuk, and RuYe Xing. 1987. "Role of Amino Acids and Vitamins in Nutrition of Mesophilic Methanococcus Spp.." *Applied and Environmental Microbiology* 53 (10). American Society for Microbiology (ASM): 2373–78.

Yang, Jianyi, Renxiang Yan, Ambrish Roy, Dong Xu, Jonathan Poisson, and Yang Zhang. 2015. "The I-TASSER Suite: Protein Structure and Function Prediction." *Nature Methods* 12 (1): 7–8. doi:10.1038/nmeth.3213.

C h a p t e r 2

ARTIFICIAL ELECTRON ACCEPTORS DECOUPLE ARCHAEAL METHANE OXIDATION FROM SULFATE REDUCTION

Silvan Scheller[1], Hang Yu[1], Grayson L. Chadwick[1], Shawn E. McGlynn[1,2], and Victoria J. Orphan[1]

[1]Division of Geological and Planetary Sciences, California Institute of Technology, Pasadena, CA 91125, USA.

[2]Present Affiliation: Department of Biological Sciences, Tokyo Metropolitan University, Tokyo 192-0397, Japan and Biofunctional Catalyst Research Team, RIKEN Center for Sustainable Resource Science, Saitama 351-0198, Japan.

Originally published in Science, volume 351 issue 627 pages 703–7 (2016)

doi:10.1126/science.aad7154.

.

2.1 ABSTRACT

The oxidation of methane with sulfate is an important anaerobic microbial metabolism in the global carbon cycle. In marine methane seeps, this process is mediated by consortia of methanotrophic archaea (ANME) that live in syntrophy with sulfate-reducing bacteria (SRB). The underlying interdependencies within this uncultured symbiotic partnership are poorly understood. We used a combination of rate measurements and single-cell stable isotope probing to demonstrate that ANME in deep-sea sediments can be catabolically and anabolically decoupled from their syntrophic SRB partners using soluble artificial oxidants. The ANME still sustain high rates of methane oxidation in the absence of sulfate as the terminal oxidant, lending support to the hypothesis of interspecies extracellular electron transfer as the syntrohic mechanism for the anaerobic oxidation of methane.

2.2 REPORT

Biological methane oxidation in the absence of oxygen is restricted to anaerobic methanotrophic archaea (ANME) that are phylogenetically related to methanogens (*1, 2*). These organisms evolved to carry out C1-metabolism from methane to CO_2 near thermodynamic equilibrium ($E^{\circ\prime}$ = -245 mV for CH_4/CO_2) via the pathway of reverse methanogenesis (*3*), which includes the chemically challenging step of methane activation without oxygen-derived radicals (*4*). Reported terminal electron acceptors for anaerobic oxidation of methane (AOM) include sulfate (*1, 2*), nitrate (*5*), and metal oxides (*6*). The recently described process of nitrate reduction coupled to methane oxidation was shown to be directly mediated by a freshwater archaeal methanotroph 'Methanoperedens nitroreducens' ANME-2d (*5*); however, the electron transport mechanism coupling methane oxidation with other terminal electron acceptors (e.g. sulfate and metal oxides) is still debated [e.g. (*7-9*)].

Sulfate-coupled methane oxidation (eq. 1) is the dominant mechanism for methane removal within marine sediments, preventing the release of teragrams per year of this greenhouse gas from the oceans (*10*).

$$CH_4 + SO_4^{2-} = HCO_3^- + HS^- + H_2O \quad \Delta G^{\circ\prime} = -17 \text{ kJ mol}^{-1} \quad (1)$$

Multiple methanotrophic archaeal lineages (ANME-1, ANME-2a,b,c and ANME-3) form syntrophic consortia with sulfate-reducing deltaproteobacteria (SRB) that drive AOM in areas of methane release at the seabed (*11*). The metabolism of AOM with sulfate appears to be partitioned between the two partners, requiring exchange of electrons or intermediates. The mechanism underlying this syntrophic association has been studied using microcosm experiments, with AOM microorganisms exhibiting doubling times of 2-7 months (*12-17*), as well as through the application of stable isotope analyses (*2*), radiotracer rate measurements (*18*), metagenomics (*3, 5, 19, 20*) and theoretical modeling (*21, 22*).

Attempts to metabolically decouple the syntrophic association and identify the intermediate compound passaged between ANME archaea and their SRB partners have been unsuccessful using diffusive intermediates such as hydrogen, acetate, formate, and some redox active organic electron shuttles (*16, 23*). Culture-independent evidence for direct interspecies electron transfer in sulfate-coupled AOM by members of the ANME and their SRB partners (*8, 9*), supports earlier genomic predictions of this process occurring in the methanotrophic ANME-1 (*19*).

Guided by the recent evidence of direct interspecies electron transfer from ANME-2 to SRB (*8*), we probed whether artificial electron acceptors can substitute for the role of the SRB partner as a terminal oxidant for AOM. Respiration of the artificial electron acceptor 9,10-anthraquinone-2,6-disulfonate (AQDS, E°' = -186 mV) has been previously reported in methanogens [e.g. (*24*)]. We tested AQDS as a sink for methane-derived electrons generated by the ANME archaea in incubations with deep-sea methane seep sediment. The stoichiometry of methane oxidation coupled to AQDS predicts the reduction of 4 equivalents of AQDS per methane (eq. 2).

$$CH_4 + 4\ AQDS + 3\ H_2O = HCO_3^- + H^+ + 4\ AQH_2DS \quad \Delta G^{\circ\prime} = -41\ kJ\ mol^{-1} \quad (2)$$

To quantify AOM with AQDS, we performed anaerobic microcosm experiments using methane seep sediment from the Santa Monica basin that had been rendered sulfate- and sulfide-free (*25*) and amended with 50 μmol AQDS and ^{13}C-labeled methane [0.35 MPa (*25*)]. After a 21-day incubation at 4 °C, approximately 12.5 μmol dissolved inorganic carbon (DIC) formed from the ^{13}C-methane (Fig. 1A), concomitant with the reduction of AQDS close to the predicted 1:4 stoichiometry (Table S1). The initial rates of AOM with AQDS were equivalent to the rates measured with sulfate over the first 6 days (Fig. 1B), and later diverged as the AQDS was depleted from solution. At 22.5 °C, where AQDS has a higher solubility (Table S2), the AOM rates with AQDS exceeded those with sulfate (Fig. S3).

To confirm that the observed methane oxidation with AQDS was not coupled to traces of sulfate, we tracked AOM in the presence of sodium molybdate, a competitive inhibitor for sulfate reduction (*26*). With the addition of 25 mM molybdate, rates of sulfate-coupled AOM decreased by approximately 5-fold relative to controls, consistent with previous reports (*16*). Notably, the high rates of methane oxidation in our sulfate-free incubations containing AQDS showed no inhibitory response if molybdate was included, indicating a decoupling of AOM from sulfate-reduction (Fig. 1A+B).

Stimulation of AOM without sulfate is not restricted to AQDS. Regioisomers of AQDS (1,5-AQDS and 2,7-AQDS), humic acids, and soluble iron(III)-complexes (ferric citrate and ferric-EDTA) also stimulated anaerobic oxidation of methane at rates that were at least 0.1 μmol cm^{-3} d^{-1} (Fig. 1B; a list of all oxidants tested is provided in Table S3). In control incubations without an added electron acceptor, we measured a small apparent methane oxidation activity (1.5% relative to sulfate-coupled AOM, Fig. 1B) that is likely attributed to enzyme catalyzed isotope exchange between methane and DIC without net methane oxidation (*27, 28*). In killed control experiments (formaldehyde addition), we did not detect any conversion of ^{13}C-methane to DIC (Fig. 1B).

The archaeal 16S rRNA gene diversity of the seep sediment used in our AOM microcosm experiments was dominated by ANME-2 of the subgroups ANME-2a and ANME-2c, with a low relative abundance of ANME-1 phylotypes (Fig. S4). To identify the active archaea potentially involved in methane oxidation in our experiments, we sequenced expressed archaeal 16S rRNA and the alpha subunit of the methyl coenzyme M reductase (mcrA) after 4 weeks from the sulfate, AQDS, and no added electron acceptor microcosm treatments. The archaeal sequences recovered from the 16S rRNA and mcrA cDNA clone libraries were similar in the 3 treatments, with each containing only representatives of ANME-2a, and 2c (Fig. 2). The detection of transcripts from multiple subgroups of ANME-2 in each treatment suggest that the same ANME lineages are active in AOM, independent of whether sulfate or AQDS is supplied as the oxidant. In contrast to

the similar ANME composition, the relative abundance of recovered bacterial SEEP-SRB1 clones in the cDNA libraries decreased in treatments lacking sulfate compared to microcosms supporting active sulfate-coupled AOM (Table S4), and suggest that ANME may be capable of utilizing AQDS directly without syntrophic interaction.

To directly test this hypothesis, we used cell-specific stable isotope analysis to quantify the anabolic activity of ANME-2 (including ANME-2c) and their co-associated syntrophic partners in consortia recovered from incubations supplied with different oxidants (including sulfate, AQDS, humic acids, and ferric iron). Using $^{15}NH_4^+$ stable isotope probing combined with fluorescence *in situ* hybridization and nanoscale secondary ion mass spectrometry (FISH-SIMS (*2*)), we measured the cell specific anabolic activity (^{15}N cellular enrichment) for paired ANME and SRB populations in consortia (*8*). After 18 days of incubation with $^{15}NH_4^+$, consortia were phylogenetically identified by FISH using ANME-2c and Desulfobacteraceae-targeted oligonucleotide probes, and analyzed by nanoSIMS to quantify the assimilation of $^{15}NH_4^+$ for each paired population of ANME-2 and SRB (*25*).

In AOM microcosms containing sulfate, the $^{15}NH_4^+$ assimilation by co-associated bacteria and archaea in consortia from 2 sets of experiments (n=20 and n=19 consortia) was positively correlated at approximately 1:1, indicating balanced syntrophic growth during AOM similar to (*8*); (Fig. 3C and Fig. 4A+B). ANME-SRB consortia recovered from sulfate-free incubations amended with AQDS also showed high levels of $^{15}NH_4^+$ assimilation, however, in this case, anabolic activity within each of these consortia occurred only in the ANME archaea and not in their co-associated bacterial partners (Fig. 3F and Fig. 4A). This is consistent with the weak FISH signal observed for the Desulfobacteraceae. These data offer direct validation of results based on RNA analysis, demonstrating that when AQDS is supplied as the terminal electron acceptor for AOM, the ANME-2 archaea (directly shown for ANME-2c (n=10) and inferred for ANME-2a based on nanoSIMS results from the 9 non-ANME-2c aggregates that were all anabolically active) sustain active biosynthesis that is decoupled from the activity of the SRB partner. Consortia from

incubations with methane and $^{15}NH_4^+$ but lacking an electron acceptor showed no measurable anabolic activity in either partner (n=9 ANME-SRB consortia; Fig. 4A inset, and Fig. S5).

Notably, the ANME cells paired with SRB in consortia from AQDS incubations showed similar levels of anabolic activity [3.3 months doubling time based on average ^{15}N incorporation (*25*)] as ANME archaea conserving energy through conventional sulfate-coupled AOM [2.9 months doubling time (*25*)] in parallel incubations, suggesting equivalent potential for growth (Fig. 4A). Apparently, ANME-2 archaea are capable of conserving energy for biosynthesis independent of sulfate availability and, importantly, separated from the activity of their syntrophic bacterial partners.

AOM incubations with iron(III)-citrate and humic acids as the alternative electron acceptors also demonstrated exclusive biosynthetic activity of ANME-2c and other ANME-2 cells (Fig. 4B and Fig. S6). In contrast to incubations with sulfate or AQDS, only a few, and mostly small AOM consortia [14/31 for iron(III)-citrate and 4/46 for humic acids] were anabolically active [>10% archaeal activity relative to cells in the sulfate treatments, or >0.8 atom% ^{15}N], despite the high rates of AOM measured with those compounds (Fig. 1B).

All compounds that were able to replace the role of the SRB partners during AOM, including AQDS-isomers, humic acids, and iron(III)-complexes, have the ability to accept single electrons. Mechanistically, extracellular electron transfer (*8, 9*) from ANME-2 to single electron acceptors can account for all our findings. Large, S-layer associated multi-heme *c*-type cytochromes in members of the ANME-2 (*8*) putatively conduct electrons [discussed in (*29*)] derived from reverse methanogenesis from the archaeal membrane to the outside of the cell, where they can be taken up by a suitable electron acceptor. A congruent path of extracellular electron transfer has been proposed for the bacterium *Geobacter sulfurreducens* when oxidizing acetate coupled to the reduction of AQDS or humic acids (*30*). The similar catabolic and anabolic activities observed within ANME-2 archaea, independent of whether the terminal electron acceptor is AQDS or sulfate, suggest that the biochemistry

within these organisms may follow the same pathway under AQDS-conditions as when syntrophically coupled to sulfate-reducing bacteria. Our data therefore also lend experimental evidence in support of the hypothesis of direct interspecies electron transfer as the syntrophic coupling mechanism between methane-oxidizing ANME-2 and SRB in the environment (*8*).

The apparent ability of ANME-2 to oxidize methane via release of single electrons constitutes a versatile half-metabolism. This physiology suggests that methanotrophic ANME-2 archaea should also be able to respire solid electron acceptors directly via extracellular metal reduction, which would explain methane oxidation coupled to insoluble iron(III) and manganese(IV) reduction reported previously (*6*). Evolutionarily, methane oxidation with metal oxides could have served as a transient life-style for ANME prior to the establishment of a syntrophic association with SRB. According to this hypothesis, methanogenic archaea first evolved the capability to conserve energy as a methanotroph coupled with respiration of solid metal oxides as electron acceptors. In a subsequent evolutionary step, SRB developed a symbiosis with ANME archaea, gaining a direct source of electrons for sulfate reduction and leading to the highly structured syntrophic consortia common today in seep environments. This physiology of using extracellular electron transfer to enable syntrophic interaction (*8, 9*) has the advantage that intermediates cannot be lost due to diffusion, and that electrical conductance is much faster than diffusive transfer of reducing equivalents (*8*). Further, this described metabolism may have industrial utility, providing a mechanism for conversion of methane to CO_2 + single electrons that can be catalyzed reversibly at low temperatures with potential to convert methane to electricity at high overall efficiencies. Finally, these findings offer a promising path forward for isolating members of the ANME-2 in pure culture, enabling detailed characterization of the ecophysiology of these key players in the global methane cycle.

2.3 FIGURES

Fig. 1: DIC production per vial in incubations with 1.0 cm^{-3} methane seep sediment. A Methane oxidation coupled to sulfate-reduction (140 µmol SO_4^{2-} (28 mM), methane oxidation unlimited, • symbol). Methane oxidation coupled to AQDS reduction (50 µmol AQDS (10 mM) in the absence of sulfate, Δ symbol). Due to the 1:4 stoichiometry between CH_4, and AQDS, the amount of DIC formed plateaus at approximately 12.5 µmol (dashed line). Open symbols depict incubations with the addition of the sulfate-reduction inhibitor sodium molybdate (25 mM). Control incubations without electron acceptors added (x symbol). **B** Initial rates of methane oxidation with different electron acceptors for individual incubation bottles. Values from linear regression of time points 1-6 days (4 points) are calculated per cm^3 wet sediment, error bars represent 95% confidence interval. Time course measurements for these experiments are provided in Fig. S1; raw data is provided in Fig. S2.

A

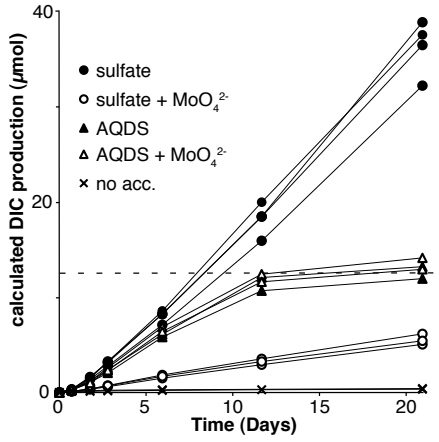

B

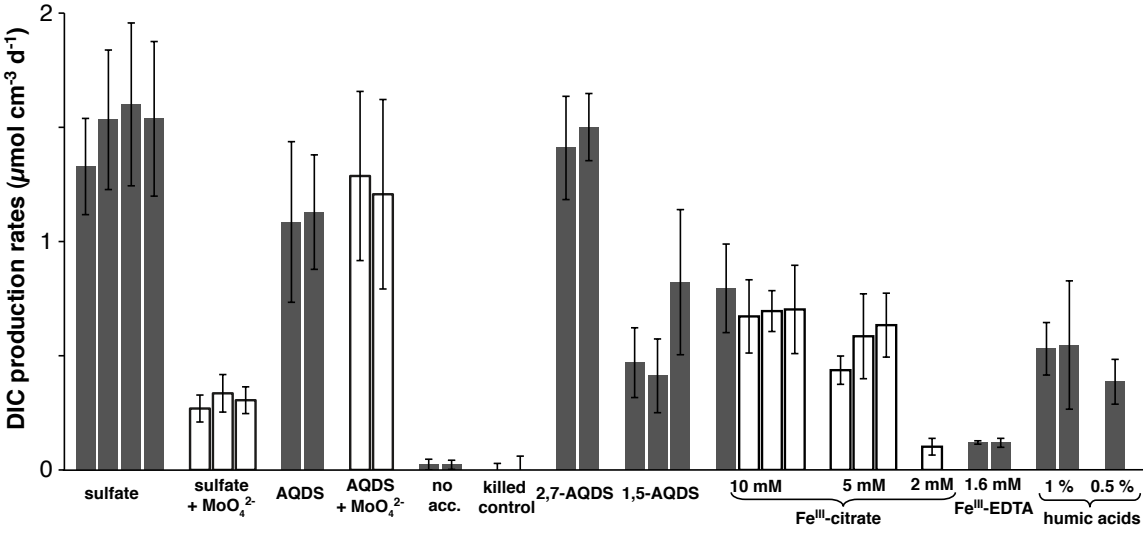
DIC production rates (µmol cm-3 d-1)
2
1
0
sulfate
sulfate + MoO4 2-
AQDS
AQDS + MoO4 2-
no acc.
killed control
2,7-AQDS
1,5-AQDS
10 mM
5 mM
2 mM
Fe III-citrate
1.6 mM
Fe III-EDTA
1 %
0.5 %
humic acids

Fig. 2: Bayesian phylogeny of expressed archaeal RNA recovered from different AOM microcosms. 16S rRNA (left) and mcrA (right) transcripts obtained from AOM incubations with either sulfate or AQDS as the primary oxidant or no electron acceptor added. Numbers at major nodes represent Bayesian likelihood values. Scale bars represent estimated sequence divergence or amino acid changes.

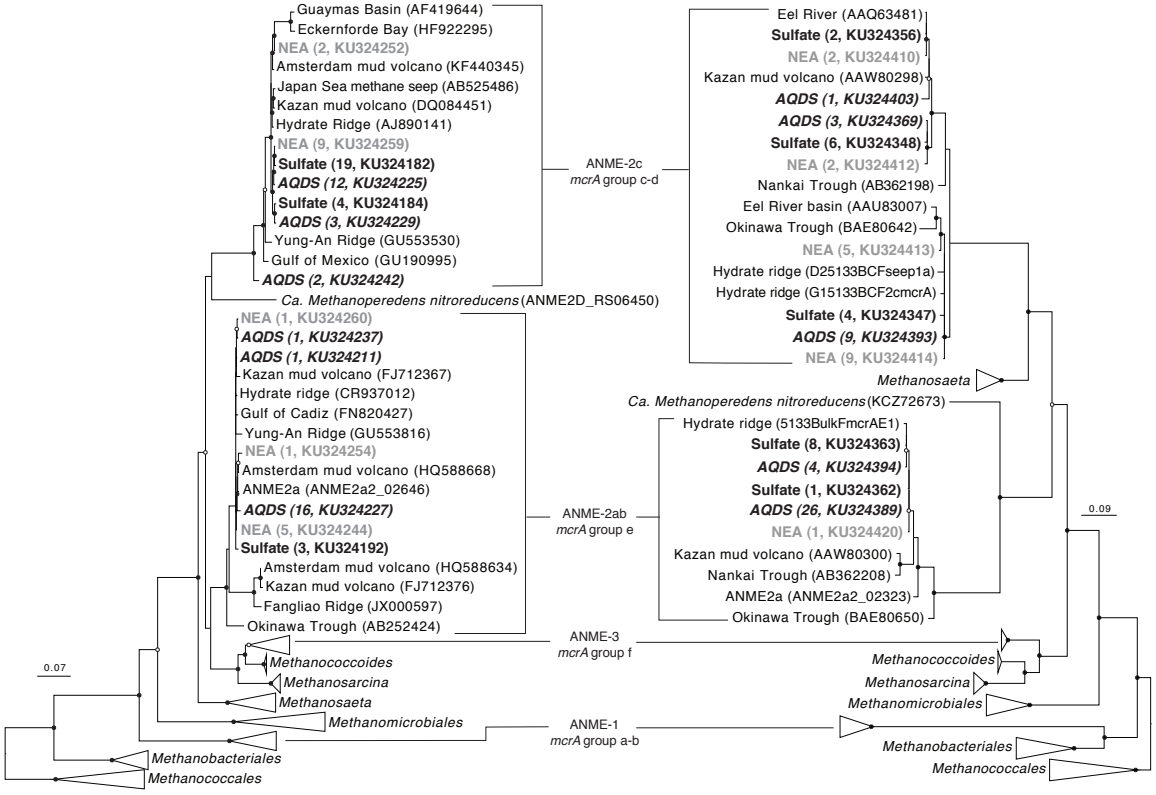

Fig. 3: Representative FISH-nanoSIMS images from sulfate and AQDS microcosms. Correlation between phylogenetic identity (FISH) and anabolic activity (^{15}N enrichment) for example consortia of ANME-2 archaea and sulfate-reducing bacteria analyzed from AOM incubations amended with sulfate or AQDS. **A-C**: AOM consortium from microcosm with sulfate; **D-F**: Consortium from microcosm with AQDS as the sole electron acceptor. In each case, the atom percent ^{15}N isotope enrichment was calculated from ratios of secondary ion images of $^{12}C^{15}N^-$ and $^{12}C^{14}N^-$. **Panels A & D**: FISH images, ANME-2c (in red), Desulfobacteraceae (in green), note the FISH signal for the bacterial cells in panel D is weak likely due to the low abundance of cellular rRNA in SRB in the AQDS treatment without sulfate. **Panels B & E**: nanoSIMS ion image of $^{12}C^{14}N^-$ for cellular biomass, linear scale; **Panels C & F**: fractional abundance of ^{15}N (in AT%) as a proxy for anabolic activity.

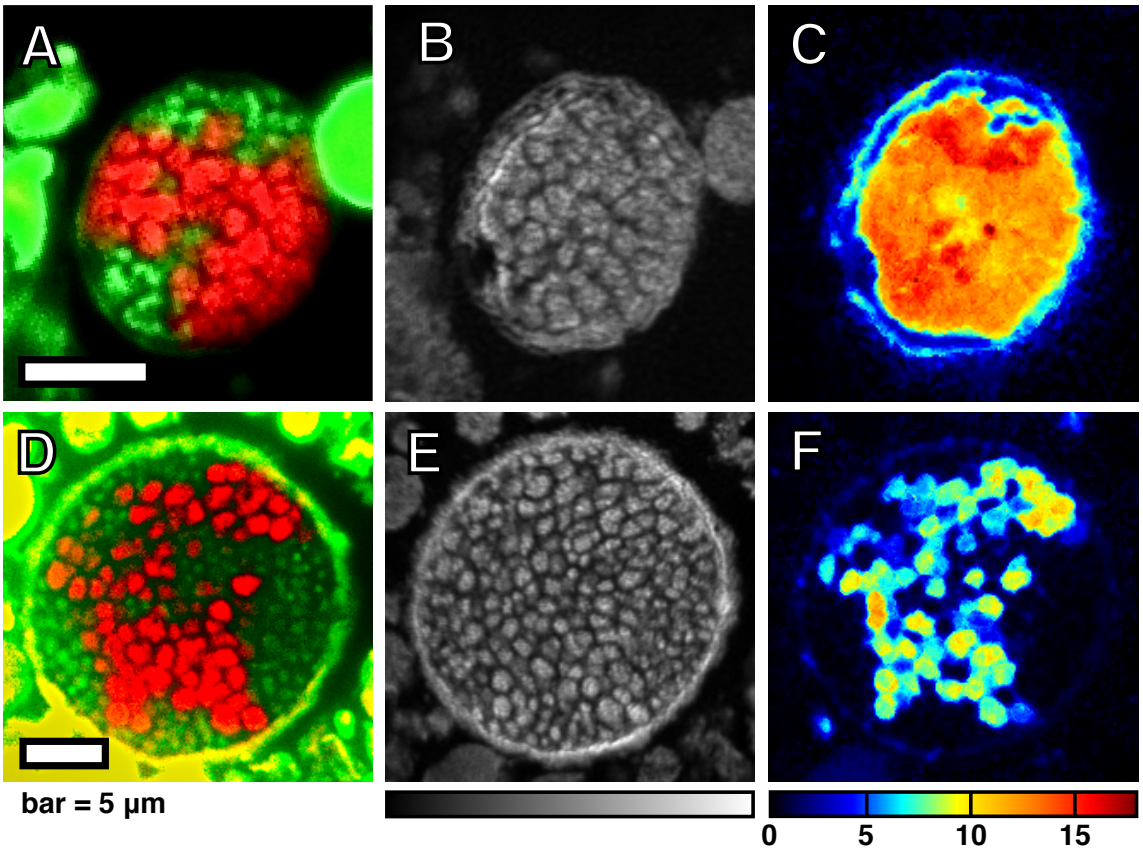

Fig. 4: Summary of FISH-nanoSIMS ^{15}N incorporation data. Average anabolic activity for paired ANME and SRB population in each AOM consortia from incubations with different terminal electron experiments. Each symbol represents the average ^{15}N atom percent for the population of paired ANME cells relative to bacterial cells in a single consortium. Inset: ^{15}N atom percent values close to natural abundance value (0.36 AT% ^{15}N). FISH-nanoSIMS images of consortia marked with an arrow are displayed in Fig 3, Fig. S5+S6. Note: Panel A and B constitute 2 independent sets of experiments, experiments in A contained ca. 80% $^{15}NH_4^+$, while B contained ca. 40% (*25*). Numeric data for each aggregate is provided in Table S5. The activity of bacterial cells (b) relative to the archaeal cell activity (a) was determined via linear regression: **A**: sulfate: b=0.97a + 2.17, R^2=0.75; AQDS: b=0.070a + 0.39, R^2=0.69. **B**: sulfate: b=1.09a + 1.07, R^2=0.74; Iron citrate: b=0.28a + 0.25, R^2=0.71; Humic acids: b=0.21a + 0.29, R^2=0.60. The data point in brackets (Panel A) was not included for the linear regression (see Fig. S7 for single cell analysis and further discussion). The small apparent ^{15}N enrichment in bacteria from Panel A (n=19 consortia) was found to be due to inaccuracies in pixel assignments for SRB cells during data processing, determined by manual inspection of each nanoSIMS image.

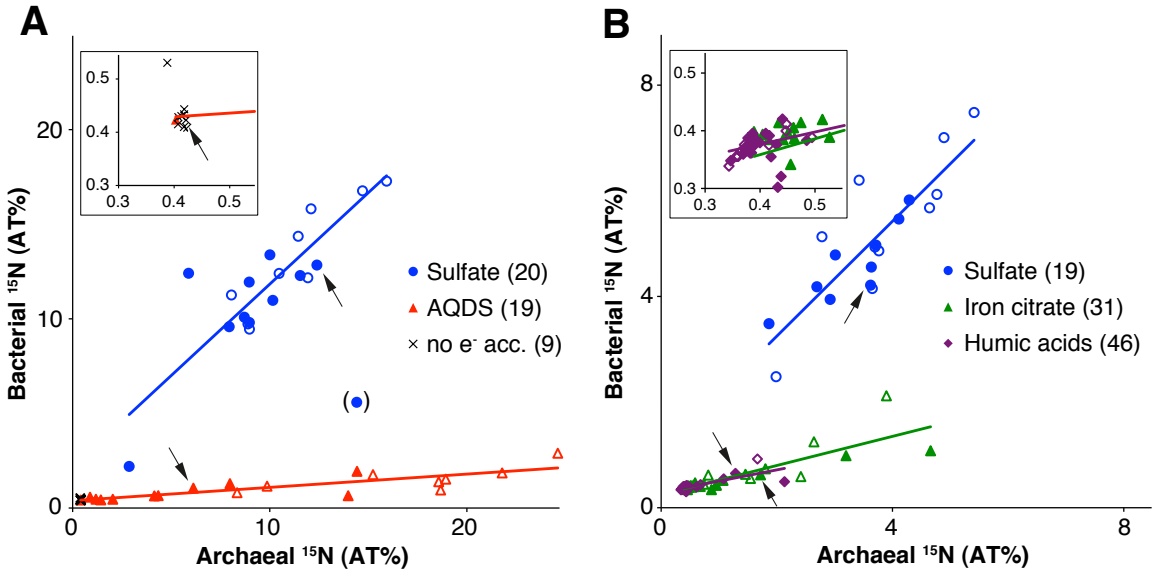

Fig. S1: AOM with different oxidants. Time courses for rates described in Fig. 1B (red curves); AOM rates with sulfate are included as a reference (blue curves, representing identical data as shown in Fig. 1A).

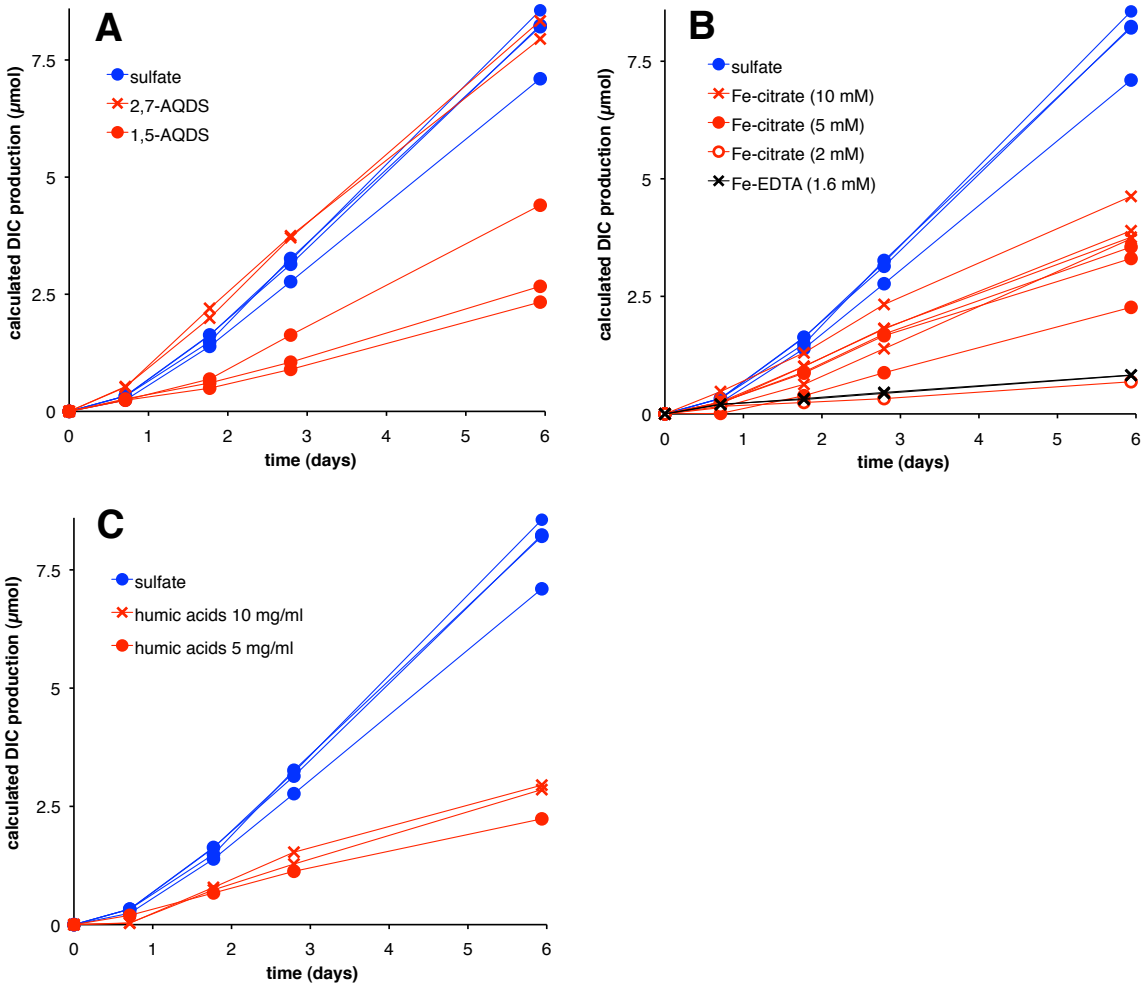

Fig. S2: Comparison of raw data and calculated concentrations of DIC. Data for two replicate incubations with sulfate-coupled AOM (Table S3, incubations "Sulfate [28 mM] A+B") that are used for Fig. 1A and Table S1B are shown as examples. **A**: Time course of AT% ^{13}C measured in DIC. **B**: Calculated concentrations of total (black) and newly formed (red) DIC (see methods). **Red**: Calculation used throughout this publication that yields the concentration of newly formed DIC. This method relies on knowing the AT% ^{13}C in the methane employed and the initial concentration and isotopic composition of DIC. **Black:** Independent method via standard addition that directly yields the absolute concentration of DIC for any time point. We employed this method to provide evidence for net DIC increase during incubations. This method does not account for the inorganic carbon present as gaseous CO_2 in the headspace.

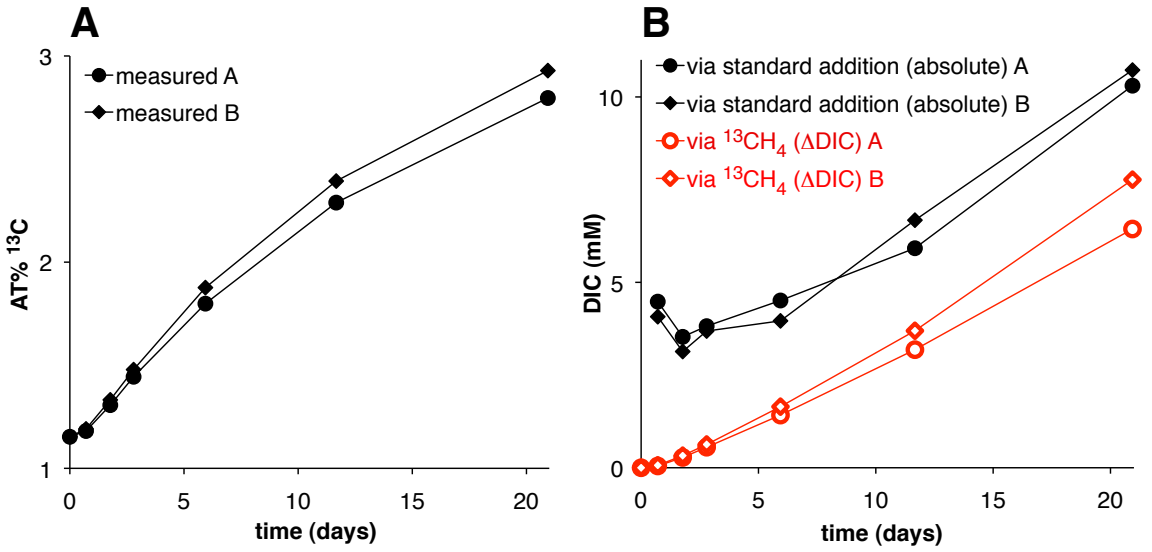

Fig. S3: Time course of AOM with sulfate and AQDS at 22.5 °C. Data from experiments at 4 °C included as a reference (• symbol, identical data as in Fig. 1A).

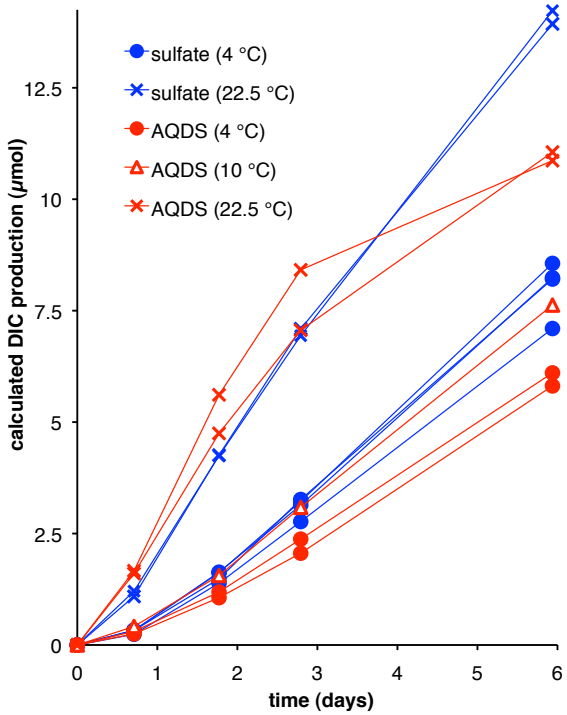

Fig. S4: Top 10 most abundant archaeal and bacterial genera in PC61. 16S rRNA gene Illumina TAG sequencing of the microbial assemblage in the initial PC61 sediment used for the microcosm experiments. Sequences were classified using the SILVA database release 119.

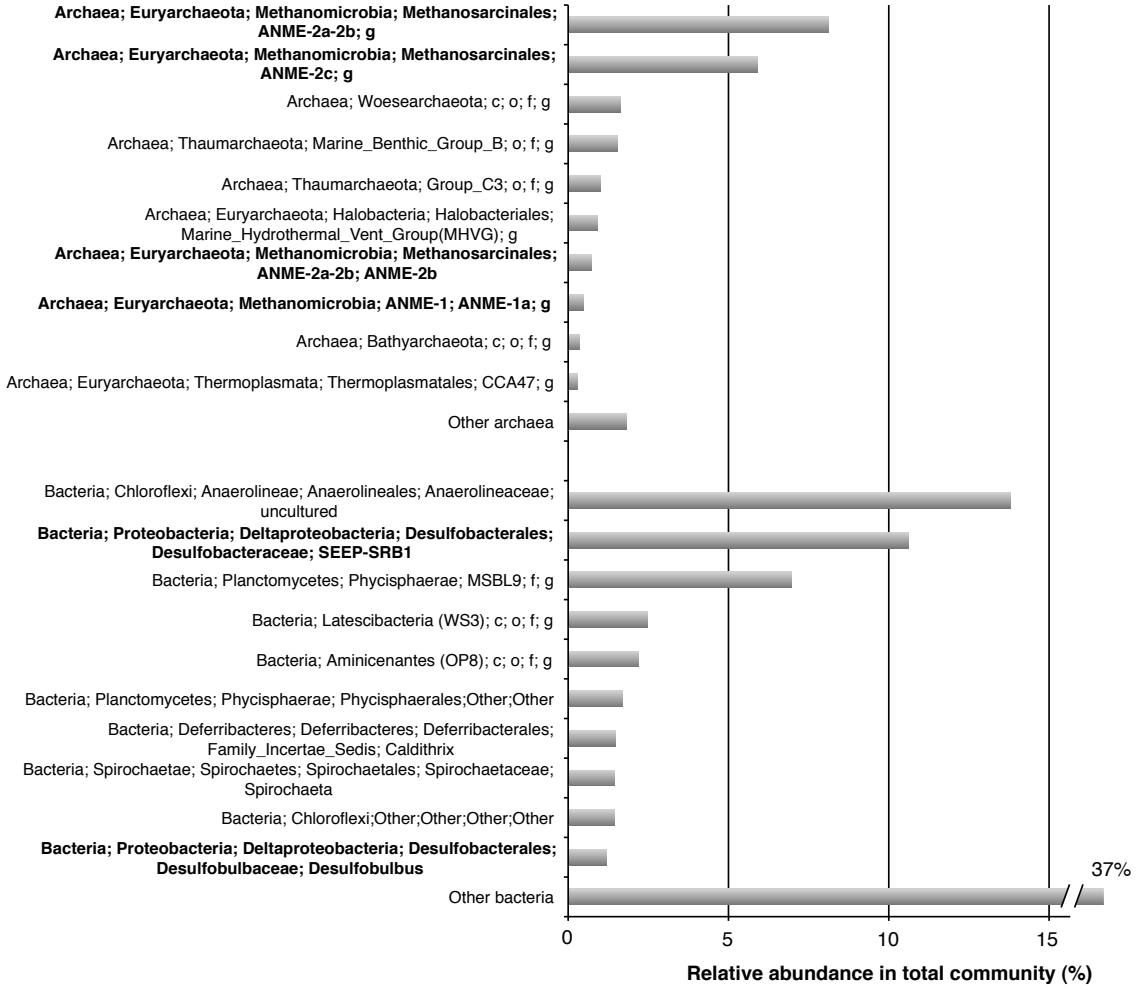

Fig. S5: Example FISH-nanoSIMS of consortium incubated without an oxidant. ANME-2c/ DSS consortium recovered from the microcosm treatment supplied with a methane headspace but no added electron acceptor. Data was acquired after 18 days of incubation in the presence of $^{15}NH_4^+$ (see Fig. 3A, inset). Panel **A**: FISH images, ANME-2c (in red), Desulfobacteraceae (in green). Panel **B**: nanoSIMS ion image of $^{12}C^{14}N^-$ showing cell biomass, linear scale. Panel **C**: fractional abundance of ^{15}N (in AT%) as a proxy for newly synthesized biomass.

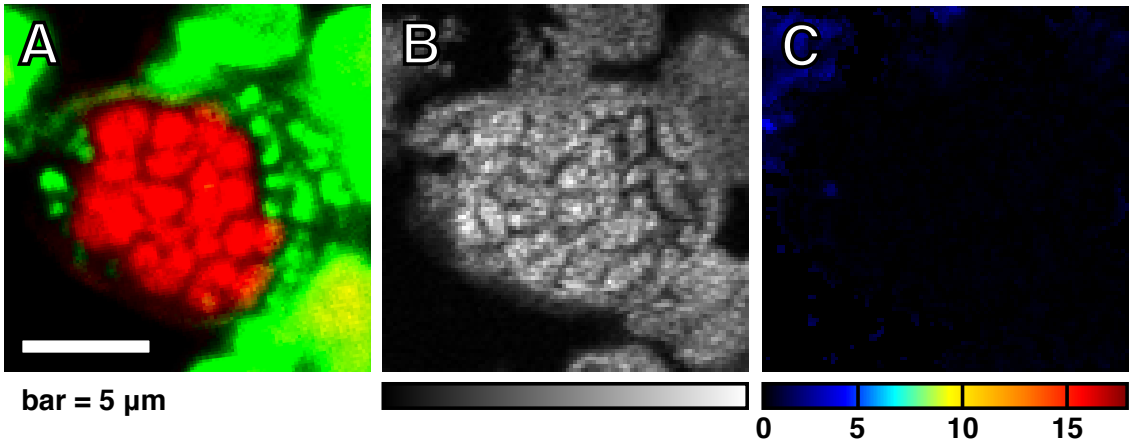

Fig. S6: FISH-nanoSIMS analysis of consortia incubated with different oxidants. Representative consortia recovered from a second set of experiments with PC61 (see Fig. 4B) incubated with ferric citrate, humic acids, or sulfate. Panels **A**-**C**: with sulfate; Panels **D**-**F**: with ferric citrate in the presence of the sulfate-reducing inhibitor sodium molybdate (25 mM); Panels **G**-**I**: with humic acids as the oxidant. Panels **A** & **D** & **G**: FISH images, ANME-2c (in red), Desulfobacteraceae (in green); for panel A DAPI image (in blue) included. Scale bar = 5 μm for all FISH images. Panels **B** & **E** & **H**: nanoSIMS ion image of $^{12}C^{14}N^-$ showing cell biomass, linear scale. Panel **C** & **F** & **I**: fractional abundance of ^{15}N (in AT%) measured by nanoSIMS as a proxy for newly synthesized biomass. Here, the minimum value on the scale was set to 0.3 AT% (black), close to the natural abundance ^{15}N (0.36 AT%).

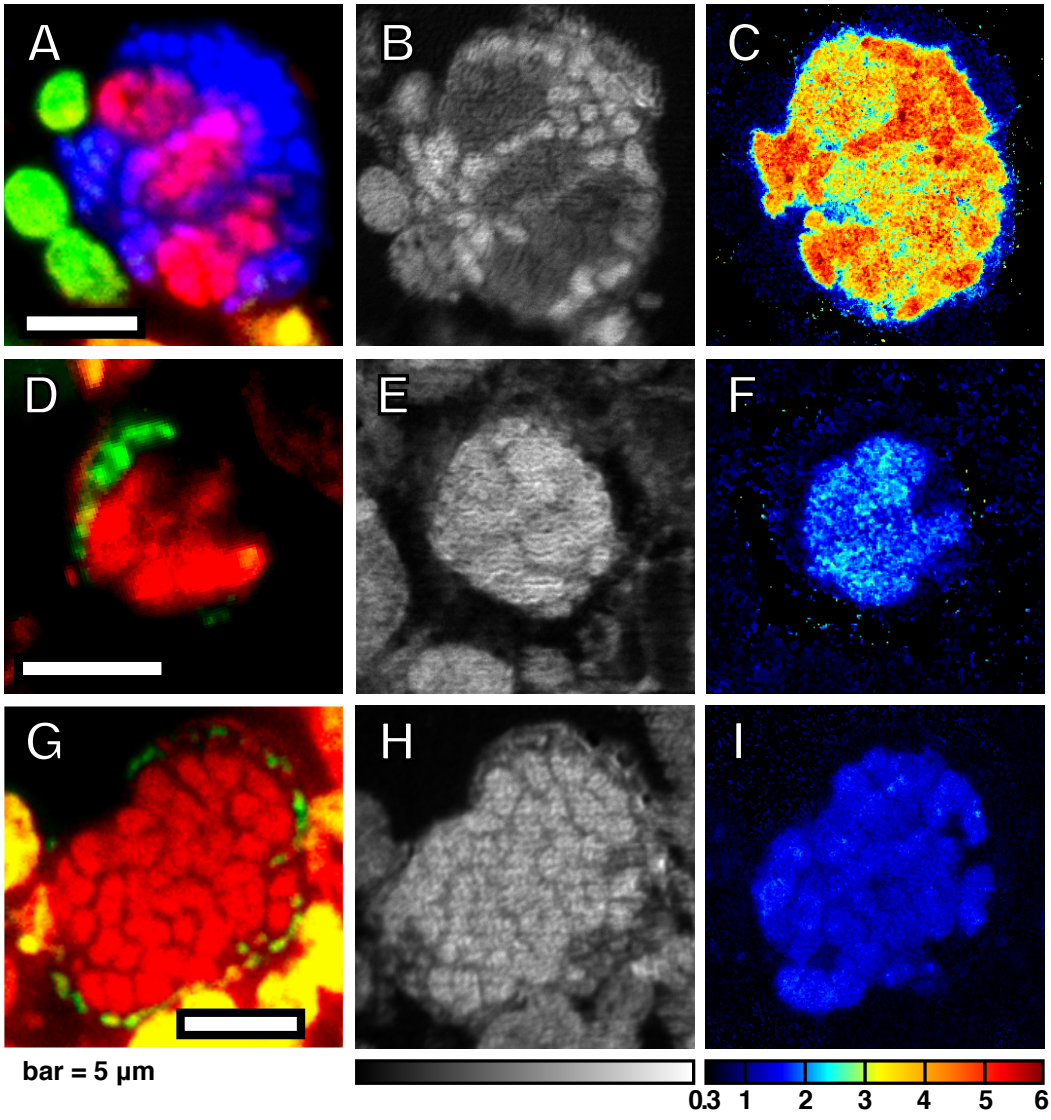

Fig. S7: FISH-nanoSIMS data from the outlier ANME-2c consortium. This consortium was excluded from the activity correlation (see Fig. 4A).* Panel **A**: FISH images, ANME-2c (in red), Desulfobacteraceae, DSS (in green), DAPI (in blue). Panel **B**: nanoSIMS ion image of $^{12}C^{14}N^-$ showing cell biomass, linear scale. Panel **C**: fractional abundance of ^{15}N (in AT%) as a proxy for newly synthesized biomass.

* The low ratio of bacterial/archaeal ^{15}N incorporation (ratio = 0.386) for incubations with sulfate is represents an outlier from all other analyzed consortia from this treatment as well as our previously published FISH-nanoSIMS experiments. For this reason, we excluded this ANME-2c aggregate (with an unidentified bacterial partner) from the linear regression of the overall activities displayed in Fig. 4A.

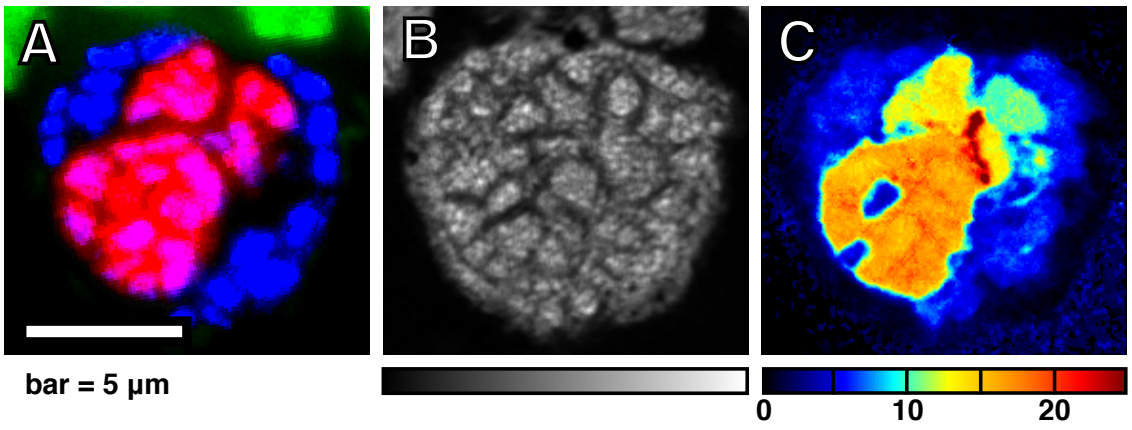

Table S1: Final concentration of reduced electron acceptors AQH_2DS and sulfide. Concentrations measured after a 21 day incubation (experiments in Fig. 1A) and calculated stoichiometry per DIC formed from methane.

A) Final concentrations of reduced AQDS (AQH_2DS):

Experiment	DIC formed [mM]	AQH_2DS [mM]	Stoichiometry*
AQDS 10 mM	2.39	8.6	3.60
AQDS 10 mM	2.64	9.6	3.62
AQDS 10 mM + MoO_4^{2-} 25 mM	2.82	9.8	3.45
AQDS 10 mM + MoO_4^{2-} 25 mM	2.59	9.2	3.55

* The lower amount of AQH_2DS found than expected (4:1 stoichiometry) may be attributed to partial oxidation during the process of sampling and titration.

B) Final concentrations of sulfide:

Experiment	DIC formed [mM]	sulfide [mM]*	Stoichiometry†
Sulfate 28 mM (A)	6.44	5.9	0.92
Sulfate 28 mM (B)	7.77	6.5	0.84
Sulfate 28 mM (C)	7.51	7.0	0.93
Sulfate 28 mM (D)	7.29	6.1	0.84

* sulfide [mM] = sum of HS^- and H_2S.

† The lower amount of aqueous sulfide measured relative to the expected 1:1 stoichiometry may be attributed to a combination of factors resulting in a loss of sulfide. These include some sulfide partitioning into the headspace as gaseous H_2S and possibly escaping as gaseous H_2S during sampling, partial sulfide oxidization during the sampling and centrifugation on the benchtop, or possibly precipitation with divalent cations during the incubation.

Table S2: Solubility of different AQDS regioisomers in the incubation medium.

Compound	4 °C	22.5 °C
2,6-AQDS (AQDS)	0.9 mM	1.9 mM
2,7-AQDS	>25 mM	>25 mM
1,5-AQDS	2.5 mM	not determined

Table S3: List of all oxidants tested for AOM. The percentage AOM rates are reported relative to sulfate-coupled AOM (1.50 µmol cm^{-3} day^{-1}). **Top**: Summary of compounds described in Fig. 1B; **Bottom**: Oxidants resulting in an AOM rate less than 0.10 µmol cm^{-3} day^{-1} (< 7% rel. to sulfate as oxidant).

Oxidant [conc.], replicates	E°' (mV)	Addition of 25 mM MoO_4^{2-}	Rate relative to AOM with sulfate (%)
Sulfate [28 mM] A,B,C*,D	-220	−	100
Sulfate [28 mM] E,F,G		+	20
AQDS [10 mM] A,B	-186 (*36*)	−	74
AQDS [10 mM] C,D		+	83
No oxidant A,B		−	1.5 †
No oxidant + H_2CO (4%) A,B		−	0
2,7-AQDS [10 mM] A,B	-185 (*36*)	−	97
1,5-AQDS [10 mM] A,B,C	-175 (*36*)	−	38
Fe(III)-citrate [10 mM] A	372 (*52*)	−	53
Fe(III)-citrate [10 mM] B*,C,D		+	46
Fe(III)-citrate [5 mM] A,B,C		+	37
Fe(III)-citrate [2 mM]		+	7
Fe(III)-EDTA [1.6 mM] A,B	96 (*53*)	−	8
Humic acids [1%] A*,B	n.a.‡	−	36
Humic acids [0.5%]		−	26
Melanin [8 mg/ml]	n.a.‡	+	6.4 §
Melanin [2 mg/ml]		+	4.3
Melanin [0.5 mg/ml]		+	2.6
Fe(III)-citrate [25 mM]	372 (*52*)	+	2.5
Fe(III)-NTA [1 mM]		−	2.5
Fe(III)-NTA [10 mM]	385 (*52*)	−	≤ 1.5 †
Fe(III)-EDTA [10 mM] A,B	96 (*53*)	−	≤ 1.5 †
Phenazine methosulfate [1 mM]	80 (*54*)	−	≤ 1.5 †
Methylene blue [1 mM]	11 (*54*)	−	≤ 1.5 †
Indigo tetrasulfonate [10 mM; 1 mM]	-46 (*54*)	−	≤ 1.5 †
Resazurin [10 mM]	-51 (*55*)	−	≤ 1.5 †
1-Hydroxynaphthoquinone [10 mM; 1 mM]	-137 (*54*)	−	≤ 1.5 †
Phenosafranine [10 mM; 1.6 mM]	-252 (*54*)	−	≤ 1.5 †
Safranine T [10 mM; 1.6 mM]	-289 (*54*)	−	≤ 1.5 †

* Replicate that was analyzed via nanoSIMS (see Fig. 4B and Fig. S6).

† No net methane oxidation can be deduced, because incubations without oxidant show an apparent AOM rate of 0.023 µmol cm^{-3} day^{-1} (1.5% relative to sulfate). This label conversion of $^{13}CH_4$ to ^{13}C-DIC arises via enzyme catalyzed isotope exchange between $^{13}CH_4$ and DIC without net methane oxidation [(*27, 28*), also discussed in main part and in the methods section].

‡ The midpoint reduction potentials of humic acids and melanin are not well defined. Both compounds can act as single electron acceptors due to their quinone moieties as shown experimentally for humic acids (*56*) and for melanin (*57*). The melanin used was a gift from Kenneth Nealson (University of Southern California) that is kindly acknowledged.

§ AOM occurs linearly, rates per wet sediment: with 8 mg/ml melanin: 0.096 ± 0.020 µmol cm^{-3} day^{-1}; with 2 mg/ml melanin: 0.064 ± 0.012 µmol cm^{-3} day^{-1}; with 0.5 mg/ml melanin: 0.039 ± 0.015 µmol cm^{-3} day^{-1}.

Table S4: Bacterial 16S rRNA diversity. Recovered from AOM microcosms supplied with sulfate, AQDS, or no added oxidant.

Bacterial 16S cDNA sequences recovered*	Oxidant		
	Sulfate	AQDS†	none
Proteobacteria/Deltaproteobacteria/Desulfobacterales_Desulfobacteraceae/SEEP-SRB1	**18**	**2**	**0**
Proteobacteria/Deltaproteobacteria/Desulfuromonadales/Desulfuromonadaceae_Pelobacter_2	2	3	0
Bacteroidetes/Sphingobacteriia_Sphingobacteriales_1/WCHB1-69	2	0	0
Chlorobi/Ignavibacteria_Ignavibacteriales/BSV26	2	0	0
Proteobacteria/Deltaproteobacteria/Desulfarculales_Desulfarculaceae/uncultured	2	0	0
Proteobacteria/Gammaproteobacteria_1/Pseudomonadales_Pseudomonadaceae/Pseudomonas_1	1	3	0
Chloroflexi/Anaerolineae_Anaerolineales_Anaerolineaceae/uncultured	1	1	1
Proteobacteria/Deltaproteobacteria/Sva0485	1	1	0
Acidobacteria/Subgroup 22	1	0	0
Candidate division OP8	1	0	1
Proteobacteria/Deltaproteobacteria/Sh765B-TzT-29	1	0	0
Proteobacteria_Deltaproteobacteria_Desulfobacterales_Nitrospinaceae/uncultured	1	0	0
Spirochaetae_Spirochaetes/Spirochaetales/Spirochaetaceae/Spirochaeta_2	0	9	1
Proteobacteria/Betaproteobacteria/Burkholderiales/Oxalobacteraceae/Herbaspirillum_1	0	4	0
Candidate division JS1	0	2	3
Proteobacteria/Epsilonproteobacteria/Campylobacterales_Helicobacteraceae/Sulfurimonas	0	2	1
Bacteroidetes/Flavobacteriia_Flavobacteriales/Flavobacteriaceae_1/Maritimimonas	0	1	0
Chloroflexi/Ardenticatenia/uncultured	0	1	1
Firmicutes_Clostridia_1/Clostridiales/Family XII/Fusibacter	0	1	0
Proteobacteria/Alphaproteobacteria/Rhizobiales_1/Brucellaceae/Ochrobactrum_1	0	1	0
Actinobacteria/Acidimicrobiia_Acidimicrobiales/OM1 clade	0	0	3
Bacteroidetes/BD2-2	0	0	2
Bacteroidetes/Bacteroidia_Bacteroidales/Porphyromonadaceae_4/uncultured	0	0	1
Candidate division WS3	0	0	1
Chloroflexi/Dehalococcoidia/GIF9	0	0	1
Lentisphaerae/B01R017	0	0	1
Planctomycetes/Phycisphaerae/MSBL9	0	0	1
Planctomycetes/Phycisphaerae/Phycisphaerales/AKAU3564 sediment group	0	0	1
Proteobacteria/Gammaproteobacteria_2/Chromatiales_Ectothiorhodospiraceae_Acidiferrobacter	0	0	1
Spirochaetae_Spirochaetes/Spirochaetales/Leptospiraceae/uncultured	0	0	1
TOTAL NUM OF CLONES	33	31	21

* Data based on 16S cDNA clone libraries.

† PCR amplification and cloning of bacterial cDNA from the AQDS treatment was challenging due to weak amplification, few insert containing clones, and chimeric sequences.

Table S5: nanoSIMS ^{15}N and ^{14}N total ion counts. Calculation of ^{15}N fractional abundance (anabolic activity proxy) for paired archaea (a) and bacteria (b) in consortia from all 6 incubation conditions supplied with $^{15}NH_4^+$.

Set 1: Sulfate	a ^{14}N counts	a ^{15}N counts	b ^{14}N counts	b ^{15}N counts	a ^{15}N fraction	b ^{15}N fraction
1	8186903	910346	4986312	770403	0.1001	0.1338
2*	13234012	2228293	9988379	591393	0.1441	0.0559
3	1017392	100206	4734445	514724	0.0897	0.0981
4	10447750	1350011	16572950	2779724	0.1144	0.1436
5	2896866	327406	4306194	530991	0.1015	0.1098
6	5173791	509800	10152972	1060263	0.0897	0.0946
7	8069719	1053146	10253054	1436464	0.1154	0.1229
8	9548875	1646186	11052811	2226646	0.1470	0.1677
9	15412698	1470548	7454752	836300	0.0871	0.1009
10	1254227	172559	434489	81620	0.1209	0.1581
11	523351	45850	455947	57855	0.0806	0.1126
12	586645	57716	467545	63416	0.0896	0.1194
13	9284639	274089	992128	22318	0.0287	0.0220
14	13355485	2529941	10646441	2223613	0.1593	0.1728
15	8150920	509359	7548831	1069396	0.0588	0.1241
16	9090606	1285688	3806417	560889	0.1239	0.1284
17	4446504	383623	2105270	223125	0.0794	0.0958
18	6543141	886483	4962457	687646	0.1193	0.1217
19	5192683	506817	3032520	326993	0.0889	0.0973
20	4772514	558378	5406186	765379	0.1047	0.1240
Set 1: AQDS						
1	6072396	126268	3174807	14796	0.0204	0.0046
2	6738562	291479	2337765	15076	0.0415	0.0064
3	4174136	678303	6944724	45479	0.1398	0.0065
4	4421657	39358	3701860	21362	0.0088	0.0057
5	9024087	1521364	2290624	45313	0.1443	0.0194
6	12497523	3481819	1829789	34577	0.2179	0.0185
7	14933629	1359298	5258297	43004	0.0834	0.0081
8	34700825	3797466	14097837	164882	0.0986	0.0116
9	1400937	5689	1219111	5187	0.0040	0.0042
10	4102974	1339454	656114	19576	0.2461	0.0290
11	1932351	87738	2609306	17195	0.0434	0.0065
12	5872808	85174	11129659	48086	0.0143	0.0043

13	21909385	1429092	16271732	172963	0.0612	0.0105
14	25267632	301796	14219942	66618	0.0118	0.0047
15	5632270	1292904	2895095	27853	0.1867	0.0095
16	27058715	4864118	7520936	135132	0.1524	0.0177
17	18133896	4135568	10299199	145195	0.1857	0.0139
18	23419015	5468125	7276084	112843	0.1893	0.0153
19	29832362	2586694	10923964	142677	0.0798	0.0129

Set 1: no oxidant

1	27743268	116427	26164833	108451	0.0042	0.0041
2	10368296	44295	5406673	22582	0.0043	0.0042
3	5725992	23424	2571274	10786	0.0041	0.0042
4	2337391	9594	1496614	6431	0.0041	0.0043
5	4006009	16847	2432421	10715	0.0042	0.0044
6	796822	3103	637887	3373	0.0039	0.0053
7	2168580	9002	913893	3964	0.0041	0.0043
8	2027340	8569	533112	2280	0.0042	0.0043
9	594977	2510	250708	1120	0.0042	0.0044

Set 2: Sulfate

1	8087694	305021	9201606	439261	0.0363	0.0456
2	14667860	628799	5998433	346787	0.0411	0.0547
3	15123316	455273	15751906	646736	0.0292	0.0394
4	6143931	236920	5971520	312392	0.0371	0.0497
5	6096641	123600	5619590	142946	0.0199	0.0248
6	910494	32272	655354	43321	0.0342	0.0620
7	4214918	158386	9693657	426387	0.0362	0.0421
8	33488023	1268969	15216001	658815	0.0365	0.0415
9	11309440	214881	7779576	280883	0.0186	0.0348
10	15482854	594463	5301457	275310	0.0370	0.0494
11	1786420	91861	1233988	92978	0.0489	0.0701
12	9145651	409931	3955885	244739	0.0429	0.0583
13	3867661	107011	1599231	69821	0.0269	0.0418
14	50990162	2917348	27076729	2189768	0.0541	0.0748
15	8328778	405356	7942316	478070	0.0464	0.0568
16	36187900	1123734	15598271	783987	0.0301	0.0479
17	118836163	3398649	24451232	1322277	0.0278	0.0513
18	12972873	507426	16102047	823092	0.0376	0.0486
19	14351082	718547	5907655	372495	0.0477	0.0593

Set 2: Fe^{III}-citrate

1	13958433	256405	2142551	15908	0.0180	0.0074
2	80658680	426938	40755590	159073	0.0053	0.0039
3	7945594	76309	2466373	10663	0.0095	0.0043
4	25346261	103012	30689462	121272	0.0040	0.0039
5	24940312	115912	9047431	35106	0.0046	0.0039
6	28445673	128781	7571431	30020	0.0045	0.0039
7	17070092	79021	10395414	42311	0.0046	0.0041
8	33377158	145571	26132592	108667	0.0043	0.0041
9	11158319	82807	4238780	18974	0.0074	0.0045
10	90768537	415556	32521432	111492	0.0046	0.0034
11	5730271	84783	4685776	29842	0.0146	0.0063
12	1771637	9949	734437	3142	0.0056	0.0043
13	1079883	7359	672707	2715	0.0068	0.0040
14	13358256	63664	5039684	20964	0.0047	0.0041
15	521199	5641	421875	2195	0.0107	0.0052
16	12034615	487803	4495900	97325	0.0390	0.0212
17	67354991	648685	23031378	98321	0.0095	0.0043
18	26683636	137727	18050449	76041	0.0051	0.0042
19	34660589	858122	5156201	30589	0.0242	0.0059
20	2726245	10646	1167407	4668	0.0039	0.0040
21	12633567	103769	3697589	23008	0.0081	0.0062
22	1582971	9352	741502	3509	0.0059	0.0047
23	80592797	1264580	47868634	266877	0.0154	0.0055
24	7272802	197358	1815950	22945	0.0264	0.0125
25	726949	3227	869859	3359	0.0044	0.0038
26	10556506	59782	2868653	11472	0.0056	0.0040
27	3799183	66454	753031	4718	0.0172	0.0062
28	249351	8235	159039	1582	0.0320	0.0098
29	17565368	858385	8662755	94449	0.0466	0.0108
30	4004142	16716	1971058	7616	0.0042	0.0038
31	26175206	229809	10609375	36439	0.0087	0.0034

Set 2: Humic acids

1	55117751	205562	33614478	126802	0.0037	0.0038
2	25490787	110116	16573079	62509	0.0043	0.0038
3	16355923	62061	11353534	42632	0.0038	0.0037
4	1714610	7232	2068626	7368	0.0042	0.0035
5	15484727	68166	7298135	23485	0.0044	0.0032
6	27861590	191027	5821760	25592	0.0068	0.0044

7	21308772	78013	9206680	33601	0.0036	0.0036
8	5096678	18894	1266090	4568	0.0037	0.0036
9	51484560	184292	30993892	110596	0.0036	0.0036
10	60947497	220325	28581153	101978	0.0036	0.0036
11	8698946	32672	7242871	26593	0.0037	0.0037
12	1706409	6586	4794201	17402	0.0038	0.0036
13	25317446	96727	7293172	27065	0.0038	0.0037
14	3012438	65659	1078289	5336	0.0213	0.0049
15	1589700	17382	132418	727	0.0108	0.0055
16	2982865	10376	2787514	9735	0.0035	0.0035
17	12071094	204435	3823404	35601	0.0167	0.0092
18	62533691	257650	29351492	116502	0.0041	0.0040
19	4661401	18127	3330721	12872	0.0039	0.0038
20	1411693	5478	994683	3947	0.0039	0.0040
21	12452346	48188	10019896	37442	0.0039	0.0037
22	2756054	13427	2934052	11289	0.0048	0.0038
23	2230184	10036	1424952	5890	0.0045	0.0041
24	25175520	113101	9529710	38242	0.0045	0.0040
25	46314144	230182	13121757	51152	0.0049	0.0039
26	30810467	118178	21636937	80911	0.0038	0.0037
27	25912507	101075	25529653	95841	0.0039	0.0037
28	6613731	27686	1335995	5250	0.0042	0.0039
29	2821470	10703	494632	1923	0.0038	0.0039
30	32229781	121891	12349381	46419	0.0038	0.0037
31	29021850	128491	15403182	64994	0.0044	0.0042
32	13268313	51047	3640947	13699	0.0038	0.0037
33	3919208	24209	942992	3784	0.0061	0.0040
34	4830697	20192	1996265	7515	0.0042	0.0038
35	105728195	1376562	16280903	106545	0.0129	0.0065
36	27989361	109408	20585970	78464	0.0039	0.0038
37	35846128	139036	5793441	22969	0.0039	0.0039
38	21421209	82112	23012457	86891	0.0038	0.0038
39	48875263	168401	54750403	186101	0.0034	0.0034
40	49043583	188027	6873982	25469	0.0038	0.0037
41	2307701	8846	630923	2289	0.0038	0.0036
42	40320950	154632	18812307	71445	0.0038	0.0038
43	20353901	81696	9496510	36161	0.0040	0.0038
44	72837724	316207	27141409	82236	0.0043	0.0030
45	18002993	66271	8274426	30362	0.0037	0.0037
46	17935549	70220	10335920	40134	0.0039	0.0039

*This aggregate was classified as outlier in Fig 4A (see also Fig. S7).

2.4 REFERENCES IN THE REPORT

1. A. Boetius *et al.*, A marine microbial consortium apparently mediating anaerobic oxidation of methane. *Nature* 407, 623 (2000).
2. V. J. Orphan, C. H. House, K. U. Hinrichs, K. D. McKeegan, E. F. DeLong, Methane-consuming archaea revealed by directly coupled isotopic and phylogenetic analysis. *Science* 293, 484 (2001).
3. S. J. Hallam *et al.*, Reverse methanogenesis: Testing the hypothesis with environmental genomics. *Science* 305, 1457 (2004).
4. S. Scheller, M. Goenrich, R. Boecher, R. K. Thauer, B. Jaun, The key nickel enzyme of methanogenesis catalyses the anaerobic oxidation of methane. *Nature* 465, 606 (2010).
5. M. F. Haroon *et al.*, Anaerobic oxidation of methane coupled to nitrate reduction in a novel archaeal lineage. *Nature* 501, 567 (2013).
6. E. J. Beal, C. H. House, V. J. Orphan, Manganese- and Iron-Dependent Marine Methane Oxidation. *Science* 325, 184 (2009).
7. J. Milucka *et al.*, Zero-valent sulphur is a key intermediate in marine methane oxidation. *Nature* 491, 541 (2012).
8. S. E. McGlynn, G. L. Chadwick, C. P. Kempes, V. J. Orphan, Single cell activity reveals direct electron transfer in methanotrophic consortia. *Nature* 526, 531 (2015).
9. G. Wegener, V. Krukenberg, D. Riedel, H. E. Tegetmeyer, A. Boetius, Intercellular wiring enables electron transfer between methanotrophic archaea and bacteria. *Nature* 526, 587 (2015).
10. W. S. Reeburgh, Oceanic methane biogeochemistry. *Chem. Rev.* 107, 486 (2007).
11. K. Knittel, A. Boetius, Anaerobic oxidation of methane: progress with an unknown process. *Annu. Rev. Microbiol.* 63, 311 (2009).
12. P. R. Girguis, A. E. Cozen, E. F. DeLong, Growth and population dynamics of anaerobic methane-oxidizing archaea and sulfate-reducing bacteria in a continuous-flow bioreactor. *Appl. Environ. Microbiol.* 71, 3725 (2005).
13. V. J. Orphan, K. A. Turk, A. M. Green, C. H. House, Patterns of N-15 assimilation and growth of methanotrophic ANME-2 archaea and sulfate-reducing bacteria within structured syntrophic consortia revealed by FISH-SIMS. *Environmental Microbiology* 11, 1777 (2009).
14. R. J. W. Meulepas *et al.*, Enrichment of Anaerobic Methanotrophs in Sulfate-Reducing Membrane Bioreactors. *Biotechnol. Bioeng.* 104, 458 (2009).
15. T. Holler *et al.*, Thermophilic anaerobic oxidation of methane by marine microbial consortia. *Isme J.* 5, 1946 (2011).
16. K. Nauhaus, T. Treude, A. Boetius, M. Krueger, Environmental regulation of the anaerobic oxidation of methane: A comparison of ANME-I and ANME-II communities. *Environmental Microbiology* 7, 98 (2005).
17. K. Nauhaus, M. Albrecht, M. Elvert, A. Boetius, F. Widdel, In vitro cell growth of marine archaeal-bacterial consortia during anaerobic oxidation of methane with sulfate.

Environmental Microbiology 9, 187 (2007).
18. S. B. Joye *et al.*, The anaerobic oxidation of methane and sulfate reduction in sediments from Gulf of Mexico cold seeps. *Chem. Geol.* 205, 219 (2004).
19. A. Meyerdierks *et al.*, Metagenome and mRNA expression analyses of anaerobic methanotrophic archaea of the ANME-1 group. *Environmental Microbiology* 12, 422 (2010).
20. F. P. Wang *et al.*, Methanotrophic archaea possessing diverging methane-oxidizing and electron-transporting pathways. *Isme J.* 8, 1069 (2014).
21. M. J. Alperin, T. M. Hoehler, Anaerobic Methane Oxidation by Archaea/Sulfate-Reducing Bacteria Aggregates: 1. Thermodynamic And Physical Constraints. *Am. J. Sci.* 309, 869 (2009).
22. B. Orcutt, C. Meile, Constraints on mechanisms and rates of anaerobic oxidation of methane by microbial consortia: process-based modeling of ANME-2 archaea and sulfate reducing bacteria interactions. *Biogeosciences* 5, 1587 (2008).
23. R. J. W. Meulepas, C. G. Jagersma, A. F. Khadem, A. J. M. Stams, P. N. L. Lens, Effect of methanogenic substrates on anaerobic oxidation of methane and sulfate reduction by an anaerobic methanotrophic enrichment. *Appl. Microbiol. Biotechnol.* 87, 1499 (2010).
24. D. R. Bond, D. R. Lovley, Reduction of Fe(III) oxide by methanogens in the presence and absence of extracellular quinones. *Environmental Microbiology* 4, 115 (2002).
25. Additional supplementary information is available on Science Online.
26. L. G. Wilson, R. S. Bandurski, Enzymatic Reactions Involving Sulfate, Sulfite, Selenate, and Molybdate. *J. Biol. Chem.* 233, 975 (1958).
27. T. Holler *et al.*, Carbon and sulfur back flux during anaerobic microbial oxidation of methane and coupled sulfate reduction. *Proc. Natl. Acad. Sci. U. S. A.* 108, E1484 (2011).
28. M. Y. Yoshinaga *et al.*, Carbon isotope equilibration during sulphate-limited anaerobic oxidation of methane. *Nat. Geosci.* 7, 190 (2014).
29. S. Pirbadian, M. Y. El-Naggar, Multistep hopping and extracellular charge transfer in microbial redox chains. *Phys. Chem. Chem. Phys.* 14, 13802 (2012).
30. J. W. Voordeckers, B. C. Kim, M. Izallalen, D. R. Lovley, Role of Geobacter sulfurreducens Outer Surface c-Type Cytochromes in Reduction of Soil Humic Acid and Anthraquinone-2,6-Disulfonate. *Appl. Environ. Microbiol.* 76, 2371 (2010).
31. K. Nauhaus, A. Boetius, M. Kruger, F. Widdel, In vitro demonstration of anaerobic oxidation of methane coupled to sulphate reduction in sediment from a marine gas hydrate area. *Environmental Microbiology* 4, 296 (2002).
32. J. J. Marlow *et al.*, Carbonate-hosted methanotrophy represents an unrecognized methane sink in the deep sea. *Nat. Commun.* 5, 5094 (2014).
33. A. Green-Saxena, A. E. Dekas, N. F. Dalleska, V. J. Orphan, Nitrate-based niche differentiation by distinct sulfate-reducing bacteria involved in the anaerobic oxidation of methane. *Isme J.* 8, 150 (2014).
34. J. D. Cline, Spectrophotometric Determination of Hydrogen Sulfide in Natural Waters. *Limnol. Oceanogr.* 14, 454 (1969).
35. R. Gamage, A. J. McQuillan, B. M. Peake, Ultraviolet Visible and Electron-Paramagnetic Resonance Spectroelectrochemical Studies of the Reduction Products of some

Anthraquinone Sulfonates in Aqueous-Solutions. *J. Chem. Soc.-Faraday Trans.* 87, 3653 (1991).
36. J. B. Conant, H. M. Kahn, L. F. Fieser, S. S. Kurtz, An electrochemical study of the reversible reduction of organic compounds. *J. Am. Chem. Soc.* 44, 1382 (1922).
37. A. E. Dekas, G. L. Chadwick, M. W. Bowles, S. B. Joye, V. J. Orphan, Spatial distribution of nitrogen fixation in methane seep sediment and the role of the ANME archaea. *Environmental Microbiology* 16, 3012 (2014).
38. E. Trembath-Reichert, A. Green-Saxena, V. J. Orphan, in *Microbial Metagenomics, Metatranscriptomics, and Metaproteomics,* E. F. DeLong, Ed. (Elsevier Academic Press Inc, San Diego, 2013), vol. 531, pp. 21-44.
39. C. Quast *et al.*, The SILVA ribosomal RNA gene database project: improved data processing and web-based tools. *Nucleic Acids Res.* 41, D590 (2013).
40. S. F. Altschul *et al.*, Gapped BLAST and PSI-BLAST: a new generation of protein database search programs. *Nucleic Acids Res.* 25, 3389 (1997).
41. W. Ludwig *et al.*, ARB: a software environment for sequence data. *Nucleic Acids Res.* 32, 1363 (2004).
42. F. Ronquist *et al.*, MrBayes 3.2: Efficient Bayesian Phylogenetic Inference and Model Choice Across a Large Model Space. *Syst. Biol.* 61, 539 (2012).
43. A. Rambaut, *FigTree 1.4. 2 software. Institute of Evolutionary Biology, Univ. Edinburgh* (2014).
44. O. Mason *et al.*, Comparison of Archaeal and Bacterial Diversity in Methane Seep Carbonate Nodules and Host Sediments, Eel River Basin and Hydrate Ridge, USA. *Microb. Ecol.* 70, 766 (2015).
45. J. G. Caporaso *et al.*, QIIME allows analysis of high-throughput community sequencing data. *Nat. Methods* 7, 335 (2010).
46. B. M. Fuchs, J. Pernthaler, R. Amann, Single cell identifcation by fuorescence in situ hybridization. *Methods for general and molecular microbiology* 3, 886 (2007).
47. R. I. Amann, L. Krumholz, D. A. Stahl, Fluorescent-Oligonucleotide Probing of Whole Cells for Determinative, Phylogenetic, and Environmental-Studies In Microbiology. *J. Bacteriol.* 172, 762 (1990).
48. K. Knittel, T. Losekann, A. Boetius, R. Kort, R. Amann, Diversity and distribution of methanotrophic archaea at cold seeps. *Appl. Environ. Microbiol.* 71, 467 (2005).
49. W. Manz, M. Eisenbrecher, T. R. Neu, U. Szewzyk, Abundance and spatial organization of Gram-negative sulfate-reducing bacteria in activated sludge investigated by in situ probing with specific 16S rRNA targeted oligonucleotides. *FEMS Microbiol. Ecol.* 25, 43 (1998).
50. T. Losekann *et al.*, Diversity and abundance of aerobic and anaerobic methane oxidizers at the Haakon Mosby mud volcano, Barents Sea. *Appl. Environ. Microbiol.* 73, 3348 (2007).
51. L. Polerecky *et al.*, Look@NanoSIMS - a tool for the analysis of nanoSIMS data in environmental microbiology. *Environmental Microbiology* 14, 1009 (2012).
52. B. Thamdrup, Bacterial manganese and iron reduction in aquatic sediments. *Advances in Microbial Ecology* 16, 41 (2000).

53. G. S. Wilson, Determination of oxidation-reduction potentials. *Methods in enzymology* 54, 396 (1978).
54. M. L. Fultz, R. A. Durst, Mediator Compounds for the Electrochemical Study of Biological Redox Systems - a Compilation. *Anal. Chim. Acta* 140, 1 (1982).
55. R. S. Twigg, Oxidation-Reduction Aspects of Resazurin. *Nature* 155, 401 (1945).
56. M. Aeschbacher, D. Vergari, R. P. Schwarzenbach, M. Sander, Electrochemical Analysis of Proton and Electron Transfer Equilibria of the Reducible Moieties in Humic Acids. *Environ. Sci. Technol.* 45, 8385 (2011).
57. H. S. Mason, D. J. E. Ingram, B. Allen, The Free Radical Property of Melanins. *Arch. Biochem. Biophys.* 86, 225 (1960).

2.5 MATERIALS AND METHODS

Materials

Sediment collection and processing

Santa Monica basin seep sediments overlain by a white mat were collected from the Santa Monica Mounds site in a push core (PC 61) deployed by the ROV *Doc Ricketts*. Samples were collected in May 2013 during a research cruise organized by the Monterey Bay Aquarium Research Institute (MBARI) using the R/V *Western Flyer*. PC61 was collected during dive 463 at 860 m depth with an *in situ* temperature of 4 °C (lat. 33.78905, long. -118.66833). The intact sediment core was extruded shipboard and then heat-sealed in a large mylar bag flushed for 5 minutes with argon. Sediments were stored at 4 °C until processed in the lab (40 days after collection). The whole push core (ca. 12 cm, yielding 800 ml wet sediment) was suspended in 1600 ml filter sterilized N_2 sparged bottom seawater from the site (1 in 3 ratio) in an anaerobic chamber (3% H_2 in N_2). The anaerobic sediment slurry was then distributed into three 1L pyrex bottles, sealed with a large butyl rubber stopper, and pressurized with methane (0.25 MPa). Aggregate counts at the start of the experiment were determined by DAPI staining and epifluorescence microscopy, yielding approximately 9.7 x 10^5 aggregates per ml wet weight sediment. The initial sulfate-coupled AOM activity of the sediment was assessed via sulfide production measurements, showing the generation of 2.8 mM sulfide within the first 15 days.
All manipulations of the sediment incubations were done anaerobically at 4 °C or on ice. Prior to establishment of the microcosm experiments, the seep sediment was maintained for 12 months at 4 °C under methane (0.25 MPa) in anoxic bottom seawater that was exchanged every 3 months. For all reported experiments in this study, the seawater above the sediment was exchanged with a modified artificial seawater (see below) that contained 10x less Ca^{2+}, no sulfate, no sulfide, and 25 mM HEPES buffer at pH 7.5. The low Ca^{2+} concentration and lower pH prevent carbonate precipitation, which allows quantitative analysis of the ^{13}C-bicarbonate formed in solution during ^{13}C-methane oxidation. Methane was added (0.30 MPa), shaken and the sediment allowed to settle for 48 hours (sediment/total volume = 1:3). The supernatant was exchanged 3 times with the described medium following the same procedure in order to obtain sulfate and sulfide-free sediment.

Medium composition:

The final composition in the medium was: NaCl 457 mM, $MgCl_2$ 47 mM, Na^+-HEPES (pH=7.5) 25 mM, KCl 7.0 mM, $NaHCO_3$ 5.0 mM, $CaCl_2$ 1.0 mM, K_2HPO_4 1.0 mM, NH_4Cl 1.0 mM, SeO_3^{2-} 0.01 μM, WO_4^{2-} 0.007 μM, 0.1% trace element solution, containing per liter: nitrilotriacetic acid 150 mg, $MnCl_2$ x 4 H_2O 610 mg, $CoCl_2$ x 6 H_2O 420 mg, $ZnCl_2$ 90 mg, $CuCl_2$ x 2 H_2O 7 mg, $AlCl_3$ 6 mg, H_3BO_3 10 mg, Na_2MoO_4 x 2 H_2O 20 mg, $SrCl_2$ x 6 H_2O 10 mg, NaBr 10 mg, KI 70 mg, $FeCl_3$ x 6

H_2O 500 mg, $NiCl_2$ x 6 H_2O 25 mg. No vitamins, indicators, reducing agents, or other substances were added.

The sulfate concentration of the final sediment slurry was below detection limit (< 10 μM). Before the start of the microcosm experiments, the sediment slurry was flushed with methane (ca. 20 min) to remove traces of sulfide. The presence of sulfide (e.g. 0.5 mM in previous studies (*16, 31*) can chemically reduce AQDS, preventing methane oxidation with AQDS (*16*). It is possible that under these conditions, AOM is inhibited by the polysulfides formed from sulfide + AQDS rather than directly by reduced AQDS, as reduced AQDS was observed to accumulate in our experiments with no apparent inhibition of AOM (Table S1A).

Sediment characterization

AOM rates with sulfate (1.5 μmol methane (cm^3 wet sediment)$^{-1}$ d^{-1}, see main text) were comparable to active methane-seep sediments described previously (*31, 32*). The dominant groups of archaea included ANME-2a and ANME-2c based on Illumina Tag sequencing using the Earth Microbiome primer set (Fig. S4). FISH hybridization and aggregate counts based on DAPI staining yielded 47% (69 of 146 aggregates) ANME-2a affiliated consortia and 43% ANME-2c (47 of 109 DAPI stained aggregates). The remaining 10% of aggregates likely represented other ANME not targeted by the specific FISH probes or possibly weakly hybridized ANME-2a or 2c aggregates that were below detection by FISH.

Chemicals and reagents

AQDS (=2,6-AQDS, >98% purity) and Fe(III)-EDTA was purchased from Sigma. Humic acids (sodium salt, tech. batch no. 10121HA) were obtained from Aldrich. 2,7-AQDS and 1,5-AQDS (>98% purity) were purchased from TCI chemicals. The different AQDS isomers were found to contain variable amounts of residual sulfate as determined by Ion Chromatography: 11 μM sulfate per 10 mM AQDS; 176 μM sulfate per 10 mM 2,7-AQDS; 344 μM sulfate per 10 mM 1,5-AQDS. 1,5-AQDS was re-crystallized from boiling water to remove traces of sulfate present in the purchased product. Residual sulfate in the re-crystallized 1,5-AQDS: 13 μM per 10 mM 1,5-AQDS. 2,7-AQDS, AQDS and all other chemicals were used as received. 50 mM Fe(III)-citrate stock solution was prepared by dissolving 2.0 mmol citric acid in a small amount of DI water, followed by the addition of 1.0 mmol $FeCl_3$ x 6 H_2O and pH adjustment to pH = 7.5 with NaOH. The solution was then diluted to 50 mM ferric ions (20 ml final volume).

Methods for metabolic measurements

General description of methane oxidation measurements via ^{13}C-methane

Methane oxidation was quantified by determining the production of inorganic carbon ("CO_2"). Accurate quantification of the concentration of inorganic carbon formed from methane oxidation is challenging due to 4 main reasons:
1) Inorganic carbon is present as a mixture of CO_2(g) in the headspace, and CO_2(aq.), H_2CO_3, HCO_3^- or CO_3^{2-} in solution (dissolved inorganic carbon, DIC)
2) Inorganic carbon may also be produced from respiration of organic carbon sources other than methane
3) Inorganic carbon can also be slowly produced via dissolution of carbonates (a major component of seep sediments)
4) Inorganic carbon may also precipitate with divalent cations as insoluble carbonates

For our experiments, we found that quantifying methane oxidation using the stable isotope tracer $^{13}CH_4$ in incubations with a known amount of unlabelled (dissolved inorganic carbon, DIC) by analyzing the ^{13}C enrichment in DIC was the most accurate (Fig. S2A).We used a defined amount of added DIC in artificial, buffered seawater with a low calcium concentration to prevent carbonate precipitation (see medium composition). As $^{13}CH_4$ was the only ^{13}C-enriched carbon source added, the newly formed ^{13}C-DIC must be derived from methane. For low methane oxidation rates (less than ca. 5% relative to sulfate as the oxidant), however, enzyme-catalyzed isotope exchange between methane and DIC (*27, 28*) needs to be taken into account, because it contributes to ^{13}C enrichment of the DIC without net methane oxidation, resulting in an overestimation of net methane oxidation. To illustrate the utility of this approach for quantifying rates of AOM, we used 2 AOM incubations amended with ^{13}C-methane and sulfate and compared our calculation of newly formed DIC based on $^{13}CH_4$ (Fig. S2B, red) with an independent method used in analytical chemistry based on standard addition that yields the absolute amounts of DIC formed during the incubations more directly (Fig. S2B, black). Details of both methods, the $^{13}CH_4$ experiments and the standard addition are described below. The method via standard addition provides evidence for net DIC increase during incubations, and is consistent with the progressive enrichment of ^{13}C-DIC observed from $^{13}CH_4$. In this comparative analysis, however, we observed an initial decrease in the absolute concentration of DIC within the first 2 days for the standard addition method, which we mainly attribute to diffusion of CO_2 into the headspace of the vial (Fig. S2B, black).

Incubation conditions for AOM rate measurement
Each incubation vial was set up with 1.0 cm^3 wet sediment (wet sediment = volume of sediment after allowing the sediment slurry settle for 48 h) in total slurry volume of 5 ml as follows: Sterile serum vials were closed with butyl rubber stoppers (volume = 12.9 ml after closing) and flushed with methane. 1.0 ml $^{13}CH_4$ (99% ^{13}C, Cambridge Isotope Laboratories, containing 0.05 vol% $^{13}CO_2$ as an impurity) was introduced anaerobically. 2.0 ml of artificial, anaerobic seawater containing 2.5x the target concentration of the corresponding electron acceptor was injected into the serum vial cooled on ice. For AQDS and 1,5-AQDS, this was a suspension corresponding to 25 mM (see Table S2).

The 1L pyrex bottle with the sediment in the sulfate-free medium (1 part wet sediment in 3 parts of slurry volume) was vigorously shaken each time and 3.0 ml of slurry immediately removed and injected into the individual serum bottles. Each stoppered serum vial was supplemented with unlabelled methane (0.250 MPa overpressure: pressure gauge SSI Technologies, Inc., Media Gauge™), shaken and stored inverted at 4 ˚C (final headspace: 0.35 MPa methane, with ca. 4 % $^{13}CH_4$). The exact fractional abundance of ^{13}C in the methane was quantified via ^1H-NMR spectroscopy for individual incubations.

AOM rate measurements (quantification of newly formed DIC based on $^{13}CH_4$)
For ^{13}C-DIC analysis, 0.25 ml of the medium above the settled sediment in the microcosm was sampled with a disposable needle and syringe at each time point (same intervals for all experiments) and centrifuged (16000 rcf, 5 min). The supernatant was transferred into 0.6 ml eppendorf tubes, flash frozen in N_2(l), and stored at -20 ˚C until measurement. 150 µl of the thawed supernatant was then added to He-flushed vials containing 100 µl H_3PO_4 (85%). The resulting CO_2 was analyzed for the isotopic enrichment ($^{13}F(t_n)$) on a GC-IR-MS GasBench II (Thermo Scientific). The amount of DIC newly formed ($\Delta[DIC](t_n)$, see Fig. 2B) was calculated from the measured ^{13}F (fractional abundance of ^{13}C), neglecting isotope effects on AOM:

$$\Delta[DIC](t_n) = [DIC](t_0) * (^{13}F(t_n) - {}^{13}F(t_0)) / (^{13}F(CH_4) - {}^{13}F(t_n))$$

[DIC] = sum of carbonate, bicarbonate and CO_2, $[DIC](t_0)$ = 5.0 mM
$^{13}F(t_0)$ = 0.01153 (higher than medium due to $^{13}CO_2$-impurity in the $^{13}CH_4$ used)
$^{13}F(CH_4)$ = ^{13}C in the methane used (measured via ^1H-NMR spectroscopy)

Amount of DIC formed per vial (Fig. 1A, S1, S3) = 5 mL * $\Delta[DIC](t_n)$

Calculation of specific AOM rates per volume sediment
For each incubation, the methane oxidation rate per volume sediment slurry was determined via linear regression of the time points 1, 2, 3 and 4 (17 h, 42.5 h, 67 h and 142.5 h). The 95% confidence intervals were calculated. Rates per cm^3 wet sediment are 5x higher than for the sediment slurry (sediment + modified HEPES-buffered seawater), as displayed in Fig 1B (wet sediment = 20% of total slurry volume).

Quantification of absolute DIC concentrations via standard addition
For two incubations with sulfate, we quantified the absolute concentrations of DIC for the full time course of the incubations (Fig. S2B) using the standard addition method. 75 µl of each sample was mixed with 75 µl of a DIC standard (10.0 mM $NaHCO_3$) and analyzed for its isotopic enrichment ($^{13}F_{mix}(t_n)$). The absolute DIC-concentration of the sample ($[DIC](t_n)$, see Fig. S2B) was calculated as follows:

$$[DIC](t_n) = 10\ mM * (^{13}F_{mix}(t_n) - {}^{13}F_{std}) / (^{13}F(t_n) - {}^{13}F_{mix}(t_n))$$

Quantification of fractional abundance of $^{13}CH_4$ in the headspace used
The exact fraction of $^{13}CH_4$ (ca. 4.0 %) was quantified for individual incubations at the end of the 21 day incubation period via ^{1}H-NMR spectroscopy (Varian 400 MHz Spectrometer with broadband auto-tune OneProbe). Methane in the headspace was passed through chloroform-d (99.8% D, Cambridge Isotope laboratories) via a long 23G needle and acquired at 400 MHz with a repetition time of 10 s. Fractional abundances of ^{13}C in the methane were obtained via integration of the $^{12}CH_4$ signal and of the $^{13}CH_4$-satellites (iNMR version 4.3.0).

Quantification of residual sulfate
Residual sulfate was quantified via Ion chromatography on a DX-500 or DX-2000 instrument (Dionex, Sunnyvale, CA, USA) housed at the Caltech Environmental Analysis Center following the protocol outlined in (*33*). The DI water used throughout this study contained <10 μM residual sulfate. Incubations with 2,7-AQDS contained a maximum of 200 μM residual sulfate, from traces of sulfate present in the purchased material (176 μM per 10 mM 2,7-AQDS), which could not be removed via re-crystallization due to the high solubility of 2,7-AQDS (described in the chemicals and reagents section above). For all other incubations, the sulfate concentration remained below 50 μM throughout the incubation period.

Quantification of sulfide
Supernatant was removed via syringe and centrifuged in 0.6 ml eppendorf tubes (16000 rcf, 30 s). 20 μl of the clear supernatant was removed and added to 400 μl $Zn(OAc)_2$ (500 mM) to preserve the sulfide. Analysis was carried out in triplicate via the methylene blue method (*34*) using standards of 0.1, 0.25, 0.5, 1, 2, 5, 10 and 25 mM sulfide added to $Zn(OAc)_2$ (500 mM) in the same ratios as for the samples. Quantification was carried out in a plate reader (TECAN Sunrise™) by monitoring the absorbance at 670 nm.

Quantification of AQDS solubility in the incubation medium (data for Table S2)
Different regioisomers of AQDS (1,5-AQDS, 2,6-AQDS and 2,7-AQDS) were separately added to the modified artificial seawater described above, to a targeted final concentration of 25 mM. The suspensions were ultra-sonicated at room temperature to dissolve as much of the AQDS as possible. The tubes were kept at 4 °C or at 22.5 °C overnight. The tubes were centrifuged at 4 °C or 22.5 °C (16000 rcf, 30 min). The supernatant (300 μl) was mixed with 300 μl acetate (10.0 mM) as the internal standard and 100 μl deuterated water (99.9% D, Cambridge Isotope Laboratories) was added. The concentration of AQDS was obtained from integration of the ^{1}H-NMR spectra by comparison relative to the acetate standard.

Identity of reduced AQDS by UV-Vis and NMR
Reduced AQDS was identified photospectrometrically matching the spectra reported previously (*35*). Solutions containing reduced AQDS were paramagnetic (ca. 1000 Hz

line width, ^{1}H-NMR spectroscopy), putatively due to the presence of the semiquinone-radical. Supernatant from an incubation that contained ca. 10 mM reduced AQDS was sparged with air for 30 min in order to re-oxidize AQH_2DS back to AQDS. ^{1}H-NMR spectroscopy shows full conversion to AQDS, undistinguishable from the AQDS used initially. No signals other than AQDS or HEPES buffer were visible in the spectrum, proving reversible reduction and oxidation without detectable formation of side products.

Quantification of reduced AQDS by iodometry

Reduced AQDS (2,6-AQH_2DS) was quantified via iodimetric titration in the anaerobic chamber. A standard solution of ca. 20 mM KI_3 was prepared as follows: iodine (254 mg, 2.0 mmol) and potassium iodide (1.66 g, 10 mmol) were dissolved in 100 ml DI water. After 2 days, the clear, dark solution was N_2-sparged and brought into the anaerobic chamber. The exact concentration of the KI_3 standard solution was quantified to be 19.5 mM via duplicate titration with sodium thiosulfate (exactly 101.5 mM, N_2-sparged). Procedure for the quantification of reduced AQDS in the incubations: 1000 µl anaerobic assay solution centrifuged in the anaerobic chamber + 200 µl anaerobic HEPES (1.0 M, pH = 7.5) + KI_3 standard solution as needed until color minimum, added in steps of 100 µl first, than in steps of 10 µl when closer to the equivalence point.

Control experiments without methane

Sediment incubations with AQDS (10 mM) under nitrogen did not generate substantial amounts of reduced AQDS (less than 1 mM after 3 weeks). To confirm that the methanotrophic microorganisms in the sediment had not been killed during the nitrogen + AQDS incubation, methane was later injected into these incubation bottles after 3 weeks. Upon addition of methane, AQDS was reduced at rates similar to that shown in Fig. 1.

Check for methanogenic activity

Sediment slurries were incubated under a nitrogen headspace in duplicates without an added oxidant to probe for endogenous methanogenic activity. After 6 days, methane in the headspace was quantified via GC-MS (Hewlett Packard 5890 Series II gas chromatograph with mass selective detector 5972) by triplicate injections. For the first biological replicate, methane was found at a concentration that was close to the detection limit, corresponding to a specific methanogenesis rate of 0.5 ± 0.25 nmol methane (cm^3 wet sediment)$^{-1}$ d^{-1}. For the second replicate, the methane peak was too small for accurate quantification, but we can state an upper limit of 0.25 nmol (cm^3 wet sediment)$^{-1}$ d^{-1}. Based on these measurements, the endogenous methanogenesis rate [and/or enzymatic equilibration rate (*27, 28*) is ca. 3000x lower than methane oxidation with sulfate.

Thermodynamic calculations

The standard free energy for AOM with AQDS was calculated from the corresponding redox-potentials:

HCO_3^- + 4 H_2 + H^+ = CH_4 + 2 H_2O $\Delta G^{\circ\prime}$ = -135.3 kJ mol^{-1}
$E^{\circ\prime}$ for CH_4/HCO_3^- = -414 mV - $\Delta G^{\circ\prime}/(nF)$ = -239 mV
$E^{\circ\prime}$ for 2,6-AQDS = -186 mV [E° = +228 mV (*36*)]
$\Delta E^{\circ\prime}$ = 53 mV, $\Delta G^{\circ\prime}$ = -n$F\Delta E^{\circ\prime}$ = -41 kJ mol^{-1}

Methods for microbial anabolic activity measurements

Incubations for FISH-nanoSIMS and RNA analysis

For AOM incubations with sulfate or AQDS that were used for nanoSIMS (Fig. 3 and Fig. 4A) and RNA analysis (Fig. 2), incubations experiments were set up following the AOM-rate measurements described above (initially containing 1.0 mM ammonium without ^{15}N label). Methane oxidation rates were tracked in these incubations via the ^{13}C label. After 11 days, ca. 3.5 ml of supernatant remained in the serum bottles to which 3.0 ml artificial seawater without ammonium containing either 25 mM AQDS, 28 mM sulfate, or no oxidant was added. Next, 0.1 ml $^{15}NH_4^+$ (100 mM) was injected to yield about 2.0 mM ammonium with ca. 75% ^{15}N. Methane oxidation was monitored. After additional 8 days, the medium of the AQDS incubations was exchanged by 5.0 ml new medium containing 25 mM AQDS and 2.0 mM $^{15}NH_4^+$. Now the AQDS incubations contained ca. 95% $^{15}NH_4^+$ in the ammonium pool. The cultures were incubated for additional 10 days before harvest. Total incubation time with labeled ammonium: 18 days. Average labeling strength: ca. 75% for sulfate and no oxidant control; ca. 86% for the AQDS incubations.
For the second independent set of experiments with iron citrate, humic acids and sulfate (Fig. 4B), the medium contained 1.0 mM ammonium with ca. 40% ^{15}N label throughout the incubation period. These experiments were carried out from identical incubations that were for the AOM rate measurements (highlighted in Table S3).

Sampling for FISH-nanoSIMS and RNA

After 18 days incubation in the presence of $^{15}NH_4^+$, each incubation was shaken to suspend the sediment and 1.0 ml sediment slurry was sampled using a disposable sterile needle and syringe (ca. 0.3 ml wet sediment). The sediment aliquot was briefly centrifuged (4000 rcf) in an eppendorf tube and 0.5 ml of the supernatant was removed for DIC and metabolite analysis. 0.5 ml 4% paraformaldehyde in PBS (100 mM phosphate pH=7.4, salinity=10 g l^{-1}) was then added to the remaining 0.5 ml sediment slurry (2% formaldehyde final), resuspended and fixed for 120 min at 4 °C. The fixed sediment was subsequently washed 3 times with 1X PBS, followed by a single wash in EtOH/PBS (1:1) and then re-suspended in EtOH/PBS (1:1) to a final volume of 0.5 ml that was used for microscopy and nanoSIMS.
All remaining sediment from the identical incubations (ca. 0.7 ml wet sediment, see above) was removed for RNA analysis using a disposable sterile needle and syringe. The sediment slurry was immediately centrifuged (16000 rcf, 15 s), followed by removal of the

supernatant and flash-freezing of the sediment pellet in liquid N_2. Frozen sediment was stored at -80 ˚C until RNA extraction.

RNA extraction, PCR, clone library construction, and phylogenetic analysis

RNA was extracted from the 0.7 ml frozen wet sediment described above using the RNA Powersoil Total RNA Isolation Kit (cat # 12866-25; MO BIO Laboratories, Inc., Carlsbad, CA, USA) with modifications (*37*). The eluted RNA was immediately DNase treated using the MO BIO RTS DNase Kit (cat no. 15200-50, MO BIO Laboratories, Inc., Carlsbad, CA, USA), purified and concentrated to 24 µl using the Qiagen RNeasy Plus Micro Kit (cat # 74034, Qiagen, Valencia, CA, USA), and converted to cDNA using the Invitrogen Superscript III First-Strand Synthesis SuperMix (cat no. 18080-400, ThermoFisher Scientific, Grand Island, NY, USA) with no reverse transcriptase (NRT) controls following manufacturer's instructions. cDNA was stored at -80 ˚C until further processing.

PCR conditions were as follows: 1 x 5 PRIME HotMasterMix buffer (cat # 2200400; 5 PRIME, Inc., Gaithersburg, MD, USA), 0.4 µM of each forward and reverse primer, and 1 µl of cDNA in a final volume of 25 µl. Methyl-coenzyme reductase alpha subunit (mcrA, primers ME1: GCMATGCARATHGGWATGTC /ME2 TCATKGCRTAGTTDGGRTAGT) and archaeal and bacterial 16S rRNA (primers Arc23F: TTCCGGTTGATCCYGCCGGA or Bac27F: AGAGTTTGATYMTGGCTC with U1492R: GGYTACCTTGTTACGACTT) were amplified with 40 cycles as described in (*38*). The cDNA from the sulfate microcosm was diluted 1/50 to have similar amount of amplicons compared with other cDNA samples. 5 µl of the PCR products was quantified in 1% (w/v) agarose electrophoresis with SYBR safe stain under ultraviolet light, and NRT controls did not show any amplification. The remainder of the PCR product for each sample was immediately cleaned by filtration (MultiScreen PCR Filter Plate #MSNU03010, Millipore) and resuspended to the original volumes using Tris–HCl (pH 8). 1 µl of the cleaned PCR product was used per ligation reaction and cloning according instructions in the TOPO TA Cloning Kit for Sequencing using the pCR4-TOPO Vector and One Shot Top 10 chemically competent *Escherichia coli* (Life Technologies). Recombinant clones were checked for inserts by PCR, gel electrophoresis and sequenced using primers M13F (5′-GTAAAACGACGGCCAG-3′) and M13R (5′-CAGGAAACAGCTATGAC-3′) on an ABI Prism 3730 DNA sequencer using the BigDye Terminator v3.1 cycle sequencing kit (Applied Biosystems Inc., Foster City, CA, USA).

Sequences were manually checked and contigs assembled using the Sequencer v4.1.4 software. Sequences were then compared against the SILVA 16S rRNA database [version 119 (*39*)] or GenBank DNA database by using the BLAST algorithm (*40*). Alignment against reference sequences was completed using the SILVA online aligner (*39*) for 16S rRNA and ClustalO for mcrA, and aligned sequences were then imported into the ARB package version 6.0.2 (*41*) and manually verified. An additional 80 16S rRNA sequences were retrieved from SILVA database and 44 mcrA sequences were

retrieved from NCBI Refseq and used as references for the phylogenetic analyses. The Bayesian phylogeny was generated using 1421 aligned 16S rRNA nucleic acid positions (inverse gamma rates) and 248 aligned mcrA amino acid positions (mixed amino acid model) using MrBayes v3.2.2 (*42*) until split frequencies were less than 0.01. Clone library sequences fall into several clades of high phylogenetic support. Clone library sequences fall into several groups of high phylogenetic support. One representative sequence is used to represent highly similar sequences; the number of sequences represented and the representative accession number are indicated in brackets in Figure 2. mcrA sequences were classified into groups as previously (*43*). Clone library sequences for archaeal 16S rRNA and mcrA genes, and bacterial 16S rRNA genes were deposited in NCBI under accession numbers KU324182 to KU324260, KU324346 to KU324428, and KU324261 to KU324345, respectively.

Illumina Tag sequencing (data for Fig. S4)
DNA was extracted from 0.25 g of wet weight sediment using the PowerSoil DNA Isolation Kit (Cat#12888-05, Mo Bio Laboratories, Carlsbad, CA). PCR amplification and barcoding of the 16S rRNA gene were performed as described previously (*44*). Amplicons for deep sequencing were outsourced to Laragen, Inc (Culver City, CA) and run on an Illumina MiSeq platform (*44*). Data was analyzed using QIIME 1.8.0 (*45*) and processed sequences were assigned to phylotypes using a 99% similarity cutoff to the SILVA database version 115 (*39*) following previous procedures (*44*).

Sample preparation for aggregate embedding, sectioning, FISH, and nanoSIMS
Sample preparation was carried out following the recently optimized protocol in our lab outlined in (*8*). Briefly: Paraformaldehyde fixed consortia were detached from the sediment particles via sonication on ice with a sterile remote-tapered microtip probe (Branson) inserted into the liquid. Aggregates were concentrated on a 3 μm filter, covered in molten noble agar (2%) and embedded in glycol methacrylate (Heraeus Kulzer - Technovit® 8100). Sections of ca. 1 μm thickness were cut and stretched on a water droplet on a polylysine coated slide with teflon wells (Tekdon Inc) and analyzed by fluorescence *in situ* hybridization (FISH). Images of the FISH-stained consortia were collected and the location of these consortia were mapped for subsequent nanoSIMS analysis as described below.

FISH conditions and probes for this study
The FISH hybridization on thin sections of resin embedded microbial aggregates followed the recently optimized protocol described in (*8*). The phylogenetic identity of microorganisms in the thin sections were determined using conventional FISH using oligonucleotide probes fluorescently labeled on both the 5' and 3' ends (dual labeled) as outlined below. The FISH hybridization followed a standard protocol (*46*) and used a hybridization buffer containing 60% formamide and incubation at 46 ˚C for 120 min, followed by a wash step at 48 ºC for 10 min. remove excess of probes. Visualization via

epifluorescence microscopy (light source EXFO, X-Cite, Series 120 Q) was accomplished by mounting the hybridized sample with a mixture of DAPI-Citifuor (5 μg DAPI/ml) and imaging with a 100x objective (Microscope Olympus BX51, objective UPlan FL N, 100x /1.30 Oil, ∞/0.17/FN 26.5). The following FISH probes were used in this study (final concentration 2.5 ng/μl for each):
S-D-Arch-0915-a-A-20 in FITC, dual labeled: 5' to 3'= GTGCTCCCCCGCCAATTCCT (*47*)
S-*-ANME2c-0760-a-A-18 in Cy3, dual labeled: 5' to 3'= CGCCCCCAGCTTTCGTCC (*48*)
S-*-Dsb-0658-a-A-18 in Cy5, dual labeled: 5' to 3'= TCCACTTCCCTCTCCCAT (*49, 50*)

The overlay figures (Fig. 3 and Fig. S5-7) were contrast-adjusted for display purposes. FITC channel (Arc 915) is not shown. For aggregates that were positively stained for both ANME-2c and DSS, the DAPI channel was omitted for the overlay image.

nanoSIMS procedures and parameters for this study
After FISH and mapping (described above), the glass slides were scored and broken to size to fit in the Cameca "Geology" holder for the nanoSIMS, and coated with 50 nM gold to enhance conductivity. Secondary ion mass spectrometry analysis was carried out on a nanoSIMS 50L instrument (Cameca) using a primary Cs^+ ion beam. Pre- sputtering of target consortia was conducted with 100 pA current at D1=1 until 70,000-1,000,000 counts were reached on the ^{12}C detector. Analytical conditions included a 256x256 raster (or 512x512 raster for frames larger than 35 μm), ES=2, D1=4 (0.5 pA of current). Chained analyses were set up using SIBC, EOS, and HMR automatic peak centering every 2 frames using the $^{14}N^{12}C^-$ ion as reference. The following secondary ions were collected during the analysis: $^{12}C^-$, $^{13}C^-$, $^{12}C^{14}N^-$, $^{12}C^{15}N^-$, $^{32}S^-$, $^{33}S^-$ and $^{34}S^-$. 1-4 frames were collected for each aggregate. The ions $^{12}C^{14}N^-$ and $^{12}C^{15}N^-$ were used for the fractional abundances of ^{15}N reported in this study.

nanoSIMS data processing
Raw nanoSIMS data files were initially processed in the Matlab-based program Look@NanoSIMS (*51*) to align and accumulate frames and extract ion count data. FISH images of aggregates (described above) were used to define regions of interest (ROIs) on the nanoSIMS ion images that correspond to archaeal or bacterial biomass. Total ion counts in each ROI for $^{12}C^{15}N^-$ and $^{12}C^{14}N^-$ were used to calculate partner-specific relative biosynthetic activity ($^{15}N/(^{14}N+^{15}N)$) for each aggregate (data for Fig. 4A and 4B). For display purposes the median image filter medfilt2 from the Matlab Image Processing Toolbox was applied to the images of aggregate fractional abundance ^{15}N to reduce the noise of abnormally bright pixels. This filter was not applied to the raw data for any analyses.

Calculation of doubling times from average cellular ^{15}N after 18 days ($^{15}F_{18days}$)

Fraction of new biomass: $x = [B_{18days}-B_0] /B_{18days}$
With exponential growth: $x = 1 - \exp(-\mu * 18 \text{ days})$
With $^{15}F_0 \approx 0$: $^{15}F_{18days} = x * {}^{15}F_{NH4+}$
Specific growth rate: $\mu = -\ln(1-{}^{15}F_{18days}/{}^{15}F_{NH4+})/18 \text{ days}$
Doubling time: $t_d = \ln(2)/\mu$

$^{15}F_{NH4+}$ = 0.75 for sulfate and 0.86 for AQDS (see "Incubations for FISH-nanoSIMS")

2.6 REFERENCES IN THE MATERIALS AND METHODS

1. A. Boetius *et al.*, A marine microbial consortium apparently mediating anaerobic oxidation of methane. *Nature* **407**, 623 (2000).
2. V. J. Orphan, C. H. House, K. U. Hinrichs, K. D. McKeegan, E. F. DeLong, Methane-consuming archaea revealed by directly coupled isotopic and phylogenetic analysis. *Science* **293**, 484 (2001).
3. S. J. Hallam *et al.*, Reverse methanogenesis: Testing the hypothesis with environmental genomics. *Science* **305**, 1457 (2004).
4. S. Scheller, M. Goenrich, R. Boecher, R. K. Thauer, B. Jaun, The key nickel enzyme of methanogenesis catalyses the anaerobic oxidation of methane. *Nature* **465**, 606 (2010).
5. M. F. Haroon *et al.*, Anaerobic oxidation of methane coupled to nitrate reduction in a novel archaeal lineage. *Nature* **501**, 567 (2013).
6. E. J. Beal, C. H. House, V. J. Orphan, Manganese- and Iron-Dependent Marine Methane Oxidation. *Science* **325**, 184 (2009).
7. J. Milucka *et al.*, Zero-valent sulphur is a key intermediate in marine methane oxidation. *Nature* **491**, 541 (2012).
8. S. E. McGlynn, G. L. Chadwick, C. P. Kempes, V. J. Orphan, Single cell activity reveals direct electron transfer in methanotrophic consortia. *Nature* **526**, 531 (2015).
9. G. Wegener, V. Krukenberg, D. Riedel, H. E. Tegetmeyer, A. Boetius, Intercellular wiring enables electron transfer between methanotrophic archaea and bacteria. *Nature* **526**, 587 (2015).
10. W. S. Reeburgh, Oceanic methane biogeochemistry. *Chem. Rev.* **107**, 486 (2007).
11. K. Knittel, A. Boetius, Anaerobic oxidation of methane: progress with an unknown process. *Annu. Rev. Microbiol.* **63**, 311 (2009).
12. P. R. Girguis, A. E. Cozen, E. F. DeLong, Growth and population dynamics of anaerobic methane-oxidizing archaea and sulfate-reducing bacteria in a continuous-flow bioreactor. *Appl. Environ. Microbiol.* **71**, 3725 (2005).
13. V. J. Orphan, K. A. Turk, A. M. Green, C. H. House, Patterns of N-15 assimilation and growth of methanotrophic ANME-2 archaea and sulfate-reducing bacteria within structured syntrophic consortia revealed by FISH-SIMS. *Environmental Microbiology* **11**, 1777 (2009).
14. R. J. W. Meulepas *et al.*, Enrichment of Anaerobic Methanotrophs in Sulfate-Reducing Membrane Bioreactors. *Biotechnol. Bioeng.* **104**, 458 (2009).
15. T. Holler *et al.*, Thermophilic anaerobic oxidation of methane by marine microbial consortia. *Isme J.* **5**, 1946 (2011).
16. K. Nauhaus, T. Treude, A. Boetius, M. Krueger, Environmental regulation of the anaerobic oxidation of methane: A comparison of ANME-I and ANME-II communities. *Environmental Microbiology* **7**, 98 (2005).
17. K. Nauhaus, M. Albrecht, M. Elvert, A. Boetius, F. Widdel, In vitro cell growth of marine archaeal-bacterial consortia during anaerobic oxidation of methane with sulfate.

Environmental Microbiology **9**, 187 (2007).
18. S. B. Joye *et al.*, The anaerobic oxidation of methane and sulfate reduction in sediments from Gulf of Mexico cold seeps. *Chem. Geol.* **205**, 219 (2004).
19. A. Meyerdierks *et al.*, Metagenome and mRNA expression analyses of anaerobic methanotrophic archaea of the ANME-1 group. *Environmental Microbiology* **12**, 422 (2010).
20. F. P. Wang *et al.*, Methanotrophic archaea possessing diverging methane-oxidizing and electron-transporting pathways. *Isme J.* **8**, 1069 (2014).
21. M. J. Alperin, T. M. Hoehler, Anaerobic Methane Oxidation by Archaea/Sulfate-Reducing Bacteria Aggregates: 1. Thermodynamic And Physical Constraints. *Am. J. Sci.* **309**, 869 (2009).
22. B. Orcutt, C. Meile, Constraints on mechanisms and rates of anaerobic oxidation of methane by microbial consortia: process-based modeling of ANME-2 archaea and sulfate reducing bacteria interactions. *Biogeosciences* **5**, 1587 (2008).
23. R. J. W. Meulepas, C. G. Jagersma, A. F. Khadem, A. J. M. Stams, P. N. L. Lens, Effect of methanogenic substrates on anaerobic oxidation of methane and sulfate reduction by an anaerobic methanotrophic enrichment. *Appl. Microbiol. Biotechnol.* **87**, 1499 (2010).
24. D. R. Bond, D. R. Lovley, Reduction of Fe(III) oxide by methanogens in the presence and absence of extracellular quinones. *Environmental Microbiology* **4**, 115 (2002).
25. Additional supplementary information is available on Science Online.
26. L. G. Wilson, R. S. Bandurski, Enzymatic Reactions Involving Sulfate, Sulfite, Selenate, and Molybdate. *J. Biol. Chem.* **233**, 975 (1958).
27. T. Holler *et al.*, Carbon and sulfur back flux during anaerobic microbial oxidation of methane and coupled sulfate reduction. *Proc. Natl. Acad. Sci. U. S. A.* **108**, E1484 (2011).
28. M. Y. Yoshinaga *et al.*, Carbon isotope equilibration during sulphate-limited anaerobic oxidation of methane. *Nat. Geosci.* **7**, 190 (2014).
29. S. Pirbadian, M. Y. El-Naggar, Multistep hopping and extracellular charge transfer in microbial redox chains. *Phys. Chem. Chem. Phys.* **14**, 13802 (2012).
30. J. W. Voordeckers, B. C. Kim, M. Izallalen, D. R. Lovley, Role of Geobacter sulfurreducens Outer Surface c-Type Cytochromes in Reduction of Soil Humic Acid and Anthraquinone-2,6-Disulfonate. *Appl. Environ. Microbiol.* **76**, 2371 (2010).
31. K. Nauhaus, A. Boetius, M. Kruger, F. Widdel, In vitro demonstration of anaerobic oxidation of methane coupled to sulphate reduction in sediment from a marine gas hydrate area. *Environmental Microbiology* **4**, 296 (2002).
32. J. J. Marlow *et al.*, Carbonate-hosted methanotrophy represents an unrecognized methane sink in the deep sea. *Nat. Commun.* **5**, 5094 (2014).
33. A. Green-Saxena, A. E. Dekas, N. F. Dalleska, V. J. Orphan, Nitrate-based niche differentiation by distinct sulfate-reducing bacteria involved in the anaerobic oxidation of methane. *Isme J.* **8**, 150 (2014).
34. J. D. Cline, Spectrophotometric Determination of Hydrogen Sulfide in Natural Waters. *Limnol. Oceanogr.* **14**, 454 (1969).
35. R. Gamage, A. J. McQuillan, B. M. Peake, Ultraviolet Visible and Electron-Paramagnetic Resonance Spectroelectrochemical Studies of the Reduction Products of some

Anthraquinone Sulfonates in Aqueous-Solutions. *J. Chem. Soc.-Faraday Trans.* **87**, 3653 (1991).
36. J. B. Conant, H. M. Kahn, L. F. Fieser, S. S. Kurtz, An electrochemical study of the reversible reduction of organic compounds. *J. Am. Chem. Soc.* **44**, 1382 (1922).
37. A. E. Dekas, G. L. Chadwick, M. W. Bowles, S. B. Joye, V. J. Orphan, Spatial distribution of nitrogen fixation in methane seep sediment and the role of the ANME archaea. *Environmental Microbiology* **16**, 3012 (2014).
38. E. Trembath-Reichert, A. Green-Saxena, V. J. Orphan, in *Microbial Metagenomics, Metatranscriptomics, and Metaproteomics,* E. F. DeLong, Ed. (Elsevier Academic Press Inc, San Diego, 2013), vol. 531, pp. 21-44.
39. C. Quast *et al.*, The SILVA ribosomal RNA gene database project: improved data processing and web-based tools. *Nucleic Acids Res.* **41**, D590 (2013).
40. S. F. Altschul *et al.*, Gapped BLAST and PSI-BLAST: a new generation of protein database search programs. *Nucleic Acids Res.* **25**, 3389 (1997).
41. W. Ludwig *et al.*, ARB: a software environment for sequence data. *Nucleic Acids Res.* **32**, 1363 (2004).
42. F. Ronquist *et al.*, MrBayes 3.2: Efficient Bayesian Phylogenetic Inference and Model Choice Across a Large Model Space. *Syst. Biol.* **61**, 539 (2012).
43. S. J. Hallam, P. R. Girguis, C. M. Preston, R. M. Richardson, E. F. Delong, Identification of methyl coenzyme M reductase A (mcrA) genes associated with methane-oxidizing archaea. *Appl Environ Microbiol* **69**, 5483 (2003).
44. O. Mason *et al.*, Comparison of Archaeal and Bacterial Diversity in Methane Seep Carbonate Nodules and Host Sediments, Eel River Basin and Hydrate Ridge, USA. *Microb. Ecol.* **70**, 766 (2015).
45. J. G. Caporaso *et al.*, QIIME allows analysis of high-throughput community sequencing data. *Nat. Methods* **7**, 335 (2010).
46. B. M. Fuchs, J. Pernthaler, R. Amann, Single cell identifcation by fuorescence in situ hybridization. *Methods for general and molecular microbiology* **3**, 886 (2007).
47. R. I. Amann, L. Krumholz, D. A. Stahl, Fluorescent-Oligonucleotide Probing of Whole Cells for Determinative, Phylogenetic, and Environmental-Studies In Microbiology. *J. Bacteriol.* **172**, 762 (1990).
48. K. Knittel, T. Losekann, A. Boetius, R. Kort, R. Amann, Diversity and distribution of methanotrophic archaea at cold seeps. *Appl. Environ. Microbiol.* **71**, 467 (2005).
49. W. Manz, M. Eisenbrecher, T. R. Neu, U. Szewzyk, Abundance and spatial organization of Gram-negative sulfate-reducing bacteria in activated sludge investigated by in situ probing with specific 16S rRNA targeted oligonucleotides. *FEMS Microbiol. Ecol.* **25**, 43 (1998).
50. T. Losekann *et al.*, Diversity and abundance of aerobic and anaerobic methane oxidizers at the Haakon Mosby mud volcano, Barents Sea. *Appl. Environ. Microbiol.* **73**, 3348 (2007).
51. L. Polerecky *et al.*, Look@NanoSIMS - a tool for the analysis of nanoSIMS data in environmental microbiology. *Environmental Microbiology* **14**, 1009 (2012).
52. B. Thamdrup, Bacterial manganese and iron reduction in aquatic sediments. *Advances*

in Microbial Ecology **16**, 41 (2000).
53. G. S. Wilson, Determination of oxidation-reduction potentials. *Methods in enzymology* **54**, 396 (1978).
54. M. L. Fultz, R. A. Durst, Mediator Compounds for the Electrochemical Study of Biological Redox Systems - a Compilation. *Anal. Chim. Acta* **140**, 1 (1982).
55. R. S. Twigg, Oxidation-Reduction Aspects of Resazurin. *Nature* **155**, 401 (1945).
56. M. Aeschbacher, D. Vergari, R. P. Schwarzenbach, M. Sander, Electrochemical Analysis of Proton and Electron Transfer Equilibria of the Reducible Moieties in Humic Acids. *Environ. Sci. Technol.* **45**, 8385 (2011).
57. H. S. Mason, D. J. E. Ingram, B. Allen, The Free Radical Property of Melanins. *Arch. Biochem. Biophys.* **86**, 225 (1960).

2.7 ACKNOWLEDGEMENTS

We thank Y. Guan for assistance with the nanoSIMS and M. Aoki for FISH analysis of ANME-2a and ANME-2c consortia and S. Goffredi and C. Skennerton for editorial comments. We are grateful to P. Brewer from the Monterey Bay Aquarium Research Institute for providing the opportunity to participate on the May 2013 research expedition with the R/V Western Flyer and A. Pasulka and K. Dawson for their contributions with shipboard sample collection and processing. This work was supported by the Department of Energy BER program (DE-SC0010574 and DE-SC0004940) and funding by the Gordon and Betty Moore Foundation through Grant GBMF3306 and Grant GBMF3780 (to VJO). S.S. was supported in part by the Swiss National Science Foundation (Grant# PBEZP2_142903). All data are available in the supplementary materials. Sequence data is submitted to NCBI.

2.8 AUTHOR CONTRIBUTIONS

SS, HY, and VJO devised the study. SS, HY, GLC, and SM conducted the experiments and analyses. SS and VJO wrote the manuscript with contributions from all authors, including data analysis, figure generation, and the final manuscript.

Chapter 3

TRANSCRIPTIONAL RESPONSES OF DEEP-SEA ARCHAEA DECOUPLED FROM THEIR SYNTROPHIC SULFATE-REDUCING BACTERIA PARTNER

Hang Yu[1,2], Connor T. Skennerton[1], Grayson L. Chadwick[1], Andy O. Leu[3], Roland Hatzenpichler[1,6], Danielle Goudeau[4], Rex R. Malmstrom[4], Tanja Woyke[4], Gene W. Tyson[3,5], Victoria J. Orphan[1]

[1]Division of Geological and Planetary Sciences, California Institute of Technology, Pasadena, CA 91125, USA

[2]Ronald and Maxine Linde Center for Global Environmental Science, California Institute of Technology, Pasadena, CA 91125, USA

[3]Australian Centre for Ecogenomics, University of Queensland, St. Lucia, QLD 4072, Australia

[4]Joint Genome Institute, Department of Energy, Walnut Creek, CA 94598, USA

[5]Advanced Water Management Centre, University of Queensland, St. Lucia, QLD 4072, Australia

[6]Present Address: Department of Chemistry and Biochemistry, Montana State University, Bozeman, MT 59717, USA

This chapter is in preparation for publication.

3.1 ABSTRACT

A syntrophic partnership of anaerobic methane-oxidizing archaea (ANME) and sulfate-reducing bacteria (SRB) consumes teragrams of methane annually in marine ecosystems, yet the basic mechanism of this symbiotic interaction remains poorly understood. Recent imaging, genomic, and physiological studies suggest direct interspecies electron transfer as the underlying mechanism of ANME-SRB metabolic coupling in the anaerobic oxidation of methane (AOM) with sulfate. Here we use paired metagenomics and metatranscriptomics to understand the pathways in individual AOM consortium for the canonical ANME-SRB syntrophic association and for ANME alone with AQDS, a humic acid analog as their electron sink. The overall expression profiles indicate that SRB are transcriptionally inactive in the presence of AQDS, hypothesized to be due to a lack of methane-derived electrons from ANME. This corroborates the single-cell anabolic activity patterns observed with $^{15}NH_4^+$ stable isotope probing using nanoscale secondary ion mass spectrometry. Metagenomes were created from paired bulk methane seep sediment incubations, and individual active AOM consortia labelled by bioorthogonal noncanonical amino acid tagging were separated from methane seep sediment using flow cytometry and individually sequenced to provide a better genomics framework for specific ANME-SRB partnerships. All known sulfate reduction genes in SRB were inactive in the metatranscriptome, indicating that pathways of methane oxidation and sulfate reduction was not linked in one organism as proposed previously. Comparing genes expressed by ANME with or without their syntrophic partner reveals and validates previous genomic hypotheses on the use of membrane and periplasmic cytochrome-containing complexes to directly transfer electrons extracellularly. Furthermore, expression of metabolic genes over a period of 3-9 days showed an initial upregulation but little variation afterwards, suggesting a controlled short-term gene expression in the ANME-SRB consortia that double on average every 3-7 months. Lastly, in the presence of low levels of sulfate, ANME show comparable methane oxidizing and biosynthetic activity while reducing AQDS. By studying

transcriptional responses together with metagenomics and single-cell activity probing of individual consortia, we provide evidence for direct interspecies electron transfer using multiheme cytochromes between ANME and their SRB partner as well as insight into the cellular machineries that facilitate the extracellular electron flow in AOM.

3.2 INTRODUCTION

Anaerobic oxidation of methane (AOM) with sulfate is an important biogeochemical process in the global carbon cycle. It consumes over 90% of the methane fluxing out of marine sediment annually (Knittel and Boetius 2009). This process is mediated by a symbiosis between anaerobic methanotrophic archaea (ANME) and sulfate reducing bacteria (SRB). Since the discovery of these consortia over 15 years ago, the mechanism of how ANME and SRB are able to couple their metabolisms through electron sharing has remained elusive. It was first hypothesized that a diffusible intermediate such as hydrogen could be involved in this syntrophy, but experimental work with the addition of such diffusible compounds failed to decouple the syntrophy (Nauhaus et al. 2005; Meulepas et al. 2010; Wegener et al. 2016). Milucka and colleagues proposed an alternative hypothesis in which ANME performs both methane oxidation and sulfate reduction to zero-valent sulfur, which is then transferred to SRB and disproportionated (Milucka et al. 2012). As yet there is no genomic evidence that dissimilatory sulfate reduction occurs in ANME, based on my detailed analysis of putative sulfur metabolic genes in known ANME genomes covered in Chapter 1 of this thesis. Microcosm experiments using samples from different methane seeps also provided results inconsistent with zero-valent sulfur as the intermediate in AOM syntrophy (McGlynn et al. 2015; Wegener et al. 2015; Wegener et al. 2016). An alternative hypothesis has recently emerged, supported by genomic, modeling and physiological evidence, that point to direct extracellular transfer of electrons from ANME to SRB using multiheme cytochromes (Meyerdierks et al. 2010; McGlynn et al. 2015; Wegener et al. 2015). This was further supported by experimental evidence that ANME maintained net anaerobic methane

oxidation and were biosynthetically active in the absence of sulfate (Scheller et al. 2016). Under sulfate-free condition, ANME reduced alternative electron acceptors such as anthraquinone-2,6-disulfonate (AQDS) and iron citrate, and showed biosynthetic activity in the absence of activity in their associated syntrophic SRB partner, a first example of this symbiosis decoupled. There are still important questions remaining regarding how ANME couples AOM to AQDS reduction, and changes in transcriptional activities in the absence of an active syntrophic partners.

Here we used metatranscritompics to study uncultivated AOM consortia in complex environmental samples. These consortia grow slowly with doubling times range from 3-7 months (Girguis, Cozen, and DeLong 2005; Nauhaus et al. 2007; Meulepas et al. 2009) and therefore it is difficult to assess the active processes in the cells and their responses to experimental perturbation. Metatranscriptomics has been successful in circumventing this issue, and provides direct genetic insights into active processes in uncultivated microbes (Moran et al. 2013). To focus on transcriptional responses of specific ANME-SRB partnership, we used bioorthogonal noncanonical amino acid tagging coupled to fluorescence-activated cell sorting (BONCAT-FACS). Environments such as deep-sea methane seeps often host thousands of species (Ruff et al. 2015), and even the dominant groups such as AOM consortia, a large diversity often exist (Knittel and Boetius 2009). Multiple clades of ANME such as ANME-1 and ANME-2a, ANME-2b and ANME-2c coexist and partner up with different clades of SRB including SEEP-SRB-1 and SEEP-SRB-2 (Orphan et al. 2002; Pernthaler et al. 2008). We reduced sample complexity and sequenced genomes of individual active ANME-SRB from methane seep sediments using the BONCAT-FACS method (Hatzenpichler et al. 2016).

In this study, we used multiple types of activity measurements to study the response of ANME with or without active syntrophic SRB partner. The metabolic activities of AOM consortia were tracked over 9 days, representing at most one tenth of doubling time. Afterwards, the incorporation of $^{15}NH_4^+$ was used as a proxy for cellular biosynthetic activities

and measured using fluorescence in situ hybridization coupled to nanoscale secondary ion mass spectrometry (FISH-nanoSIMS) to understand the short-term responses of ANME to different electron acceptors. RNA samples were also taken during this time course experiment. The resulting metatranscriptomes were mapped onto paired metagenomes obtained using BONCAT-FACS to understand the transcriptional responses of single AOM consortium. Our anabolic analysis showed slow-growth of these microbes, but by sampling RNA at 3-9 days, we were able to gain insights into short-term responses of AOM consortia to different electron acceptors.

3.3 MATERIALS AND METHODS

3.3.1 Sample collection and microcosm setup

The methane seep sediment sample (sediment #7142 or PC61) was collected from Santa Monica basin (lat. 33.78905, long. -118.66833) below a white microbial mat during a research cruise organized by the Monterey Bay Aquarium Research Institute (MBARI) on board of *R/V Western Flyer* using *R/V Doc Ricketts* in May 2013. The intact sediment core was stored in a heat-sealed mylar bag flushed with argon for 5 minutes. The sediment was then transferred into a 1 L bottle and incubated with methane (0.2 MPa) with natural seawater (collected around the seep site) for ca. 30 months with periodic replacement and addition of anoxic natural seawater. Prior to the experiments, the sediment was washed 3 times with anoxic sulfate-free artificial seawater (ASW) and incubated under methane headspace (0.2 MPa) for 6 months. Sample manipulations were done on ice and incubations were kept at 4°C. Further details on ASW composition and initial sediment characterization can be found in Chapter 2.

Prior to setting up the microcosm experiments, the sediment headspace was switched to N_2:CO_2 (80:20, 0.2 MPa) by flushing for 5 minutes and then incubated overnight at 4°C to allow stabilization. Microcosms were setup in 30-mL serum bottles (Wheaton, USA)

capped with black butyl rubber stoppers (Geo-Microbial Technologies, Inc., Ochelata, OK) each containing 2 ml of wet sediment (wet sediment = sediment after settling for at least 48 hours) and 8 ml of sulfate-free ASW. For incubations with methane and different electron acceptors, each serum bottle was sparged with N_2 for 5 minutes followed by unlabeled CH_4 for 2 minutes, before injecting 0.9 ml of $^{13}CH_4$ (99% ^{13}C, Cambridge Isotope Laboratories, previously determined to containing 0.05 vol% $^{13}CO_2$ as an impurity (Scheller et al. 2016)). 2 ml of 0.22 μm filtered anoxic solutions containing 12.5 mM Na_2SO_4 (Macron Fine Chemicals™), 50 mM AQDS (anthraquinone-2,6-disulfonate, >98%, Sigma Chemicals), or both 12.5 mM Na_2SO_4 and 50 mM AQDS dissolved in MilliQ deionized water was injected into each bottle and mixed with 2 ml of 2x ASW without sulfate. For bottles with no electron acceptor (methane only control), 2 ml of MilliQ deionized water was injected into each instead. For bottles with N_2:CO_2 headspace instead of methane, N_2:CO_2 gas was used instead of methane for flushing before electron acceptor addition. All bottles (total = 45) were incubated on ice for 1 hour before 6 ml of well-mixed 7142 slurry was injected into each and pressurized with unlabelled CH_4 or N_2:CO_2. Final concentrations for sulfate and AQDS in the incubations were 2.5 mM and/or 10 mM, and final pressures for both CH_4 and N_2:CO_2 were 0.35 MPa.

3.3.2 Geochemistry measurements

Geochemistry measurements were performed on subsamples of the microcosms over a 9-day period immediately following the setup. 0.5 ml of supernatant was sampled anaerobically from each microcosm after 1.5 hour (day 0), 24 hours (day 1), 72 hours (day 3), 144 hours (day 6), and 216 hours (day 9) post initial setup (Supplementary Table 1A). This supernatant was filtered through a 0.22 μm filter; 0.15 ml of the filtrate was immediately flash frozen for DIC measurement, stored at -20°C, and analyzed as described previously (Scheller et al. 2016). The remaining filtrate (ca. 0.3 ml) of the filtrate was injected into a 10-ml serum bottle (Wheaton, USA) capped with blue butyl rubber stopper (Chemglass Life Sciences, Vineland, NJ, USA) that had been previously flushed with N_2 for 5 minutes. In an

anaerobic chamber (N2:H2=95:5), the 10-ml serum bottles were opened. 50 µl of the filtrate was mixed with 450 µl of pH 2 anoxic seawater and measured photospectrometrically by quantifying absorption at 428 nm compared to known concentrations of AQDS reduced with dithionite. 100 µl of the filtrate was preserved in 400 µl of 0.5 M zinc acetate solution and later measured by quantifying the absorbance at 670 nm via the methylene blue method (Cline 1969). The remaining filtrate was flash frozen and stored in -20°C; later, 30 µl was used for sulfate quantification via ion chromatography (Dionex ICS-3000, using an AS-19 column and bicarbonate eluent at the Caltech Environmental Analysis Center).

For microscopy and RNA preservation for metatranscriptomics, all supernatant from the microcosm was removed anaerobically and saved for geochemistry measurement as described above (Supplementary Table 1B). 8 ml of N_2-sparged Lifeguard™ Soil Preservation Solution (MoBio Laboratories, Carlsbad, CA) was immediately injected into the serum bottle and thoroughly mixed on ice. 1 ml of the Lifeguard-sediment mixture was subsampled and fixed in 1.33% paraformaldehyde at 4°C for 2 hours for microscopy, and the rest of the mixture was kept at 4°C overnight in the serum bottle to allow complete reaction of the LifeGuard solution with the RNA samples. Microscopy samples were later washed twice with 1x phosphate-buffered saline (PBS; 145 mM NaCl, 1.4 mM NaH_2PO_4, 8 mM Na_2HPO_4 at pH 7.4), resuspended in PBS:ethanol (1:1), and stored at -20°C. RNA samples in LifeGuard solution were pelleted next day by centrifuging at 5250 x g for 20 minutes at 4°C in 15-ml falcon tubes; the supernatant was discarded and the remaining pellet was flash frozen and stored at -80°C.

3.3.3 Metagenomics of bulk sediment and individually sorted active consortia

DNA was extracted from flash frozen sediment #7142 (ca. 2 mL slurry) using the FastDNA SPIN kit for soil (MPBio) according to the manufacturer's protocol. DNA concentrations were quantified using the Quant-iT dsDNA HS assay kit (Invitrogen) as per the manufacturer's instructions. The paired-end library was prepared using the Nextera XT

DNA library preparation kit (Illumina, USA) for DNA extracted. The libraries were sequenced on a NextSeq500 (Illumina, USA) platform at the University of Queensland, generating 2×150 bp paired-end reads with an average insert length of 300 bp.

The draft genomes from an active ANME-2a/Seep-SRB1a consortia (G09) was generated at the DOE Joint Genome Institute (JGI) using the BONCAT-FACS method (Hatzenpichler et al. 2016). A 300 bp insert standard shotgun library was constructed and sequenced using the Illumina NextSeq platform which generated 15,936,036 reads totaling 2,390.4 Mbp. All general aspects of library construction and sequencing performed at the JGI can be found at http://www.jgi.doe.gov. BBTools software tools (https://sourceforge.net/projects/bbmap/) was used to remove Illumina artifacts, PhiX, reads with more than one "N" or with quality scores (before trimming) averaging less than 8 or reads shorter than 51 bp (after trimming), reads with >95% identity mapped to masked versions of human, cat, and dog references. Then, reads with high k–mer coverage (>100X average k–mer depth) were normalized and error corrected to an average depth of 100X. Reads with an average k–mer depth of less than 2X were removed. These reads were assembled using SPAdes (version 3.6.2) (Bankevich et al. 2012), and any contigs with length is <1 kbp were discarded. Parameters for the SPAdes assembly were –t 16 –m 120 —sc –k 25,55,95 —12. The final draft assembly contained 554 contigs in 525 scaffolds, totaling 5.043 Mbp in size.

3.3.4 FISH-nanoSIMS analysis

PFA-fixed AOM consortia in the microscopy samples were concentrated by percoll, followed by embedding and sectioning as previously (McGlynn et al. 2015). FISH was done on 1 μm thin sections using protocols as described previously (McGlynn et al. 2015). The following oligonucleotide probes fluorescently labeled on both the 5' and 3' ends and 40% formamide concentrations were used in the FISH reactions: ANME-2a-828 dual labelled with Alexa488, ANME-2c dual labelled with Cy3, and DSS658 dual labelled with Cy5. 5

μg/ml of DAPI-Citifluor solution was added prior to visualization. After imaging with a 100x objective (Olympus), DAPI-Citifluor was washed off the thin sections and prepared for nanoSIMS analysis. nanoSIMS sample preparation, analysis, and data processing were done as previously (McGlynn et al. 2015; Scheller et al. 2016). ^{15}N atom percentage in the cells was used as a proxy for biosynthetic activity and calculated using ions collected from the nanoSIMS as follows: $^{15}N^{12}C^{-}/(^{15}N^{12}C^{-}+^{14}N^{12}C^{-})$ (McGlynn et al. 2015).

3.3.5 RNA extraction and analysis

RNA was extracted from microcosm samples in replicates (Supplementary Table 1B) using RNA PowerSoil Total RNA Isolation kit (MoBio Laboratories) according to manufacturer's protocol. Turbo DNA-free kit (Ambion) was used to remove genomic DNA and purified using RNeasy MinElute cleanup kit (Qiagen). rRNA subtraction was performed using Ribo-Zero Magnetic kit (Epicentre) as per the manufacturer's instructions. RNA was prepared for sequencing using the ScriptSeq stranded mRNA library prep kit (Illumina, USA) following the manufacturer's protocol. The library was sequenced on a NextSeq500 (Illumina, USA) platform at the University of Queensland, generating 2×150 bp paired-end reads with an average insert length of 300 bp.

RNA reads were mapped to a database containing multiple single aggregate metagenomes generated from sediment #7142 using kallisto and sleuth software packages (Bray et al. 2016; Pimentel et al. 2016). A normalized ratio expressed as transcripts per million (TPM) values, after taking into account differential read length and sequencing depth between samples, were used for further analysis and plots. To obtain taxonomy information of the transcripts, each assembled transcript was determined by comparing them to the NCBI refseq proteins as a database using diamond v0.8.11.73 and then finding the lowest common ancestor of the blast hits using the program blast2lca v0.400 (https://github.com/emepyc/Blast2lca). All sequences were assigned to one of eight groups based on their taxonomy string. To obtain metabolic pathway information for the transcripts,

assembled transcripts were functionally annotated using the ghostKOALA webserver provided by KEGG (http://www.kegg.jp/ghostkoala/), using the "genus_prokaryotes" database. For both taxonomic and metabolic analyses, the sum of the TPM was calculated for each replicate of each condition for each of the taxonomic groups or kegg pathways. The mean and standard deviation was then calculated for each taxonomic group or pathway between the triplicates.

3.4 RESULTS AND DISCUSSION

3.4.1 Incubation setup and geochemistry

Methane seep sediment (#7142) quickly resumed AOM activity after sulfate addition, as evident in the linear increases in concentrations of ^{13}C-labelled dissolved inorganic carbon (DIC) and sulfide, as products of ^{13}C-labelled methane and sulfate (Figure 1A). The ratio between sulfide and DIC produced are off from the predicted 1:1 reaction stoichiometry; compared to the amount of sulfate consumed, 25-50% of sulfide or DIC produced could be partially oxidized during sampling or precipitated over the course of this experiment. In the absence of sulfate, the humic acid analog AQDS can serve as the electron acceptor for AOM as described previously (Figure 1B) (Scheller et al. 2016). Interestingly, when both sulfate and AQDS were added to incubations with CH_4, only AQDS was reduced. Sulfate was not consumed but a higher rate of DIC production and AQDS reduction was observed relative to microcosms with CH_4 and AQDS (Figure 1C). Negligible amounts of DIC were consumed or produced in the methane only control without an added terminal electron accetpro (sulfate or AQDS) (Figure 1D), indicating an absence of methanogenesis or methanotrophy coupled to endogenous electron acceptors in the sediment under our experimental conditions. Corresponding controls lacking CH_4 also showed negligible amounts of sulfate or AQDS reduction (Figure 1A-C), indicating minor contributions of non-methane coupled sulfate or AQDS reduction from organics in the sediment over the course of our experiment.

We further probed the nearly two-fold stimulatory effect observed of sulfate on AOM coupled to AQDS reduction with decreasing levels of sulfate. Under canonical AOM with sulfate conditions, sulfate (50-2500 μM) was consumed down to 4-25 μM (detection limit = 1 μM) after 16 days (Supplementary Figure 1A). In incubations containing both AQDS and sulfate however, sulfate concentrations remain largely unchanged (Supplementary Figure 1B), but AQDS reduction rates increased in the presence of sulfate

compared to the microcosm without sulfate addition (Supplementary Figure 1C). The sulfate stimulatory effect was found to be most pronounced between 100 to 2500 μM of sulfate added, and with less of an effect at 50 μM sulfate (Supplementary Figure 1C). The lack of appreciable sulfate reduction concurrent with stimulated AQDS reduction could be explained by two scenarios depending on the activity of ANME and SRB. One scenario is that ANME reduce AQDS, and they require or assimilate or are stimulated by low levels of sulfate, but their SRB partners remain inactive during this process. Alternatively, both ANME and SRB are active, with ANME reducing AQDS and SRB reducing sulfate. In this scenario, the sulfide produced from sulfate reduction is chemically oxidized by AQDS generating zero-valent sulfur, which could further increase its reduction rate through disproportionation reaction by SRB, as described in a previous hypothesis (Milucka et al. 2012). SRB would switch its metabolism to zero-valent sulfur disproportionation, creating a cycling of sulfur using AQDS without sulfate consumption. ANME has two electron sinks, one being the direct interaction with AQDS and the other being its SRB partner, increasing the AOM rate. Schematics of these two scenarios can be found in Supplementary Figure 2.

3.4.2 FISH-nanoSIMS activity probing

AOM consortia incubated with $^{15}NH_4^+$ and different terminal electron acceptors were analyzed after 9 days using FISH-nanoSIMS in order to distinguish these two scenarios. This approach revealed both the phylogenetic identity of the two partners in the AOM consortia and their biosynthetic activity from $^{15}NH_4^+$ assimilation at the single-cell level (Figure 2). Comparing incubations with sulfate or AQDS as electron acceptor, the results were consistent with AOM consortia or ANME only activities as observed previously, with a much lower SRB activity compared to ANME in the presence of AQDS (Figure 3A) (McGlynn et al. 2015; Scheller et al. 2016). The methane only control incubation without an added electron acceptor showed no biosynthetic activity in either partners (Supplementary Table 2). Single-cell level analysis of ANME showed comparable activity in the Sulfate and AQDS+Sulfate conditions, both are higher than the biosynthetic activity observed in the

AQDS condition (Figure 3B and Supplementary Table 2). SRB was only biosynthetically active in the sulfate condition (Figure 3B and Supplementary Table 2). The larger deviation and small portion of active SRB cells observed with ^{15}N atom percentage higher than natural nitrogen abundance might be due to mismatches between FISH and nanoSIMS cell identification. Taken together, these results support the first scenario in which SRB is inactive in the presence of AQDS and ANME or AOM is stimulated by sulfate for reasons unknown, as shown by single-cell and population biosynthetic activities. It remains possible that SRB reduce sulfate or AQDS without conserving energy, but it is unlikely that residual proteins in SRB can sustain the same rate of AQDS reduction or AOM over the course of this experiment without energy input by reducing sulfate and synthesis of new proteins.

3.4.3 Metatranscriptomics of an individual AOM consortium

Metatranscriptomics was performed on these microcosms to gain further insight into the active processes during AOM syntrophy involving ANME-2a/2b/2c archaea and their SRB partners with sulfate as the electron acceptor, in comparison to conditions involving active ANME but inactive SRB partners with AQDS or AQDS+Sulfate as the electron acceptor. A majority of transcripts in the Sulfate, AQDS, and AQDS+Sulfate treatments were associated with the *Methanosarcinales* (Figure 4A). This is expected since the dominant ANME groups in this sediment sample (ANME-2a and ANME-2c) both belong to *Methanosarcinales*, and are actively oxidizing methane. Transcripts belonging to *Deltaproteobacteria*, which contain the dominant SRB group in this sample (Seep-SRB1), were a large portion of the total transcripts when sulfate was used as the electron acceptor, but not with AQDS or AQDS+Sulfate. This further supports that SRB are not active either biosynthetically or transcriptionally in the presence of AQDS, and ANME activity can be decoupled from their partner using AQDS as the electron acceptor for AOM either with or without sulfate. Looking at the major metabolic pathways, the majority of the mRNA transcripts can be assigned to methane metabolism, which increase significantly with electron acceptor addition (Figure 4B). Transcripts assigned to sulfur metabolism was the second

most abundant metabolism with sulfate as the electron acceptor, but not with AQDS+Sulfate as the electron acceptor (Figure 4B). Sulfur metabolism transcripts remained low in both AQDS and AQDS+Sulfate conditions, matching the FISH-nanoSIMS result showing biosynthetically active ANME but inactive SRB. These independent lines of evidences demonstrate that ANME-2a and ANME-2c can remain both biosynthetically and transcriptionally active without their SRB partner.

A large diversity of ANME and SRB groups co-exist in methane seep sediments. The specificity and selectivity in these partnerships are poorly understood, and may employ different symbiotic mechanisms. To gain insight into a particular AOM partnership, individual active AOM consortia were separated using BONCAT-FACS, and subsequently lysed and amplified prior genome sequencing to obtain information on specific ANME-SRB partnerships in our microcosms. Previous 16S rRNA gene sequencing result showed a representative sorting of dominant ANME and SRB groups from the bulk sediment and provided partnership information of AOM consortia in this sediment sample (Hatzenpichler et al. 2016). Our metatranscriptomic analysis then focused on one consortium of ANME-2a and Seep-SRB1a with the highest genomic coverage of both partners (52% and 67% genome completeness for ANME-2a and Seep-SRB1a, respectively) from the same sediment sample. In this consortium, all genes in the AOM pathway were expressed in our experimental conditions, but the sulfate reduction pathway in Seep-SBR1a was significantly downregulated with AQDS (Figure 4). It was hypothesized that membrane b-type cytochrome (cytB) couples methanephenazine (MP) oxidation to reduction of multiheme c-type cytochromes (MHC) that may be bound to the S-layer (McGlynn et al. 2015). All these components in ANME-2a were expressed with either sulfate or AQDS as the electron acceptor, indicating that they are likely important for the extracellular electron transfer (EET) from ANME to either their SRB partner or artificial electron acceptor AQDS. Complementary MHC-containing operons have been identified in SRB genomes (Skennerton et al. In review), and were expressed with sulfate but not with AQDS or AQDS+Sulfate as the electron acceptor (Figure 5). This indicates that Seep-SRB1a in this

specific partnership with ANME-2a are transcriptionally inactive with AQDS, in agreement with the observations of the bulk metatranscriptome (Figure 4). Interestingly, the expression of Seep-SRB1a genes with AQDS are even lower than that of control with methane only, possibly due to fast degradation of mRNA transcripts without active transcription (Figure 4). Over the time course of our experiment from 3-9 days, transcription of genes in methane oxidation, sulfate reduction, and extracellular electron transfer show differences in transcriptional responses of ANME compared to that of SRB: transcripts of ANME genes show steady increase over time, whereas transcripts of SRB genes increase rapidly by day 3 and then show similar levels of expression afterwards (Supplementary Figure 3). This may indicate differences in transcriptional regulation between archaea and bacteria.

3.4.4 Conclusions

Our combined results from geochemical measurements, FISH-nanoSIMS, metagenomics, and metatranscriptomics of individual AOM consortium provide insights into the enigmatic syntrophy in AOM. ANME can be decoupled from their SRB partner using AQDS as the electron acceptor and remain both biosynthetically and transcriptionally active. By tracking the rates of AOM and AQDS reduction, it is observed that sulfate stimulates ANME and AOM while SRB are inactive either biosynthetically or transcriptionally. The reason for this stimulation is currently unknown, but likely due to a direct effect of sulfate on ANME. Metatranscriptomics also show active transcription of different multiheme cytochromes in ANME and SRB that have been proposed for AOM syntrophy, supporting the hypothesis of direct interspecies electron transfer as the symbiotic mechanism in AOM. Moreover, the genes in AOM, sulfate reduction, and extracellular electron transfer all show sustained transcriptional levels from 3 to 9 days, suggesting that an initial fast response to electron acceptor addition followed by a sustained level of transcription in these slow-growing microbes. By combining different activity measurements together, this study provides insights into symbiosis and the specific cellular machineries that are used to facilitate the extracellular electron flow in AOM.

3.5 TABLES AND FIGURES

Figure 1. Geochemical measurements of microcosms with different electron acceptors (sulfate in A, AQDS in B, AQDS+Sulfate in C, and no electron acceptor or methane only control in D). Concentrations of dissolved inorganic carbon (DIC), sulfate, sulfide and reduced AQDS (AQH2DS) are tracked as proxies for AOM consortia activities.

A

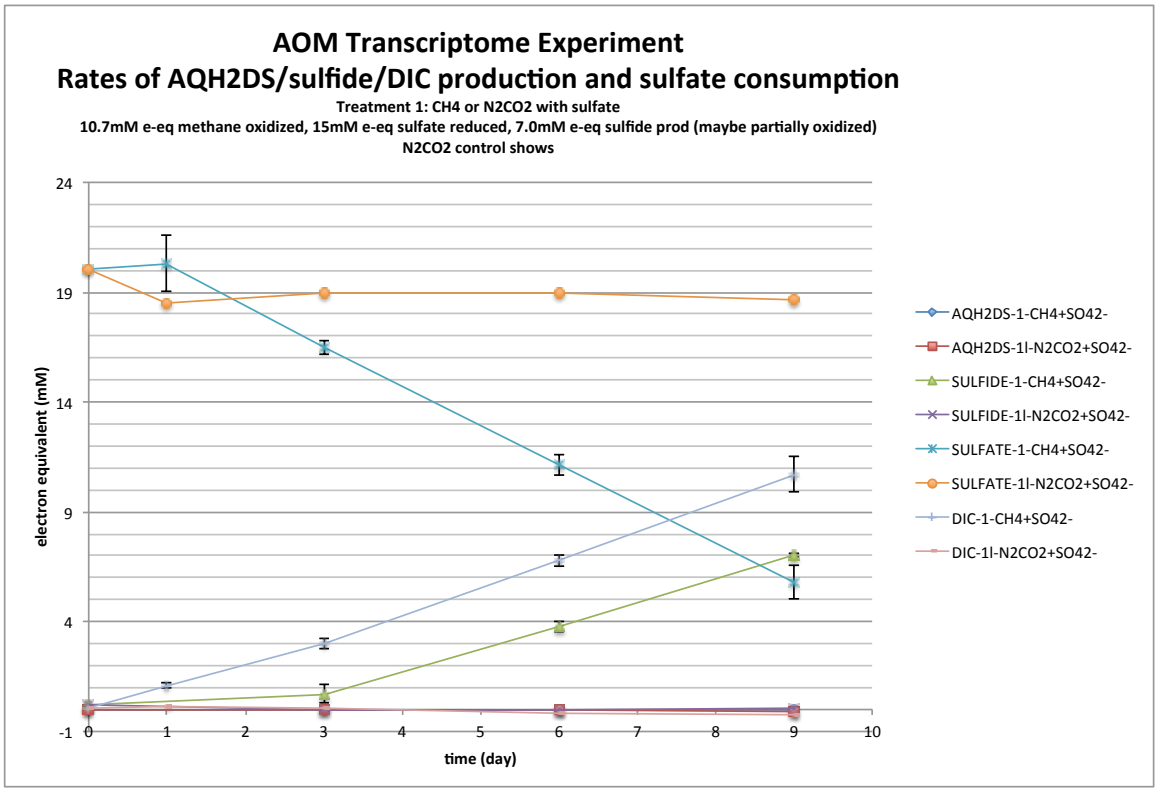

B

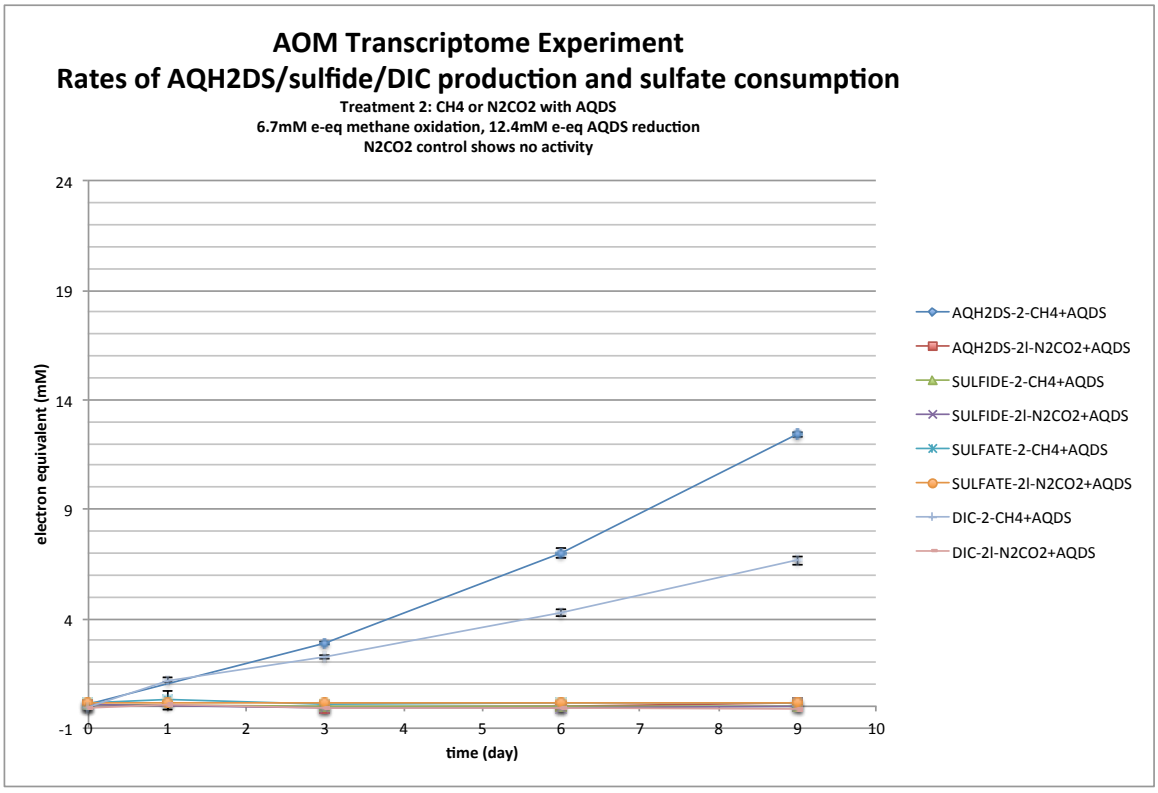
AOM Transcriptome Experiment
Rates of AQH2DS/sulfide/DIC production and sulfate consumption
Treatment 2: CH4 or N2CO2 with AQDS
6.7mM e-eq methane oxidation, 12.4mM e-eq AQDS reduction
N2CO2 control shows no activity
electron equivalent (mM)
time (day)
AQH2DS-2-CH4+AQDS
AQH2DS-2l-N2CO2+AQDS
SULFIDE-2-CH4+AQDS
SULFIDE-2l-N2CO2+AQDS
SULFATE-2-CH4+AQDS
SULFATE-2l-N2CO2+AQDS
DIC-2-CH4+AQDS
DIC-2l-N2CO2+AQDS

C

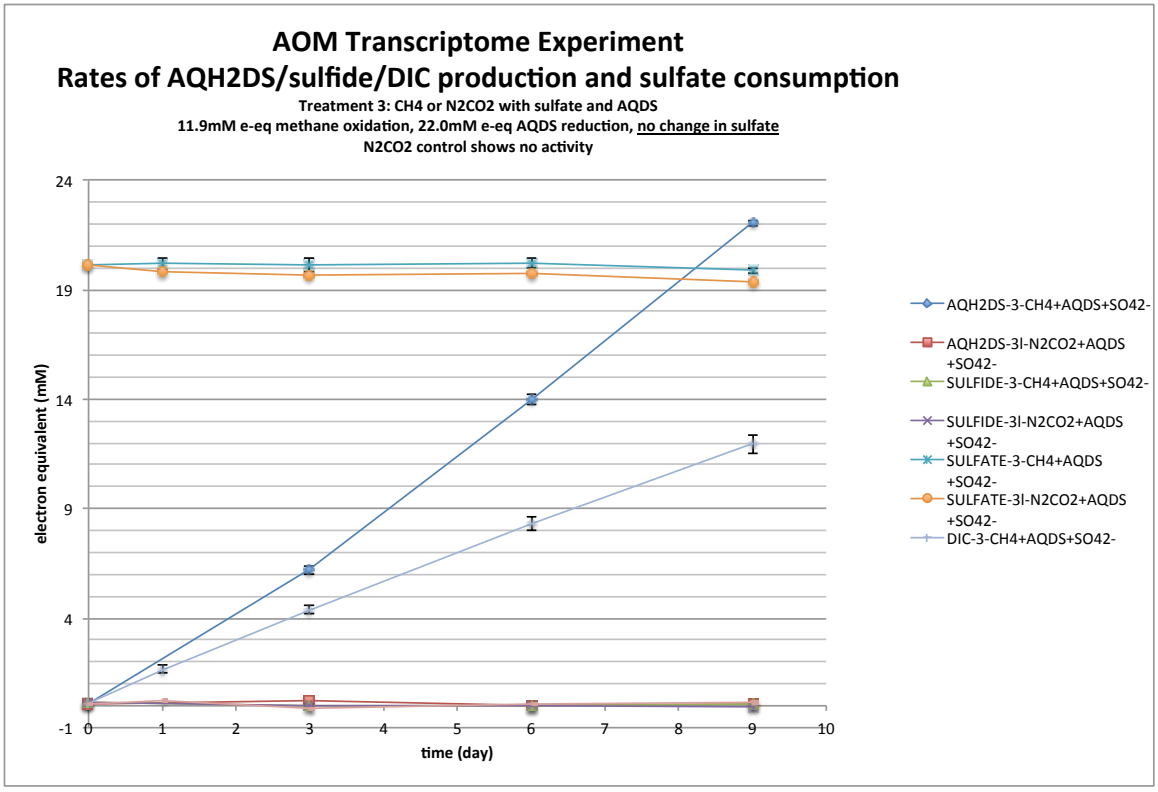
AOM Transcriptome Experiment
Rates of AQH2DS/sulfide/DIC production and sulfate consumption
Treatment 3: CH4 or N2CO2 with sulfate and AQDS
11.9mM e-eq methane oxidation, 22.0mM e-eq AQDS reduction, no change in sulfate
N2CO2 control shows no activity
electron equivalent (mM)
time (day)
AQH2DS-3-CH4+AQDS+SO42-
AQH2DS-3l-N2CO2+AQDS +SO42-
SULFIDE-3-CH4+AQDS+SO42-
SULFIDE-3l-N2CO2+AQDS +SO42-
SULFATE-3-CH4+AQDS +SO42-
SULFATE-3l-N2CO2+AQDS +SO42-
DIC-3-CH4+AQDS+SO42-

D

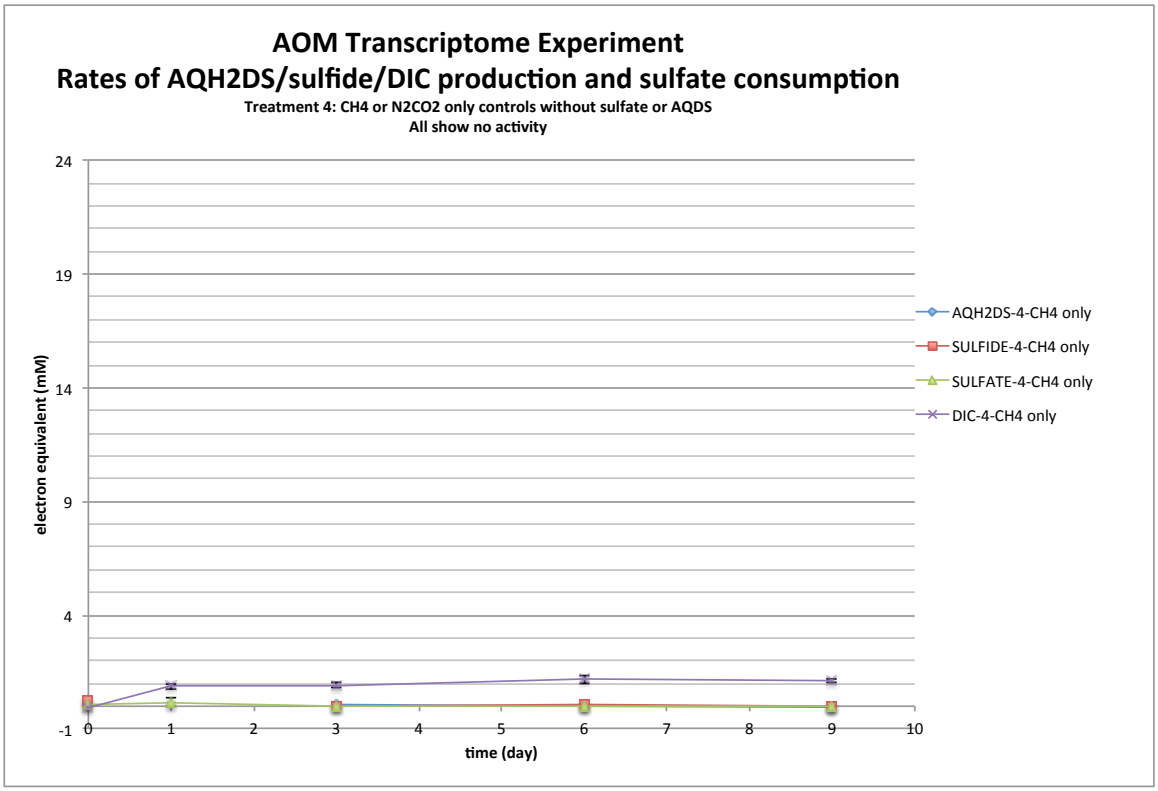
AOM Transcriptome Experiment
Rates of AQH2DS/sulfide/DIC production and sulfate consumption
Treatment 4: CH4 or N2CO2 only controls without sulfate or AQDS
All show no activity
electron equivalent (mM)
24
19
14
9
4
-1
0
1
2
3
4
5
6
7
8
9
10
time (day)
AQH2DS-4-CH4 only
SULFIDE-4-CH4 only
SULFATE-4-CH4 only
DIC-4-CH4 only

Figure 2. Examples of paired phylogenetic identification and anabolic activity of AOM consortia with different electron acceptors revealed by FISH-nanoSIMS. A, D, G, J) FISH images of AOM consortia with ANME in red and SRB in green. B, E, H, K) Corresponding nanoSIMS ion images of $^{14}N^{12}C^-$ as a proxy for biomass, with scale bars shown on the right. C, F, I, L) Single cell activity shown as ^{15}N atom percentage in regions of interest (ROI). ANME ROIs are outlined in red and SRB ROIs are outlined in green. Assimilation of $^{15}NH_4^+$ into the biomass is used as a proxy for cellular anabolic activity, with scale bars showing ^{15}N atom percentages on the right.

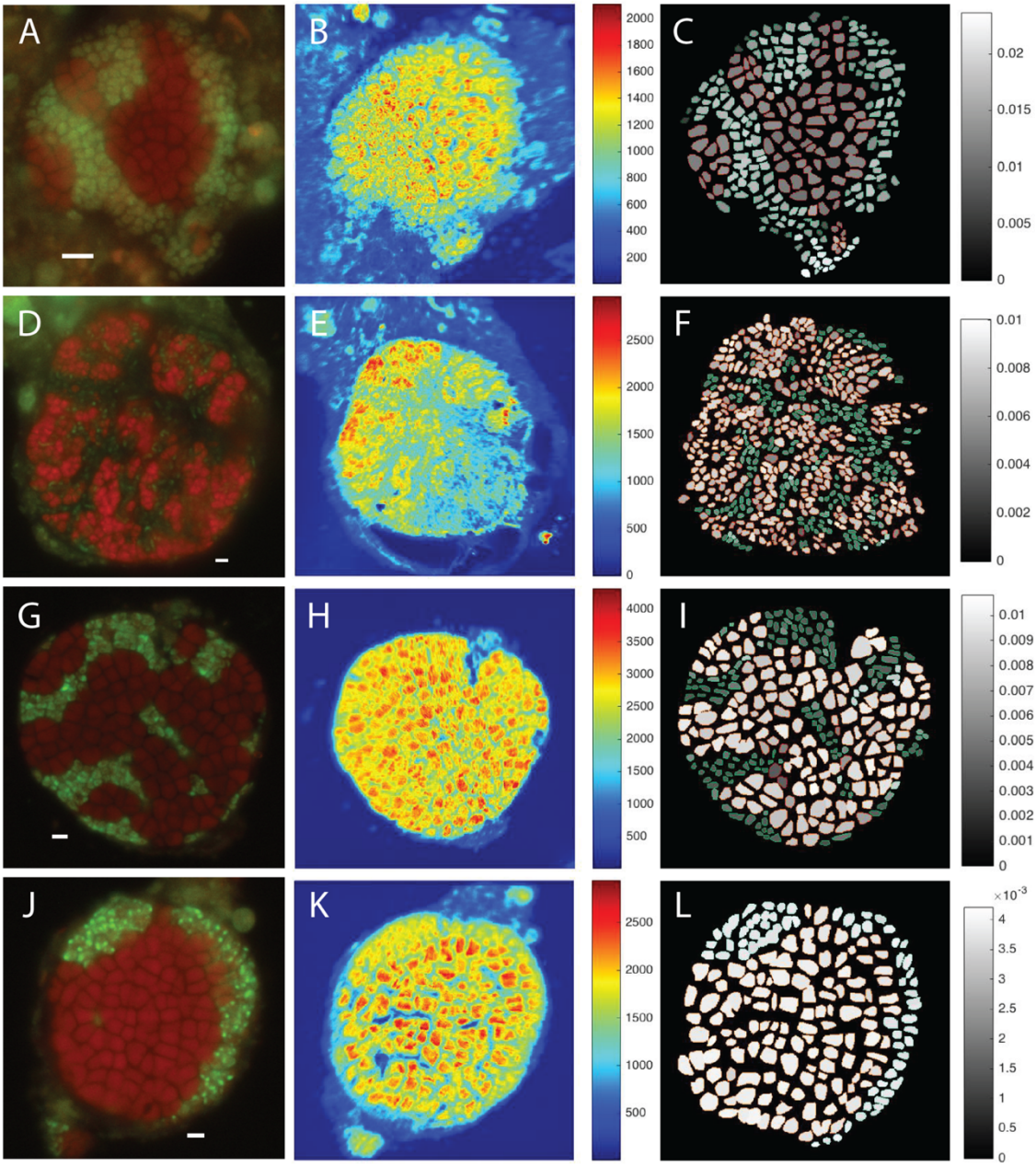

Figure 3. Population and single cell activities of AOM consortia with different electron acceptors. **A**) Population activities of AOM consortia with sulfate (n=6, green), AQDS (n=28, red), AQDS+Sulfate (n=32, orange) and no electron acceptor (methane only, n=10, blue) incubated under methane. Each point represents the ratio of average ^{15}N atom percentage between SRB and ANME populations in individual AOM consortium as revealed in FISH-nanoSIMS. Solid and dashed lines show linear regressions and 95% confidence intervals in slopes for plotted data. R^2 values are 0.53, 0.14, 0.25, and 0.81 for sulfate, AQDS, AQDS+Sulfate and methane only conditions respectively. The 1:1 line is shown in black. **B**) Single cell activity distributions of ANME (red) and SRB (green) with different electron acceptors. ^{15}N atom percentages of 188 ANME and 249 SRB with sulfate, 1305 ANME and 1248 SRB with AQDS, 1725 ANME and 1759 SRB with AQDS+Sulfate, and 609 ANME and 493 SRB of ANME and SRB with no electron acceptor (no methane) as identified as ROI in FISH-nanoSIMS from all AOM consortia in **A** are used.

A

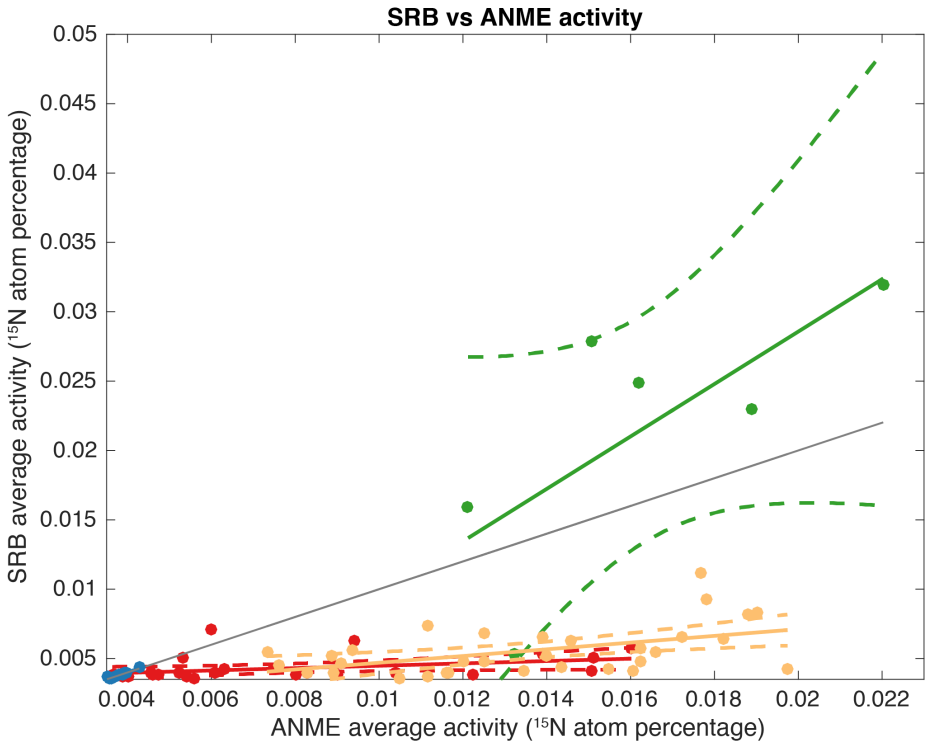

B

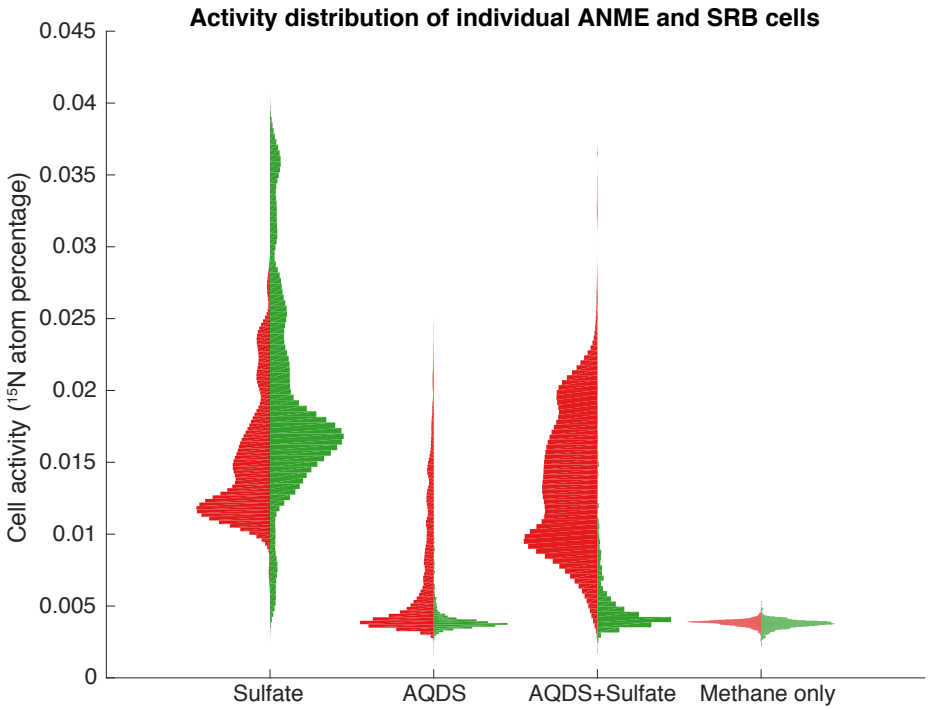
Activity distribution of individual ANME and SRB cells
Cell activity (15N atom percentage)
0.045
0.04
0.035
0.03
0.025
0.02
0.015
0.01
0.005
0
Sulfate
AQDS
AQDS+Sulfate
Methane only

Figure 4. Overview of metatranscriptome with different electron acceptors. A) Taxonomy assignment of mRNA reads based on NCBI Refseq database. B) Major metabolic pathway assignment of mRNA reads based on KEGG database. Error bars represent standard deviations of triplicate day 9 samples.

A

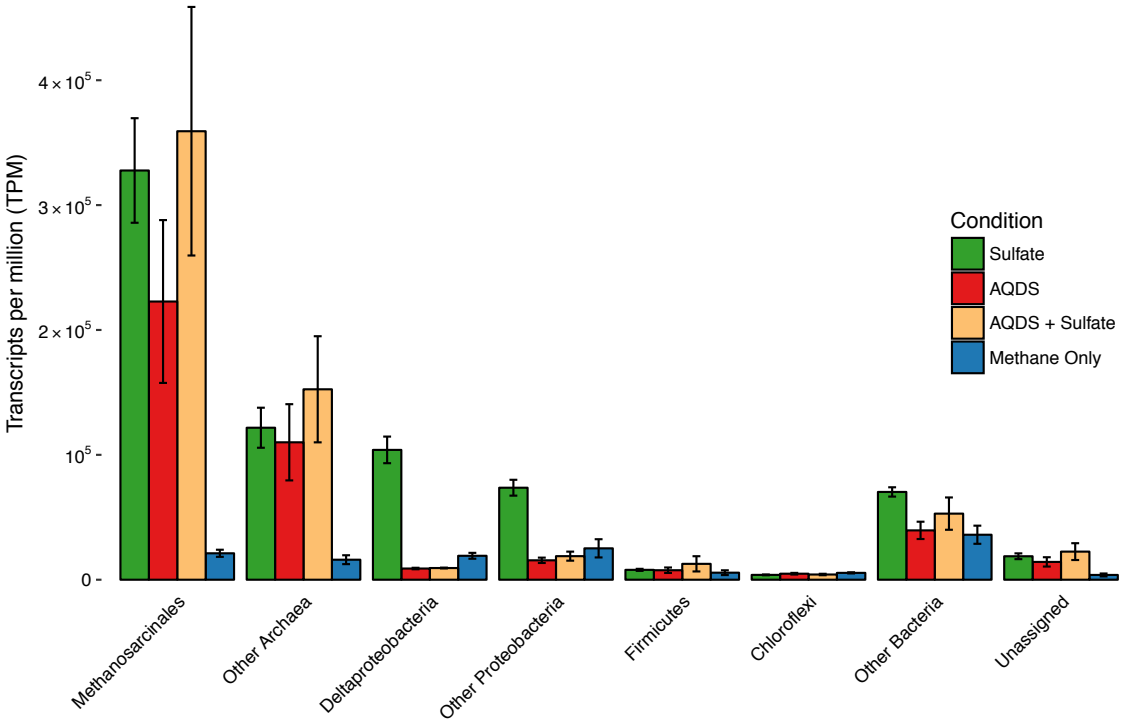

B

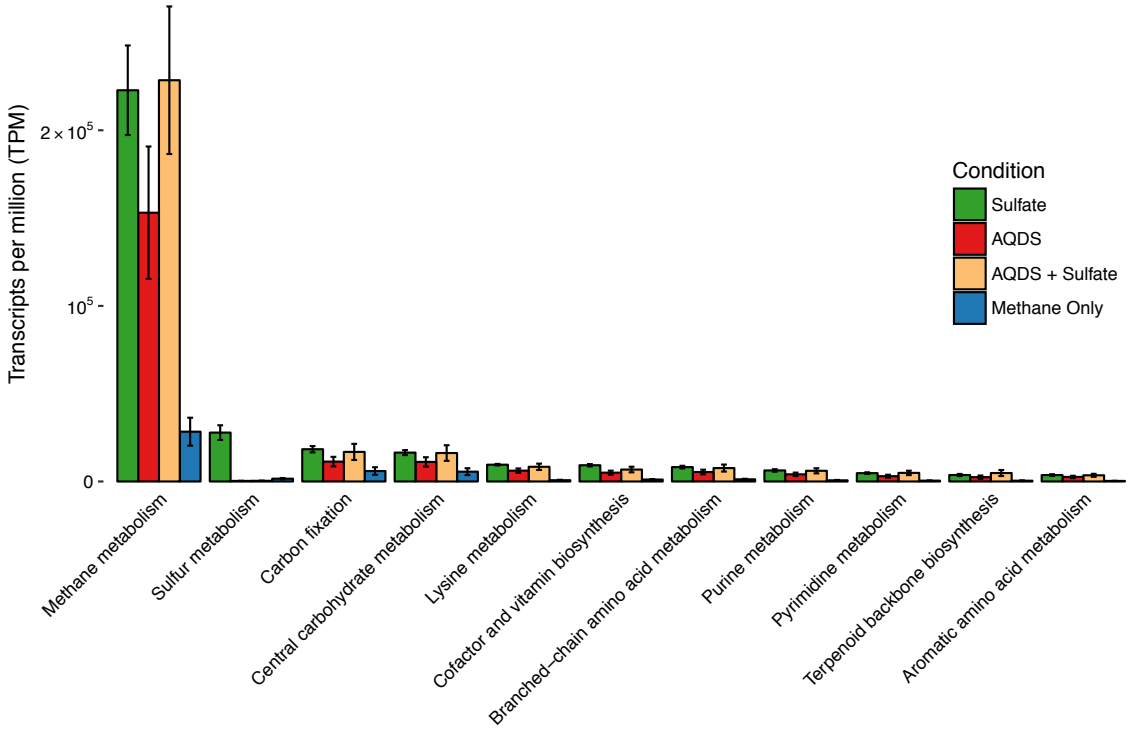
Transcripts per million (TPM)
2 × 10^5
10^5
0
Condition
Sulfate
AQDS
AQDS + Sulfate
Methane Only
Methane metabolism
Sulfur metabolism
Carbon fixation
Central carbohydrate metabolism
Lysine metabolism
Cofactor and vitamin biosynthesis
Branched−chain amino acid metabolism
Purine metabolism
Pyrimidine metabolism
Terpenoid backbone biosynthesis
Aromatic amino acid metabolism

Figure 5. Expression of metabolic and direct interspecies electron transfer genes in AOM consortia. Only three conditions are shown here with sulfate (green), AQDS (red) or none (methane only control, blue) as the electron acceptor. The analysis is based on a single aggregate (G09) of ANME-2a and SEEP-SRB1a. Methane oxidation proteins are in red, sulfate reduction proteins are in green, and potential proteins involved in direct interspecies electron transfer are in yellow for ANME and light green for SRB.

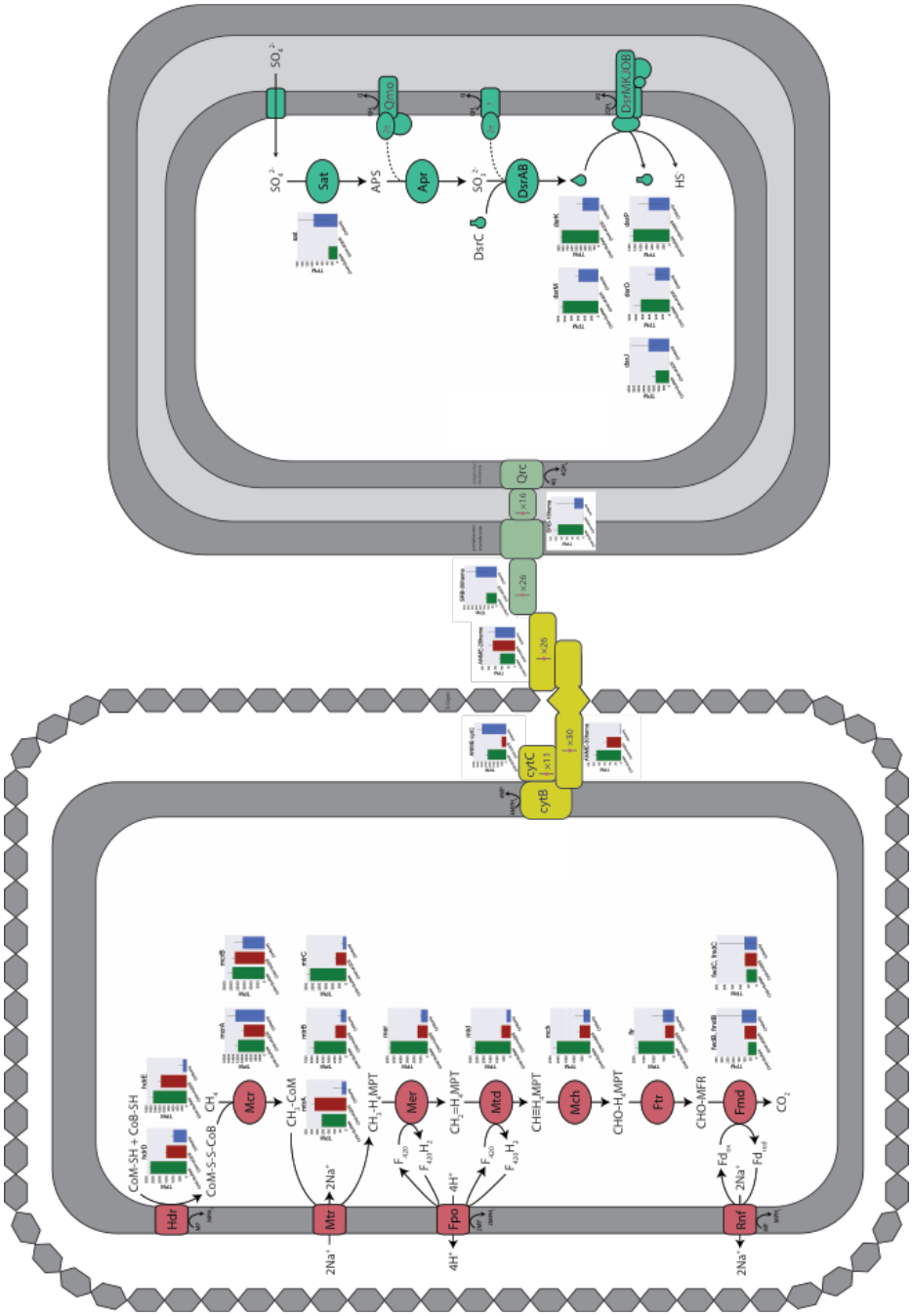

Supplementary Figure 1. The stimulatory effect of sulfate on AOM. A) Sulfate concentrations in incubations without AQDS. B) and C) Sulfate and AQH_2DS concentrations in incubations with both sulfate and AQDS (B, sulfate concentration; C, AQH_2DS concentration). A stimulatory effect of sulfate on AQDS reduction is observed with different amounts of sulfate.

A

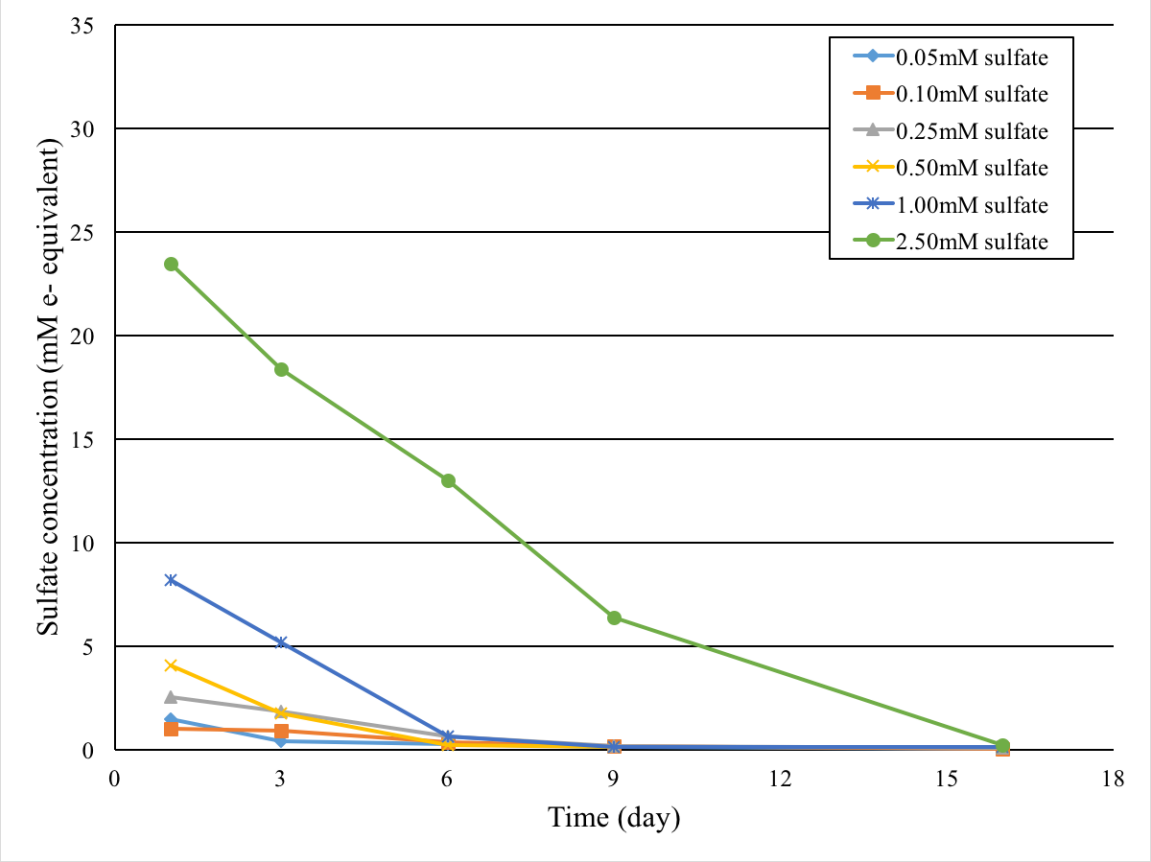

B

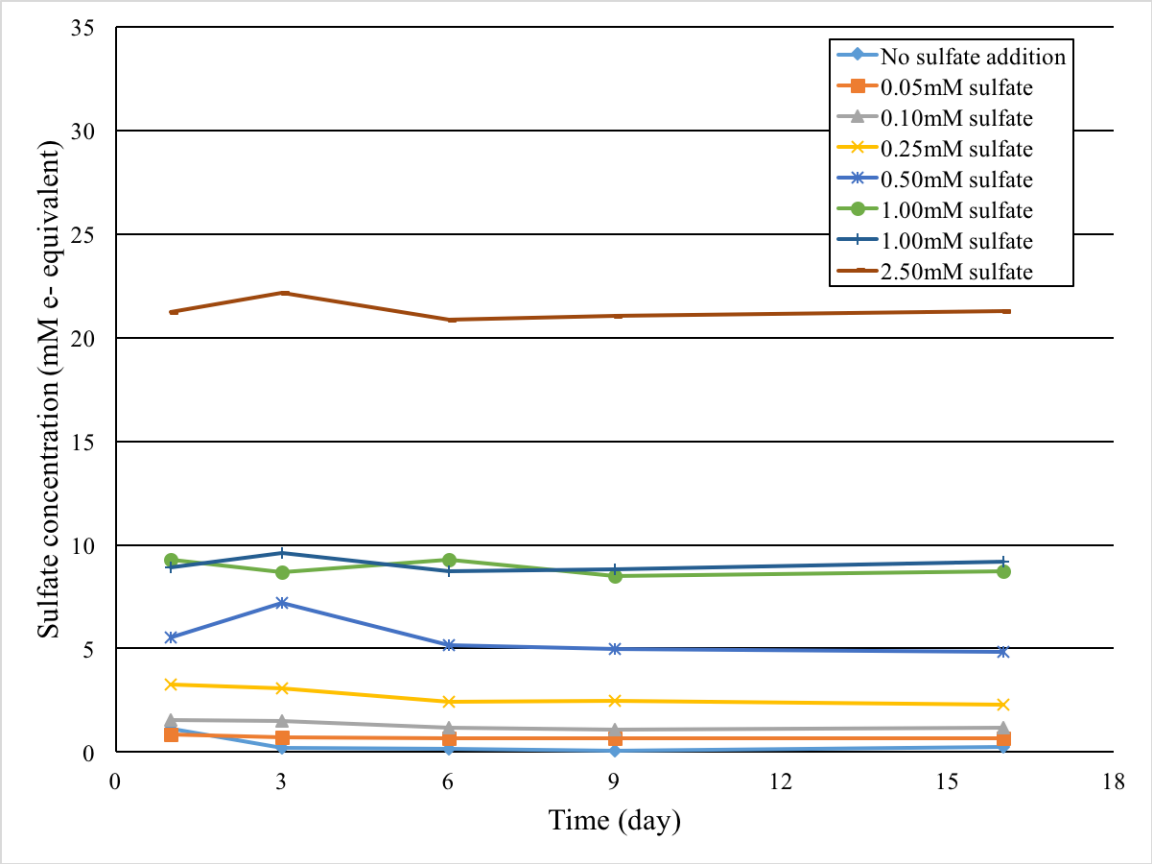
Sulfate concentration (mM e- equivalent)
Time (day)
No sulfate addition
0.05mM sulfate
0.10mM sulfate
0.25mM sulfate
0.50mM sulfate
1.00mM sulfate
1.00mM sulfate
2.50mM sulfate
0
5
10
15
20
25
30
35
0
3
6
9
12
15
18

C

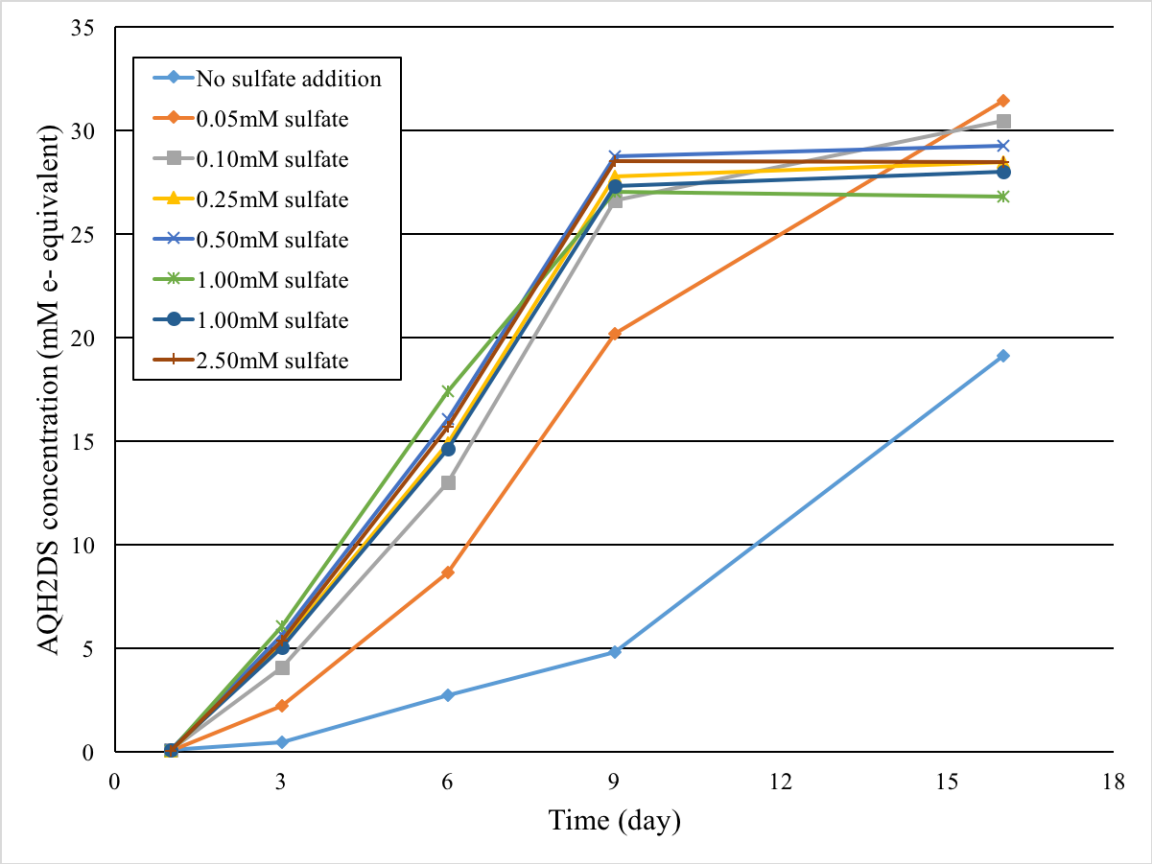
No sulfate addition
0.05mM sulfate
0.10mM sulfate
0.25mM sulfate
0.50mM sulfate
1.00mM sulfate
1.00mM sulfate
2.50mM sulfate
AQH2DS concentration (mM e- equivalent)
Time (day)
0
5
10
15
20
25
30
35
0
3
6
9
12
15
18

Supplementary Figure 2. Schematics showing two different scenarios of AQDS interaction with AOM consortia.

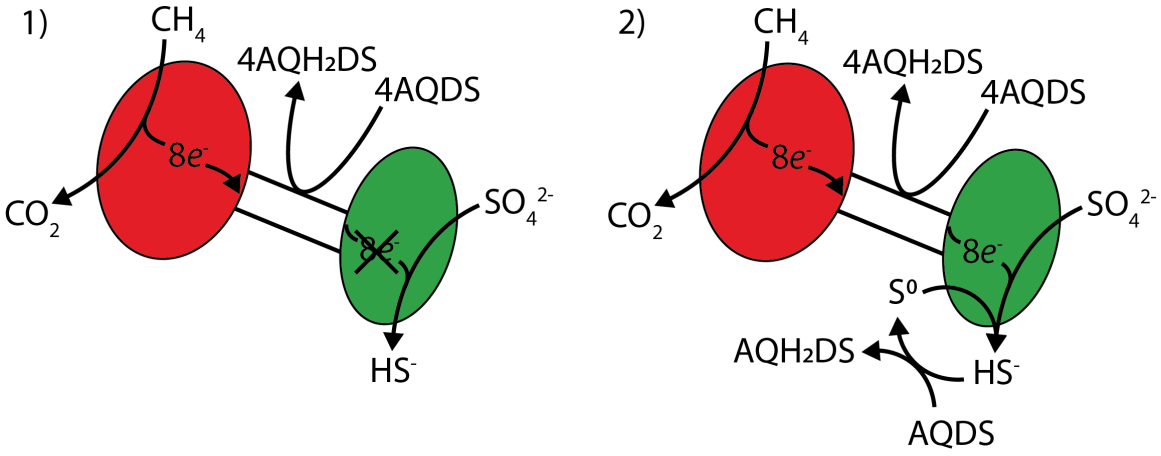

Supplementary Figure 3. Expression of key genes in methane oxidation, sulfate reduction and extracellular electron transfer over time with methane as electron donor and either sulfate or AQDS as the electron acceptor.

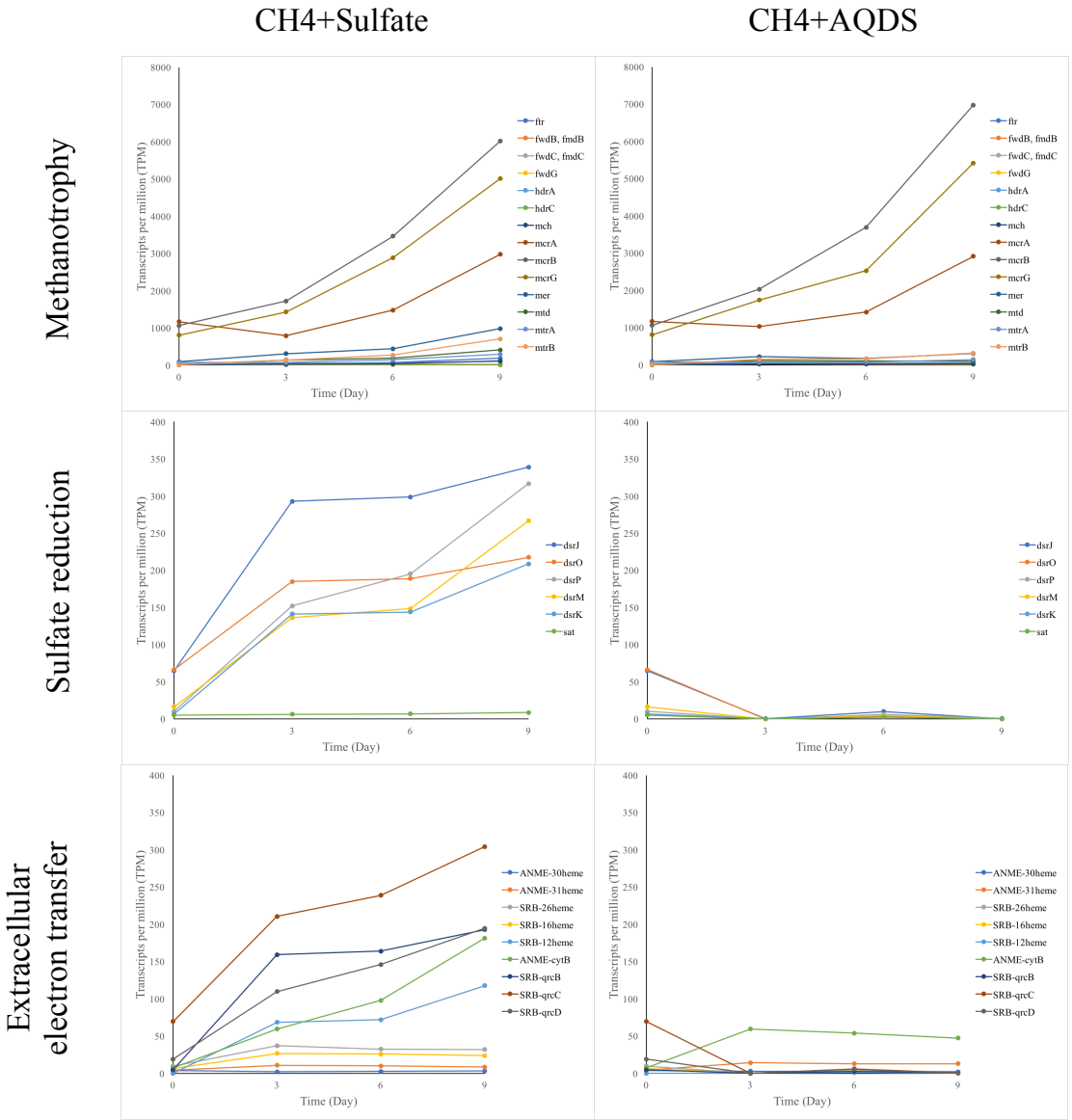

Supplementary Table 1. Sampling detail for A) geochemistry measurements and B) metatranscriptomics.

A

	day 0	day 3	day 6	day 9	total
CH4+sulfate	1	5	2	3	11
CH4+AQDS	1	4	3	3	11
CH4+sulfate+AQDS	1	4	3	3	11
CH4 only	1	3	2	3	9
N2CO2+sulfate				1	1
N2CO2+AQDS				1	1
N2CO2+sulfate+AQDS				1	1
				Grand total	45

B

	day 0	day 3	day 6	day 9	total
CH4+sulfate	1	1	2	3	7
CH4+AQDS		1	1	3	5
CH4+sulfate+AQDS		1	2	3	6
CH4 only	1	1	1	3	6
N2CO2+sulfate				1	1
N2CO2+AQDS				1	1
N2CO2+sulfate+AQDS				1	1
				Grand total	27

Supplementary Table 2. FISH-nanoSIMS analysis of ANME-SRB consortia at single-cell level with different electron acceptors.

	Number analyzed			**ANME 15N percentage**		**SRB 15N percentage**	
	Consortia	ANME	SRB	Mean	SD	Mean	SD
Sulfate	6	188	249	0.0151	0.0042	0.0193	0.0069
AQDS	28	1305	1248	0.0073	0.0043	0.0041	0.0012
AQDS+Sulfate	32	1725	1759	0.0137	0.0046	0.0053	0.0029
CH4 only	10	609	493	0.0038	0.0002	0.0037	0.0003

3.6 AUTHOR CONTRIBUTIONS

HY, RRM, TW, GWT, VJO devised the study. HY, CTS, GLC, AOL, RH, DG, conducted the experiments and analyses. HY and VJO wrote the manuscript with contributions from all authors, including data analysis, figure generation, and the final manuscript.

3.7 REFERENCES

Bankevich, Anton, Sergey Nurk, Dmitry Antipov, Alexey A Gurevich, Mikhail Dvorkin, Alexander S Kulikov, Valery M Lesin, et al. 2012. "SPAdes: a New Genome Assembly Algorithm and Its Applications to Single-Cell Sequencing." *Journal of Computational Biology* 19 (5): 455–77. doi:10.1089/cmb.2012.0021.

Bray, Nicolas L, Harold Pimentel, Páll Melsted, and Lior Pachter. 2016. "Near-Optimal Probabilistic RNA-Seq Quantification.." *Nature Biotechnology* 34 (5). Nature Research: 525–27. doi:10.1038/nbt.3519.

Cline, J D. 1969. "Spectrophotometric Determination of Hydrogen Sulfide in Natural Waters." *Limnology and Oceanography* 14: 454–58.

Girguis, P R, A E Cozen, and E F DeLong. 2005. "Growth and Population Dynamics of Anaerobic Methane-Oxidizing Archaea and Sulfate-Reducing Bacteria in a Continuous-Flow Bioreactor." *Applied and Environmental Microbiology* 71 (7). American Society for Microbiology: 3725–33. doi:10.1128/AEM.71.7.3725-3733.2005.

Hatzenpichler, Roland, Stephanie A Connon, Danielle Goudeau, Rex R Malmstrom, Tanja Woyke, and Victoria J Orphan. 2016. "Visualizing in Situ Translational Activity for Identifying and Sorting Slow-Growing Archaeal–Bacterial Consortia." *Proceedings of the National Academy of Sciences of the United States of America*, June. National Acad Sciences, 201603757. doi:10.1073/pnas.1603757113.

Knittel, Katrin, and Antje Boetius. 2009. "Anaerobic Oxidation of Methane: Progress with an Unknown Process.." *Annual Review of Microbiology* 63: 311–34. doi:10.1146/annurev.micro.61.080706.093130.

McGlynn, Shawn E, Grayson L Chadwick, Christopher P Kempes, and Victoria J Orphan. 2015. "Single Cell Activity Reveals Direct Electron Transfer in Methanotrophic Consortia.." *Nature* 526 (7574). Nature Publishing Group: 531–35. doi:10.1038/nature15512.

Meulepas, Roel J W, Christian G Jagersma, Ahmad F Khadem, Alfons J M Stams, and Piet N L Lens. 2010. "Effect of Methanogenic Substrates on Anaerobic Oxidation of Methane and Sulfate Reduction by an Anaerobic Methanotrophic Enrichment.." *Applied Microbiology and Biotechnology* 87 (4): 1499–1506. doi:10.1007/s00253-010-2597-0.

Meulepas, Roel J W, Christian G Jagersma, Ahmad F Khadem, Cees J N Buisman, Alfons J M Stams, and Piet N L Lens. 2009. "Effect of Environmental Conditions on Sulfate Reduction with Methane as Electron Donor by an Eckernförde Bay Enrichment." *Environmental Science & Technology* 43 (17): 6553–59. doi:10.1021/es900633c.

Meyerdierks, Anke, Michael Kube, Ivaylo Kostadinov, Hanno Teeling, Frank Oliver Glöckner, Richard Reinhardt, and Rudolf Amann. 2010. "Metagenome and mRNA Expression Analyses of Anaerobic Methanotrophic Archaea of the ANME-1 Group.." *Environmental Microbiology* 12 (2). Blackwell Publishing Ltd: 422–39. doi:10.1111/j.1462-2920.2009.02083.x.

Milucka, Jana, Timothy G Ferdelman, Lubos Polerecky, Daniela Franzke, Gunter Wegener,

Markus Schmid, Ingo Lieberwirth, Michael Wagner, Friedrich Widdel, and Marcel M M Kuypers. 2012. "Zero-Valent Sulphur Is a Key Intermediate in Marine Methane Oxidation.." *Nature* 491 (7425): 541–46. doi:10.1038/nature11656.

Moran, Mary Ann, Brandon Satinsky, Scott M Gifford, Haiwei Luo, Adam Rivers, Leong-Keat Chan, Jun Meng, et al. 2013. "Sizing Up Metatranscriptomics.." *The ISME Journal* 7 (2): 237–43. doi:10.1038/ismej.2012.94.

Nauhaus, Katja, Melanie Albrecht, Marcus Elvert, Antje Boetius, and Friedrich Widdel. 2007. "In Vitro Cell Growth of Marine Archaeal-Bacterial Consortia During Anaerobic Oxidation of Methane with Sulfate.." *Environmental Microbiology* 9 (1): 187–96. doi:10.1111/j.1462-2920.2006.01127.x.

Nauhaus, Katja, Tina Treude, Antje Boetius, and Martin Krüger. 2005. "Environmental Regulation of the Anaerobic Oxidation of Methane: a Comparison of ANME-I and ANME-II Communities.." *Environmental Microbiology* 7 (1): 98–106. doi:10.1111/j.1462-2920.2004.00669.x.

Orphan, Victoria J, Christopher H House, Kai-Uwe Hinrichs, Kevin D McKeegan, and Edward F DeLong. 2002. "Multiple Archaeal Groups Mediate Methane Oxidation in Anoxic Cold Seep Sediments.." *Proceedings of the National Academy of Sciences of the United States of America* 99 (11). National Acad Sciences: 7663–68. doi:10.1073/pnas.072210299.

Pernthaler, Annelie, Anne E Dekas, C Titus Brown, Shana K Goffredi, Tsegereda Embaye, and Victoria J Orphan. 2008. "Diverse Syntrophic Partnerships From Deep-Sea Methane Vents Revealed by Direct Cell Capture and Metagenomics.." *Proceedings of the National Academy of Sciences of the United States of America* 105 (19). National Acad Sciences: 7052–57. doi:10.1073/pnas.0711303105.

Pimentel, Harold J, Nicolas Bray, Suzette Puente, Páll Melsted, and Lior Pachter. 2016. "Differential Analysis of RNA-Seq Incorporating Quantification Uncertainty." *bioRxiv*. Cold Spring Harbor Labs Journals, 058164. doi:10.1101/058164.

Ruff, S Emil, Jennifer F Biddle, Andreas P Teske, Katrin Knittel, Antje Boetius, and Alban Ramette. 2015. "Global Dispersion and Local Diversification of the Methane Seep Microbiome.." *Proceedings of the National Academy of Sciences* 112 (13): 4015–20. doi:10.1073/pnas.1421865112.

Scheller, Silvan, Hang Yu, Grayson L Chadwick, Shawn E McGlynn, and Victoria J Orphan. 2016. "Artificial Electron Acceptors Decouple Archaeal Methane Oxidation From Sulfate Reduction.." *Science* 351 (6274): 703–7. doi:10.1126/science.aad7154.

Wegener, Gunter, Viola Krukenberg, Dietmar Riedel, Halina E Tegetmeyer, and Antje Boetius. 2015. "Intercellular Wiring Enables Electron Transfer Between Methanotrophic Archaea and Bacteria." *Nature* 526 (7574). Nature Publishing Group: 587–90. doi:10.1038/nature15733.

Wegener, Gunter, Viola Krukenberg, S Emil Ruff, Matthias Y Kellermann, and Katrin Knittel. 2016. "Metabolic Capabilities of Microorganisms Involved in and Associated with the Anaerobic Oxidation of Methane." *Frontiers in Microbiology* 7 (17). Frontiers: 869. doi:10.3389/fmicb.2016.00046.

A p p e n d i x A

INVESTIGATING THE EFFECTS OF DIFFUSIBLE METABOLITES ON ANAEROBIC METHANE OXIDIZING CONSORTIA

Hang Yu*, Silvan Scheller*, Victoria Orphan

Division of Geological and Planetary Sciences, California Institute of Technology, Pasadena, CA 91125, USA

*These authors contributed equally to this work

This appendix contains unpublished material.

EXPLANATION FOR APPENDIX

The biology that facilitates anaerobic oxidation of methane (AOM) with sulfate was discovered by a series of studies around the year 2000, and involves a symbiosis between anaerobic methanotrophic archaea (ANME) and sulfate reducing bacteria (SRB). Based on their phylogenetic identity and genomic composition, it was generally accepted that ANME mediate methane oxidation and SRB mediate sulfate reduction. Together, this partnership has great impact on the cycling of methane and sulfur on Earth, mediating the release of a potent greenhouse gas and capturing this energy-rich molecule in the deep-sea. For a decade since their discovery, researchers have been pondering and puzzled by these syntrophic consortia. Mainly due to the fact that for the metabolism of AOM with sulfate to function, a metabolic intermediate must exist to transfer electrons from ANME to SRB cells. ANME are phylogenetically related to methanogenic archaea that produce methane from a range of substrates such as hydrogen, formate, acetate, methanol, and other methylated compounds. The relatives of syntrophic SRB in *Deltaproteobacteria* can often be found to form symbiosis with methanogenic archaea, with the former consuming organic substrates and producing a diffusible metabolite for methanogenesis. This knowledge led to the hypothesis that ANME and SRB use a methanogenic substrate as the metabolic intermediate in AOM. There were a number of studies testing these metabolites, but no compelling evidences were offered then in my opinion to support or to refute this hypothesis.

I started my Ph.D. in 2011, and set out to find this metabolic intermediate in AOM. In 2012, Silvan Scheller joined as a post-doc in the lab, and we teamed up to set up a series of microcosm experiments to test potential metabolic intermediates and various ideas we had to selectively grow or inhibit ANME or SRB. Also in 2012, a new hypothesis came out that proposed zero-valent sulfur as the metabolic intermediate, with ANME producing zero-valent sulfur using a novel sulfate reduction mechanism and SRB disproportionating this product to sulfate and sulfide. This hypothesis had a great influence on our understanding of AOM, and Silvan and I investigated the effect of sulfur compounds on AOM consortia

experimentally. During this process, we developed and applied new methodologies to better track the activities of methane oxidation and sulfate reduction. This appendix represents a synopsis of these microcosm experiments from 2012 to 2015. The synthesis and result of this collaborative work eventually led to a new understanding on the symbiosis between ANME and SRB, as detailed in the main part of this thesis, and a method for decoupling what was thought as an obligate syntrophic association in AOM.

ABSTRACT

The symbiotic mechanism in AOM syntrophy remains enigmatic mainly due to a lack of identification of an intermediate that links ANME and SRB metabolisms. Here we investigate various diffusible metabolites as possible metabolic intermediates in AOM. Microcosms containing methane seep sediments were monitored for their sulfate reduction and methane oxidation rates in the presence of these metabolites. For the metabolites that showed promise, new methods for tracking AOM and sulfate reduction using stable isotope probing were applied to study short-term responses of AOM consortia to a spike in these compounds. Moreover, community profiling using 16S rRNA gene was also done to check for possible growth of ANME or SRB after 9 months of incubation. Methanogenic substrates such as hydrogen, formate, acetate, methanol, and methyl sulfide, as well as various organic and sulfur compounds, were ruled out as the intermediate in AOM as a result. Various inhibitors and antibiotics were tested, and two were found to be selective for ANME or SRB. This work adds to a growing body of literature that suggest diffusible metabolites are unlikely to mediate the symbiosis in AOM.

INTRODUCTION

Ever since the discovery of the biological identities that mediate AOM with sulfate (Hoehler et al. 1994; Hinrichs et al. 1999; Boetius et al. 2000; Orphan et al. 2001), researchers have been speculating on how these syntrophic consortia are metabolically linked. For AOM to be coupled to sulfate reduction, a metabolic intermediate was hypothesized to exist to shuttle the electrons obtained from methane oxidation in ANME to SRB for sulfate reduction. Possible intermediates include hydrogen, formate, acetate, and other methanogenic substrates (Hoehler et al. 1994; Valentine and Reeburgh 2000; Moran, House, et al. 2008; Alperin and Hoehler 2009). However, experimental studies have not found an effect of these metabolites on AOM consortia, and therefore concluded that these were unlikely the metabolic intermediate in AOM (Nauhaus et al. 2002; Nauhaus et al. 2005; Meulepas et al. 2010; Wegener et al. 2016). A notable exception here is the partner SRB, namely HotSeep-1, to ANME-1 in thermophilic AOM. HotSeep-1 was able to couple hydrogen oxidation to sulfate reduction, and subsequently isolated (Wegener et al. 2015; Krukenberg et al. 2016). However, hydrogen is not the intermediate in thermophilic AOM, since that the rate of hydrogen production when sulfate reduction is inhibited does not match the rate needed to sustain AOM (Wegener et al. 2015). An alternative hypothesis was proposed, in which ANME reduce sulfate to zero-valent sulfur and this intermediate is subsequently disproportionated by their partner bacteria (Milucka et al. 2012). However, no genetic mechanism has been found for sulfate reduction in ANME (Yu et al. In prep), and experimental and modeling results do not support zero-valent sulfur as the metabolic intermediate (McGlynn et al. 2015; Wegener et al. 2015; Wegener et al. 2016).

Here we test the hypothesis that diffusible intermediates link the AOM syntrophic partners. Microcosms of two different methane seep sediments were designed to decouple the AOM partnership, and the activities of methane oxidation and sulfate reduction were tracked to better understand the effects of these metabolites. Additionally, we monitored the community profiles in these microcosms to observe potential shifts that may indicate selective

growth of ANME or SRB in the system. Moreover, a range of inhibitors or antibiotics were characterized for their impact on the metabolism in AOM consortia. Our findings are consistent to other studies that were conducted during the same time (McGlynn et al. 2015; Wegener et al. 2015; Wegener et al. 2016), together suggesting that diffusible metabolites are not the metabolic intermediate in AOM.

MATERIALS AND METHODS

Two methane seep sediments collected from Hydrate Ridge (sediment #5207) or Santa Monica Basin (sediment #7142) were used in this study. 16S iTag sequencing was done on the bulk sediment to understand the community composition as described previously (Case 2016), and fluorescence in situ hybridization (FISH) microscopy was used to better characterize dominant ANME groups in sediment #7142 (Scheller et al. 2016).

Microcosms were setup from sediment #5207 as described in Chapter 1 of this thesis. Briefly, 30 ml serum bottles were used each with 20 ml slurry (1:2 sediment:seawater ratio) and ca. 12 ml headspace. Natural seawater collected from Hydrate Ridge was used, and bottles were pressurized with methane (99%, 0.3 MPa), hydrogen (0.2 MPa) or nitrogen (0.2 MPa). The amendments were added to the following final concentrations: 15 mM for H_2S, ca. 10-15 mM for synthesized polythionate (Steudel, Göbel, and Holdt 1988), ca. 50 mg of yellow sulfur powder, 5 mM for Na_2SO_3, 10 mM for $ZnSO_4$, 300 mg/L for ampicillin, 300 mg/L for kanamycin, 100 mg/L for tetracycline, 10 mg/L for mevastatin, 100 mg/L for monensin, ca. 1% or 0.03 kPa for difluoromethane, 300 mg/L for vancomycin, 10 mM for formate, 10 mM for acetate, 10 mM for methanol, 10mM for $Na_2S_2O_6$, 10 mM for polysulfide synthesized by mixing Na2S and S^0 and dissolving at 32°C overnight (Ikeda et al. 1972), 10 mM for $Na_2S_2O_3$, 10 mM for lactate, 10 mM for propionate, 10 mM for ethanol, 10 mM for methanol, and 0.1 mM or 1 mM for L-Azidohomoalanine (AHA). Subsamples of the overlaying seawater were taken at the beginning and the end of every incubation interval. 0.75 ml of seawater was centrifudged at 16.1 x kg for 30 seconds; 0.2 ml

of the supernatant was mixed with 0.2 ml of 0.5 M zinc acetate to preserve the sulfide; the rest of the supernatant was frozen and stored at -20°C until further analysis for sulfate or DIC. Pressure was monitored using a pressure gauge (SSI Technologies, Inc., Media Gauge). Periodically, 0.5 ml of mixed sediment slurry was fixed in 2.67% paraformaldehyde overnight at 4°C, washed twice by centrifudging at 16.1 x kg for 1 minute with 1x PBS, and resuspended in 0.6 ml of 50:50 EtOH:PBS and stored at -20°C.

Microcosms were setup from sediment #7142 as described previously (Scheller et al. 2016). These incubations are in 10 ml serum bottles with 1 ml of wet sediment and 4 ml of artificial seawater. The following compounds were spiked in at the following final concentrations: 1 kPa for hydrogen, 0.1 or 1 mM for formate, 0.1 or 1 mM for acetate, 1 mM for methyl sulfide, 0.05 to 0.5 mM for zero-valent sulfur, 100 mg/L for monensin, and 25 mM for sodium molybdate.

Sulfide samples preserved in zinc acetate were measured later using the methylene blue method (Cline 1969); Sulfate was measured using ion chromatography (Dionex ICS-500, 2000 or 3000 at the Caltech Environmental Analysis Center). DIC was measured as previously described (Scheller et al. 2016).

RESULTS AND DISCUSSIONS

Hydrogen

Hydrogen was the first intermediate proposed to link the metabolisms of ANME and SRB (Hoehler et al. 1994). In microcosms of sediment #5207, hydrogen is quickly consumed within 5 days of addition (data not shown). This is coupled to sulfide production from sulfate in the natural seawater (Table 1). Note that the sulfide production is lower relative to the methane controls due to reaction stoichiometry differences between methane and hydrogen with sulfate, and hydrogen becomes the limiting substrate during each of the incubation intervals.

Given the quick consumption of hydrogen, more sensitive methods are needed to study its effect on AOM consortia, specifically on ANME. Stable isotope probing using $^{13}CH_4$ can detect changes in AOM rate by measuring the production of ^{13}C-DIC, and this provides time resolution on the order of hours in our microcosms (Scheller et al. 2016). Microcosms of sediment #7142 are first setup and confirmed for active AOM, as observed in linear increases in ^{13}C-DIC concentrations (Figure 1A). Hydrogen is spiked in after 4 days of incubation and AOM rates are continuously measured. If hydrogen is the metabolic intermediate produced by ANME, then addition of hydrogen should inhibit ANME or AOM as a result of product inhibition. No effect of hydrogen addition is observed, indicating that hydrogen is not produced by ANME from AOM and not the metabolic intermediate in AOM syntrophy.

Formate

Even though formate is a methanogenic substrate, it was first thought as an unlikely metabolic intermediate in AOM. The main reason is because known methanogens that use formate are too distantly related phylogenetically to ANME (Boetius et al. 2000; Valentine

2002). We still tested the possibility of formate as the intermediate by adding it to microcosms of sediment #5207. Without methane, formate is consumed coupled to sulfide generation (Table 1). With methane, sulfide production increase slightly compared to the controls without formate addition (Table 1). This is expected if sulfate reduction was maximized under our experimental conditions: without methane, SRB couple formate oxidation to sulfate reduction, but the rate could be lower due to diffusion of formate in the system; with methane, SRB could receive formate from both ANME and the media, resulting in a slightly higher overall rate of sulfate reduction. Also, we observe a rapid isotopic exchange between formate and DIC, indicating active formate dehydrogenases in the system (data not shown).

We then tested this possibility by measuring the impact of formate on ANME with the production of ^{13}C-DIC. Microcosms of sediment #7142 are tracked to confirm active AOM, then formate is spiked in after 4 days of incubation. No effect on AOM rate is observed, indicating that ANME is not product inhibited by formate addition (Figure 1B). Therefore, formate is unlikely the metabolic intermediate in AOM.

Acetate

Acetate is a methanogenic substrate used by methanogens, namely by the order of *Methanosarcinales* which contain ANME-2a/b/c and Candidatus Methanoperedens, and therefore could be an intermediate in AOM (Valentine and Reeburgh 2000). Microcosms of sediment #5207 show little or no acetate oxidation coupled to sulfide production (Table 1). However, with both acetate and polythionate, sulfide production is much higher than with polythionate alone (Table 1). This result is puzzling, but could be explained by a double-metabolic-intermediate scenario in which both acetate and polythionate are produced by ANME; only when both acetate and polythionate are present do the SRB become active and produce high levels of sulfide.

To further investigate the role of acetate in AOM, both acetate of natural isotope abundance and $^{13}CH_4$ are added to microcosms of sediment #5207. If acetate were produced by ANME, then isotope exchange between methane and acetate must occur from AOM coupled acetate pathway. After one month incubation, the isotope composition of acetate shows little isotope exchange has occurred, indicating that acetate is unlikely an AOM intermediate that is actively turned over in the system (Figure 2). In addition, acetate spiked into microcosms of sediment #7142 showed no effect on AOM, suggesting again that acetate is not the metabolic intermediate in AOM (Figure 1B).

Other organic compounds

Other organic compounds are tested as possible intermediate in AOM or potential growth substrate for SRB, because they are known substrates for methanogenic archaea or sulfate-reducing *Deltaproteobacteria* related to the syntrophic SRB groups in AOM (Liu and Whitman 2008; Rabus, Hansen, and Widdel 2013). These substrates include methanol, lactate, propionate, and ethanol. Methanol is added to microcosms of sediment #5207. Only a small amount of methanol is consumed for sulfate reduction, as indicated by the small increase in sulfide production with or without methane (Table 1). We also examine the community shifts in microcosms with the addition of these metabolites using 16S rRNA gene iTag sequencing. After 9 months of incubation, the known syntrophic SRB groups, namely Seep-SRB1 and Seep-SRB2, either have a similar or decreased relative abundance (Figure 4 and Table 3). This indicates that these SRB groups cannot grow with methanol, lactate, propionate, or ethanol, while other bacteria showing increased relative abundance may be responsible in consuming these organic compounds in methane seep ecosystems.

Methyl sulfide was proposed as a possible intermediate in AOM (Moran, Beal, et al. 2008). We find that methyl sulfide does not affect AOM rate in microcosms of sediment #7142, and is therefore unlikely to be the intermediate in AOM (Figure 1C).

Sulfur compounds

The possibility of a sulfur based intermediate has been examined in Chapter One of this thesis. Here we provide additional experiments on the effect of sulfide, polythionate, polysulfide, elemental sulfur, sulfite, and thiosulfate on AOM. Mostly, addition of these sulfur compounds to microcosms of sediment #5207 has a negative effect on the sulfide production relative to the controls (Table 1). This suggests that polythionate, polysulfide, elemental sulfur, and sulfite are not only unlikely candidates to be the intermediate in AOM, but also inhibitory or toxic to the AOM consortia. By tracking sulfate concentration, we find that sulfate is not consumed in the presence of polythionate or sulfur powder (Table 2). This indicates that polythionate and sulfur powder are more favorable substrates for sulfide production in our microcosms. In the presence of sulfite, sulfate is consumed, suggesting that sulfite likely remains in the microcosms and not consumed (Table 2). With thiosulfate addition, comparable levels of sulfide production are observed over time as compared to controls without thiosulfate (Table 1). However, sulfate concentrations remain the same or increase, suggesting a preferential usage of thiosulfate via either direct reduction or disproportionation (Table 2). This is likely coupled to AOM, as seen by comparable levels methane oxidation measured using either DIC concentration or headspace pressure (Table 2). Amounts of DIC produced in these microcosms do not match the amounts of sulfur reduction to sulfide, likely due to precipitation of DIC in natural seawater. Pressure measurements show large variations between duplicates, indicating a low precision in measurements of headspace pressure. Further investigation of microcosms of sediment #7142 in Chapter 1 show that thiosulfate addition does not affect the rates of sulfate reduction, suggesting that it is unlikely the intermediate or substrate for AOM or ANME.

While sulfite, thiosulfate, and zero-valent sulfur such as polythionate, polysulfide and sulfur powder are unlikely to be the intermediate in AOM, zero-valent sulfur has a puzzling effect on the AOM consortia with polysulfide inhibition observed (Table 1). We further explore this inhibition effect with a range of zero-valent sulfide concentrations. At

concentrations of zero-valent sulfur great than 0.1 mM, AOM rates decrease or stop in microcosms of sediment #7142 (Figure 1D). This result is consistent with zero-valent sulfur being the intermediate in AOM, as the ANME partner is product inhibited by high concentrations of this metabolite. However, this does not explain a lack of sulfide production observed (Table 1). Also, long-term incubations of sediment #5207 with different sulfur compounds do not show an increase in the relative abundance of 16S rRNA gene in the syntrophic SRB groups (Figure 3). Furthermore, genome mining results in Chapter 1 found no dissimilatory sulfate reduction pathway in ANME. Together, the effect of zero-valent sulfur on ANME may be toxic rather than inhibitory. The reason for this toxicity is unknown at the present.

Inhibitors

Instead of decoupling AOM consortia by providing alternative electron donors or acceptors, it might be possible to decouple AOM consortia using inhibitors that selectively act on ANME or SRB. We investigate potential inhibitors that have been reported to be effective for methanotrophs, methanogens, archaea, or *Deltaproteobacteria*. Possible inhibitors include diflouromethane (CH_2F_2) (Miller, Sasson, Oremland 1998), mevastatin (Miller and Wolin 2001), and monensin (Thornton and Owens 1981) for ANME, as well as various antibiotics such as ampicillin, kanamycin, tetracycline, and vancomycin in addition to molybdate for sulfate-reducing *Deltaproteobacteria* (Saleh, Macpherson, and Miller 1964; Hoehler et al. 1994). The ANME inhibitors chosen have different mechanisms of action: diflouromethane inhibits enzymes in methanogenesis, mevastatin inhibits HMG-CoA reductase in isoprenoid synthesis, and monensin is an ionophore that disrupts the membrane potentials. The antibiotics for SRB chosen have different mechanisms of action as well: ampicillin and vancomycin inhibit cell wall synthesis, whereas kanamycin and tetracycline inhibits protein synthesis, and molybdate competitively inhibits enzymes associated with sulfate reduction.

These inhibitors or antibiotics are added to microcosms of sediment #5207, approximately 10-fold excess concentration of the values reported previously for pure cultures or gut communities. No effect on sulfide production is observed with mevastatin, difluoromethane, ampicillin, kanamycin, or tetracycline (Table 1). This could be due to reactions of these molecules with sulfide, fast degradation by sediment microorganisms, or inability to penetrate into the AOM aggregates. Vancomycin is found to be partially inhibitory to AOM consortia, as shown by the slow decrease in sulfide production over time (Table 1). Monensin is the only compound that inhibited AOM consortia effectively with little or no sulfide production after its addition (Table 1).

We further tested the short-term effectiveness of monensin on ANME, along with molybdate, a reported inhibitor on SRB in AOM consortia (Saleh, Macpherson, and Miller 1964; BANAT and Nedwell 1984; Hoehler et al. 1994). Both compounds are found to inhibit AOM, as seen in the immediate decrease in DIC production in microcosms of sediment #7142 (Figure 4A). After amendments, three types of responses are observed: 1) rates continue at same speed indicating no effect on metabolism, 2) rates stop and no more labelled product is formed indicating complete inhibition to the metabolic process, and 3) labelled product continue to be formed but at a much slower rate. The controls without addition show the first type of response as expected. Monensin shows the second type of reponse, whereas molybdate shows the third type of response. This is interesting because the third type of response is likely caused by natural isotopic exchange catalyzed by active enzymes, but the metabolic process is no longer energetically favorable and no more net production of metabolites such as DIC is observed (Holler et al. 2011). The reverse effect is observed for sulfate reduction: after monensin addition, ^{34}S-sulfide continues to form at a slow rate, whereas after molybdate addition, ^{34}S-sulfide formation stops (Figure 4B). Taken together, these results show that monensin and molybdate selectively inhibit ANME or SRB, respectively. AOM consortia no longer carry out methane oxidation or sulfate reduction, because only one of the partners remains active, waiting for their electron donor or acceptor.

TABLES AND FIGURES.

Figure 1. Short term effects of various metabolites on the rate of AOM. A) Hydrogen, B) formate and acetate, C) methyl sulfide, D) zero-valent sulfur in the form of polysulfides, are spiked into active microcosms containing methane seep sediment. Black arrows indicate the time of spike.

A

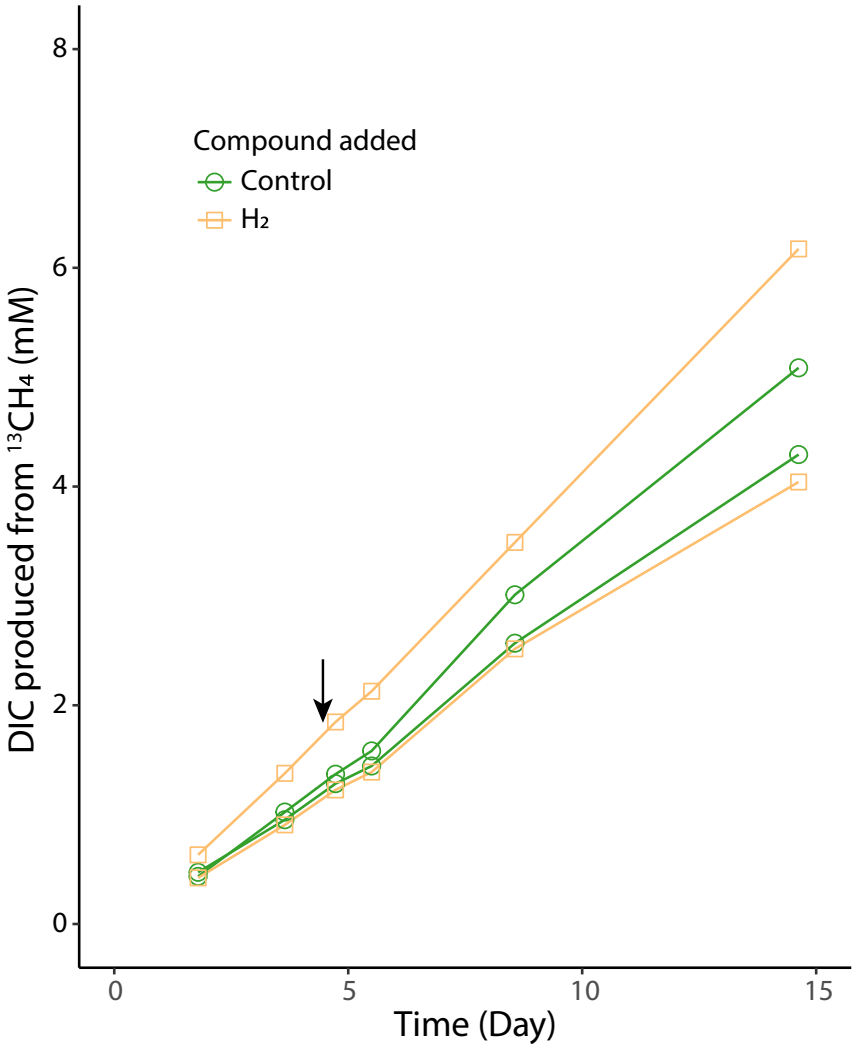

B

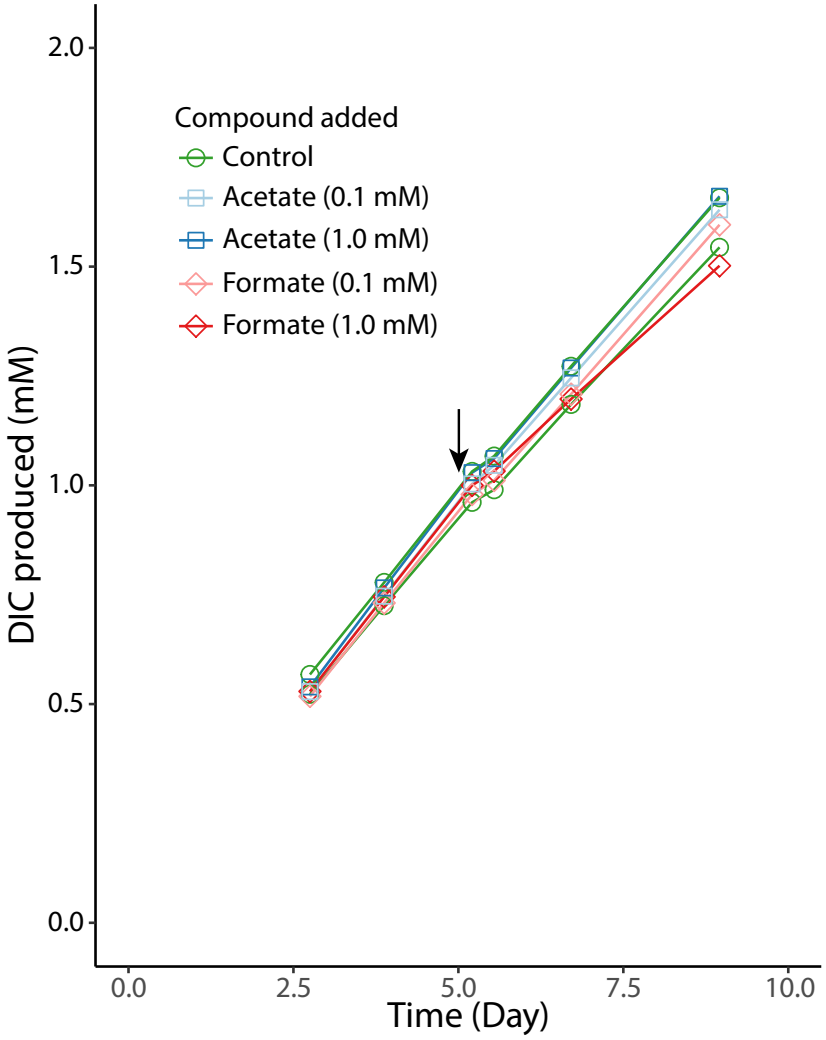
Compound added
Control
Acetate (0.1 mM)
Acetate (1.0 mM)
Formate (0.1 mM)
Formate (1.0 mM)
DIC produced (mM)
2.0
1.5
1.0
0.5
0.0
0.0
2.5
5.0
7.5
10.0
Time (Day)

C

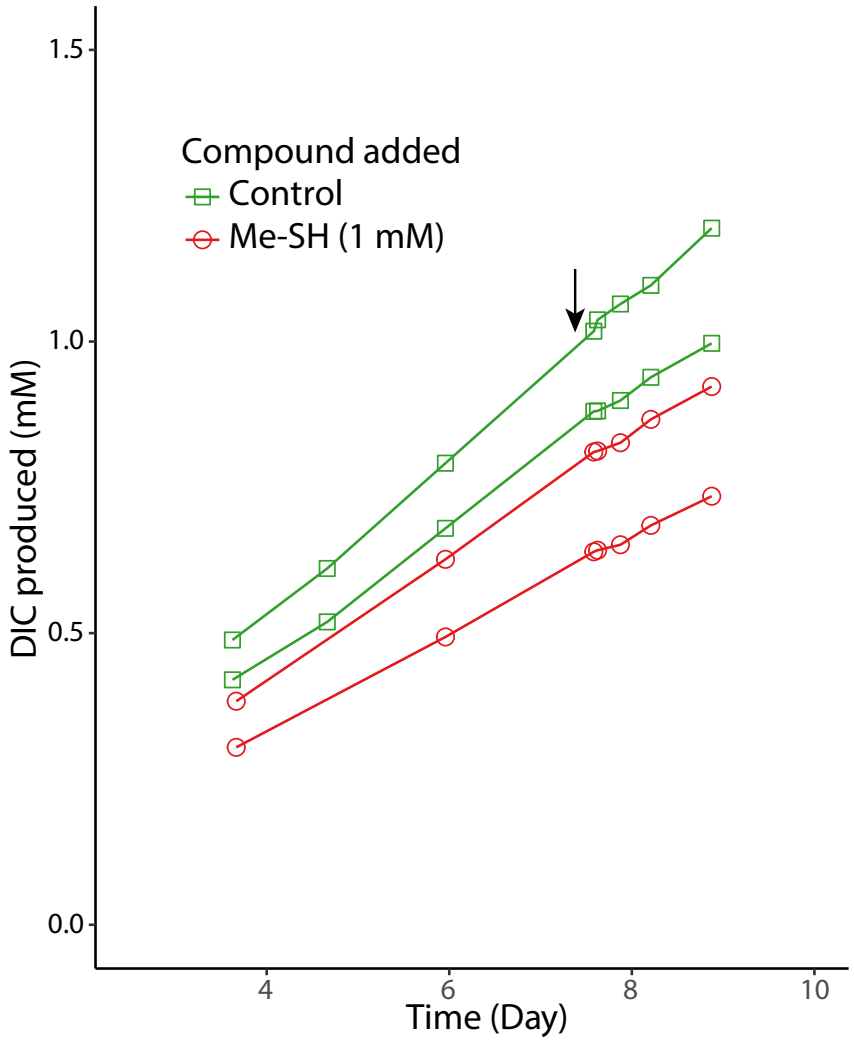
Compound added
Control
Me-SH (1 mM)
DIC produced (mM)
1.5
1.0
0.5
0.0
4
6
8
10
Time (Day)

D

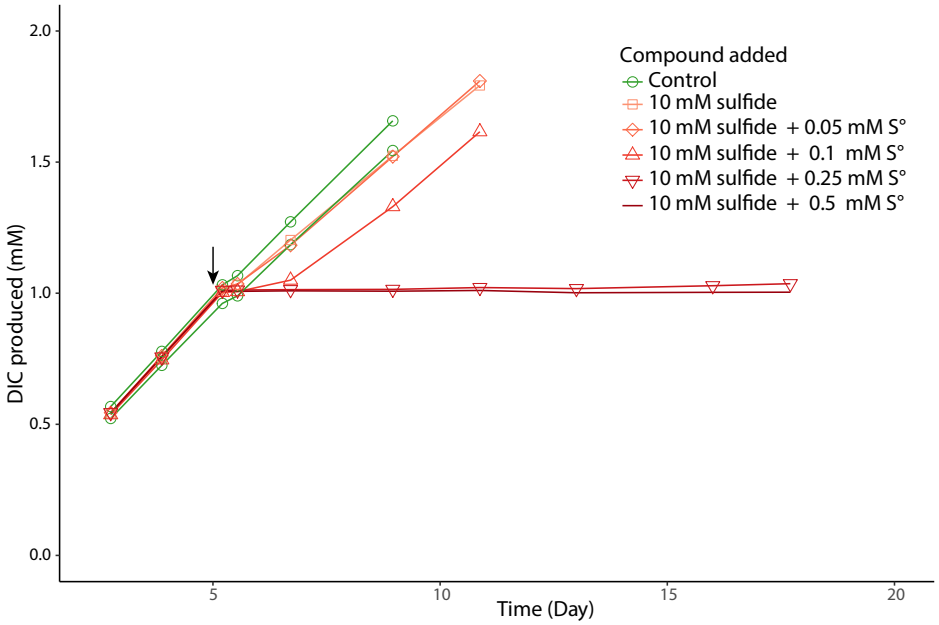
DIC produced (mM)
2.0
1.5
1.0
0.5
0.0
5
10
15
20
Time (Day)
Compound added
Control
10 mM sulfide
10 mM sulfide + 0.05 mM S°
10 mM sulfide + 0.1 mM S°
10 mM sulfide + 0.25 mM S°
10 mM sulfide + 0.5 mM S°

Figure 2. NMR spectra of acetate from a month-long microcosm experiment with natural seawater amended with 2 bar $^{13}CH_4$ and 10 mM acetate (natural carbon isotope abundance). Blue line indicates simulated acetate isotopic abundance, and red line indicates measured acetate isotopic abundance. Overlapping of simulated and measured data suggest that no 13C labelled acetate was produced from $^{13}CH_4$, and acetate is unlikely an AOM intermediate that is turned over in the system.

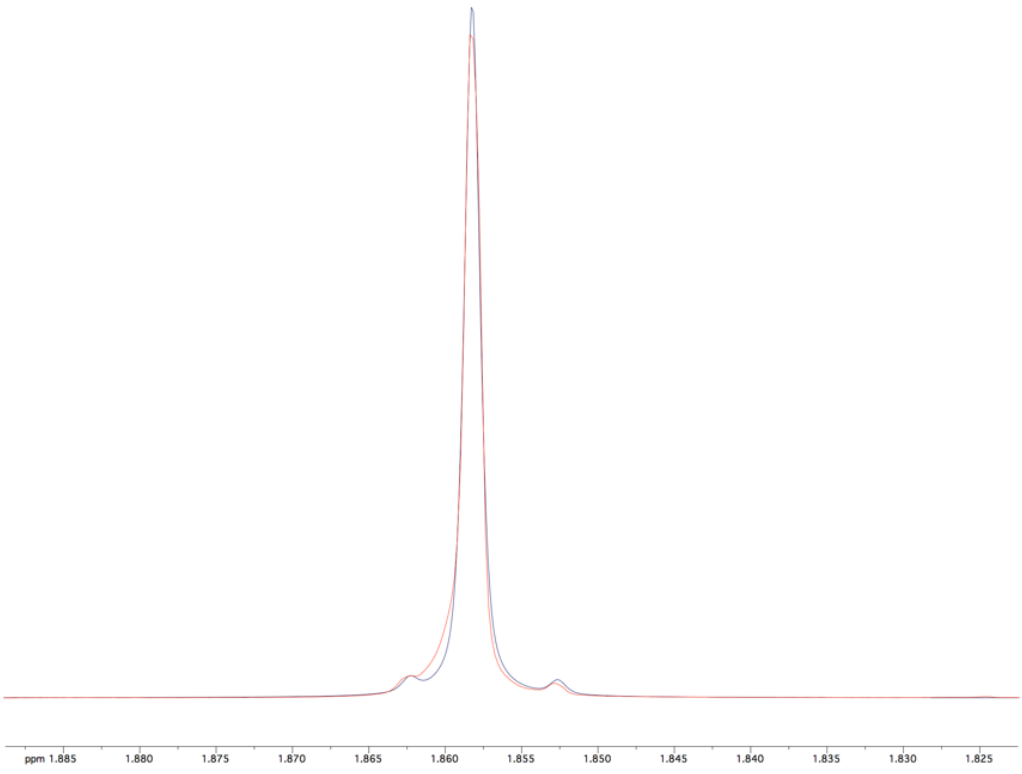

Figure 3. 16s tag sequencing of microbial communities in methane seep sediment microcosms. All incubations were 5 months long with monthly seawater replacement and amendment addition except in the "original". Natural seawater was used with 28 mM sulfate. Taxonomy is based on SILVA database and only species with >1% relative abundance are shown.

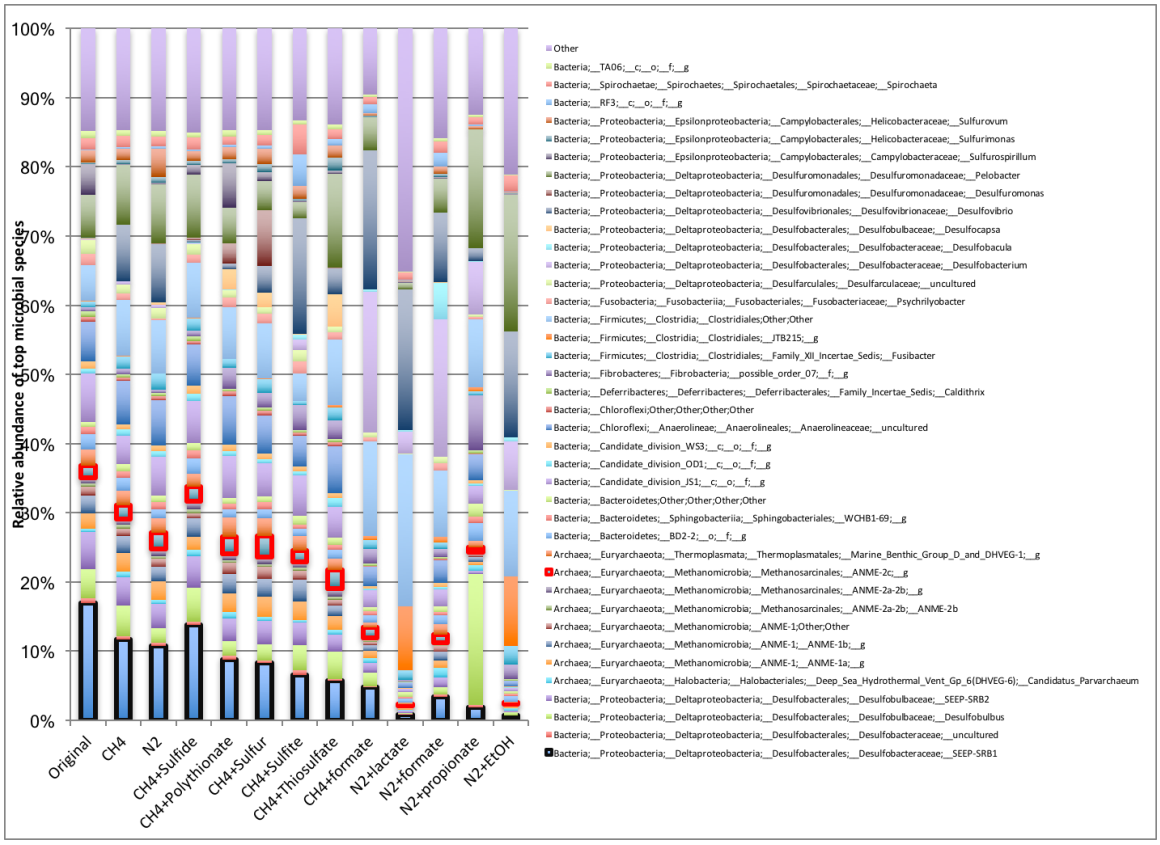

Figure 4. Molybdate and monensin exhibit selective inhibition on sulfate reduction and methane oxidation respectively. A) Rate of methane oxidation rate measured via ^{13}C-DIC production from $^{13}CH_4$, and B) rate of sulfate reduction measured via ^{34}S-sulfide production from $^{34}SO_4^{2-}$, in different AOM microcosms.

A

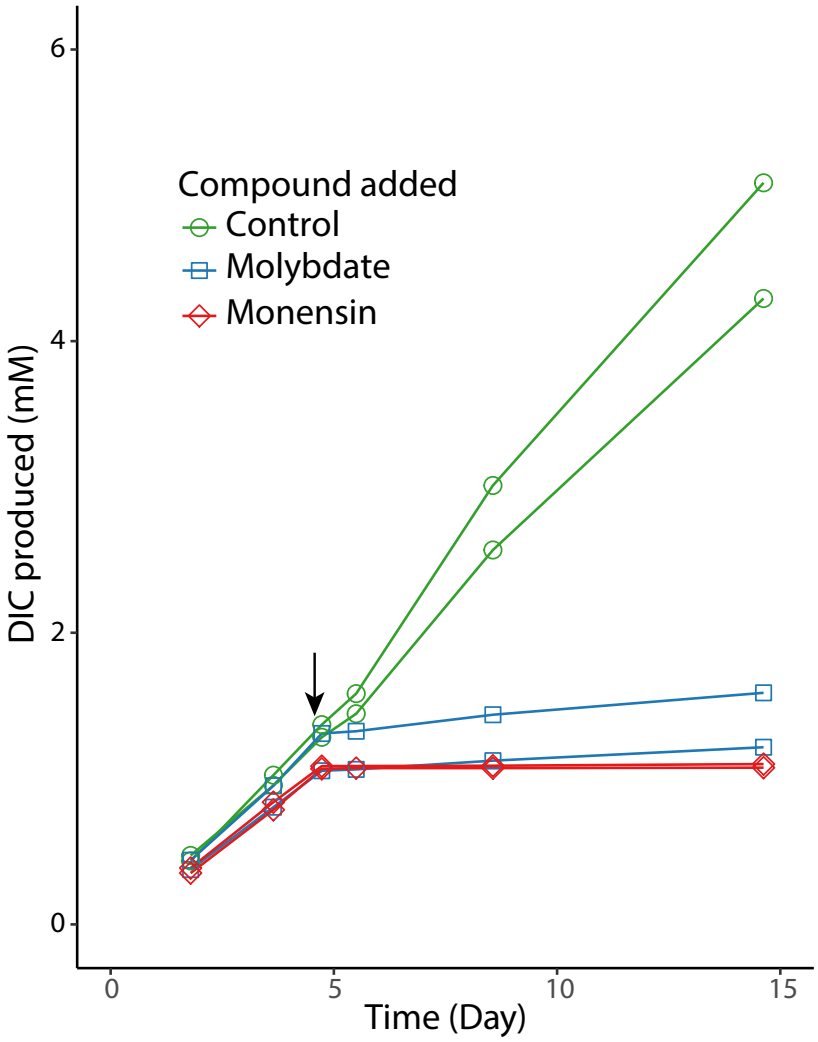

B

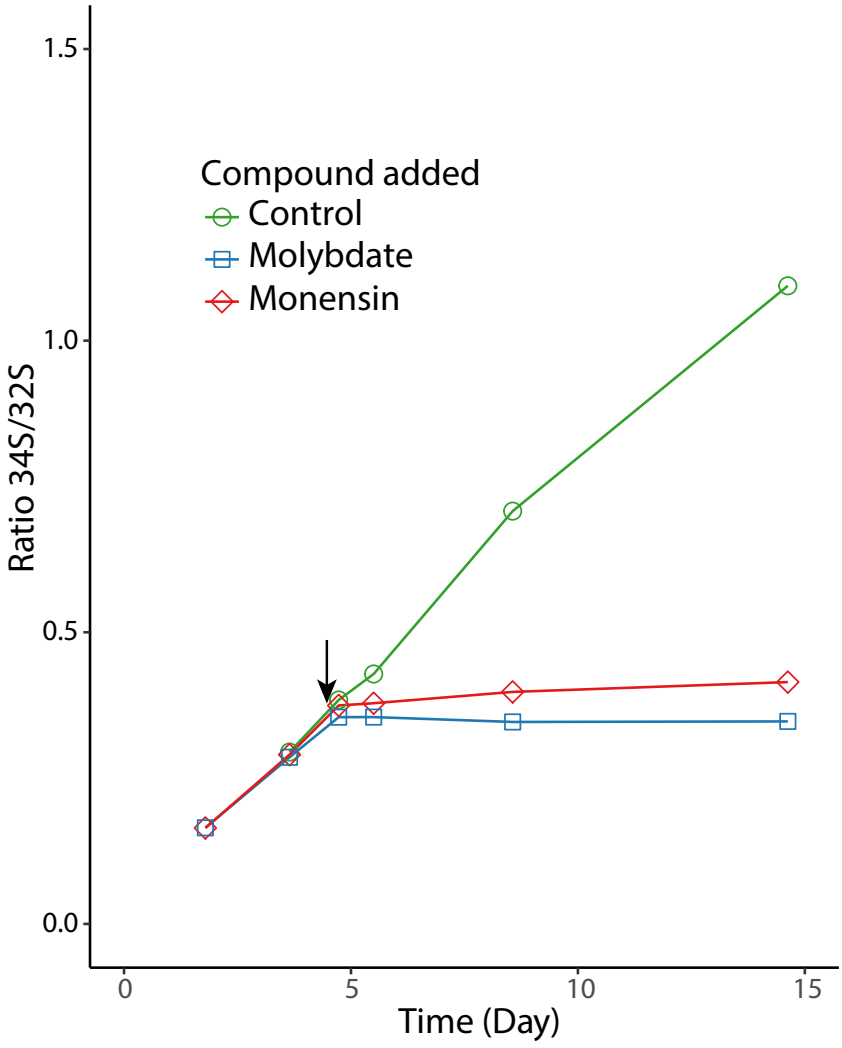
Compound added
Control
Molybdate
Monensin
Ratio 34S/32S
1.5
1.0
0.5
0.0
0
5
10
15
Time (Day)

Table 1. Sulfide production in microcosms with different amendments. (This table is attached separately as an Excel file)

Table 1. Sulfide production in microcosms with different amendments

	Incubation days	28	28	28	50	43	61
*	Treatment	T2-T3	T3-T4	T4-T5	T5-T6	T6-T7	T7-T8
Sulfide production (mM) in CH4 controls							
HS001	CH_4, control	5.9	3.8	5.2	7.0	8.8	9.5
HS002	CH_4, control	5.6	3.1	6.2	6.9	8.4	10.5
Sulfide production RELATIVE to CH4 controls (average of HS001+HS002)							
Controls							
HS001	CH_4, control	1.0	0.9	0.9	1.0	1.0	1.0
HS002	CH_4, control	1.0	0.7	1.1	1.0	1.0	1.0
HS090	CH_4, control	1.0	1.0	1.0	0.9	1.0	1.0
HS091	CH_4, control	1.0	1.0	1.0	1.1	1.0	1.0
HS003	N_2 (no CH_4), control	0.0	0.1	0.0	0.0	0.0	0.0
HS004	N_2 (no CH_4), control	0.0	0.0	0.0	0.0	0.0	0.0
HS089	N_2 (no CH_4), control	0.3	0.1	0.1	0.0	0.0	0.0
HS007	Control fixed (2 % HCHO)		0.0	0.0	0.0	0.0	0.0
Hydrogen							
HS005	Control H2		0.4	0.5	0.4	0.3	
HS006	Control H2		0.6	0.7	0.3	0.3	
HS013	Polythionate + H2		1.2	1.5	0.9	0.7	
HS014	Polythionate + H2		0.5	1.5	0.9	0.9	
HS017	S0 + H2		1.5	1.5	1.5	0.8	
HS018	S0 + H2		1.5	2.0	1.4	1.3	
Sulfur							
HS009	H2S/HS- pH = 7.7	2.0	1.9	0.5	1.4	1.1	1.0
HS010	H2S/HS- pH = 7.7	1.6	2.0	1.4	1.3	1.1	1.0
HS011	Polythionate	0.6	0.1	0.6	0.5	0.4	0.3
HS012	Polythionate	0.9	0.4	0.6	0.5	0.4	0.3
HS015	S0	0.5	0.3	0.5	0.4	0.4	0.3
HS016	S0	1.1	0.1	0.5	0.5	0.4	0.3
HS019	SO32-	0.3	0.4	0.3	0.2	0.2	0.2
HS020	SO32-	0.3	0.4	0.3	0.2	0.2	0.2
HS069	Polysulfide	2.7	0.5	-0.1	-0.3	-0.2	
HS070	Polysulfide	2.1	0.9	0.1	-0.2	0.0	
HS071	$Na_2S_2O_3$	1.5	1.0	1.2	0.9	0.7	0.7
HS072	$Na_2S_2O_3$	1.5	1.1	1.2	1.0	0.9	0.8
Inhibitors							
HS029	Bact inh. 1 Amp	1.0	1.0	1.1	1.0	0.7	1.0
HS030	Bact inh. 1 Amp	1.0	1.0	1.1	1.1	0.8	1.0
HS031	Bact inh. 2 Kan	1.1	1.1	1.0	1.0	0.7	0.9
HS032	Bact inh. 2 Kan	1.1	1.1	1.1	1.2	0.8	1.0
HS033	Bact inh. 3 Tet	0.9	1.0	0.8	0.7	0.6	0.7
HS034	Bact inh. 3 Tet	0.8	1.2	0.9	0.7	0.7	0.7
HS035	Arch inh. 1 Mev	1.3	1.1	1.1	1.0	0.8	1.1
HS036	Arch inh. 1 Mev	1.2	1.1	1.2	1.1	0.8	1.1
HS037	Arch inh. 2 Mon	0.0	0.1				
HS038	Arch inh. 2 Mon	0.0	0.1				
HS039	Arch inh. 3 = CH2F2	1.1	0.9				
HS040	Arch inh. 3 = CH2F2	1.0	1.0				
HS041	Bact inh. 4 Van	0.8	0.6	0.5	0.3	0.1	0.1
HS042	Bact inh. 4 Van	0.9	0.6	0.5	0.3	0.1	0.1
HS075	amp/kan/tet + polythionate	0.3	0.2	0.1	0.0	0.0	
HS098	amp/kan/tet + polythionate	0.3	0.2	0.3	0.1	0.1	
HS099	amp/kan/tet + polythionate	0.4	0.3	0.2	0.1	0.1	
Organics							
HS065	CH_4 + formate	1.1	1.1	1.2	0.9	0.7	
HS066	CH_4 + formate	1.1	1.2	1.3	1.0	0.8	
HS053	CH_4 + methanol	1.1	1.0				
HS054	CH_4 + methanol	1.0	1.0				
HS077	N_2 (no CH_4), + lactate	1.2	0.9	1.0	0.6	0.6	
HS078	N_2 (no CH_4), + lactate	1.3	0.8	1.0	0.6	0.5	
HS079	N_2 (no CH_4), + acetate	0.0	0.1				
HS080	N_2 (no CH_4), + acetate	0.0	0.2				
HS081	N_2 (no CH_4), + formate	0.5	0.7	0.8	0.4	0.4	
HS082	N_2 (no CH_4), + formate	0.5	0.5	0.8	0.4	0.4	
HS083	N_2 (no CH_4), + propionate	0.5	0.7	1.3	0.9	0.8	
HS084	N_2 (no CH_4), + propionate	0.9	1.3	1.6	1.0	0.9	
HS085	N_2 (no CH_4), + ethanol	1.0	1.0	1.0	0.6	0.7	
HS086	N_2 (no CH_4), + ethanol	0.9	1.0	1.1	0.7	0.6	
HS087	N_2 (no CH_4), + methanol	0.1	0.2				
HS088	N_2 (no CH_4), + methanol	0.1	0.1				
Misc							
HS021	ZnSO4	0.0					
HS022	ZnSO4	0.0					
HS023	Ellman	0.0					
HS024	Ellman	0.0					
HS025	Dithiodibenzoic acid (Ellman derivatieve)	0.0					
HS026	Dithiodibenzoic acid (Ellman derivatieve)	0.0					
HS027	TCEP	0.0					
HS028	TCEP	0.0					
HS043	[13C]-Me-*S*-CoM	1.0					
HS044	[13C]-Me-*S*-CoM	0.9					
HS047	DCOO- + polythionate	1.1	1.4				
HS048	DCOO- + polythionate	1.2	1.2				
HS051	acetate + polythionate	1.7	2.0	1.8	1.6	1.5	0.9
HS052	acetate + polythionate	1.5	1.9	2.1	2.1	1.5	1.1
HS049	acetate/triple antibiotics at t3	1.2	1.2				
HS050	acetate/triple antibiotics at t3	1.1	1.0				
HS059	H13CO3-	1.0	1.0				
HS060	H13CO3-	1.1	1.0				
HS061	room temp	1.0	0.5				
HS062	room temp	1.0	0.5				
HS063	37 °C	0.0					
HS064	37 °C	0.0					
HS092	L-Azidohomoalanine (0.1mM)			1.0	0.9	0.6	0.6
HS093	L-Azidohomoalanine (0.1mM)			1.0	0.8	0.6	0.6
HS094	L-Azidohomoalanine (1mM)			0.9	0.7	0.6	0.5
HS095	L-Azidohomoalanine (1mM)			0.9	0.7	0.4	0.3
HS067	$Na_2S_2O_6$	0.0	0.0	0.0	0.2	0.6	0.6
HS068	$Na_2S_2O_6$	0.0	0.0	0.0	0.0	0.6	0.6
HS096	tetrathionate	0.0	0.0	0.0	0.0	0.0	0.0
HS097	tetrathionate	0.0	0.0	0.0	0.0	0.0	0.0

Table 2. Geochemistry measurements of two time intervals in microcosms with different amendments. (This table is attached separately as an Excel file)

TABLE 2. Geochemistry measurements of two time intervals in microcosms with different amendments

	Incubation days	28			61		
Sample ID	**Treatment**	**Interval 1 (T4-T5)**			**Interval 2 (T7-T8)**		
Change in concentrations measured in mM for sulfide/sulfate/DIC and in bar for pressure							
		sulfide	**sulfate**	**DIC**	**sulfide**	**sulfate**	**Pressure (Bar overpressured)**
HS001	CH_4, control	5.15	-5.86	1.76	8.8	-11.0	1.0
HS002	CH_4, control	6.16	-6.02	1.57	8.6	-11.9	1.0
RELATIVE change in concentrations compared to CH4 controls (average of HS001+HS002)							
Controls							
		sulfide	**sulfate**	**DIC**	**sulfide**	**sulfate**	**Pressure**
HS001	CH_4, control	0.9	1.0	1.1	1.0	1.0	1.0
HS002	CH_4, control	1.1	1.0	0.9	1.0	1.0	1.0
HS090	CH_4, control	0.9			1.0	1.0	0.6
HS091	CH_4, control	0.9		1.3	1.0	1.0	1.4
HS003	N_2 (no CH_4), control	0.0		-0.2	0.0	0.1	
HS004	N_2 (no CH_4), control	0.0		0.0	0.0	0.1	
HS089	N_2 (no CH_4), control	0.1		-0.2			
HS007	Control fixed (2 % HCHO)	0.0			0.0		
Sulfur							
HS009	H2S/HS- pH = 7.7	0.5			1.0	0.9	1.5
HS010	H2S/HS- pH = 7.7	1.4			1.0	0.9	1.7
HS011	Polythionate	0.6	-0.1	1.0	0.3	0.0	0.1
HS012	Polythionate	0.6	-0.1	1.2	0.3	-0.1	-0.2
HS015	S0	0.5	-0.1	0.6	0.3	0.0	0.4
HS016	S0	0.5	-0.1	0.8	0.3	-0.1	0.2
HS019	SO32-	0.3	0.4	0.1	0.2	0.4	0.5
HS020	SO32-	0.3	0.5	0.1	0.2	0.4	0.1
HS069	Polysulfide	-0.1	0.0	-0.2			0.2
HS070	Polysulfide	0.0	0.1	-0.1			0.4
HS071	$Na_2S_2O_3$	1.1	0.0	1.2	0.7	-0.3	0.4
HS072	$Na_2S_2O_3$	1.1		0.9	0.8	-0.1	0.8
Inhibitors							
HS029	Bact inh. 1 Amp	1.1		1.7	1.0	0.8	1.1
HS030	Bact inh. 1 Amp	1.1		1.4	1.0	0.9	0.3
HS031	Bact inh. 2 Kan	1.0		1.9	0.9	0.9	1.2
HS032	Bact inh. 2 Kan	1.1		1.8	1.0	1.0	0.8
HS033	Bact inh. 3 Tet	0.8		1.5	0.7	0.6	0.6
HS034	Bact inh. 3 Tet	0.9		1.2	0.7	0.6	1.1
HS035	Arch inh. 1 Mev	1.1		2.1	1.1	1.1	0.7
HS036	Arch inh. 1 Mev	1.2		1.7	1.1	0.8	0.8
HS037	Arch inh. 2 Mon						
HS038	Arch inh. 2 Mon						
HS039	Arch inh. 3 = CH2F2						
HS040	Arch inh. 3 = CH2F2						
HS041	Bact inh. 4 Van	0.5	0.3	0.3	0.1	0.0	0.0
HS042	Bact inh. 4 Van	0.5		0.3	0.1	0.1	0.7
HS075	amp/kan/tet + polythionate	0.1		0.1			0.2
HS098	amp/kan/tet + polythionate	0.2	0.0	0.4			1.1
HS099	amp/kan/tet + polythionate	0.2	-0.1	-0.1			-0.1
Organics							
HS065	CH_4 + formate	1.2	1.3	3.5			0.5
HS066	CH_4 + formate	1.3	1.4	3.0			1.0
HS053	CH_4 + methanol						
HS054	CH_4 + methanol						
HS077	N_2 (no CH_4), + lactate	0.9		3.9			
HS078	N_2 (no CH_4), + lactate	0.9		3.5			
HS079	N_2 (no CH_4), + acetate						
HS080	N_2 (no CH_4), + acetate						
HS081	N_2 (no CH_4), + formate	1.2	0.6	3.1			
HS082	N_2 (no CH_4), + formate	1.4	0.6	3.2			
HS083	N_2 (no CH_4), + propionate	0.9	1.1	2.9			
HS084	N_2 (no CH_4), + propionate	1.0	1.4	3.9			
HS085	N_2 (no CH_4), + ethanol	0.0		1.0			
HS086	N_2 (no CH_4), + ethanol	0.0					
HS087	N_2 (no CH_4), + methanol						
HS088	N_2 (no CH_4), + methanol						
Misc							
HS021	ZnSO4						-0.1
HS022	ZnSO4						0.1
HS051	acetate + polythionate	1.8	1.3	3.1	0.9	0.8	1.0
HS052	acetate + polythionate	2.1	1.4	3.5	1.1	0.7	0.2
HS092	L-Azidohomoalanine (0.1mM)	0.9			0.6		3.5
HS093	L-Azidohomoalanine (0.1mM)	0.9			0.6		0.2
HS094	L-Azidohomoalanine (1mM)	0.8		1.0	0.5		0.8
HS095	L-Azidohomoalanine (1mM)	0.8		1.4	0.3		1.0
HS067	$Na_2S_2O_6$	0.0	-0.2	0.3	0.6		0.8
HS068	$Na_2S_2O_6$	0.0		0.4	0.6	-1.1	0.3
HS096	tetrathionate	0.0	0.0	0.2	0.0	0.0	1.8
HS097	tetrathionate	0.0		0.8	0.0	-0.1	1.1

Table 3. Relative abundances of community members in microcosms of sediment #5207 before and after amendment addition. (Full table is attached separately as an Excel file)

Taxon	Original	CH4	N2	CH4+Sulfide	CH4+Polythi	CH4+Sulfur	CH4+Sulfite	CH4+Thiosulf	CH4+formate	N2+lactate	N2+formate	N2+propiona	N2+EtOH
Bacteria;__Proteobacteria;__Deltaproteobacteria;__Desulfobacteraceae;__SEEP-SRB1	0.169	0.117	0.108	0.137	0.088	0.083	0.066	0.057	0.048	0.008	0.034	0.019	0.007
Bacteria;__Proteobacteria;__Deltaproteobacteria;__Desulfobacteraceae;__uncultured	0.007	0.005	0.004	0.005	0.006	0.004	0.006	0.003	0.002	0.001	0.003	0.003	0.001
Bacteria;__Proteobacteria;__Deltaproteobacteria;__Desulfobulbaceae;__Desulfobulbus	0.042	0.043	0.021	0.049	0.021	0.023	0.036	0.040	0.020	0.002	0.011	0.189	0.005
Bacteria;__Proteobacteria;__Deltaproteobacteria;__Desulfobulbaceae;__SEEP-SRB2	0.054	0.041	0.035	0.046	0.032	0.033	0.033	0.024	0.014	0.003	0.014	0.005	0.002
Archaea;__Euryarchaeota;__Halobacteriales;__Deep_Sea_Hydrothermal_Vent_Gp_6(DHVEG-6);__Candidatus_Parvarchaeum	0.005	0.009	0.006	0.009	0.009	0.007	0.003	0.007	0.006	0.002	0.013	0.008	0.003
Archaea;__Euryarchaeota;__Methanomicrobia;__ANME-1a;__g	0.022	0.027	0.027	0.018	0.027	0.029	0.027	0.020	0.011	0.002	0.011	0.005	0.003
Archaea;__Euryarchaeota;__Methanomicrobia;__ANME-1;__ANME-1b;__g	0.026	0.024	0.021	0.027	0.028	0.026	0.031	0.015	0.008	0.002	0.013	0.006	0.001
Archaea;__Euryarchaeota;__Methanomicrobia;__ANME-1;Other;Other	0.012	0.011	0.012	0.007	0.016	0.018	0.013	0.009	0.004	0.001	0.007	0.005	0.001
Archaea;__Euryarchaeota;__Methanomicrobia;__Methanosarcinales;__ANME-2a-2b;__ANME-2b	0.005	0.006	0.004	0.007	0.003	0.003	0.004	0.005	0.002	0.000	0.002	0.001	0.000
Archaea;__Euryarchaeota;__Methanomicrobia;__Methanosarcinales;__ANME-2a-2b;__g	0.008	0.008	0.010	0.011	0.010	0.010	0.008	0.012	0.004	0.001	0.003	0.002	0.001
Archaea;__Euryarchaeota;__Methanomicrobia;__Methanosarcinales;__ANME-2c;__g	0.018	0.019	0.024	0.020	0.025	0.030	0.017	0.027	0.014	0.002	0.011	0.007	0.002
Archaea;__Euryarchaeota;__Thermoplasmata;__Thermoplasmatales;__Marine_Benthic_Group_D_and_DHVEG-1;__g	0.023	0.022	0.021	0.019	0.027	0.026	0.020	0.016	0.007	0.002	0.015	0.009	0.002
Bacteria;__Bacteroidetes;__BD2-2;__o__f__g	0.022	0.019	0.013	0.022	0.012	0.013	0.012	0.013	0.011	0.005	0.013	0.025	0.008
Bacteria;__Bacteroidetes;__Sphingobacteriia;__Sphingobacteriales;__WCHB1-69;__g	0.010	0.009	0.010	0.012	0.009	0.011	0.006	0.006	0.006	0.002	0.005	0.010	0.003
Bacteria;__Bacteroidetes;Other;Other;Other;Other	0.007	0.011	0.009	0.011	0.007	0.009	0.012	0.011	0.005	0.007	0.007	0.019	0.004
Bacteria;__Candidate_division_JS1;__c__o__f__g	0.070	0.040	0.056	0.060	0.061	0.047	0.058	0.044	0.025	0.004	0.025	0.025	0.004
Bacteria;__Candidate_division_OD1;__c__o__f__g	0.007	0.010	0.008	0.011	0.007	0.006	0.006	0.013	0.002	0.000	0.003	0.003	0.001
Bacteria;__Candidate_division_WS3;__c__o__f__g	0.011	0.007	0.009	0.011	0.009	0.008	0.007	0.007	0.004	0.002	0.006	0.005	0.001
Bacteria;__Chloroflexi;__Anaerolineae;__Anaerolineales;__uncultured	0.058	0.062	0.065	0.060	0.070	0.056	0.044	0.069	0.028	0.008	0.033	0.037	0.008
Bacteria;__Chloroflexi;Other;Other;Other	0.007	0.005	0.006	0.005	0.007	0.007	0.004	0.005	0.002	0.000	0.002	0.001	0.000
Bacteria;__Deferribacteres;__Deferribacteres;__Family_Incertae_Sedis;__Calditrix	0.008	0.005	0.005	0.007	0.004	0.004	0.004	0.004	0.003	0.001	0.002	0.004	0.002
Bacteria;__Fibrobacteres;__Fibrobacteria;__possible_order_07;__f__g	0.006	0.008	0.005	0.009	0.030	0.021	0.036	0.027	0.021	0.002	0.012	0.079	0.022
Bacteria;__Firmicutes;__Clostridia;__Clostridiales;__Family_XII_Incertae_Sedis;__Fusibacter	0.009	0.017	0.022	0.018	0.012	0.020	0.005	0.019	0.012	0.015	0.009	0.007	0.026
Bacteria;__Firmicutes;__Clostridia;__Clostridiales;__JTB215;__g	0.000	0.001	0.001	0.000	0.001	0.001	0.000	0.004	0.006	0.091	0.008	0.006	0.101
Bacteria;__Firmicutes;__Clostridia;__Clostridiales;Other;Other	0.052	0.080	0.077	0.080	0.075	0.080	0.040	0.095	0.137	0.220	0.097	0.098	0.123
Bacteria;__Fusobacteria;__Fusobacteriia;__Fusobacteriales;__Fusobacteriaceae;__Psychrilyobacter	0.016	0.010	0.002	0.011	0.013	0.014	0.017	0.010	0.005	0.000	0.010	0.004	0.000
Bacteria;__Proteobacteria;__Deltaproteobacteria;__Desulfarculales;__Desulfarculaceae;__uncultured	0.020	0.013	0.015	0.015	0.011	0.009	0.017	0.008	0.007	0.001	0.009	0.004	0.001
Bacteria;__Proteobacteria;__Deltaproteobacteria;__Desulfobacteraceae;__Desulfobacterium	0.001	0.004	0.005	0.002	0.000	0.000	0.016	0.001	0.204	0.032	0.199	0.076	0.071
Bacteria;__Proteobacteria;__Deltaproteobacteria;__Desulfobacteraceae;__Desulfobacula	0.000	0.000	0.000	0.000	0.000	0.000	0.006	0.000	0.003	0.002	0.053	0.001	0.006
Bacteria;__Proteobacteria;__Deltaproteobacteria;__Desulfobulbaceae;__Desulfocapsa	0.001	0.001	0.003	0.000	0.029	0.021	0.001	0.046	0.000	0.000	0.001	0.000	0.000
Bacteria;__Proteobacteria;__Deltaproteobacteria;__Desulfovibrionales;__Desulfovibrionaceae;__Desulfovibrio	0.001	0.081	0.085	0.004	0.008	0.038	0.167	0.038	0.202	0.204	0.101	0.019	0.152
Bacteria;__Proteobacteria;__Deltaproteobacteria;__Desulfuromonadales;__Desulfuromonadaceae;__Desulfuromonas	0.001	0.000	0.001	0.003	0.029	0.080	0.000	0.001	0.000	0.000	0.000	0.000	0.000
Bacteria;__Proteobacteria;__Deltaproteobacteria;__Desulfuromonadales;__Pelobacter	0.061	0.086	0.086	0.091	0.052	0.042	0.023	0.136	0.047	0.008	0.049	0.171	0.198
Bacteria;__Proteobacteria;__Epsilonproteobacteria;__Campylobacteraceae;__Sulfurospirillum	0.044	0.001	0.003	0.014	0.064	0.014	0.003	0.005	0.001	0.003	0.002	0.000	0.002
Bacteria;__Proteobacteria;__Epsilonproteobacteria;__Campylobacteriales;__Helicobacteraceae;__Sulfurimonas	0.003	0.006	0.008	0.005	0.006	0.012	0.002	0.019	0.001	0.000	0.004	0.001	0.000
Bacteria;__Proteobacteria;__Epsilonproteobacteria;__Campylobacteriales;__Helicobacteraceae;__Sulfurovum	0.017	0.016	0.041	0.014	0.018	0.021	0.019	0.017	0.004	0.001	0.010	0.004	0.002
Bacteria;__RF3;__c__o__f__g	0.002	0.003	0.003	0.003	0.003	0.005	0.045	0.009	0.013	0.001	0.021	0.003	0.001
Bacteria;__Spirochaetae;__Spirochaetes;__Spirochaetales;__Spirochaetaceae;__Spirochaeta	0.016	0.016	0.015	0.018	0.013	0.015	0.044	0.015	0.010	0.011	0.015	0.011	0.024
Bacteria;__TA06;__c__o__f__g	0.010	0.008	0.008	0.007	0.009	0.007	0.006	0.006	0.003	0.001	0.005	0.003	0.001
Other	0.149	0.147	0.148	0.150	0.147	0.147	0.133	0.139	0.096	0.351	0.158	0.125	0.212

REFERENCES

Alperin, Marc J, and Tori M Hoehler. 2009. "Anaerobic Methane Oxidation by Archaea/Sulfate-Reducing Bacteria Aggregates: 1. Thermodynamic and Physical Constraints." *American Journal of Science* 309 (10): 869–957. doi:10.2475/10.2009.01.

Banat, Ibrahim M, and David B Nedwell. 1984. "Inhibition of Sulphate Reduction in Anoxic Marine Sediment by Group VI Anions." *Estuarine, Coastal and Shelf Science* 18 (3): 361–66. doi:10.1016/0272-7714(84)90077-5.

Boetius, Antje, Katrin Ravenschlag, Carsten J Schubert, Dirk Rickert, Friedrich Widdel, Armin Gieseke, Rudolf Amann, Bo Barker Jørgensen, Ursula Witte, and Olaf Pfannkuche. 2000. "A Marine Microbial Consortium Apparently Mediating Anaerobic Oxidation of Methane." *Nature* 407 (6804): 623–26. doi:10.1038/35036572.

Case, David H. 2016. "Carbonate-Associated Microbial Ecology at Methane Seeps: Assemblage Composition, Response to Changing Environmental Conditions, and Implications for Biomarker Longevity." doi:10.7907/Z9TD9V84.

Cline, Joel D. 1969. "Spectrophotometric Determination of Hydrogen Sulfide in Natural Waters." *Limnology and Oceanography* 14: 454–58.

Hinrichs, Kai U, John M Hayes, Sean P Sylva, Peter G Brewer, and Edward F DeLong. 1999. "Methane-Consuming Archaebacteria in Marine Sediments.." *Nature* 398 (6730): 802–5. doi:10.1038/19751.

Hoehler, Tori M, Marc J Alperin, Daniel B Albert, and Christopher S Martens. 1994. "Field and Laboratory Studies of Methane Oxidation in an Anoxic Marine Sediment: Evidence for a Methanogen-Sulfate Reducer Consortium." *Global Biogeochemical Cycles* 8 (4): 451–63. doi:10.1029/94GB01800.

Holler, Thomas, Gunter Wegener, Helge Niemann, Christian Deusner, Timothy G Ferdelman, Antje Boetius, Benjamin Brunner, and Friedrich Widdel. 2011. "Carbon and Sulfur Back Flux During Anaerobic Microbial Oxidation of Methane and Coupled Sulfate Reduction.." *Proceedings of the National Academy of Sciences* 108 (52): E1484–90. doi:10.1073/pnas.1106032108.

Ikeda, Sanae, Hiromu Satake, Takeo Hisano, and Toshio Terazawa. 1972. "Potentiometric Argentimetric Method for the Successive Titration of Sulphide and Dissolved Sulphur in Polysulphide Solutions.." *Talanta* 19 (12): 1650–54.

Krukenberg, Viola, Katie Harding, Michael Richter, Frank Oliver Glöckner, Harald R Gruber Vodicka, Birgit Adam, Jasmine S Berg, et al. 2016. "Candidatus Desulfofervidus Auxilii, a Hydrogenotrophic Sulfate-Reducing Bacterium Involved in the Thermophilic Anaerobic Oxidation of Methane.." *Environmental Microbiology* 18 (9): 3073–91. doi:10.1111/1462-2920.13283.

Liu, Yuchen, and William B Whitman. 2008. "Metabolic, Phylogenetic, and Ecological Diversity of the Methanogenic Archaea.." *Annals of the New York Academy of Sciences* 1125 (1). Blackwell Publishing Inc: 171–89. doi:10.1196/annals.1419.019.

McGlynn, Shawn E, Grayson L Chadwick, Christopher P Kempes, and Victoria J Orphan.

2015. "Single Cell Activity Reveals Direct Electron Transfer in Methanotrophic Consortia.." *Nature* 526 (7574). Nature Publishing Group: 531–35. doi:10.1038/nature15512.

Meulepas, Roel J W, Christian G Jagersma, Ahmad F Khadem, Alfons J M Stams, and Piet N L Lens. 2010. "Effect of Methanogenic Substrates on Anaerobic Oxidation of Methane and Sulfate Reduction by an Anaerobic Methanotrophic Enrichment.." *Applied Microbiology and Biotechnology* 87 (4): 1499–1506. doi:10.1007/s00253-010-2597-0.

Miller, Sasson, Oremland. 1998. "Difluoromethane, a New and Improved Inhibitor of Methanotrophy ." *Applied and Environmental Microbiology* 64 (11): 4357–62.

Miller, Terry L, and Meyer J Wolin. 2001. "Inhibition of Growth of Methane-Producing Bacteria of the Ruminant Forestomach by Hydroxymethylglutaryl-SCoA Reductase Inhibitors.." *Journal of Dairy Science* 84 (6): 1445–48.

Milucka, Jana, Timothy G Ferdelman, Lubos Polerecky, Daniela Franzke, Gunter Wegener, Markus Schmid, Ingo Lieberwirth, Michael Wagner, Friedrich Widdel, and Marcel M M Kuypers. 2012. "Zero-Valent Sulphur Is a Key Intermediate in Marine Methane Oxidation.." *Nature* 491 (7425): 541–46. doi:10.1038/nature11656.

Moran, James J, Christopher H House, Jennifer M Vrentas, and Katherine H Freeman. 2008. "Methyl Sulfide Production by a Novel Carbon Monoxide Metabolism in Methanosarcina Acetivorans.." *Applied and Environmental Microbiology* 74 (2): 540–42. doi:10.1128/AEM.01750-07.

Moran, James J, Emily J Beal, Jennifer M Vrentas, Victoria J Orphan, Katherine H Freeman, and Christopher H House. 2008. "Methyl Sulfides as Intermediates in the Anaerobic Oxidation of Methane.." *Environmental Microbiology* 10 (1): 162–73. doi:10.1111/j.1462-2920.2007.01441.x.

Nauhaus, Katja, Antje Boetius, Martin Krüger, and Friedrich Widdel. 2002. "In Vitro Demonstration of Anaerobic Oxidation of Methane Coupled to Sulphate Reduction in Sediment From a Marine Gas Hydrate Area.." *Environmental Microbiology* 4 (5): 296–305.

Nauhaus, Katja, Tina Treude, Antje Boetius, and Martin Krüger. 2005. "Environmental Regulation of the Anaerobic Oxidation of Methane: a Comparison of ANME-I and ANME-II Communities.." *Environmental Microbiology* 7 (1): 98–106. doi:10.1111/j.1462-2920.2004.00669.x.

Orphan, Victoria J, Christopher H House, Kai U Hinrichs, Kevin D McKeegan, and Edward F DeLong. 2001. "Methane-Consuming Archaea Revealed by Directly Coupled Isotopic and Phylogenetic Analysis.." *Science* 293 (5529). American Association for the Advancement of Science: 484–87. doi:10.1126/science.1061338.

Rabus, Ralf, Theo A Hansen, and Friedrich Widdel. 2013. "Dissimilatory Sulfate- and Sulfur-Reducing Prokaryotes." In *The Prokaryotes*, 309–404. Berlin, Heidelberg: Springer Berlin Heidelberg. doi:10.1007/978-3-642-30141-4_70.

Saleh, A M, R Macpherson, and J D A Miller. 1964. "The Effect of Inhibitors on Sulphate Reducing Bacteria: a Compilation." *Journal of Applied Bacteriology* 27 (2): 281–93. doi:10.1111/j.1365-2672.1964.tb04914.x.

Scheller, Silvan, Hang Yu, Grayson L Chadwick, Shawn E McGlynn, and Victoria J Orphan.

2016. “Artificial Electron Acceptors Decouple Archaeal Methane Oxidation From Sulfate Reduction..” *Science* 351 (6274): 703–7. doi:10.1126/science.aad7154.

Steudel, Ralf, Thomas Göbel, and Gabriele Holdt. 1988. “The Molecular Composition of Hydrophilic Sulfur Sols Prepared by Acid Decomposition of Thiosulfate [1].” *Zeitschrift Für Naturforschung B* 43 (2). doi:10.1515/znb-1988-0212.

Thornton, J H, and F N Owens. 1981. “Monensin Supplementation and Methane Production by Steers.” *Journal of Animal Science* 52 (3): 628. doi:10.2527/jas1981.523628x.

Valentine, D L, and W S Reeburgh. 2000. “New Perspectives on Anaerobic Methane Oxidation..” *Environmental Microbiology* 2 (5). Blackwell Science Ltd: 477–84. doi:10.1046/j.1462-2920.2000.00135.x.

Valentine, David L. 2002. “Biogeochemistry and Microbial Ecology of Methane Oxidation in Anoxic Environments: a Review..” *Antonie Van Leeuwenhoek* 81 (1-4): 271–82.

Wegener, Gunter, Viola Krukenberg, Dietmar Riedel, Halina E Tegetmeyer, and Antje Boetius. 2015. “Intercellular Wiring Enables Electron Transfer Between Methanotrophic Archaea and Bacteria.” *Nature* 526 (7574). Nature Publishing Group: 587–90. doi:10.1038/nature15733.

Wegener, Gunter, Viola Krukenberg, S Emil Ruff, Matthias Y Kellermann, and Katrin Knittel. 2016. “Metabolic Capabilities of Microorganisms Involved in and Associated with the Anaerobic Oxidation of Methane.” *Frontiers in Microbiology* 7 (17). Frontiers: 869. doi:10.3389/fmicb.2016.00046.

AOM with sulfate is a large sink for methane in the global carbon cycle. The energy yield for this reaction is low ($\Delta G^{\circ\prime}$ = -17 kJ/mol) and fuels a symbiosis between two microorganisms, namely ANME and SRB. Our understanding on the mechanism of this symbiosis has greatly improved in the past six years, with work presented here and many more from other researchers cited in this thesis. Diffusible intermediates such as hydrogen, carbon-based compounds and zero-valent sulfur are unlikely the metabolic intermediate linking the AOM consortia together (Chapter 1 and Appendix A). Instead, a picture starts to emerge that involves electrons being passed directly between ANME and SRB. This is supported by experimental evidences that soluble electron acceptors such as AQDS could be used by ANME as an alternative electron acceptor (Chapter 2 and 3), and multiheme cytochromes in both ANME and SRB genomes critical in extracellular electron transfer are expressed under syntrophic conditions (McGlynn *et al.* 2015, Skennerton *et al.* In review., Chapter 3).

AOM research has been hampered by the slow-growth of the microorganisms carrying out this reaction, as well as the complex chemical and biological ecosystems they inhabit. Technological advances and methodological developments such as stable isotope probing, FISH-nanoSIMS, BONCAT-FACS and metatranscriptomics have been successful in circumventing these two issues, and successfully characterizing the AOM consortia. However, ultimately, cultivation of ANME or SRB is needed to make the next leap forward in this research area. Even though these microorganisms double on the timescale of months, the ability to make direct measurements on a simple, reproducible, cultured biological system is worth the wait. This has recently been accomplished with thermophilic AOM consortia involving ANME-1 (Wegener *et al.* 2015), leading to the isolation of its SRB partner *Candidatus* Desulfofervidus auxilii (Krukenberg *et al.* 2016). Other enrichments with ANME-2a/2b/2c and their SRB partners are also start to emerge

(Wegener *et al.* 2016 and Yu *et al.* Unpublished). These cultured systems will greatly assist and accelerate discoveries in AOM research.

Experiments that continue to investigate the hypothesis of direct interspecies electron transfer in AOM symbiosis are the next logical step. One focus could be characterizing the intercellular space between ANME and SRB. What chemicals, proteins, organic compounds or minerals are there and how are they arranged to facilitate electron transfer between two cells? Also, anaerobic methane oxidation is not unique to one phylogenic group but evolved multiple times independently to give rise to ANME-1, ANME-2ab, ANME-2c and *Candidatus* Methanoperedens clades. What are the commonalities between these groups to allow reverse methanogenesis to occur? While multiple partnerships exist, research so far on both ANME-1 and ANME-2a/2c are pointing to a similar symbiosis mechanism of direct interspecies electron transfer. What then distinguishes the bacterial partners of different ANME clades and from other related bacterial groups? Furthermore, can we use our understanding to engineer an ANME strain or build one *de novo* that grows fast for future energy applications? These are all exciting directions forward and will require close partnerships between individuals with not only skills in multiple scientific disciplines but also tremendous amounts of curiosity and patience to accomplish.

[This page is intentionally left blank]

[This page is intentionally left blank]